A UNIT CELL APPROACH FOR LIGHTWEIGHT STRUCTURE AND COMPLIANT MECHANISM

A Dissertation

Presented to

The Academic Faculty

By

Hongqing Vincent Wang

In Partial Fulfillment

Of the Requirements for the Degree

Doctor of Philosophy in Mechanical Engineering

Georgia Institute Of Technology

December 2005

A UNIT CELL APPROACH FOR LIGHTWEIGHT STRUCTURE AND COMPLIANT MECHANISM

Approved by:

David W. Rosen, Chair
Professor
Mechanical Engineering

Farrokh Mistree
Professor
Mechanical Engineering

Imme Ebert-Uphoff
Associate Professor
Mechanical Engineering

Hamid Garmestani
Professor
Materials Science and Engineering

David L. McDowell
Regents' Professor
Mechanical Engineering

Jarek Rossignac
Professor
College of Computing

Date Approved: November 28, 2005

ACKNOWLEDGEMENTS

I would like to thank, first of all, my advisor Dr. David Rosen for his continuous encouragement and guidance throughout my years at Georgia Tech. Without him, the completion of this work would be impossible.

The committee members of this dissertation, Drs. Imme Ebert-Uphoff, Jarek Rossignac, David McDowell, Farrokh Mistree, and Hamid Garmestani, deserve many thanks for their comments and suggestions.

I specially thank Yong Chen for his contribution to geometric modeling, Markus Wahlberg for his contribution to design synthesis of cellular structure, Giorgos Hatzilias for teaching me to use SLA, Steven Sheffield for teaching me to use the CMM PFx-5, Guan Yuan for helping me on PDMS modeling, Chris Williams for providing information about cellular material manufacturing and commercializing TrussCreator, Carolyn Seepersad for her insightful discussion on topology optimization, Aijun Wang for his inputs about nonlinearity and buckling, Sebastien Wolff for discussion on MASTAN2, and Krister Svanburg for supplying the MMA algorithm. I would like to thank all of the faculty and students for their friendship and challenging discussions and for making the SRL a wonderful place to learn, work and grow. The people listed below deserve special recognitions for their friendships and helps: Benay Sager, Yao Lin, Angran Xiao, Shiva Sambu, and Sundiata Jhangha.

The financial supports from the RPMI and the NSF Digital Clay project are greatly appreciated. I would like to thank Rick Pressley at Pratt Whitney for his continuous support to my work.

Finally I would like to thank my dear wife, Chunchun Ni, my parents, Guorong He and Guanfu Wang for their support without which I wouldn't have been here. I am grateful to my friends Sai Zeng, Lizheng Zhang, Jiantao Zheng, Guoan Wang, Yong Huang and Zhihuang Dai.

TABLE OF CONTENTS

ACKNOWLEDGEMENTS iii
LIST OF TABLES ix
LIST OF FIGURES x
LIST OF SYMBOLS xv
SUMMARY xxvi
CHAPTER 1 CELLULAR STRUCTURES: LIGHTWEIGHT STRUCTURE AND COMPLIANT MECHANISM 1
1.1 Cellular Structures from Natural Occurrence to Engineering Applications 1
1.1.1 Natural Occurrences 1
1.1.2 Artificial Cellular Structures 4
1.1.3 Stretching-dominated Structure vs. Bending-dominated Structure 7
1.2 Lightweight Structure – a Stretching-dominated Structure 11
1.2.1 Lightweight Structure 11
1.2.2 Adaptive Truss Structures 13
1.2.3 Research Opportunities: Adaptive Lightweight Structures 14
1.3 Compliant Mechanism – a Bending-dominated Structure 15
1.3.1 Compliant Mechanism 15
1.3.2 Research Opportunities: Multi-degree-of-freedom Deformation and Nonlinearity Analysis, Multiple-objective Design 16
1.4 Research Question, Hypothesis, Validation, and Contributions 17
1.4.1 Research Question and Hypothesis 18
1.4.2 Research Contributions 20
1.4.3 Applications 21
1.5 Validation Strategy and an Overview of this Dissertation 24
CHAPTER 2 FOUNDATIONS OF UNIT TRUSS APPROACH FOR ADAPTIVE CELLULAR STRUCTURES 30
2.1 Classifications of Cellular Structures 32
2.2 Uniform Cellular Structures and Adaptive Cellular Structures 33
2.2.1 Uniform Truss vs. Conformal Truss 34
2.2.2 Optimized Truss vs. Non-optimized Truss 38
2.3 Recent Developments in Structural Optimization for Adaptive Structures 39
2.3.1 Ground Truss Approach – Discrete Structural Optimization 40
2.3.2 Homogenization Method – a Continuum Structural Optimization 42
2.4 Research Issues and Possible Solutions 48
2.4.1 Research Issue 1: Representation 49
2.4.2 Research Issue 2: Mechanical Analysis 52
2.4.3 Research Issue 3: Manufacturing 56
2.4.4 Research Issue 4: Design Synthesis 58
2.4.5 Connections between Research Issues 59
2.5 Overview of Cellular Structure Design Process 60
2.6 Chapter Summary 61
CHAPTER 3 GEOMETRIC MODELING FOR CREATING CONFORMAL TOPOLOGY FOR ADAPTIVE CELLULAR STRUCTURE 63
3.1 Topology and Microstructures of Conformal Cellular Structures 64
3.2 An Overview of Parametric Modeling Approach for Conformal Topology 67

3.3 Creating Topology with Parametric Modeling 70
3.3.1 NURBS - Nonuniform Rational B-Spline 70
3.3.2 Creating a 2-D Truss Topology 73
3.3.3 Creating a 3-D Truss Topology 76
3.3.4 Forming The Approximating NURBS Surface and Creating Thin Skin for Lightweight Truss Structure 79
3.3.5 Implementation of Parametric NURBS Modeling for Creating Topology ...81
3.4 Creating Topology from FEM Mesh as Supplemental Method 86
3.4.1 Overview of Meshing Approach for Creating Initial Truss Topology 86
3.4.2 Approach to Create Topology Using FEM Mesh 88
3.5 A Comparison Between Parametric Modeling And Meshing Approaches 93
3.6 Chapter Summary....95
CHAPTER 4 MECHANICS ANALYSIS OF CELLULAR STRUCTURE WITH UNIT TRUSS APPROACH 98
4.1 Overview of Mechanics Analysis 99
4.2 Constitutive Equations of Unit Truss 101
4.2.1 Mechanics Model of 2-D Unit Truss 102
4.2.2 Mechanics Model of 3-D Unit Truss 107
4.3 Adjusting Stiffness of Unit Truss with FEM 114
4.4 Consideration of Nonlinearity....118
4.4.1 Geometric Nonlinearity and Material Nonlinearity 119
4.4.2 Tangent Stiffness Method for Nonlinearity Analysis of Cellular Structures 120
4.5 Failure Mode in Cellular Structures 125
4.5.1 Failure Modes in Lightweight Truss Structures: Yielding and Buckling....125
4.5.2 Failure Mode in Compliant Mechanism: Yielding....128
4.6 Analysis of System Using Unit Truss as Elements 128
4.6.1 Analysis of System Using Unit Truss as Elements 129
4.6.2 Implementation of Unit Truss Approach....131
4.7 Test Examples 133
4.8 Chapter Summary....137
CHAPTER 5 DESIGN SYNTHESIS OF CELLULAR STRUCTURES....139
5.1 Analysis of Problem Characteristics....139
5.1.1 A General Problem Formulation of Structural Design Synthesis Involving FEM 140
5.1.2 Design Variables....142
5.1.3 Objective functions 142
5.1.4 Design Constraints 146
5.2 Problem Formulation of Design for Rigidity and Flexibility 150
5.3 Identifying Search Algorithm for Design Synthesis 153
5.3.1 Selecting Search Algorithm 153
5.3.2 Particle Swarm Optimization 157
5.4 Constraint Consideration and System Integration Using PSO as the Search Algorithm 160
5.4.1 Penalties And Composite Exponential Barrier Functions 161
5.4.2 Considering Constraints Using Barrier Functions....164
5.4.3 Implementation in MATLAB 167
5.5 Validation Example 170
5.6 Chapter Summary....173
CHAPTER 6 A HYBRID METHOD FOR GEOMETRIC MODELING OF CELLULAR STRUCTURES 175

6.1 Overview of Geometric Modeling for Conformal Structures 176
6.2 Microstructures and Unit Truss....179
6.2.1 Topology and Microstructures....179
6.2.2 Using Unit Truss as the Microstructure....180
6.3 Directly Creating STL Model Using Hybrid Geometric Modeling....182
6.3.1 Create Solid Model of Unit Truss....182
6.3.2 Remove End Faces and Obtain STL Model of Unit Truss....184
6.3.3 Stacking Unit Trusses into the Entire Truss....185
6.4 Implementation of Hybrid Geometric Modeling and its Efficiency Analysis....185
6.5 Chapter Summary....190
CHAPTER 7 MANUFACTURING OF CELLULAR STRUCTURES....192
7.1 Overview of Cellular Structure Fabrication....194
7.1.1 Challenges of Manufacturing....194
7.1.2 Popular Manufacturing Processes for Periodic Cellular Structures....195
7.1.3 Additive Fabrication....199
7.2 Manufacturing Cellular Structure with Stereolithography Process....200
7.2.1 Identify Manufacturability and Formulate Manufacturing Rules....200
7.2.2 Considering Manufacturing Limitations at the Design Stage....206
7.3 Manufacturing Cellular Structure with Other State-of-the-art Additive Fabrication Processes....207
7.4 Chapter Summary....208
CHAPTER 8 GRADED CELLULAR STRUCTURE FOR ENHANCED STABILITY ON IMPLANT-BONE INTERFACE IN UNCEMENTED PROSTHESIS – A NEW ACETABULAR IMPLANT WITH GRADIENT POROSITY FOR HIP REPLACEMENT....210
8.1 An Overview of Implant Fixation in Hip Replacement....210
8.1.1 Fundamentals of Hip Replacement....211
8.1.2 Biologic Fixation with Porous Coating....212
8.1.3 Major Failures of Prosthesis....214
8.2 Using Graded Cellular Structure in Prosthesis for Enhanced Stability....215
8.2.1 Potential Advantages of Using Cellular Structure in Prosthesis....215
8.2.2 Formulating Design Requirements for Acetabular Component....216
8.2.3 Designing Acetabular Component with Cellular Structure....219
8.3 Critically Evaluating New Hip Prosthesis....231
8.4 Chapter Summary....233
CHAPTER 9 DESIGN SYNTHESIS OF COMPLIANT CELLULAR STRUCTURE FOR MORPHING WINGS....234
9.1 An Overview of Morphing Wings Technology....234
9.2 Morphing Wing for AAI's Shadow UAV....236
9.3 Preparing Design Synthesis of Compliant Mechanism for Variform Wing Concept....240
9.3.1 An Overview of Design Constraints and Objectives....240
9.3.2 Create Initial Topology for Design Synthesis....241
9.4 Problem Formulation of Design Synthesis....243
9.4.1 Design Variables....243
9.4.2 Design Objectives....244
9.4.3 Problem Formulation....246
9.5 Design Synthesis....246
9.5.1 Trials with Different Load Conditions....247
9.5.2 Design Synthesis Process....249
9.5.3 Refining Load Condition....251
9.6 Critically Evaluating the New Morphing Airfoil....253

9.6.1 Robustness Analysis 253
9.6.2 Nonlinear Deformation....254
9.7 Chapter Summary....255
CHAPTER 10 Closure 257
10.1 A Summary of this Dissertation....257
10.2 Answering the Research Question and Validating the Research Hypothesis 258
10.2.1 Theoretical Structural Validation and Empirical Structural Validation 259
10.2.2 Empirical Performance Validation 262
10.2.3 Theoretical Performance Validation 264
10.3 Contributions....265
10.4 Limitations and Future Work....266
REFERENCES 268
VITA....278

LIST OF TABLES

Table 2-1 Performance Improvement of Truss Structure with Size Optimization 38
Table 2-2 Typical Methods Available for Structural Synthesis 39
Table 3-1 Comparing Parametric Modeling Approach and Meshing Approach.....95
Table 4-1 Critical Slenderness Ratio and Critical Aspect Ratio 128
Table 4-2 Horizontal Deflection of N_5 in The Test Example for Linear Analysis and Nonlinear Analysis.....135
Table 4-3 Analysis Results from Unit Truss Approach and MASTAN2.....136
Table 5-1 Selecting Search Algorithms for Design Synthesis of Cellular Structures.....156
Table 2 Time and Memory Consumption of Geometric Modeling for Truss Structures.187
Table 7-1 Major Manufacturing Parameters of SLA 3500 to Build Cellular Structures..200
Table 8-1 Material Properties of Titanium Alloy and Stainless Steel.....221
Table 9-1 Profile Coordinates of Airfoil NACA 23015 (Unit: mm).....238
Table 9-2 Profile Coordinates of Airfoil FX60-126 (Unit: mm).....238
Table 9-3 Objective Function of PSO Results 250
Table 9-4 Deviations between Actual and Target Deflections of Sampled Nodes 251

LIST OF FIGURES

Figure 1.1 Lightweight Human Skull 3
Figure 1.2 Compliant Human Epiglottis....3
Figure 1.3 Linear Cellular Alloy Parts for Heat Exchanger and Combustor Liner....5
Figure 1.4 3-D Adaptive Lightweight Structure 5
Figure 1.5 Compliant Mechanism: MEMS Amplifier by Kota et al. (Kota, Joo et al. 2001) 6
Figure 1.6 3-D Compliant Mechanism: Negative Poisson's Ratio....6
Figure 1.7 Configure Structure to Be Stretching-dominated or Bending-dominated via Topology Modification 8
Figure 1.8 Stretching-dominated 2-D Triangular Truss Structure 10
Figure 1.9 Stretching-dominated 3-D Octet Truss Structure....11
Figure 1.10 Uniform Truss Structures Made of Aluminum Alloy by Gibson 12
Figure 1.11 Sandwich Plates with Truss Core by Wicks and Hutchinson....13
Figure 1.12 Frontal Longitudinal Midsection of Femur Bone....14
Figure 1.13 Conformal and Optimized Truss Adaptive to Car Body Shape and Design Requirements 14
Figure 1.14 A Cantilever Beam under Geometric Nonlinear Deformation 17
Figure 1.15 Requirement List of the Method to Design Adaptive Cellular Structures....19
Figure 1.16 Definition of Unit Truss....20
Figure 1.17 Using Unit Truss to Support the Design of Conformal Cellular Structures ...20
Figure 1.18 Possible Application in Manufacturing: Robot Arm 22
Figure 1.19 Application in Automobile: Car Bumper....22
Figure 1.20 Application in Bio-medical Engineering: Spine Surgery Implant 23
Figure 1.21 Application in Aerospace Engineering: Aircraft with Flexible Wing....24
Figure 1.22 Validation Strategy in this Dissertation by Using Validation Square....26
Figure 1.23 A Dissertation Overview and Roadmap....29
Figure 2.1 Relationship between Chapter 2 and Validation Square....31
Figure 2.2 Relationship between Constructs and Unit Truss Approach....31
Figure 2.3 Classification of Cellular Metals 32
Figure 2.4 2-D Triangular Truss and its Unit Truss....35
Figure 2.5 2-D Conformal Triangular Truss Structure 36
Figure 2.6 2-D Conformal Triangular Truss Structure 37
Figure 2.7 A Gripper Design Problem (Frecker, Ananthasuresh et al. 1997) 42
Figure 2.8 Initial Ground Truss of Gripper (Frecker, Ananthasuresh et al. 1997)....42
Figure 2.9 Designed Compliant Mechanism Using Ground Truss Approach (Frecker, Ananthasuresh et al. 1997) 42
Figure 2.10 Microstructure Approach....44
Figure 2.11 Designed Compliant Mechanism Using Homogenization Method 46
Figure 2.12 An Array of 3-D Unit Trusses....50
Figure 2.13 Representation of Triangular Truss with Unit Truss....51
Figure 2.14 A Typical Unit Truss Model....54
Figure 2.15 Stress Graph of a Unit Truss 54
Figure 2.16 Connections Between Research Issues 60
Figure 2.17 Design Process of Cellular Structures....61
Figure 3.1 Relationship between Chapter 3 and Validation Square....64
Figure 3.2 Focus of Chapter 3 in the Design Process of Cellular Structures....65

Figure 3.3 A Conformal Triangular Truss....66
Figure 3.4 Octet Truss and Tetrahedron Microstructure....66
Figure 3.5 Kelvin Foam Truss and Truncated Octahedron Microstructure....66
Figure 3.6 A Uniform Truss Structure....67
Figure 3.7 Developing Truss Topology by Mapping....68
Figure 3.8 Triangular Truss Topology for a 2-D Area....73
Figure 3.9 Truss Topology for a 3-D Volume....77
Figure 3.10 Strut Topology between Layers....78
Figure 3.11 An Algorithm to Create Truss Topology....78
Figure 3.12 Inadequate Approximation Accuracy of NURBS Curve with 4 Interpolating Surface Points....80
Figure 3.13 Increasing the Approximation Accuracy with 7 Interpolating Surface Points 81
Figure 3.14 Replacing the Original Internal Curve with the NURBS Curve for Perfect Match....81
Figure 3.15 Using NURBS to Create Truss Topology....82
Figure 3.16 Implementation Flowchart of Using NURBS to Create Truss Topology....84
Figure 3.17 TrussCreator Software Developed to Create Truss Topology....84
Figure 3.18 Gap between Part surface and Created Interior Skin Surface (NURBS)....85
Figure 3.19 Stitching Part surface and Created Interior Skin Surface for Car Body....85
Figure 3.20 Truss Topology Created between Inner Skin Surface (NURBS) and Opposite Surface (NURBS) for Car Body....86
Figure 3.21 Using FEM Meshing Approach to Create Truss Topology....89
Figure 3.22 An Turbine Blade Example of Truss Topology Creation Using FEM Meshing Approach....89
Figure 3.23 Step (1) – Offsetting Original Part CAD Model by Skin Thickness for Turbine Blade Example....91
Figure 3.24 Step (2) –Subtracting Original Part CAD Model with Offset Model to Obtain Thin Skin for Turbine Blade Example....91
Figure 3.25 Sectioned View of the Resulting Thin Skin for Turbine Blade Example....92
Figure 3.26 Step (3) - Creating FEM Mesh for Turbine Blade Example....92
Figure 3.27 Step (4) - Converting FEM Mesh into Truss Topology for Turbine Blade Example....93
Figure 3.28 Created Truss Structure for Turbine Blade Example....93
Figure 4.1 Relationship between Chapter 4 and Validation Square....99
Figure 4.2 Focus of Chapter 4 in the Design Process of Cellular Structures....100
Figure 4.3 A Unit Truss Model with Five Struts....102
Figure 4.4 Stress Graph of A Unit Truss with Five Struts....102
Figure 4.5 A 2-D Strut With Primary and Secondary Variables (or Degree of Freedom) In Local Coordinate System....103
Figure 4.6 Strut Rotated from Local Coordinate System to Global Coordinate System 105
Figure 4.7 A 3-D Strut With Primary and Secondary Variables (or Degree of Freedom) In Local Coordinate System....109
Figure 4.8 3-D Strut Rotated from Local Coordinate System to Global Coordinate System....111
Figure 4.9 3-D Unit Truss of Octet Truss in Half Space....115
Figure 4.10 Finite Element Analysis on Unit Truss....117
Figure 4.11 Comparing Effective Elasticities from Simplified Analytical Analysis and Finite Element Analysis....117
Figure 4.12 A Cantilever Beam under Geometric Nonlinear Deformation....119
Figure 4.13 Material Nonlinearity of a Typical Plastic Material....120
Figure 4.14 Euler Method for Multiple Load Step Approach....124

Figure 4.15 Buckling of a Single Strut in Lightweight Truss Structure 126
Figure 4.16 Implementation Flowchart of Mechanics Analysis 132
Figure 4.17 2-D Structure with Five Struts 133
Figure 4.18 Deformed Shape of Test Example: Structure with Five Struts 134
Figure 4.19 Horizontal Deflection of N_5 in the Test Example for Linear Analysis and Nonlinear Analysis 135
Figure 4.20 Deformed Shape of Hexagon Truss with Struts Using Unit Truss Approach 136
Figure 4.21 Deformed Shape of Hexagon Truss with Struts Using MASTAN2 136
Figure 5.1 Relationship between Chapter 5 and Validation Square 140
Figure 5.2 Research Focus of Chapter 5 in the Design Process of Cellular Structures 141
Figure 5.3 An Abstract Compliant Mechanism 145
Figure 5.4 Problem Formulation of Lightweight Truss Structure Design 151
Figure 5.5 Problem Formulation of Compliant Mechanism Design 152
Figure 5.6 Trivial Elements: Dangling and Free Elements 153
Figure 5.7 Particle Swarm Optimization Simulating A-Life 158
Figure 5.8 Global Search and Local Search in PSO 160
Figure 5.9 Composite Exponential Barrier Function for 0-1 Jump 162
Figure 5.10 Composite Exponential Barrier Function for 1-0 Jump 163
Figure 5.11 Composite Exponential Barrier Function for 0-1-0 Jump 163
Figure 5.12 Constrained Design Problem of Lightweight Truss Structure after Using Penalties 166
Figure 5.13 Constrained Design Problem of Compliant Mechanism After Using Penalties 166
Figure 5.14 Validation Example for Design Synthesis 170
Figure 5.15 Result from Homogenization Method 171
Figure 5.16 Result from Unit Truss Approach with PSO 172
Figure 6.1 Relationship between Chapter 6 and Validation Square 176
Figure 6.2 Focus of Chapter 6 in the Design Process of Cellular Structures 177
Figure 6.3 An Example of Uniform Truss 178
Figure 6.4 An Example of Conformal Truss 178
Figure 6.5 Octet Truss and Tetrahedron Microstructure 180
Figure 6.6 Kelvin Foam Truss and Truncated Octahedron Microstructure 181
Figure 6.7 Geometry Variations at Strut Joints due to Strut Size and Orientation Changes 181
Figure 6.8 Unit Truss 181
Figure 6.9 Smoothening Joint by Adding Sphere to Central Node 183
Figure 6.10 Non-manifold Entities in Truss Structures 184
Figure 6.11 Add Sphere to Avoid Non-manifold geometry 184
Figure 6.12 Removing Ending Faces from Unit Truss 185
Figure 6.13 Stacking Unit Trusses into Entire Truss 186
Figure 6.14 Connection between Two Neighboring Unit Trusses 186
Figure 6.15 Test Samples 186
Figure 6.16 Test Result: Time vs. Strut Number 187
Figure 6.17 Test Result: Used Memory vs. Strut Number 189
Figure 6.18 Chainmail and Its Suggested Microstructure for Geometric Modeling 189
Figure 7.1 Relationship between Chapter 7 and Validation Square 192
Figure 7.2 Focus of Chapter 7 in the Design Process of Cellular Structures 193
Figure 7.3 Stretching-dominated 2-D Triangular Truss Structure 194
Figure 7.4 A Stochastic Cellular Material Manufacturing Process by Gas Injection 195
Figure 7.5 Manufacture Periodic 2-D Honeycombs by Crimping and Stamping 196

Figure 7.6 Manufacturing Linear Cellular Alloy by Extruding Slurry.....197
Figure 7.7 Geodesic Structure Fabricated Using SLS by Geodesic Inc. 198
Figure 7.8 3-D Truss Panel Fabricated Using FDM and Investment Casting 198
Figure 7.9 A Tetrahedral Lattice Structure Made by Rapid Prototyping Followed by Investment Casting.....198
Figure 7.10 Truss Structures with Various Shapes and Size without Support.....201
Figure 7.11 Specimens to Identify Minimum Manufacturable Strut Diameter of the Viper System.....202
Figure 7.12 Cellular Structures with a Maximum Strut Aspect Ratio 56.7 204
Figure 7.13 QuickCast Process to Fabricate Metal Parts and a Typical Rib Pattern 205
Figure 7.14 Rib Pattern for SLA QuickCast Prototype.....205
Figure 7.15 Shelled Pattern of Cellular Structure 206
Figure 7.16 Cellular Structure Manufactured with Selective Laser Melting.....207
Figure 8.1 Total Hip Replacement and Prosthesis Components 211
Figure 8.2 Cemented and Uncemented Metal-Bone Interface in Prosthesis.....212
Figure 8.3 Porous Surfaces Available for Biologic Ingrowth.....213
Figure 8.4 New Bone Ingrowth into Porous Tantalum Acetabular Cup Retrieved Two Years after Surgery because of Recurrent Dislocation 214
Figure 8.5 New Hip Prosthesis Using a Single-Piece Acetabular Component of Cellular Structure for Enhanced Stability.....217
Figure 8.6 Requirement List of Designing Acetabular Component for Enhanced Stability 218
Figure 8.7 Effective Elasticity 223
Figure 8.8 Unit Truss in Representative Volume.....223
Figure 8.9 Porosity Decreases as Diameter Increases 225
Figure 8.10 Surface/Material Volume Ratio Decreases as Diameter Increases.....225
Figure 8.11 Pore Size of Octet Truss.....227
Figure 8.12 Geometric Specification of Graded Cellular Structure 227
Figure 8.13 Creating Conformal Truss Topology for Cellular Section.....228
Figure 8.14 A Cross-Section View of the STL Model of the New Acetabular Component with Graded Cellular Structure 228
Figure 8.15 Look-through View of the Graded Cellular Section 229
Figure 8.16 Definition of Acetabulum Anatomic Regions 230
Figure 8.17 Mechanics Analysis on 1/12 of the New Acetabular Component 230
Figure 8.18 Critical evaluation on the designed acetabular component 232
Figure 9.1 Relation between Airfoil Geometry and Performance.....235
Figure 9.2 Double Slotted Flap and Slat Airfoil (Kroo 2005).....235
Figure 9.3 AAI's Shadow 400 UAV System (2005).....236
Figure 9.4 Airfoil Morphing from NACA 23015 to FX60-126 237
Figure 9.5 Possible Fuel Bladder Configurations (Gano and Renaud 2002) 239
Figure 9.6 Known Boundary Condition and Sampling Points for Design Synthesis 241
Figure 9.7 CAD Model of NACA 23015 Airfoil Profile.....241
Figure 9.8 Meshing Profile Geometry in ANSYS 242
Figure 9.9 Initial Topology for Design Synthesis.....242
Figure 9.10 Problem Formulation of Compliant Mechanism for Variform Wing.....246
Figure 9.11 Deformed Structure with 1 Concentrated Torsion before Synthesis.....247
Figure 9.12 Deformed Structure with 1 Concentrated Torsion after Synthesis.....248
Figure 9.13 Deformed Structure with 3 Concentrated Forces before Synthesis.....248
Figure 9.14 Deformed Structure with 3 Concentrated Forces after Synthesis.....248
Figure 9.15 Deformed Structure with 5 Pairs of Opposite Forces before Synthesis 249
Figure 9.16 Deformed Structure with 5 Pairs of Opposite Forces after Synthesis.....249

Figure 9.17 Parameter Setting for Design Synthesis 250
Figure 9.18 Cleaning Topology by Removing Zero-width Struts 251
Figure 9.19 Problem Formulation of Searching for Appropriate Magnitudes of Paired Forces 252
Figure 9.20 Objective Function Changes against Load Condition Variations 253
Figure 9.21 Objective Function Changes against Width Variations of Thin Struts 254
Figure 9.22 Objective Function Changes against Width Variations of Thick Struts 254
Figure 9.23 Variations under Nonlinear Deformation 255
Figure 10.1 Test Theoretical Structural Validity by Literature Review and Critical Thinking 259
Figure 10.2 Test Theoretical Structural Validity and Empirical Structural Validity with Method Constructs and Example Problems in the Context of Validation Square ... 260
Figure 10.3 Test Empirical Performance Validity by using Example Problems in the Context of Validation Square 263

LIST OF SYMBOLS

Chapter 1

$\bar{r}$	Relative material density of a foam
b	The number of struts in a pin-jointed truss structure
j	The number of joints in a pin-jointed truss structure
t_f	Face sheet thickness of a sandwiched truss
H_c	Core thickness of a sandwiched truss
$d\,y_{\max}$	Maximum deflection of a cantilever beam
L	Length of a cantilever beam
h	Height of the rectangular cross-section of a cantilever beam
b	Width of the rectangular cross-section of a cantilever beam
P	External vertical load at the end of a cantilever beam

Chapter 2

F	Uniform force on the end face of a 2-D unit truss
q	Rotation angle of a 2-D unit truss around z axis
F_x	Equivalent force in x direction on a 2-D unit truss
F_y	Equivalent force in y direction on a 2-D unit truss
$a^{(i)}$	Cross-sectional area of the i^{th} bar in the ground truss
$l^{(i)}$	Length of the i^{th} bar in the ground truss
$E^{(i)}$	Young's modulus of the i^{th} bar in the ground truss
$v^{(i)} = a^{(i)} l^{(i)}$	Material volume of the i^{th} bar in the ground truss
$V = \sum_{i=1}^{m} v^{(i)}$	Total volume of the ground truss

$\underset{\sim}{u}$	Nodal displacement of the ground truss
$\underset{\sim}{B}$	Compatibility tensor of the ground truss
$\underset{\sim}{q}$	Axial force in a strut member of the ground truss
$\underset{\sim}{p}$	Noda force of a ground truss
$\underset{\sim}{b}^{(i)}$	The i^{th} column of compatibility tensor $\underset{\sim}{B}$ in the ground truss
$\underset{\sim}{K}^{(i)}$	Stiffness tensor of the i^{th} bar in the ground truss
r	Material density function in homogenization method
Ω	Design domain in homogenization method
Ω^m	Subdomain
Γ	Boundary of the design domain Ω in homogenization method
Γ_s	Traction boundary of the design domain in homogenization method
Γ_u	Displacement boundary of the design domain in homogenization method
$\underset{\sim}{t}$	Boundary traction on the traction boundary
$\underset{\sim}{b}$	Body force
$\underset{\sim}{u}$	Field displacements over the domain Ω
$\underset{\sim}{\tilde{E}}$	Optimal elasticity tensor over the domain Ω of statically admissible stress field
$\underset{\sim}{E}$	Elasticity tensor of a subdomain
$\underset{\sim}{E}_{ad}$	Elasticity of admissible stress field
$W_{ex}(\underset{\sim}{u})$	External work
$W_{in}(\underset{\sim}{u})$	Internal work
$dW_{ex}(\underset{\sim}{u})$	Virtual external work

$dW_{in}(\underset{\sim}{u})$	Virtual internal work
$\underset{\sim}{e}(\underset{\sim}{u})$	Linearized strain
$M_{\max}$	Maximum material mass
a , b	Sizes of rectangular microstructure
q	Orientation angle of rectangular microstructure
x_e	Design variables, material density of a microstructure e in homogenization method
$\underset{\sim}{x}$	Vector of the design variables x_e in homogenization method
k_e	Effective stiffness corresponding to density x_e of a microstructure
k_s	Stiffness of solid material for a microstructure
p	Penalization power in the power law of homogenization method
$\underset{\sim}{s}$	Stress tensor
$\underset{\sim}{C}$	Compliance tensor
C_{ijkl}	Component in compliant tensor $\underset{\sim}{C}$
E_{ijkl}	Component in compliant tensor $\underset{\sim}{E}$
R^2	2-D space
R^3	3-D space
$\underset{\sim}{f}^{(i)}$	External forces acting on the node and the end point of the i^{th} element of a unit truss in R^3.
$\underset{\sim}{u}^{(i)}$	Nodal displacement of the end point of the i^{th} element of a unit truss in R^3.
$\left[\underset{\sim}{\Psi}^{(m)}\right]$	The stiffness tensor of the m^{th} unit truss
$\left[\underset{\sim}{K}^{(i)}\right]$	Stiffness matrix $\left[\underset{\sim}{K}^{(i)}\right]$ of the i^{th} element
Φ_{11}^i, Φ_{12}^i, Φ_{21}^i, Φ_{22}^i	3×3 subsets of the 6×6 stiffness matrix $\left[\underset{\sim}{K}^{(i)}\right]$ of the i^{th} element

$\underset{\sim}{U}^{(m)}$	Nodal displacement tensor of the m^{th} unit truss
$\underset{\sim}{F}^{(m)}$	Nodal force tensor of the m^{th} unit truss
$\underset{\sim}{E}^{m}$	Elasticity tensor of the m^{th} unit truss
$\underset{\sim}{\tilde{E}}^{(m)}$	Elasticity tensor of the m^{th} unit truss after correction
$\underset{\sim}{a}^{(m)}$, $\underset{\sim}{R}^{(m)}$	Correction coefficients for elasticity correction

Chapter 3

p_{ij}	Control points of a NURB surface
h_{ij}	Weights to pull the NURBS toward the corresponding control points
$N_{i,k}(u), N_{j,k}(w)$	Basis functions for B-Spline
u, w	Parameters for a NURBS surface
$p(u,w)$	Point on a NURBS surface with parameters u, w
t_i	Knot values or a set of knot vector
k	Order of a parametric curve
B_{ij}	Control vertices of a NURBS surface
M_B	Bicubic NURBS basis transformation matrix
P	Matrix containing the surface points measured from the part surface
Δu , Δw	Primitive spacings in parametric space
U , W	Numbers of primitives in the *u* and *w* directions
V_{ij}	Truss vertex in the i^{th} row and the j^{th} column of truss vertices in 2-D
$p(V_{ij})$	Coordinate vector of vertex V_{ij}
$V_{i,j,k}$	Truss vertex in the i^{th} row and the j^{th} column and the k^{th} layer of truss vertices in 2-D
t	Part skin thickness
r	Radius of truss vertices

e	Surface approximation error

Chapter 4

$\underset{\sim}{C}$	Linear stiffness tensor
$\underset{\sim}{s}$	Infinitesimal stress tensor
$\underset{\sim}{e}$	Infinitesimal Lagrangian strain tensor
$\underset{\sim}{f}^{(i)}$	External force acting on the node and the end point of the i^{th} element of a unit truss in the global coordinate system
$\underset{\sim}{u}^{(i)}$	Nodal displacement of the end point of the i^{th} element of a unit truss in the global coordinate system
$\underset{\sim}{K}^{(i)}$	Stiffness matrix of the i^{th} strut of a unit truss in the global coordinate system
$\underset{\sim}{\overline{f}}^{(i)}$	External forces acting on the node and the end point of the i^{th} element of a unit truss in the local coordinate system
$\underset{\sim}{\overline{u}}^{(i)}$	Nodal displacement of the end point of the i^{th} element of a unit truss in the local coordinate system
$\underset{\sim}{\overline{K}}^{(i)}$	Stiffness matrix of the i^{th} strut of a unit truss in the local coordinate system
E	Young's modulus of solid material of the i^{th} beam
I	Inertia of the i^{th} beam along axis perpendicular to the plane
L	Length of the i^{th} beam
A	Cross-section area of the i^{th} beam
$\underset{\sim}{T}^{(i)}$	Transformation tensor representing the rotation of the coordinate system around y axis
$\Phi_{11}^{(i)}$, $\Phi_{12}^{(i)}$, $\Phi_{21}^{(i)}$, $\Phi_{22}^{(i)}$	Four sub-matrices in the global stiffness matrix $\underset{\sim}{K}^{(i)}$
$\underset{\sim}{K}^{e}$	Entire stiffness tensor of a unit truss
$\underset{\sim}{U}^{e}$	Nodal displacement vector of a unit truss
$\underset{\sim}{F}^{e}$	Nodal force vector of a unit truss

$\tilde{\underset{\sim}{K}}^{e}$	Entire stiffness tensor of a unit truss after correction
$\underset{\sim}{a}^{e}$, $\underset{\sim}{R}^{e}$	Correction coefficients for stiffness tensor
$W_{in}^{e}(\underset{\sim}{U}^{e})$	Energy bilinear form for internal work of a unit truss
Ω^{e}	Domain of strain field
$d\,y_{\max}$	Maximum deflection at the right end of cantilever beam
L	Length of cantilever beam
h , b	Height, width of rectangular cross-section of a cantilever beam
P	Vertical force at the end of a cantilever beam
s	Stress
s_{pl}	Proportional limit of stress-strain curve
s_{y}	Yield strength
$\underset{\sim}{L}_{x_0}(\underset{\sim}{y}) = \underset{\sim}{0}$	Linearization of the equations $\underset{\sim}{f}(\underset{\sim}{x}) = \underset{\sim}{0}$ about $\underset{\sim}{x}_0$
$d\underset{\sim}{U}$	Incremental nodal displacements
$d\underset{\sim}{F}$,	Incremental nodal forces
$\underset{\sim}{K}_t$, $\underset{\sim}{K}_t^{(i)}$	Tangent Stiffness and that for the i^{th} strut
$\underset{\sim}{K}_e$, $\underset{\sim}{K}_e^{(i)}$	Linear elastic stiffness and that for the i^{th} strut
$\underset{\sim}{K}_g$, $\underset{\sim}{K}_g^{(i)}$	Nonlinear geometric stiffness and that for the i^{th} strut
$\underset{\sim}{K}_t^{e}$	Tangent stiffness of a unit truss
$d\underset{\sim}{U}^{e}$	Incremental displacements in a unit truss
$d\underset{\sim}{F}^{e}$	Incremental forces in a unit truss
F_{x_2}	Axial force at the 2nd node in a strut
dW_{in}^{e}	Incremental energy of a unit truss
r	Radius of a cylindrical strut

P_{cr}	Critical compressional force to incur buckling
P_y	Yield force to incur strut yield
SR	Slenderness ratio of a strut
I	Area moment of cross-section
L_e	Effective length of a strut for buckling
K	Effective length factor
$\underset{\sim}{u}^{(m)}\|_{\Omega_e}$	Displacement vector of the m^{th} node in element Ω_e
$\underset{\sim}{f}^{(m)}\|_{\Omega_e}$	Force vector of the m^{th} node in element Ω_e
$[\underset{\sim}{K}]$	Stiffness matrix of the whole structural system
$[\underset{\sim}{U}]$	Nodal displacement vector of the whole structural system
$[\underset{\sim}{F}]$	Nodal load vector of the whole structural system

Chapter 5

$\{x\}$, $\{x_1, x_2, \ldots, x_n\}$	Design variables, e. g. strut diameters
$f_i(x)$	Design objective
$h_i(x) = 0$	Equality constraints
$g_i(x) \le 0$	Inequality constraints
$U = U(x)$	Nodal displacement vector as implicit functions of design variables $\{x\}$
$K(x)$	Stiffness of the structure
$F(x)$	Nodal load vector
$K(x)$	Stiffness of the structure
e	Strain under applied load
E	Stiffness
SE	Strain energy

$W_{external}(u)$	
p	Body force on domain Ω
t	Traction on traction boundary Γ_T
MSE	Mutual potential energy
$\frac{SE}{MSE}$	Ratio between mutual potential energy and strain energy
MSD	Mean squared deviation
$P_{\text{actual},i}$	Actual position of the i^{th} sampled point of the deformed structure
$P_{\text{desired},i}$	Desired position of the i^{th} sampled point of the deformed structure
MSD_w	Weighted mean squared deviation
w_i	Weight of the i^{th} sampled point of the deformed structure
$AR_{\max}$	Maximum manufacturable aspect ratio of a strut
$x_{\min}$	Minimum manufacture strut diameter
L_i	Length of the i^{th} strut
$A(x_i)$	Cross-section area of the i^{th} strut
$V_{\max}$	The maximum allowed total material volume
s_{axial}	Axial stress contributed from the axial force F_{axial}
$s_{flexure}$	Flexure stress contributed from the bending moment
s_y	Yield strength
F_{axial}	Axial force
w_1 , w_2	Weights to balance the importance between the normalized mean squared deviation and the normalized material volume in objective function $f(x)$
MSD_{norm}	Normalized mean squared deviation
V_{norm}	Normalized total volume

X_i	Position of the i^{th} particle in Particle Swarm Optimization
V_i	Moving velocity of the i^{th} particle in Particle Swarm Optimization
D	Number of design variables
P_i	Previous position of the i^{th} particle in Particle Swarm Optimization
P_g	The best particle position among all the particles
j_1, j_2	Learning factors in Particle Swarm Optimization
w	Inertia weight in Particle Swarm Optimization
R	Penalty parameter in penalty function
$P(x,R)$	Penalty function
k	Parameter for the jump slope in "Composite Exponential" penalty
s_i	The maximum stress in the i^{th} element or strut.
f_{goal}	The target value of the objective function
e_{obj}	The tolerance of objective function
e_{var}	tolerance of design variables

Chapter 6

STL_{all}	STL model for the entire structure
$ACIS_i$	Solid model of the i^{th} unit truss
$FACE_{i,j}$	End face of the j^{th} strut of the i^{th} unit truss
STL_i	STL model of the i^{th} unit truss

Chapter 7

$x_{mfg_{\min}}$	Minimum manufacturable strut size

Chapter 8

E_0	Elasticity in boundary area interfacing with spongy bone

E_s	Elasticity of solid titanium
F	Uniform axial force at end face of a unit truss
F_x, F_y, F_z	Equivalent force in x, y, z directions on a unit truss
d_x, d_y, d_z	Displacement in x, y, z directions on a unit truss
F_x, F_y, F_z	Equivalent elasticity in x, y, z directions on a unit truss
E_{eff}	Average equivalent elasticity
L	Strut length in a unit truss
L_h	Half strut length in a unit truss
d	Diameter of a circular strut cross-section
A	Area of a circular strut cross-section
$\frac{d}{L_h}$	Ratio between strut diameter and half-strut length
SR	Slenderness ratio
SR_{cr}	Critical slenderness ratio for buckling
t_{inner}	Skin thickness of the liner section
L_p	Pore size in cellular structure (foam)
$L_{p_{\max}}$	The largest opening size of a pore
R_1	Outer radius of liner section in hemispherical acetabular component
R_2	Inner radius of liner section in hemispherical acetabular component
R_0	Inner radius of cellular section in hemispherical acetabular component

Chapter 8

P_0, P_1	The most left and right points of the morphing wing example
N_i	The i^{th} node of a structure
x_i	Diameter of the i^{th} strut as design variable

x_{0^+}	Lower bound of design variable
$x_{\max}$	Upper bound of design variable
$d_{k_{\text{target}}}$	Desired deflection on node N_k
$d_{k_{\text{actual}}}$	Actual deflection on node N_k
SD_k	Squared deviation of actual deflection from desire deflection on node N_k
$(\text{mean}(SD_k))_{norm}$	Normalized mean squared deviation of all nodes
V_{norm}	Normalized total volume
w_d , w_v	Weights for normalized mean squared deviation and normalized volume in objective function
$f(x)$	Objective function
F_{pi}	The i^{th} paired forces

SUMMARY

Cellular structures are present from the atomic level all the way up to patterns found in human skeleton. They are prevailing structures in the nature and known for their excellent mechanical, thermal and acoustic properties. Two typical types of cellular structures, lightweight structures and compliant mechanisms, are investigated. Lightweight structures are rigid and designed to reduce weight, while increasing strength and stiffness. Compliant mechanisms are designed to transform motions and forces. Most available artificial lightweight structures are patterns of primitives. However, the performance of lightweight structures can be enhanced by using adaptive cellular structures with conformal strut orientations and sizes, like the trabeculae in femoral bone. Bending, torsion, and nonlinear behaviors of compliant mechanisms have not been sufficiently studied.

In order to design adaptive cellular structures, a new unit cell, the unit truss is proposed. The unit truss approach facilitates the design of adaptive cellular structures for enhanced mechanical properties via geometric modeling, finite element analysis, geometry optimization, and additive fabrication. Four research issues, which address representation, structural analysis, design synthesis, and manufacturing respectively, are raised and solved. Unit truss enables representation and mechanics analysis for adaptive cellular structures. A synthesis method using engineering optimization algorithms is developed to systematically design adaptive cellular structure. Two examples, graded cellular structure for prosthesis and compliant mechanism for morphing wings, are studied to test the unit truss approach.

CHAPTER 1

CELLULAR STRUCTURES: LIGHTWEIGHT STRUCTURE AND COMPLIANT MECHANISM

In this chapter, the natural occurrences and biomimicry of cellular structures, including lightweight structure and complaint mechanism, are discussed as well as their characteristics. Then, the author presents the research status, and identifies the research opportunities. The research question is raised and the hypothesis is proposed. The research contributions and possible applications are discussed. Finally, an overview of this dissertation and a validation strategy are given.

1.1 Cellular Structures from Natural Occurrence to Engineering Applications

This section presents the natural occurrences of cellular structures. Lightweight truss structures and compliant mechanisms are two typical cellular structures. The natural occurrences of lightweight structures and compliant mechanisms inspired the design of artificial adaptive cellular structures for engineering applications. Then, the major characteristics of lightweight structures and compliant mechanisms are presented.

1.1.1 Natural Occurrences

The inspiration for the idea of creating lightweight structures and complaint mechanisms comes from natural occurrences in living organisms, such as bones, honeycombs, cartilages, and living cells. Living organisms efficiently distribute materials to achieve high strength as lightweight structures or enhanced flexibility as compliant

mechanisms. Lightweight structures (e.g. bone) are rigid with a rather small weight relative to the applied load (Gibson and Ashby 1997; Deshpande, Fleck et al. 2001; Deshpande, Fleck et al. 2001; Wang and McDowell 2003; Xue and Hutchinson 2003; Wicks and Hutchinson 2004). Compliant mechanisms (e.g. cartilage) are flexible to transform motion, force, or energy by elastic deformation as opposed to traditional mechanisms consisting of rigid links (Midha, Norton et al. 1994; Howell 2001; Kota, Joo et al. 2001).

In recent years there has been new investigation into the mechanical structures in biology ranging from the atomic level all the way up to the patterns found in human skeletons. Biomimicry is being investigated as an emerging field, which creates breakthrough advances in material, device, and manufacturing process design. Flat bones in human skeleton, such as rib and skull bones, are sandwiched cellular structures consisting of a layer of spongy bone and two thin sandwiching layers of compact bone (Marieb, Mallatt et al. 2004). An example is human skull shown in Figure 1.1. Spongy bone is a lightweight cellular structure, which is made up of a mesh of needle-like pieces of bone with large voids between them. Compact bone is dense and forms the outer layer of all human bones. Spongy bone distributes and balances tension and compression to support external load efficiently and economically. Those cellular structures can sustain large impacts by involving neighboring elements and absorbing energy efficiently. The nature appreciates cellular structures because they are light, strong, stiff, and suited for multiple functionalities.

Human epiglottis shown in Figure 1.2 is made of flexible cartilage (Marieb, Mallatt et al. 2004). Cartilage is a compliant mechanism with certain rigidity. It changes shape when the surrounding muscles apply loads on it. The entire skeletons of sharks and rays are made of cartilages (Harris). These cartilages are strong, flexible, and light. They are

sturdy like bones, but have a much lower density. So, sharks and rays do not need bladder like other fishes. Such living organisms as cartilage possess both a high degree of moving freedom and the ability to manipulate that freedom, and thus are able to carry out diverse and soft movements as opposed to rigid links. These prevailing compliant mechanisms in the nature are sophisticated in terms of design and performance.

Figure 1.1 Lightweight Human Skull

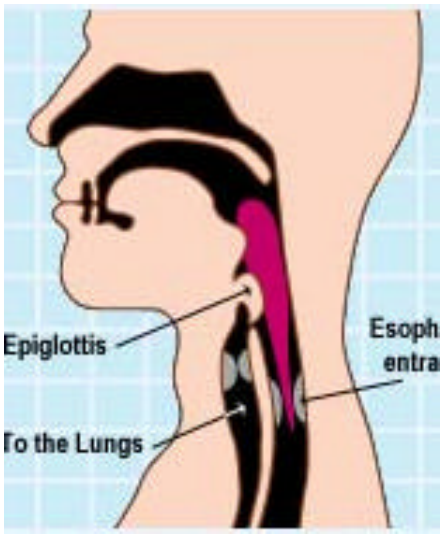

Figure 1.2 Compliant Human Epiglottis

Living cells use “geodesic architecture to organize their molecular scaffolds into porous three-dimensional forms” that simultaneously provide high mechanical strength and enhanced flexibility (Ingber 1993; Bray). These scaffolds provide not only rigidity as lightweight structures, but also flexibility as compliant mechanism by mediating internal structural transformations that enable cells to move, change shape and grow (Ingber 1998). Most living organisms are either rigidity-dominated or flexibility-dominated. Scaffolds in living cells utilize both lightweight structures and complaint mechanisms for equally important functionalities, rigidity and flexibility.

1.1.2 Artificial Cellular Structures

Big portions of space in the scaffolds of living organisms, such as bones, and cartilage are empty. The voids in living organisms reduce weight, or create moving freedom. Natural occurrences of cellular structures inspired the design of artificial cellular structures via biomimicry. Researchers are particularly interested in two typical cellular structures, lightweight structure (rigid structure) and compliant mechanism (flexible structure). Lightweight structures are suited for multifunctional applications that demand not only light weight and high strength, but also excellent performances in energy absorption, heat transfer, thermal protection, or thermal insulation (Michell 1904; Wang and Rosen 2002; Gibson 2005). Compliant mechanisms are suited for sophisticated devices that generate certain compliances to transform motions and forces with few parts. Compliant mechanisms have less weight, wear, friction, and backlash due to fewer parts.

Accordingly, two typical problems of cellular structures are formulated, design for rigidity and design for flexibility. Toward design for rigidity, non-efficient material in lightweight structures is removed to achieve desired stiffness and strength with minimum

material usage. McDowell and his lightweight structure group designed linear cellular alloys for heat exchanger and combustor liner (McDowell 1998; Seepersad 2004). Linear cellular alloy as shown in Figure 1.3 is a 2-D lightweight cellular structure and designed for enhanced multifunctionalities. In Figure 1.4, the author shows a 3-D adaptive truss structure, whose shape is conformal to the part being filled and optimized for design requirements. Adaptive cellular structures achieve better performance by conformally orienting and adaptively sizing struts.

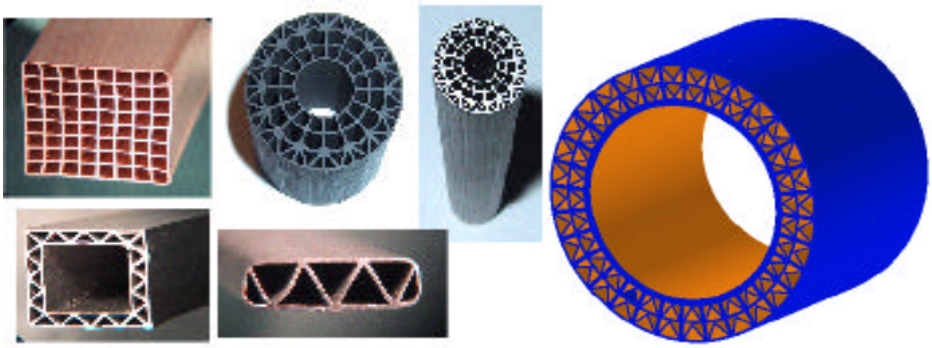

Figure 1.3 Linear Cellular Alloy Parts for Heat Exchanger and Combustor Liner

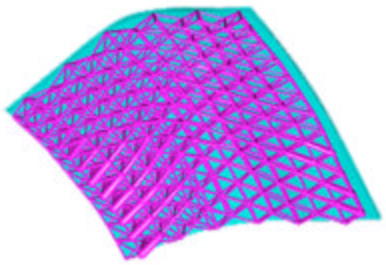

Figure 1.4 3-D Adaptive Lightweight Structure

In design for flexibility, material in structures is removed to generate moving freedom for desired compliances. A structure like this is called compliant mechanisms, which transform motion, force and energy through elastic deformation (Midha, Norton et al. 1994). A compliant mechanism consists of fewer components and products using compliant mechanisms can reduce or eliminate assembly requirements (Ananthasuresh,

Saggere et al. 1994). It has less weight, wear, friction, and backlash. It has no need for lubrication since its motion is based on deformation without inter-component sliding (Ananthasuresh and Kota 1995). Compliant mechanism can produce continuous shape changes (Ananthasuresh and Kota 1995). The built-in restore force can restore its shape to its original when the load is removed. Living organisms use their flexibility to convert motion, force, and energy. Via mimicry of living organisms, compliant mechanisms have been used to develop sophisticated devices or new material structures, such as micro-electro-mechanical-system shown in Figure 1.5 (Kota, Joo et al. 2001) and negative Poisson's-ratio material shown in Figure 1.6 (Larsen, Sigmund et al. 1997).

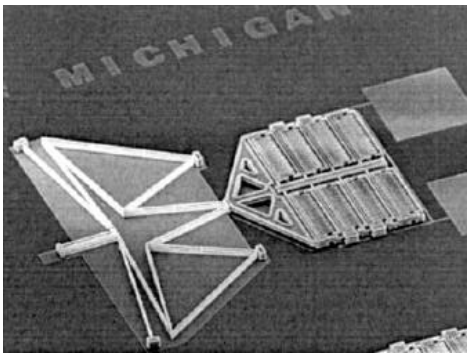

Figure 1.5 Compliant Mechanism: MEMS Amplifier by Kota et al. (Kota, Joo et al. 2001)

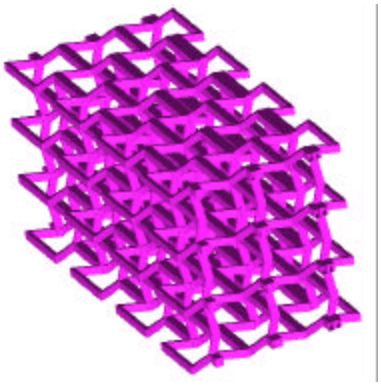

Figure 1.6 3-D Compliant Mechanism: Negative Poisson's Ratio

1.1.3 Stretching-dominated Structure vs. Bending-dominated Structure

Lightweight structures and compliant mechanisms distinguish themselves from each other by their major characteristics. Lightweight structures are stretching-dominated with their struts mainly enduring compression or tension. Compliant mechanisms are bending-dominated with a few struts undergoing significant bending or torsion. In this section, Maxwell's criterion is presented to help the design of cellular structures.

A cellular structure with either stretching-dominated or bending-dominated characteristics can significantly affect its stiffness and compliance. Gibson and Ashby demonstrated that the strength of metal and polymer foams scales as $\bar{r}^{1.5}$ when their cell (microstructure) walls are governed by bending (Gibson and Ashby 1997). $\bar{r}$ is the relative material density of foams compared with solid material. However, the strength of foams scales as $\bar{r}$ when their cell walls are governed by stretching. For $\bar{r} = 0.1$, a stretching-dominated structure is about three times as strong as a bending-dominated structure (Deshpande, Fleck et al. 2001).

Cellular structures can be configured as either stretching-dominated or bending-dominated. For example, triangular truss and four-bar mechanism with rigid joints shown in Figure 1.7 can be converted from each other by adding or removing the diagonal strut in the topology. Topology is the geometric configuration of structures, such as the strut connectivity in lightweight structures or compliant mechanisms.

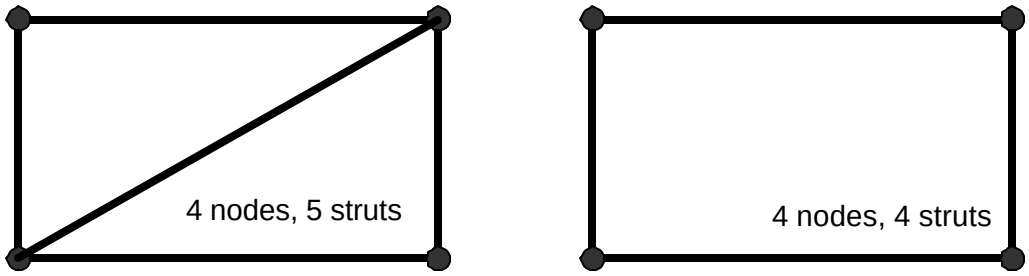

(a) Stretching-dominated triangular truss

(b) Bending-dominated four-bar mechanism with rigid joints

Figure 1.7 Configure Structure to Be Stretching-dominated or Bending-dominated via Topology Modification

In Figure 1.8, we show a stretching-dominated 2-D triangular truss, whose primitive is triangle. It is a uniform cellular structure with primitives patterned in the x and y directions. The exterior struts under external uniform pressure are modeled as beams since these struts must withstand bending moments resulting from the external pressure. All the nodes at the bottom are fixed in the y-axis direction, and the node N_1 is fixed in the x-axis direction. To demonstrate that this triangular truss is stretching-dominated, both beam (frame) element and link (truss) element are used to model the interior struts, and their stresses and deflections are compared. Link element can only withstand axial forces (compression or tension), but no bending moments. The composed structure of link elements is pin-jointed. Beam element can endure not only axial forces, but also bending moments. As shown in Figure 1.8, ANSYS was utilized to analyze stresses and deflections of a structure by using beam elements and by using link elements respectively. All struts are assumed to be under linear deformation. The maximum deflections of the structure are almost the same in both cases, and the maximum stresses differ only by 5.44%. Therefore, 2-D triangular trusses are stretching-dominated structures. Stretching-dominated structures can be stronger than traditional foam materials, which are mostly bending-dominated (Deshpande, Fleck et al. 2001). The failure in truss structures is mainly caused by the axial stress in struts, while the failure in

traditional foam materials is mainly caused by bending stress (Deshpande, Fleck et al. 2001). Axial stress is uniformly distributed on cross-section, while bending stress is non-uniformly distributed. Therefore, stretching-dominated truss structures have better strength to weight ratio. They can be a promising alternative to metal and polymer foams as new material structure (Deshpande, Fleck et al. 2001).

A pin-jointed structure consisting of b struts and j joints satisfying Maxwell's criterion shown in Equation 1.1 or Equation 1.2 is statically and kinematically determinate (Maxwell 1864).

2-D lightweight structure: $b = 2j - 3$ 1.1

3-D lightweight structure: $b = 3j - 6$ 1.2

Using Maxwell's criterion, Deshpande et al. derived that a sufficient condition for the deformation of a periodic structure to be stretching-dominated is that its unit cell (microstructure) consisting of b struts and j frictionless joints satisfies Maxwell's criterion for static determinacy shown in Equation 1.3 and Equation 1.4 (Deshpande, Fleck et al. 2001). A 2-D triangular truss shown in Figure 1.8 has triangle primitive (unit cell) with $b = 3$, $j = 3$, and $b - 2j + 3 = 0$. A 3-D octet truss shown in Figure 1.9 has tetrahedron primitive with $b = 6$, $j = 4$, and $b - 2j + 3 = 1$. Both triangle truss and octet truss are statically determinate and thus stretching-dominated.

2-D lightweight structure: $b - 2j + 3 \geq 0$ 1.3

3-D lightweight structure: $b - 3j + 6 \geq 0$ 1.4

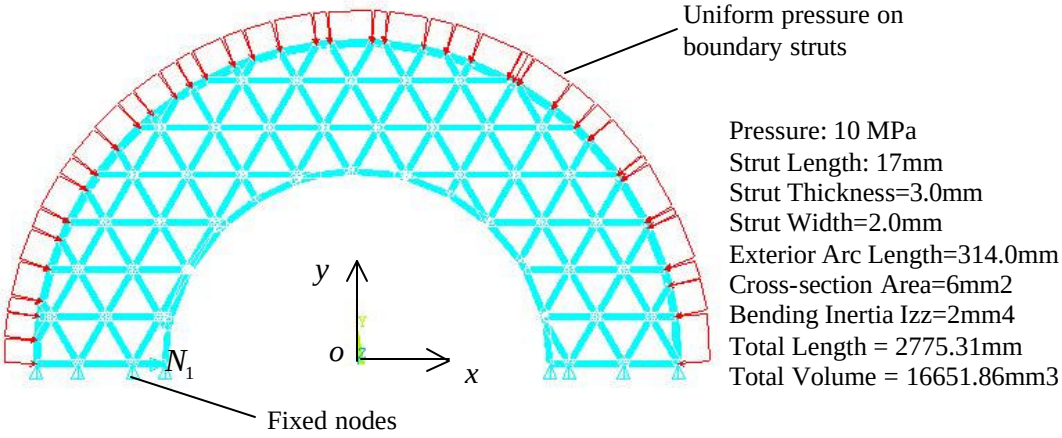

		Beam	Link	Difference
Uniform	Stress/MPa	58.664	62.038	5.44%
	Deflection/mm	26.035	25.911	-0.48%

Figure 1.8 Stretching-dominated 2-D Triangular Truss Structure

Removing struts can transform a stretching-dominated structure into a bending-dominated structure. When the numbers of struts and joints (rigid or pinned) in a structure satisfy Equations 1.5 or 1.6, the structure becomes a potential compliant mechanism. Equations 1.5 are 1.6 are the necessary conditions for an efficient compliant mechanism to convert motion, force and energy with less load. Boundary condition greatly affects degrees of freedom of a structure. Both strut connectivity and boundary condition determine whether a mechanism is compliant. The compliant mechanism shown in Figure 1.5 has $b=13$, $j=11$, and $b-2j+3=6$, and it is bending-dominated.

2-D compliant mechanism: $b-2j+3<0$ 1.5

3-D compliant mechanism: $b-3j+6<0$ 1.6

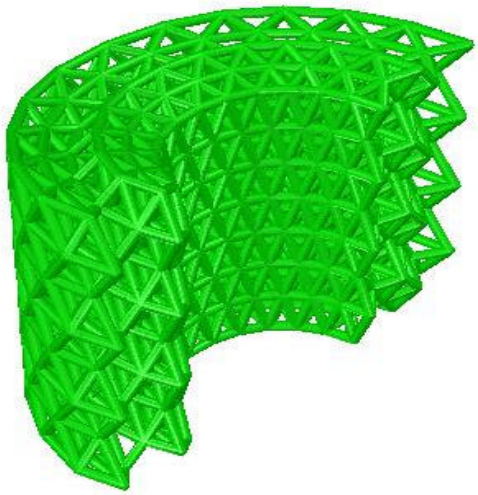

Figure 1.9 Stretching-dominated 3-D Octet Truss Structure

1.2 Lightweight Structure – a Stretching-dominated Structure

In this section, the author presents the research status of lightweight structure. It is followed by an introduction of adaptive truss structures, which have better performance than uniform lightweight structures. Then, the research opportunities of adaptive truss structures are discussed.

1.2.1 Lightweight Structure

Ashby, Gibson, Hutchinson, McDowell and their colleagues pioneered the research on the lightweight structures and focused on the topics about analysis, design, manufacturing, and applications (Gibson and Ashby 1997; Deshpande, Fleck et al. 2001; Deshpande, Fleck et al. 2001; Wang and McDowell 2003; Xue and Hutchinson 2003; Wicks and Hutchinson 2004). The benefits of designed cellular structures have been demonstrated for structural applications (stiffness/weight or strength/weight). However, most designs are uniform structures, which are just a pattern of primitives as shown in Figure 1.10. The truss geometries are not designed to be adaptive to original parts' shapes and design requirements. Polyhedra, such as tetrahedron and octahedron are

popular microstructures (unit cell) for analysis (Deshpande, Fleck et al. 2001; Deshpande, Fleck et al. 2001). However, the geometric overlaps and structural interactions between microstructures are over-simplified or neglected during analysis and their effective properties do not provide sufficient accuracy (Kanit, Forest et al. 2003). Therefore, it cannot guarantee the analysis accuracy of the entire cellular structure. Moreover, the developed mechanics model is suited to uniform cellular structures, not to non-uniform lightweight structures. Non-uniform lightweight structures include lightweight structures conformal to filled parts or adapted to design requirements.

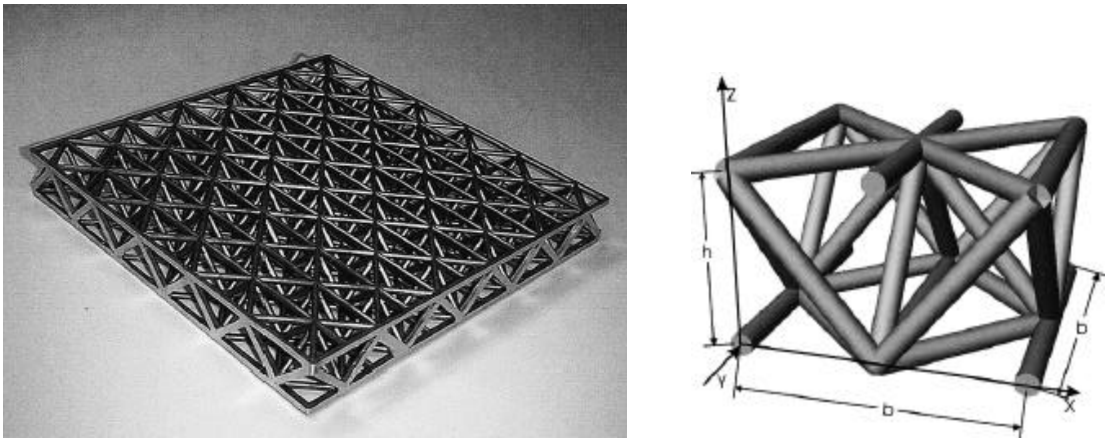

(a) 3-D Truss Panel (b) Corresponding Unit Cell

Figure 1.10 Uniform Truss Structures Made of Aluminum Alloy by Gibson

Wicks and Hutchinson first studied the minimum weight design of sandwiched panel of tetrahedral truss core subject to a prescribed combination of bending and transverse shear loads as shown in Figure 1.11. The weight is minimized when subject to the failure constraints. Circular strut length and radius, core thickness, and plate thickness are design variables for this optimization problem. However, the core is a uniform truss structure with tetrahedral primitives repeated in two directions in a plan. An optimized truss with non-uniform strut lengths and radiuses can significantly improve the performance.

Figure 1.11 Sandwich Plates with Truss Core by Wicks and Hutchinson

1.2.2 Adaptive Truss Structures

Adaptive truss structures are defined as those structures whose shapes conform to parts' geometries and strut sizes are adapted to design requirements. The orientations and positions as well as the sizes of struts in cellular structures can significantly affect the mechanical properties. Adaptive cellular structures are non-uniform in terms of strut orientations, connectivity, and sizes. Thus, they potentially have better performance than uniform cellular structures.

In Figure 1.12, the author shows the frontal longitudinal midsection of upper femur in human body and the diagram of stress lines (Gray 1918). The principal and secondary compressive trabeculae shown in Figure 1.12(a) correspond in spacings and orientations to the lines of maximum compressive stresses shown in Figure 1.12(b).

The author is particularly interested in the natural occurrence of adaptive trabeculae (spacing and orientation) in femur bone to design adaptive lightweight cellular structure via biomimicry. Figure 1.13 shows one section of an adaptive truss structure that conforms to a car body and have adaptive strut sizes for minimum deflection (Wang, Chen et al. 2005).

(a) Upper Femur

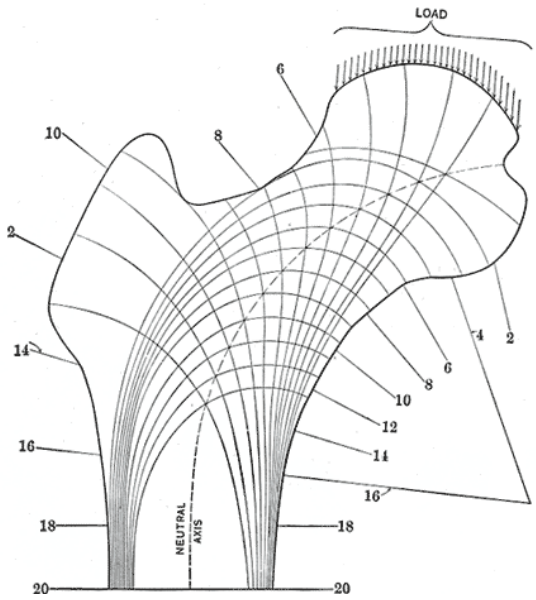

(b) Diagram Of The Lines Of Stress

Figure 1.12 Frontal Longitudinal Midsection of Femur Bone

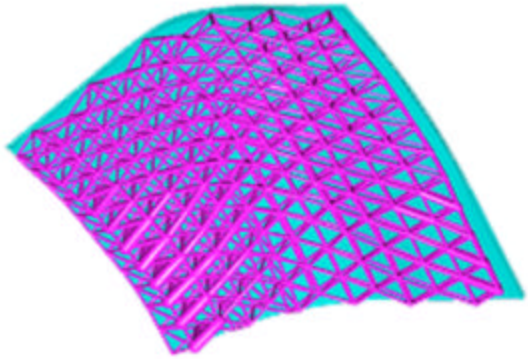

Figure 1.13 Conformal and Optimized Truss Adaptive to Car Body Shape and Design Requirements

1.2.3 Research Opportunities: Adaptive Lightweight Structures

Inspired by femur bone, adaptive lightweight structures are desired for better performances by reorienting and resizing truss struts. Adaptive lightweight cellular structures have not been sufficiently investigated and cannot be systematically designed. Research opportunities for lightweight structure design are:

Opportunity 1: To design conformal truss structures adapted to part shapes. Available engineered cellular structures are uniform with patterned primitives. Conformal cellular structures have not been sufficiently studied and cannot be designed in terms of geometric modeling.

Opportunity 2: To analyze conformal cellular structures more accurately. Various microstructures have been developed and extensively investigated for different cellular structures. However, these microstructures are only applicable to uniform structure. Moreover, the geometric overlaps and structural interactions between microstructures are over-simplified or neglected during analysis. Entire cellular structures cannot be accurately analyzed. However, it is desired to enable the analysis of conformal cellular structures, and analyze cellular structures more accurately.

Opportunity 3: To develop a systematic approach to design adaptive lightweight cellular structures. Adaptive truss by varying strut sizes can significantly enhance a structure's performance. However, adaptive lightweight structures have not been systematically designed.

1.3 Compliant Mechanism – a Bending-dominated Structure

Compliant mechanism transfers motion, force, or energy through structural deformation, mainly bending. Material in structures is removed to have more freedom to move and generate motion. In this section, the research status and opportunities of compliant mechanism are discussed.

1.3.1 Compliant Mechanism

Kota, Howell, Midha, Sigmund, Bendoe, Kikuchi and their colleagues pioneered the research of compliant mechanisms. Michell, Maxwell, et al. developed ground truss approach (a discrete structural optimization method) (Maxwell 1864; Michell 1904). Kota,

Ananthasuresh, and Frecker applied ground truss approach to analyze and design compliant mechanisms (Ananthasuresh and Kota 1995; Frecker, Ananthasuresh et al. 1997; Hetrick and Kota 1998; Kota, Joo et al. 2001). Ground truss approach includes two distinct steps, topology synthesis and dimensional synthesis. Link elements are used to analyze compliant mechanisms and only consider axial forces. However, these two steps are interrelated and should be addressed simultaneously. Moreover, bending cannot be ignored as well as torsion in 3-D compliant mechanisms since they significantly contribute to the deformation of compliant mechanisms.

Kota and his colleagues used linear beam elements and considered bending to improve analysis accuracy for 2-D compliant mechanism (Joo, Kota et al. 2000). However, a significant number of struts in compliant mechanisms are under nonlinear deformation due to geometry nonlinearity, material nonlinearity, or boundary nonlinearity. For an example shown in Figure 1.14, if the deflection at the right end, $dy_{\max}$, is more than 2% of the length L, or more than 20% of the height of the rectangular cross-section h, a cantilever beam should be considered as under nonlinear deformation. Recently, Joo and Kota presented a nonlinear formulation for dimensional synthesis of compliant mechanisms using tapered beam elements (Joo, Kota et al. 2001; Joo, Kota et al. 2001; Joo, Kota et al. 2004). However, nonlinearity in compliant mechanisms has not been sufficiently studied since linear elements cannot well represent nonlinearity. Furthermore, when beams undergo compressions, buckling is one major failure mode, which is a geometric nonlinearity problem. But buckling in compliant mechanisms has not been studied.

1.3.2 Research Opportunities: Multi-degree-of-freedom Deformation and Nonlinearity Analysis, Multiple-objective Design

Therefore, research opportunities for the compliant mechanism design are:

Opportunity 1: To simultaneously consider axial force, shear, bending and torsion to accurately analyze compliant mechanisms. The majority of designed compliant mechanisms are 2-D. 3-D compliant mechanisms cannot be designed because shear, bending and torsion cannot be considered simultaneously. It is desired to explore analysis and design methods to support the design of 3-D compliant mechanisms.

Opportunity 2: To consider nonlinearity of compliant mechanisms. Little attention has been paid to the nonlinearity of compliant mechanisms. However, nonlinearity is not negligible since compliant mechanisms are under nonlinear deformation.

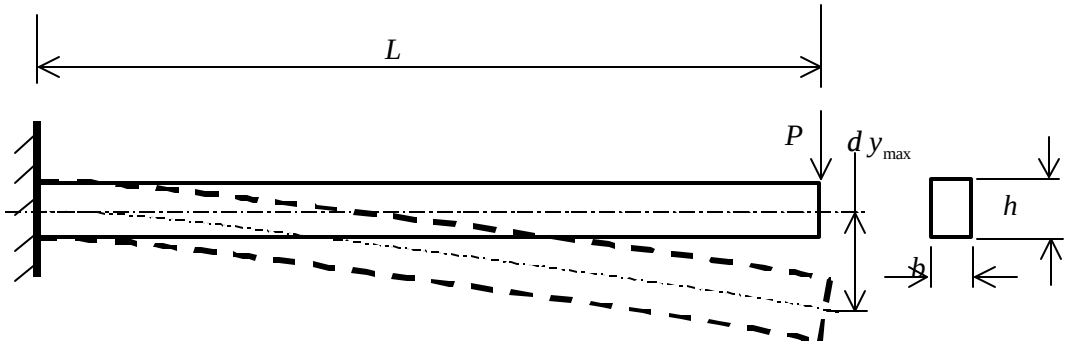

Figure 1.14 A Cantilever Beam under Geometric Nonlinear Deformation

1.4 Research Question, Hypothesis, Validation, and Contributions

In this section, the author identifies the research question and postulates the research hypothesis. Then the potential research contributions and possible applications are discussed.

1.4.1 Research Question and Hypothesis

Research Question: How can adaptive cellular structures be accurately analyzed, efficiently created, and systematically designed?

Research Hypothesis: Unit truss can be used as unit cell to facilitate the design of adaptive cellular structure via geometric modeling, finite element analysis, engineering optimization, and additive fabrication.

After discussing the research opportunities of cellular structures, the author raised a research question about the design of adaptive cellular structures. A new method is developed to realize the design of adaptive cellular structures. The requirements for the new method are elaborated from the research opportunities and listed in Figure 1.15. The first requirement is about the "representation" of conformal cellular structures to create adaptive cellular structures in terms of topology and CAD model. The second requirement is about the "analysis" of conformal cellular structures to accurately analyze cellular structures (geometric overlaps and nonlinearity), simultaneously consider axial forces, bending, and torsion. The third requirement is about "synthesis" and "manufacturing" to use unit truss approach to systematically perform design synthesis of adaptive cellular structures as well as considering the manufacturability. The new method should satisfy all requirements and the author is going to develop a new method in this dissertation.

1. Able to design conformal cellular structures adapted to part shapes.
2. Able analyze conformal cellular structures more accurately than existing approaches by considering geometric overlaps and structural interactions between microstructures, simultaneously consider axial force, shear, bending and torsion, analyze nonlinearity.
3. Suited to develop a synthesis method to systematically design adaptive cellular structures. Analysis process should be efficient; a search algorithm is available to support the design synthesis.

Figure 1.15 Requirement List of the Method to Design Adaptive Cellular Structures

In order to design adaptive cellular structures, a new unit cell, the unit truss, is proposed to represent and analyze cellular structures. Unit truss consists of the central node at a joint and the half-struts connected to the central node. An example of unit truss is shown in Figure 1.16. A strut connecting two neighboring unit trusses is separated into two half-struts, either of which belongs to one unit truss. There is no geometry overlap between any two neighboring unit trusses and the resulting interaction between them is the least complex. Unit truss approach is developed to facilitate the design of adaptive cellular structures, in particular, geometric modeling and mechanics analysis shown in Figure 1.17. Efficient geometric modeling and mechanics analysis methods can make the design synthesis potentially efficient.

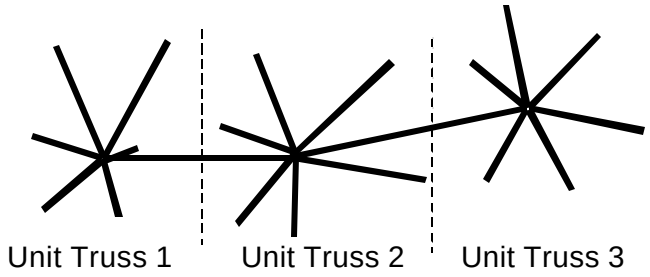

Figure 1.16 Definition of Unit Truss

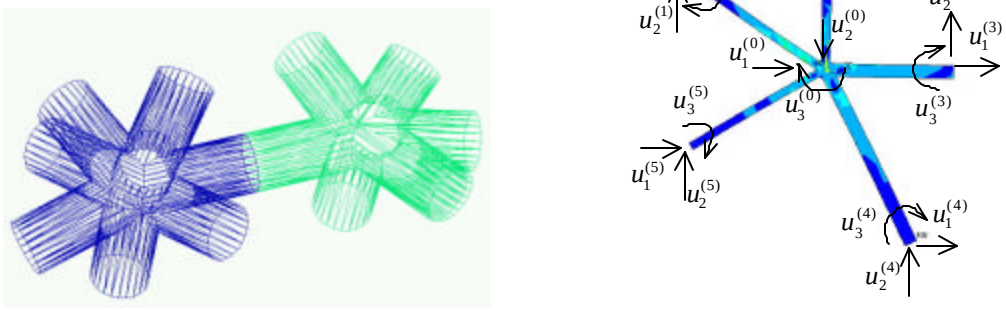

Geometric Modeling Mechanics Analysis

Figure 1.17 Using Unit Truss to Support the Design of Conformal Cellular Structures

1.4.2 Research Contributions

As a result of the research efforts, there are following principal contributions:

1. To enable the geometric modeling of large-scale conformal cellular structures by utilizing unit truss.
2. To simultaneously consider axial forces, shearing, bending, and torsion, and analyze nonlinearity and buckling.
3. To advance the understanding about the manufacturing process for cellular structures.

4. To develop a synthesis method to systematically design lightweight structures and compliant mechanisms with multiple inputs/outputs.

1.4.3 Applications

Applications include new material development, manufacturing industry, automobile industry, bio-medical engineering, and aerospace engineering. The cellular structures gives them unique properties that are exploited in a variety of applications, such as lightweight structures, energy absorption, thermal insulation, heat exchange, filtering, tissue engineering, and so on (Gibson 2003).

Henry Ford noted in 1923, "Saving even a few pounds of a vehicle's weight... could mean that they would also go faster and consume less fuel. Reducing weight involves reducing materials, which, in turn, means reducing cost as well."(1998) Cellular structures are lightweight structure and can make them as the cores of lightweight sandwich panels. Strong, stiff and light mechanisms are highly desired not only in automobile industry, but also in the manufacturing industry. For example, robotic systems are used in all areas of manufacturing, including assembly, welding, spraying, material handling and various machining processes. The major portion of the actuator torques of serial manipulators is still used to support the manipulator's own weight (An, Atkeson et al. 1988). The truss structure manufactured with additive fabrications can be used to replace the internal material of the parts to achieve high strength and stiffness while reducing the overall mass/inertia and altering its resonant frequency as desired. Using the same material, the mass of each link in a robotic manipulator could be reduced significantly through the use of truss structures without reducing its stiffness as shown in Figure 1.18 (Wang and Rosen 2002; Wang and Rosen 2002; Wang 2005). Therefore, we aim to optimally distribute material of a cellular structure for desired

strength, stiffness, design space (a 3-D CAD model), and other mechanical or dynamic properties.

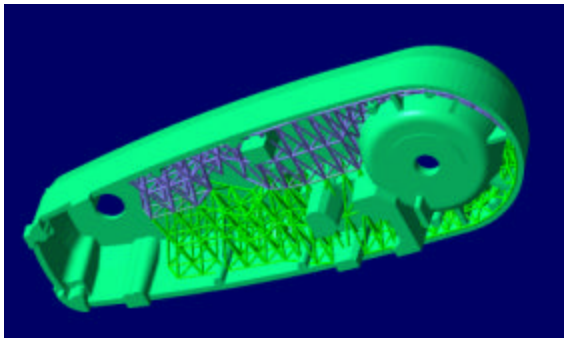

Figure 1.18 Possible Application in Manufacturing: Robot Arm

Cellular structures can withstand large strain at nearly constant stress to absorb the kinetic energy of an impact to make them as energy-absorption devices, e.g., automobile bumpers and helmets (Gibson 2003). For example, Figure 1.19 shows a car bumper filled with truss structures. The main concept is to optimize structures for lightweight, high strength and stiffness, more energy absorbance for automotive components. These components improve safety by absorbing more energy. Furthermore, these components increase automotive performance, reduce weight, and save energy due to their lightweight and high strength/stiffness characteristics.

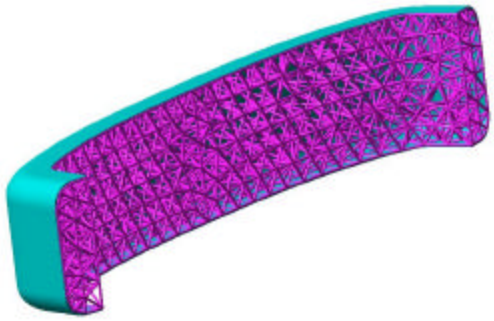

Figure 1.19 Application in Automobile: Car Bumper

Interconnected cellular structures can be used as the scaffolds in tissue engineering and allow cells to penetrate the scaffold and migrate through it due to their high porosity, surface-to-volume ratio, and reconfigurable achitecture. Interpore Cross International utilized titanium truss structures as GEO implants shown in Figure 1.20 (2003). These implanted truss structures maximize the strength of the implants with minimal amount of metal. These implants provide structural integrity and ample space to accommodate bone growth.

Figure 1.20 Application in Bio-medical Engineering: Spine Surgery Implant

The current aircraft wings are sturdy with movable panels that make aircrafts to take-off, turn and change altitude. NASA brought up a concept for a morphing aircraft that mimics bird flight behaviors shown in Figure 1.21 (Weiss 2003). This bone-and-muscle-like wing structure beneath flexible skin is a compliant mechanism with certain rigidity and flexibility. As NASA predicts, an aircraft like this may fly by 2030 (Weiss 2003).

Figure 1.21 Application in Aerospace Engineering: Aircraft with Flexible Wing

1.5 Validation Strategy and an Overview of this Dissertation

Validation: To qualitatively and quantitatively evaluate the effectiveness and efficiency of unit truss approach via Validation Square.

Simpson stated that the validation process for engineering design "is to show the research and its product to be sound, well grounded on principles of evidence, able to withstand criticism or objection, powerful, convincing and conclusive, and provable." (Simpson, Allen et al. 1998) The research question, "How can adaptive cellular structures be accurately analyzed, efficiently created, and systematically designed", was raised in Section 0. A hypothesis of using unit truss approach was postulated to answer the research question. In general, a research question is answered when the corresponding hypothesis is validated. To systematically test this hypothesis, the validation square developed by Pedersen, Allen and Mistree is applied in this dissertation as shown in Figure 1.22 (Pedersen, Emblemsvag et al. 2000). Seepersad and co-authors refined the validation square (Seepersad, Pedersen et al. 2005). This validation method consists of four phases and six steps. The four phases are theoretical structural validity, empirical structural validity, empirical performance validity, and theoretical performance validity. Structural validation is a quantitative process consisting

of three steps: “(1) accepting the individual constructs constituting the method, (2) accepting the internal consistency of the way the constructs are put together in the method, and (3) accepting the appropriateness of example problems used to verify the performance of the method.” Performance validation is a quantitative process consisting of three steps: “(4) accepting that the outcome of the method is useful with respect to the initial purpose for some chosen example problems, (5) accepting that the achieved usefulness is linked to applying the method, and (6) accepting that the usefulness of the method is beyond the example problems.” (Pedersen, Emblemsvag et al. 2000; Panchal 2005)

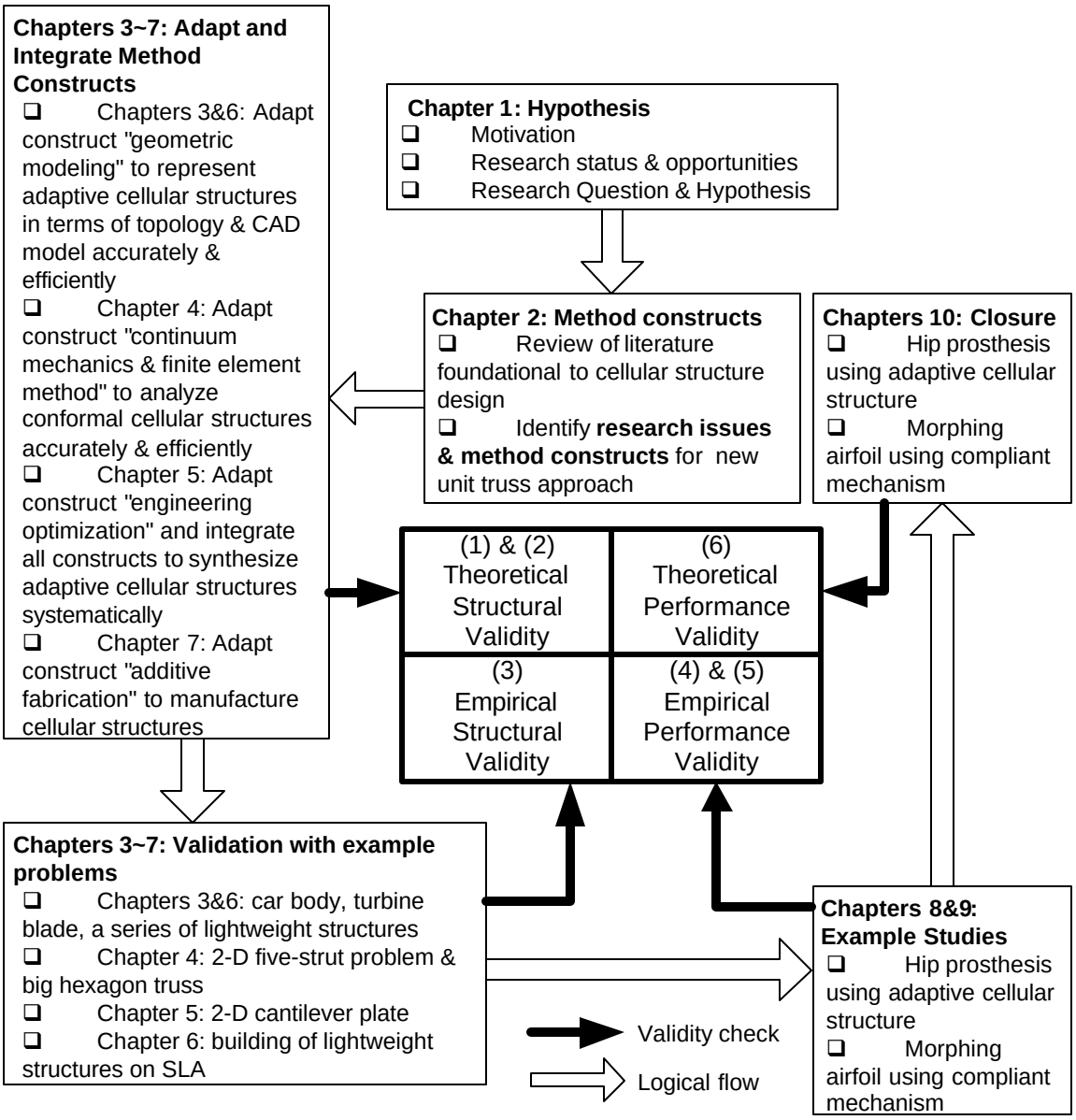

Figure 1.22 Validation Strategy in this Dissertation by Using Validation Square

In Chapter 2, the author critically evaluates the state-of-the-art approaches to design adaptive cellular structures, including ground truss approach and homogenization method. Both approaches are the theoretical foundations and leveraged for new unit truss approach. The hypothesis is dissected into four research issues in terms of representation, analysis, manufacturing and synthesis. In Chapters 3~7, the author theoretically validate the hypothesis of using new unit truss approach through

mathematical proofs and constructions, in particular, adapting the method constructs (geometric modeling, continuum mechanics and finite element method, engineering optimization, and additive fabrication) into solving these four research issues. Partial performance validation is performed by comparing new unit truss approach to the state-of-the art ground truss approach and homogenization method. Chapters 8 and 9 empirically validate the hypothesis through two examples, graded cellular structure for prosthesis and compliant mechanism for morphing wings. In Chapter 10, the author critically evaluates the new unit truss approach and argues its validity beyond the examples used in this dissertation.

The presentation of this dissertation is a process to validate the hypothesis. The organization of this dissertation is shown in Figure 1.23. In Chapters 1 and 2, the author lays the foundations of cellular structure researches. In Chapter 1 the author introduces the natural occurrences and engineered artifacts of cellular structures. Then, the research status is discussed and the research opportunities are identified. It is followed by the research question and hypothesis. A validation strategy is proposed.

In Chapter 2, the author critically reviews the reference of adaptive cellular structure for theoretical structural validation. The author shows that conformal cellular structures can enhance performances as compared to uniform cellular structures. A research review of the state-of-the-art structural synthesis methods is given. Four research issues are raised for the new unit truss approach posed in the hypothesis. The solutions to these research issues are the method constructs of the new unit truss approach and integrated into a systematic design process of adaptive cellular structures.

In Chapters 3~7, the author presents how the constructs (geometric modeling, continuum mechanics and finite element method, engineering optimization, and additive fabrication) are adapted to solve the research issues (representation, analysis,

synthesis, and manufacturing) of the new unit truss approach to design adaptive cellular structures. Successful adaptations and integration of the method constructs prove the theoretical structural validity of the hypothesis. Meantime, some examples are used to test the empirical structural validity of the hypothesis. In Chapter 3, the author proposes and discusses the conformal truss topology to represent the material distribution of cellular structures via geometric modeling; in Chapter 4, the mechanics model of unit truss is established and used as the microstructure to analyze cellular structures via continuum mechanics and finite element method; in Chapter 5, a design synthesis method using particle swarm optimization algorithm is proposed to systematically design cellular structures via engineering optimization and integration of constructs; in Chapter 6, the author presents a hybrid method to create geometric model of large-scale cellular structures via geometric modeling; in Chapter 7, the manufacturability of cellular structures is discussed and the manufacturing limitations are considered in the design stage using design for manufacturing. Cellular structures are manufactured via additive fabrication.

In Chapters 8 and 9, two examples, graded cellular structure for enhanced stability on implant-bone interface in uncemented prosthesis and compliant cellular structure for morphing wings, are used to test the proposed unit truss approach for cellular structure design. The effectiveness and efficiency of the unit truss approach is tested for their empirical performance validity.

Chapter 10 answers the research question and validates the hypothesis. The author critically evaluates the research results and expands the research achievements. For theoretical performance validation, it is argued that the research results of this dissertation are relevant beyond the two example problems.

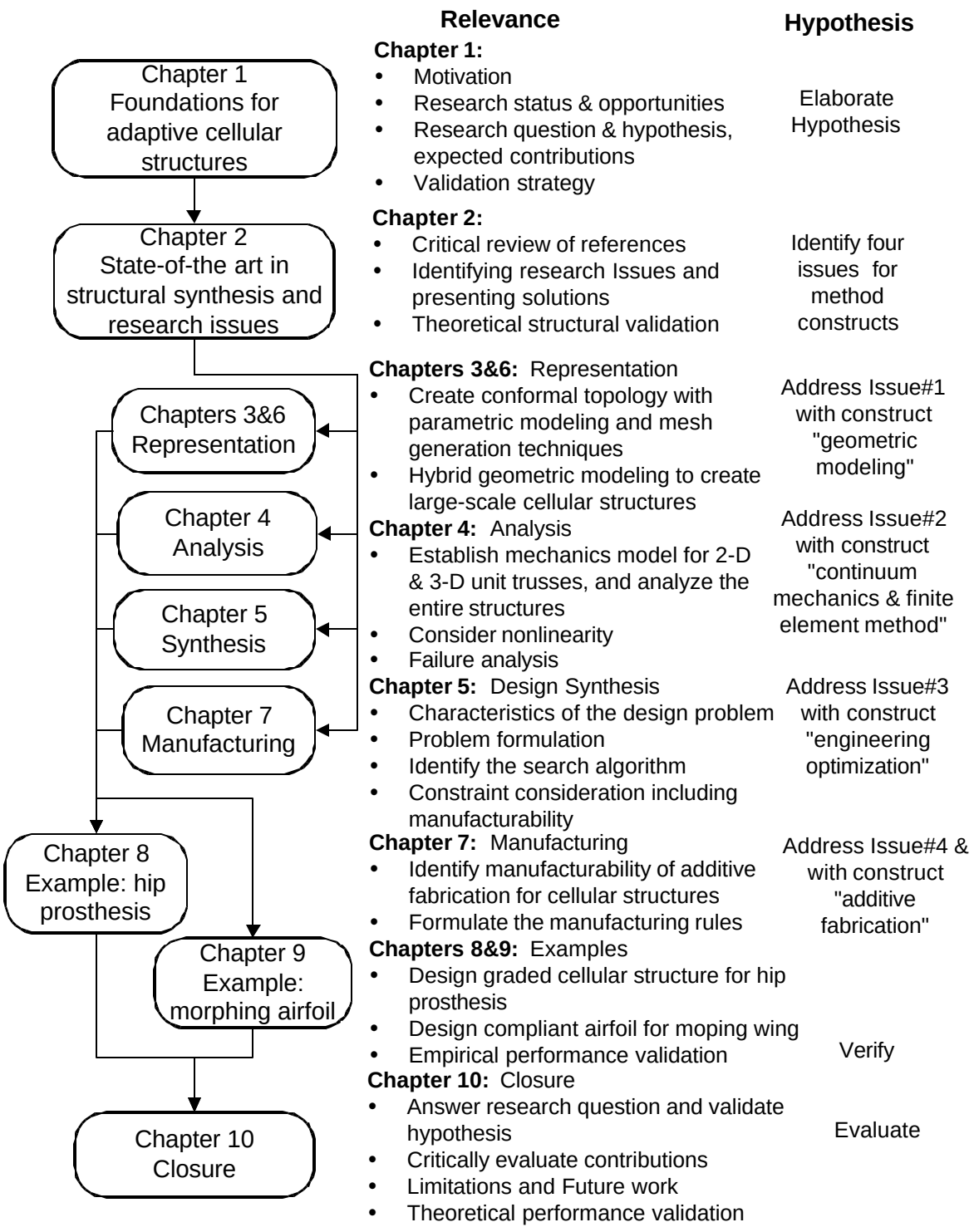

Figure 1.23 A Dissertation Overview and Roadmap

CHAPTER 2

FOUNDATIONS OF UNIT TRUSS APPROACH FOR ADAPTIVE CELLULAR STRUCTURES

In this chapter, the author lays the theoretical foundations of the proposed unit truss approach for designing adaptive cellular structures. The organization of Chapter 2 is presented in the context of the Validation Square (Figure 1.22) and shown in Figure 2.1. The author identifies the research issues of unit truss approach by: classifying cellular structures (Section 2.1); validating that adaptive cellular structures provide better performance than uniform cellular structures via analytical and numerical analyses (Section 2.2); leveraging unit cell approach to identify four research issues and propose a solution to address each research issue (Section 2.4). The solutions are adapted from method constructs (geometric modeling, continuum mechanics and finite element method, engineering optimization, and additive fabrication) that are integrated into unit truss approach as shown in Figure 2.2. The adaptation process from the method constructs to the unit truss approach will be extensively discussed in Chapters 3~7. The state-of-art methods are critically evaluated and their capability is discussed for designing adaptive cellular structures (Section 2.3). Two typical state-of-the-art design methods are ground truss approach and homogenization method discussed. These two methods are leveraged to develop the new unit truss approach. Finally, a design process of adaptive cellular structures is presented by integrating the four research solutions (Section 2.5).

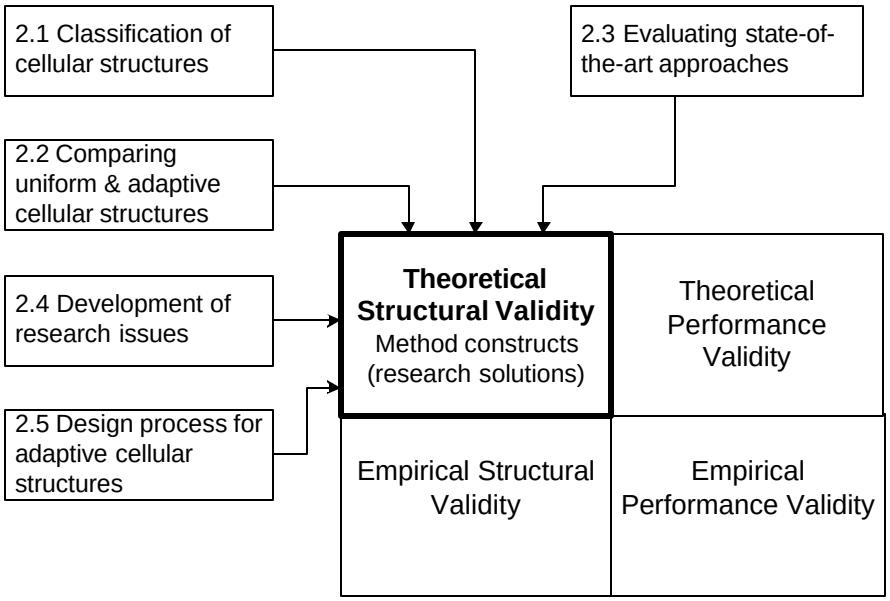

Figure 2.1 Relationship between Chapter 2 and Validation Square

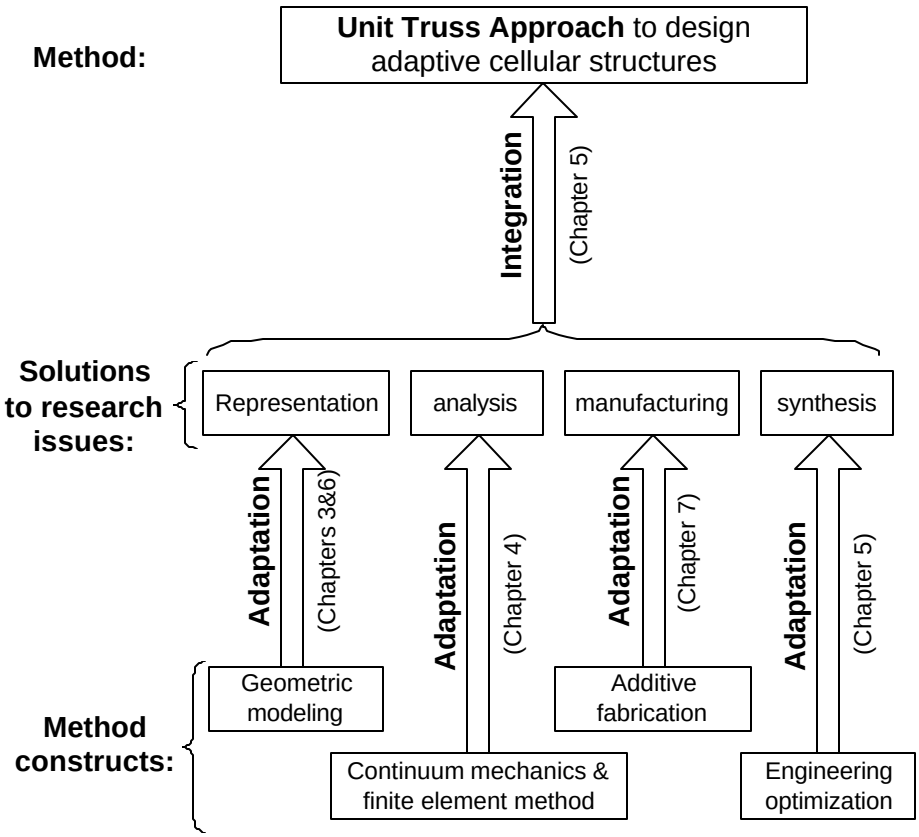

Figure 2.2 Relationship between Constructs and Unit Truss Approach

2.1 Classifications of Cellular Structures

Cellular structures can be classified in various ways, such as geometric characteristics, functionality, and manufacturing process.

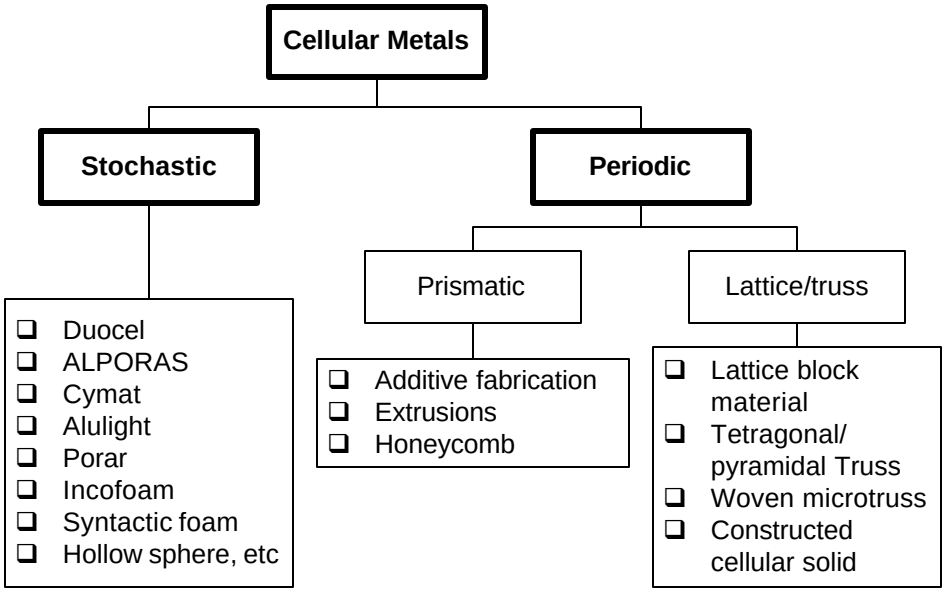

Figure 2.3 Classification of Cellular Metals

The geometries of cellular structures can be stochastic, periodic, or even a mixture of them. Cochran, Wadley and his colleagues classified the cellular structures into two main categories according to geometric characteristics: stochastic and periodic as shown in Figure 2.3 (Cochran, Lee et al. 2000; Wadley, Fleck et al. 2003). The periodic cellular structures can be classified into simple uniform structures and non-uniform periodic structures. Examples of uniform structures and non-uniform periodic structures are shown in Figure 1.3 and Figure 1.4 respectively. Actually, the natural cellular structures have much more variety than the engineered cellular structures shown in Figure 2.3. For example, the human bone structure shown in Figure 1.2 is a periodic cellular structure, but not one. The largest limitation of stochastic cellular structures is

the lack of freedom given to the designer to control the placements of voids in cellular structures (Evans, Hutchinson et al. 2002; Rosen 2003).

Cellular materials are potentially well suited to multifunctional applications that demand not only structural performance but also some other attributes such as energy absorption, heat transfer, thermal protection, or thermal insulation (Gibson 2003). Stochastic cellular solids, such as foams, have excellent thermal and acoustic insulation properties (Gibson and Ashby 1997; Gibson 2003). Periodic cellular solids, such as honeycombs and lattices, have superior mechanical properties, including energy absorption, strength, and stiffness (Gibson and Ashby 1997), as well as lower pressure drop and high surface area densities, which are important for heat transfer performance (Hayes, Wang et al. 2004). However, the periodic cellular solids, like truss structures, are configurable to enable the designers to better distribute material.

According to the manufacturing processes, cellular structures can be classified as natural structures and artificial structures, stochastic structures and repeatable structures. Namely, the classification of natural structures and artificial structures is based on natural occurrence or man-made part. Natural structures are not completely repeatable, but partially stochastic. Some artificial cellular structures are repeatable, such as periodic 2-d honeycombs made by crimping and stamping. Some artificial cellular structures are not repeatable, but stochastic, such as foam metal.

2.2 Uniform Cellular Structures and Adaptive Cellular Structures

Adaptive cellular structures are defined as those structures, whose geometries are conformal to part shapes and with topologies and individual strut sizes adapted to the design requirements. For compliant mechanisms, uniform material distribution or a

structure with uniform strut sizes usually cannot generate desired compliances. In this section, the author validates that adaptive lightweight structures can provide better performance than uniform lightweight structures by comparing uniform truss and conformal truss, as well as uniform truss and optimized truss.

The orientations and positions as well as the sizes of struts in cellular structures can greatly affect the mechanical properties. Conformal cellular structures are non-uniform in terms of strut orientations, connectivity, and sizes. Conformal cellular structures are adaptive to the design requirements. Thus, they potentially have better performance than uniform cellular structures. This section will compare uniform truss and conformal truss using simplified analytical models and a numerical example.

2.2.1 Uniform Truss vs. Conformal Truss

Uniform and conformal cellular structures have different mechanical properties in terms of compliance and strength due to their struts' orientations.

2.2.1.1 Comparison with Analytical Models

Not only the numbers of struts and joints can influence the strength (maximum stress) and stiffness of structures, but also the orientations of struts are the factors since the orientations can change the stress distributions inside structures. 2-D uniform triangular truss is shown in Figure 2.4(a) and its unit truss is shown in Figure 2.4(b). A typical 2-D unit truss consists the central node at a joint and its six connected struts in half space. Thus, each strut shown in Figure 2.4(b) only represents half of the real strut in the uniform structure. Link element is used to represent the struts. The bending moments are neglected and all struts are only under axial forces. The struts are re-oriented by rotating by q along z axis, which points outward.

For simplicity and generalization, this unit truss is assumed to exist in hydrostatic pressure and the end face of each half-strut is under uniform force F. Obviously, this unit truss is in equilibrium due to its symmetry. When this unit truss is considered as a unit cell (microstructure), the equivalent force in x direction, F_x, and, the equivalent force in y direction, F_y, are shown as Equation 2.1 and Equation 2.2 respectively.

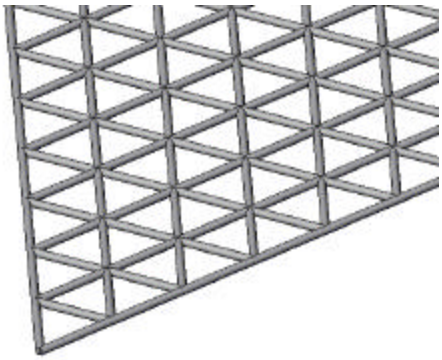

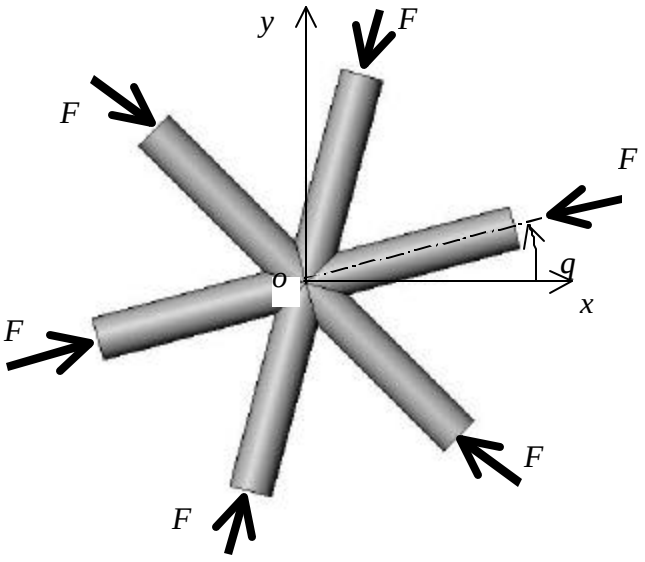

(b) A 2-D Periodic Triangle Truss (b) Unit Truss for 2-D Periodic Triangle Truss

Figure 2.4 2-D Triangular Truss and its Unit Truss

$$F_x = F\cos(q) + F\left|\cos(q+\frac{p}{3})\right| + F\cos(-q+\frac{p}{3}), q \in \left[0, \frac{p}{3}\right) \quad 2.1$$

$$F_y = F\sin(q) + F\sin(q+\frac{p}{3}) + F\sin(q+\frac{2p}{3}), q \in \left[0, \frac{p}{3}\right) \quad 2.2$$

The values of the equivalent forces F_x and F_y vary as shown in Figure 2.5, where the x direction represents the rotation q in radians changing from 0 to $\frac{p}{3}$. When $q = \frac{p}{6}$, the equivalent force F_y in the y direction reaches the maximum, while the

equivalent force F_x in the x direction reaches the minimum. Therefore, $q = \frac{p}{6}$ is the right orientation for maximum strength (least maximum stress) when under external loads in the y direction, however it is the worst orientation for the structure's strength (highest maximum stress) when under external loads in the x direction. When $q = 0$, the results are just reversed as opposite to those of $q = \frac{p}{6}$. Hence, the orientations of the struts in a truss structure can influence the strength under different load conditions.

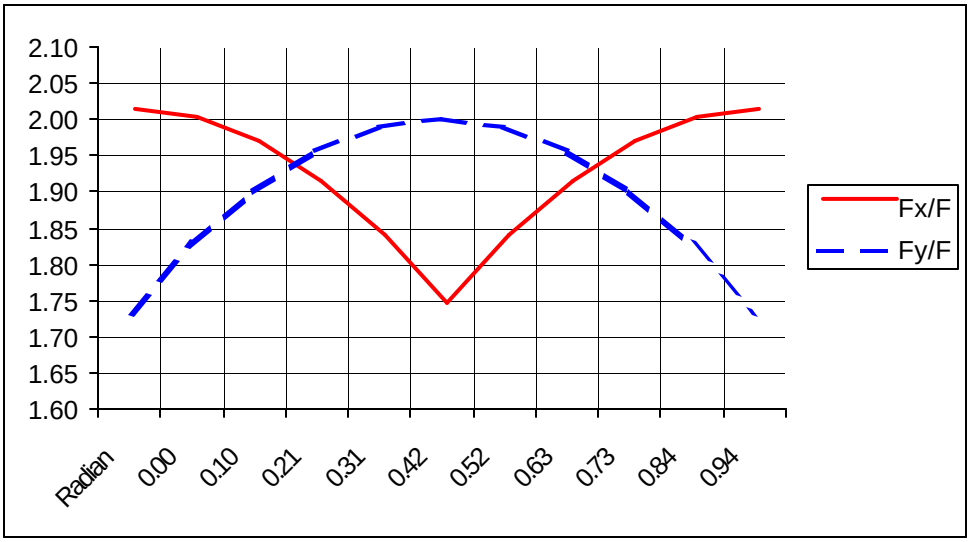

Figure 2.5 2-D Conformal Triangular Truss Structure

As long as the stress distribution changes, the deflection of the structure changes. The deflection is an integral behavior of strain, which is proportional to the stress in linear deformation. When the structure is strengthened in a certain direction represented by $\bar{u}$, the structure becomes stiffer in the $\bar{u}$ direction as well. However, the structure becomes softer in the $\bar{v}$ direction, which is perpendicular to the $\bar{u}$ direction. So there is a trade-off between strength and stiffness.

2.2.1.2 Comparison with Numerical Analysis

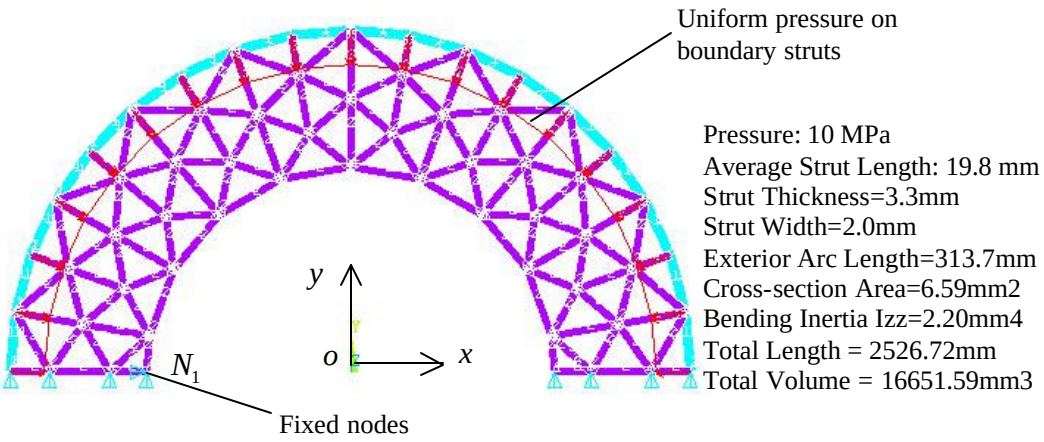

	Uniform	Conformal	Improvements
Stress/MPa	62.038	50.589	18.45%
Deflection/mm	25.911	28.472	-9.88%

Figure 2.6 2-D Conformal Triangular Truss Structure

The 2-D triangular truss shown in Figure 2.6 is a conformal truss structure, whose struts are oriented towards the boundary loads as opposed to the uniform truss shown in Figure 1.8. ANSYS was utilized to analyze the stresses and deflections of the structures. The exterior struts are modeled as beam elements since these struts need to withstand bending moments, and the interior struts are modeled as link elements. The structure is under exactly the same boundary conditions as the uniform truss shown in Figure 1.8. The finite element analysis results show that the maximum stress of the conformal truss is 18.45% less than that of the uniform truss. Thus, the strength is improved by re-orienting the struts towards the external loads. However, the maximum deflection of the conformal truss is larger than that of the uniform truss by 9.88%. The maximum deflection of the conformal truss occurs along the x axis direction since the structure is softened in the perimeter direction, which is perpendicular to the external pressure direction. These numerical analysis results are reasonable and consistent with the previous analysis results.

2.2.2 Optimized Truss vs. Non-optimized Truss

Maximizing stiffness and maximizing strength (minimizing maximum stress) cannot be obtained simultaneously by re-orienting the struts for truss structures. However, they can be balanced to reach a superior solution through optimization. Optimization technique can be leveraged to achieve a superior design for superior strength and stiffness combination with minimum material.

Generally, the structural optimization problems of truss structures can be categorized into two types of problems, size optimization and topology optimization. Size optimization defines structural parameters such as material values, cross-section dimensions and thicknesses, and then searches for the optimum sizes. Topology means the connectivity of members or elements in a structure. Topology optimization defines the structural connectivity as design parameters and then search for the best connectivity. The optimization of lightweight truss structures is a problem of size optimization. If some struts are removed, the lightweight truss structure is not statically determinate.

Table 2-1 Performance Improvement of Truss Structure with Size Optimization

		Mass (gram)	Strength (MPa)	Deflection (mm)
Before Optimization	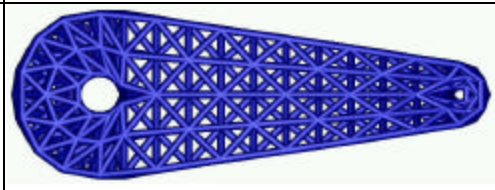	83.9	0.53	0.06
After Optimization	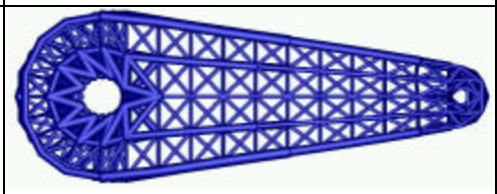	55.3	0.46	0.06
Improvement		34.08%	13.21%	0%

In Table 2-1, the author shows the performance improvement of 3-D truss structures for a robot link before and after a size optimization (Wang 2001). The joints around the left hole of the truss structure are fixed, and a vertical concentrated force is applied to the joint near the right hole of the truss structure. Both structures have an equal maximum deflection, 0.06 mm. The individual diameters of the struts are changed through optimization to achieve the same stiffness and higher strength for the robotic link, but with minimum build material. The total mass is reduced by 34.08% and the strength is improved by 13.21%. Therefore, a structure's performance can be improved significantly via structural optimization.

Table 2-2 Typical Methods Available for Structural Synthesis

Typical Method	Descriptions	Pros & Cons
Ground Structure (Discrete) Approach [Michell, Kirsch, Kota, Ananthasuresh, et al.] (Michell 1904; Rule 1994; Burns 2002)	Ground structure is a grid of potential bars connecting any two nodes in design space. The optimal truss structure is formed through choosing an optimal substructure from this pre-defined ground structure.	Pros: - Straightforward. Cons: - No consideration of bending, torsion, nonlinearity - Topology synthesis and dimensional synthesis are two separate steps, but they are interrelated
Homogenization (continuum) Method [Bendsoe, Kikuchi, et al.] (Bendsoe and Kikuchi 1988; Bendsoe 1995)	Employing a composite material as a basis for defining shape in terms of material density. Periodic microstructures are used as the equivalent homogenized material with the same effective properties.	Pros: - Relative stable - Converted the topology problem to a sizing problem - Move from macroscopic scale to microscopic scale Cons: - Non-realizable artificial elements exist - Cannot consider global behavior; computationally prohibited, difficult to design 3-D structures

2.3 Recent Developments in Structural Optimization for Adaptive Structures

Adaptive cellular structure design is a typical problem in structural optimization. Various methods have been developed for those design problems of maximum rigidity or

flexibility. Design for flexibility (compliance) is to design structures for desired compliance as opposed to design for rigidity (stiffness). Two classes of material representation methods were developed: discrete structural optimization method and continuum optimization method (Bendsoe 1995; Eschenauer and Olhoff 2001; Burns 2002). A brief overview of the discrete and continuum structural optimization approaches is given in Table 2-2. Both methods are not sufficient to accurately analyze and systematically design adaptive cellular structures. Ground truss approach can only provide a rough estimation for the geometry of desired cellular structures. Homogenization method using artificial unit cells provides better results, but it results with non-realizable elements and is computationally prohibited.

2.3.1 Ground Truss Approach – Discrete Structural Optimization

Michell and Maxwell made their pioneering works in discrete structural optimization (Michell 1904; Burns 2002). The design of discrete structures is broken down into nodal locations (geometry optimization) and strut connectivity (topology optimization). In the widely used ground truss approach, nodal locations are fixed and the resulting optimum topology is a subset of the ground truss.

The cross-sections of ground truss members are considered as continuous design variables for optimization. The members with vanishing cross-sectional areas are removed to obtain the optimum (Burns 2002). Let $a^{(i)}, l^{(i)}$ denote the cross-sectional area and length of the i^{th} bar in a ground truss. Its Young's modulus is given as $E^{(i)}$. The given truss volume is $V = \sum_{i=1}^{m} v^{(i)}$, and $v^{(i)} = a^{(i)} l^{(i)}$ $(i = 1,..., m)$ is the volume for the i^{th} bar as primary design variable. $\underset{\sim}{u}$ represents nodal displacements. For a typical single load problem to find the minimum compliance with a given volume of material, the

discrete ground truss approach is formulated as Equation 2.3 (Bendsoe 1995; Burns 2002).

$$
\begin{aligned}
&\underset{u \in u,\, t}{\text{minimize}} \quad \underset{\sim}{p} \cdot \underset{\sim}{u} \\
&\text{subject to:} \\
&\qquad \sum_{i=1}^{m} v^{(i)} \, \underset{\sim}{K}^{(i)} \cdot \underset{\sim}{u} = \underset{\sim}{p} \\
&\qquad \sum_{i=1}^{m} v^{(i)} = V, v^{(i)} \geq 0, \; i = 1, \ldots, m \\
&\text{Static equilibrium} \quad \underset{\sim}{B} \cdot \underset{\sim}{q} = \underset{\sim}{p} \\
&\text{Element stiffness matrix} \quad \underset{\sim}{K}^{(i)} = \frac{E^{(i)}}{l^{(i)^2}} \underset{\sim}{b}^{(i)} \otimes \underset{\sim}{b}^{(i)^T}
\end{aligned}
\qquad 2.3
$$

$\underset{\sim}{B}$ is the compatibility tensor, $\underset{\sim}{q}$ is the member force

$\underset{\sim}{p}$ is the nodal force, $\underset{\sim}{b}^{(i)}$ is the i^{th} column of $\underset{\sim}{B}$

Kota and his colleagues used ground truss approach to develop a two-step approach (topology and dimensional syntheses) for compliant mechanism design (Ananthasuresh, Kota et al. 1994; Joo, Kota et al. 2001). Topology synthesis is to find an optimum topology by identifying the optimum number and connectivity of structural elements for achieving specified motion requirements. Topology synthesis determines the main performance of designed compliant mechanisms and provides a kinematically functional mechanism. Dimensional synthesis starts with the resulting topology from topology synthesis and determine the sizes of individual elements in compliant mechanisms. Dimensional synthesis generates a detailed specification of the geometry of final compliant mechanisms through a sizing optimization for desired performances, such as geometric advantage and mechanical advantage (Ananthasuresh, Kota et al. 1994). An example is the gripper design problem. In Figure 2.8, we show the starting ground truss topology created in the defined design domain shown in Figure 2.7. The resulting compliant mechanism is a subset of the ground truss shown in Figure 2.9.

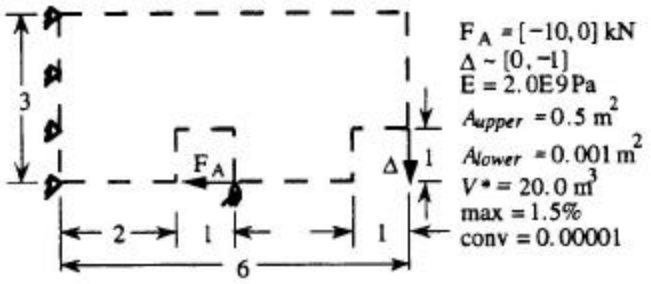

Figure 2.7 A Gripper Design Problem (Frecker, Ananthasuresh et al. 1997)

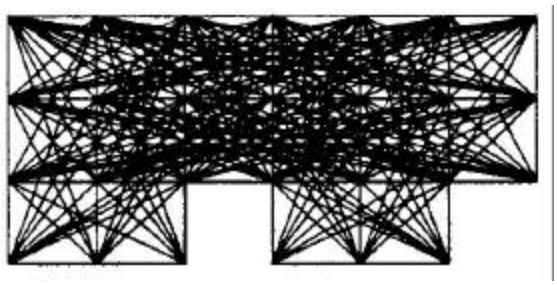

Figure 2.8 Initial Ground Truss of Gripper (Frecker, Ananthasuresh et al. 1997)

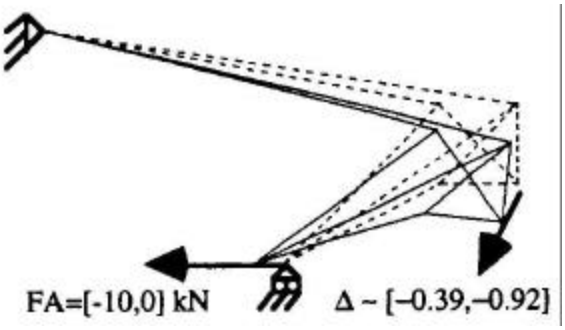

Figure 2.9 Designed Compliant Mechanism Using Ground Truss Approach (Frecker, Ananthasuresh et al. 1997)

However, topology synthesis and dimensional synthesis are interrelated. During analysis, there is no consideration of bending or torsion since only link elements are used. The ground truss approach does not consider geometric and material nonlinearity. However, bending and nonlinearity are not negligible for compliant mechanisms since they are bending-dominated and nonlinearly deformed.

2.3.2 Homogenization Method – a Continuum Structural Optimization

In continuum structural optimization methods, the design domain is represented by microstructures. Continuum structural optimization method does not need shape

parameters, such as strut diameter and plate thickness, to represent the structure's geometry. The material distribution problem is a point "on-off" (solid material-void) problem of microstructures in Evolutionary Structural Optimization, which removes or keeps microstructures using a rejection criterion during optimization (Xie and Steven 1997). Hence, microstructures has two discrete states, on or off (mathematically 1 or 0), representing solid or void respectively. However, this kind of on-off approach requires the use of discrete optimization algorithms, which would be unstable (Hassani and Hinton 1999).

This instability issue of point on-off approach was unsolved until a material density function r was introduced in homogenization method by Bendsoe and Kikuchi (Bendsoe and Kikuchi 1988). Microstructures are represented as composite materials with varying material properties as a function of material density r (r is continuous and $r \in [0,1]$) (Bendsoe 1995). From a macroscopic perspective, a point in structures can be partially occupied by structural material, with $r = 0$ corresponding to void, $r = 1$ to solid material, and $0 < r < 1$ to the porous composite with voids at micro level. Therefore, the on-off material distribution problem is converted to a sizing problem and moves from macroscopic scale to microscopic scale.

Many microstructures have been developed, but these fall into three categories: porous micro-cell, rank laminate composite, and free mixture (Burns 2002). Bendsoe and Kikuchi first proposed to use porous micro-cell with variable sizes a and b, and orientation angle q (Bendsoe and Kikuchi 1988). A more complicated microstructure, rank laminate, was developed using ranked hierarchical laminates by Allaire and Kohn later (Rozvany 1997). In the free mixture formulation, the microstructural material arrangement is not described as using holes or laminates. In Figure 2.10, the author

shows the use of microstructure approach and these three different developed microstructure formulations.

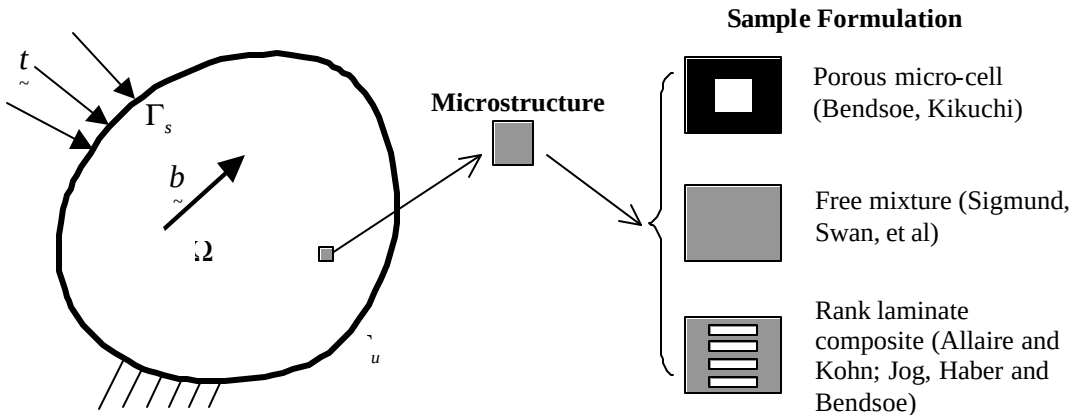

Figure 2.10 Microstructure Approach

Both Evolutionary Structural Optimization (ESO) method and Homogenization method consider a mechanical element as a body occupying a subdomain Ω^m, which is a finite section of the entire domain Ω as shown in Figure 2.10. $\tilde{\tilde{E}}(x)$ are the effective elasticity tensors, which are design variables over the domain Ω for optimization. $\tilde{t}$ is the boundary traction on the traction boundary $\Gamma_s \subset \Gamma$, and $\tilde{b}$ is the body force as shown in Figure 2.10. $\tilde{u}$ represent the field displacements over the domain Ω. The goal is to find the optimal elasticity tensors $\tilde{\tilde{E}}$ over the domain Ω of statically admissible stress field. The generalized shape design problem of optimal material distribution for maximum rigidity (stiffness) is formulated as Equation 2.4 (Bendsoe 1995). $W_{ex}(\tilde{u})$ denotes external work, and $W_{in}(\tilde{u})$ denotes internal work. When virtual external work $dW_{ex}(\tilde{u})$ is equal to virtual internal work $dW_{in}(\tilde{u})$, the system is under equilibrium.

$$\underset{u\in U,E}{\text{minimize}} \quad W_{ex}(\underset{\sim}{u})$$

subject to:

$$dW_{in}(\underset{\sim}{u}) = dW_{ex}(\underset{\sim}{u}), \text{ for all } d\,\underset{\sim}{u}\in U, \tilde{\underset{\sim}{E}} \in \underset{\sim}{E}_{ad}$$

Energy bilinear form $dW_{in}(\underset{\sim}{u}) = \int_{\Omega} \underset{\sim}{e}(\underset{\sim}{u}) : \tilde{\underset{\sim}{E}}(\underset{\sim}{x}) : d\,\underset{\sim}{e}(\underset{\sim}{u}) d\Omega$ 2.4

Linearized strains $\underset{\sim}{e}(\underset{\sim}{u}) = \frac{1}{2}\left(\overline{\nabla}\,\underset{\sim}{u} + \underset{\sim}{u}\,\overline{\nabla}\right)$

Load linear form $l(\underset{\sim}{u}) = \int_{\Omega} \underset{\sim}{p}\cdot\underset{\sim}{u}\, d\Omega + \int_{\Gamma_T} \underset{\sim}{t}\cdot\underset{\sim}{u}\, ds$

The computation of $\tilde{\underset{\sim}{E}}$ plays a key role for topology optimization in the problem of design for rigidity. It can be obtained from an analytical or numerical modeling process. Some modeling processes, such as power law methods or SIMP, even introduce artificial parameters (Rietz 2001; Sigmund 2001). $M_{\max}$ is the maximum material mass. The artificial material density r is a function of the fundamental design variables, which are those geometric variables, such as sizes and orientation of composite microstructures. For example, the geometric variables of porous micro-cell are sizes a and b, and orientation angle q. In homogenization method, the set $\tilde{\underset{\sim}{E}}(\underset{\sim}{x})$ of admissible elasticity tensors is given as Equation 2.5 (Bendsoe 1995).

Geometric variables $a, b, ..., q \in L^{\infty}(\Omega)$

$$\tilde{\underset{\sim}{E}}(\underset{\sim}{x}) = \tilde{\underset{\sim}{E}}(a(\underset{\sim}{x}), b(\underset{\sim}{x}), ..., q(\underset{\sim}{x})),$$

density of material $r(\underset{\sim}{x}) = r(a(\underset{\sim}{x}), b(\underset{\sim}{x}), ...)$ 2.5

$$\int_{\Omega} r(\underset{\sim}{x}) d\Omega \le M_{\max}; 0 \le r(\underset{\sim}{x}) \le 1, \underset{\sim}{x} \in \Omega$$

For isotropic microstructures, Sigmund proposed to use a power of the artificial density r as the coefficient of stiffness as shown in Equation 2.6 (Sigmund 2001). The stiffness k_e of a microstructure with density x_e is artificially interpolated as the stiffness

of solid material multiplied by the power law coefficient $(x_e)^p$. A typical penalization power is given as $p = 3$.

$$k_e = (x_e)^p k_s$$

where,

x_e – material density of artificial element e

k_e – stiffness of artificial element e with material density x_e

k_s – stiffness of solid element filled with regular material

p – penalization power

2.6

The optimization model of homogenization method, as shown in Equation 2.4, can be expressed in terms of the principle of minimum potential energy with respect to the stresses $\underset{\sim}{s}$ as Equation 2.7.

$$\min_{\underset{\sim}{E} \in \underset{\sim}{E}_{ad}} \min_{\underset{\sim}{s} \in \Phi} \left\{ \tfrac{1}{2} \int_{\Omega} \underset{\sim}{s} : \underset{\sim}{C} : \underset{\sim}{s} \, d\Omega \right\}$$

$$\text{Compliance tensor } C_{ijkl} = \left[E_{ijkl} \right]^{-1}$$

$$\text{Statically admissible stress field } \Phi = \left\{ \underset{\sim}{s} \mid \vec{\nabla} \underset{\sim}{s} + \underset{\sim}{p} = 0 \text{ in } \Omega, \; \underset{\sim}{n} \cdot \underset{\sim}{s} = \underset{\sim}{t} \text{ on } \Gamma_s \right\}$$

2.7

In Figure 2.11, the author shows the topology optimization result from homogenization method for the gripper problem shown in Figure 2.7 (Frecker, Ananthasuresh et al. 1997).

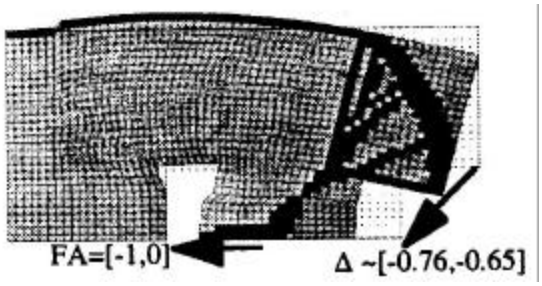

Figure 2.11 Designed Compliant Mechanism Using Homogenization Method

The above discussions are used to formulate “design for rigidity” problems. For “design for flexibility” problems, the optimization model can be expressed in terms of maximum potential energy as opposed to Equation 2.4 and Equation 2.7. In some particular cases, some researchers formulated it in terms of the maximum ratio between mutual energy and strain energy (Frecker, Ananthasuresh et al. 1997).

This power-law or other interpolation methods are used to represent the physical behavior of microstructures. However, it is a rough approximation by using the power of artificial density as the coefficient of the stiffness of microstructures. Furthermore, no physical material corresponds to artificial elements with density between 0 and 1. In homogenization method, the local behaviors of microstructures are integrated to model the global behavior of the entire structure. Therefore, some global behavior, such as buckling, cannot be considered using homogenization method, since buckling is related to the overall geometries of certain domains.

Homogenization method with optimality criteria is only suitable for the problems with continuous convex design domain, not for those with concave or discrete design domains. It needs gradients and Hessian matrices, which need huge efforts to derive. To employ homogenization method, there are a huge number of design variables. For the structural optimization with isotropic material shown in Figure 2.11, each small square (element) represents one element, which requires at least one design variable to parameterize. Sigmund used the artificial density r as design variable, and each microstructure is denoted by one variable (Sigmund 2001). In the problem shown in Figure 2.11, there are totally 1600 microstructures and 1600 design variables correspondingly. This issue becomes a showstopper to employ homogenization method to design 3-D structures. For example, for a 3-D domain with a size 3x6x5 from extruding the 2-D domain shown in Figure 2.7 in a depth of 5, around 80000 cubes are

required to fill the space and 80000 design variables should be used. Homogenization method is rarely utilized to solve 3-D structural optimization problems. Therefore, homogenization method is computationally prohibited to design large cellular structures.

2.4 Research Issues and Possible Solutions

Both methods are not sufficient to accurately analyze or systematically design adaptive cellular structures. Therefore, unit truss, a new unit cell, is proposed to represent and analyze cellular structures. Unit truss consists of the central node at a joint and the half-struts connected to the central node. Unit truss approach is a unit cell (microstructure) approach as homogenization method. However, the size of unit truss is in mesoscopic scale and much larger than the unit cells used in homogenization method. Similar to other unit cell approaches, four research issues are raised in terms of representation, analysis, manufacturing and synthesis.

The research question is “How can adaptive cellular structures be accurately analyzed, efficiently created, and systematically designed?” The hypothesis to answer the research question is “Unit truss approach can be developed and used to accurately analyze, efficiently create, and systematically design adaptive cellular structures via geometric modeling, continuum mechanics, finite element method, optimization techniques, and additive fabrications.” Four research issues related to structural design are raised, representation, analysis, manufacturing, and synthesis. The issue of “representation” is about how to represent material distribution to facilitate the design. The issue of “analysis” is about how to analyze adaptive cellular structures. The issue of “manufacturing” is about how to manufacture cellular structures and consider their manufacturability in design. The issue of “synthesis” is about how to systematically design adaptive cellular structures. Each research issue will be discussed in one of the

following subsections, where a possible solution will be proposed to address each research issue.

2.4.1 Research Issue 1: Representation

It is impossible to represent conformal cellular structures with a few shape parameters. As discussed in the last section, limitations are present in ground truss approach and homogenization method. Our solution for representation is to use unit trusses as subdomains (microstructures) to represent the entire design domain. Unit truss represents structures' joint and consists of one central node and the half-struts connected to this central node. Unit trusses are parameterizable, but in various topologies and sizes. Ground truss approach and homogenization method are leveraged to develop the proposed unit truss approach. Unit truss is used as unit cell similar to homogenization method. However, unit truss is a real unit cell, not an artificial one. The tasks are to develop conformal topology for adaptive cellular structure and to formulate unit trusses.

Issue 1: How can the material distribution of adaptive cellular structures be represented to support their design and analysis?

Solution 1: The material distribution of adaptive cellular structure (design domain) can be represented by parameterizable unit trusses (subdomains).

2.4.1.1 Microstructure: Unit Truss

Unit truss shown in Figure 2.14 is an alternative microstructure suited for topology optimization of cellular structures. Using unit truss as microstructure can directly bring such advantages as analysis accuracy and efficiency since the geometries between cellular structures and truss structures are inherently similar.

In this research, unit truss is used to replace the microstructures in homogenization method. An array of three unit trusses is shown in Figure 2.12. The size of unit trusses is larger than regular microstructures in homogenization method (Bendsoe 1995), but smaller than truss elements used in ground truss approach (Rozvany 1997). The selection of unit truss size is not discussed in this research. However, the advantages of using unit trusses are demonstrated in terms of geometric modeling and mechanics analysis.

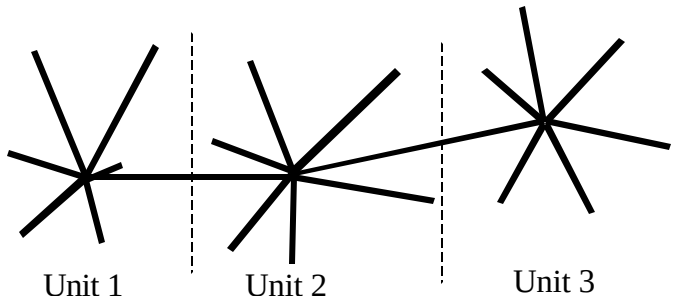

Figure 2.12 An Array of 3-D Unit Trusses

2.4.1.2 Topology Representation

The main task of the topology representation is to identify the rules to form unit trusses. The research issues that need to be investigated regarding the topology representation include: what unit trusses are appropriate, how the starting truss topology can be formed. The unit trusses are parametrically patterned to represent the design domain. A 2-D cellular (truss) structure and its unit trusses are shown in Figure 2.13. Unit trusses are the microstructured solids for mechanics analysis and represented as hexagons. The shaded hexagon in Figure 2.13 is a typical unit truss. The boundary microstructures are either one half or one quarter of regular hexagons. Each strut belongs to two neighboring unit trusses. The strain components of microstructure, shown as hexagons, include both translational displacements and rotational displacement.

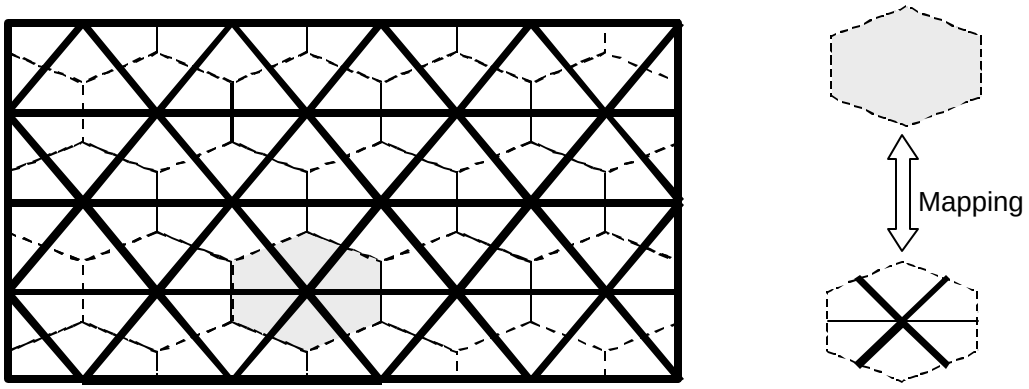

(a) 2-D Triangular Truss (b) Unit Truss

Figure 2.13 Representation of Triangular Truss with Unit Truss

The following are the advantages of using unit truss as microstructure to represent the topology of structures:

- Better analysis accuracy: the mechanics model of unit truss can more accurately describe the physical behavior of cellular structures. The geometric overlaps and interactions between neighboring struts can be considered. Some geometric features, such as rounding and fillet at joints can be estimated in the mechanics model.
- Better computational efficiency: compared to homogenization method, fewer microstructures are used and the required computation resources are reduced significantly. This is more evident for 3-D structure problems.
- Higher design reliability: the microstructure method converts layout problem to a sizing problem by varying the element sizes during optimization. The design variables can be continuously changed instead of determining an on-off point parameter. Moreover, the manufacturing limitations of cellular structures can be considered at the design stage.

2.4.2 Research Issue 2: Mechanical Analysis

Ashby, Huntington, Gibson and their colleagues developed various approaches to analyze lightweight cellular structures (Deshpande, Fleck et al. 2001; Wallach and Gibson 2001; Xue and Hutchinson 2003). Ashby and his colleagues identified the unit cell of octet-truss (combination of octahedral cell and tetrahedral cell) and derived its effective mechanical properties (e.g., elastic stress-strain relationship) for mechanics analysis. However, in Ashby's model, structures are still considered as pin-jointed trusses and bending are neglected. Eringen developed micropolar theory to analyze 2-D elastic cellular honeycombs using microstructures with coupled stresses and micro-rotations in addition to the usual components of stress and strain (Eringen 1971; Eringen 1999). In micropolar elasticity (Nowacki and International Centre for Mechanical Sciences. 1970; Eringen 1971), an additional independent deformation variable, the micro-rotation field, is introduced to represent the micro rotation gradient (Wang and Stronge 1999; Yang, Lee et al. 2003). This rotation field variable distinguishes micropolar solids from regular continuum solids. Kumar and McDowell developed generalized continuum representation of two-dimensional periodic cellular solids and treated cellular materials as micropolar continua (Kumar and McDowell 2004). Leveraged from micropolar theory, unit truss is proposed to analyze adaptive cellular structures. Not only axial forces are analyzed, but also shearing, bending, torsion, and nonlinearity in cellular structures can be considered. Unit truss approach does not consider the coupling between stresses and moments as opposed to micropolar theory. The tasks are to formulate the mechanics model of unit truss with the consideration of bending, torsion and nonlinearity, and to analyze entire structures via finite element method.

Issue 2: How can adaptive cellular structures be analyzed?

Solution 2: Unit trusses can be used as microstructures to analyze adaptive cellular structures via continuum mechanics and finite element method.

2.4.2.1 Characteristics of Unit Truss

Unit truss is parameterizable, analyzable, patternable and manufacturable. In R^2, each end point of a connected element has 3 degrees of freedom (DOFs): horizontal displacement, vertical displacement, and in-plane rotation. In R^3, each has 6 DOFs including 3 displacements and 3 rotations. In Figure 2.14, the author shows a 2-D unit truss, which has $3\times(N+1)$ DOFs. $\underset{\sim}{f}^{(i)}$ are the external forces acting on the node and the end points of the i^{th} element in R^3. The design variables of unit trusses in a given topology are strut geometric parameters, such as diameter for uniform cylindrical struts, two end diameters for conic struts, or length and width for uniform rectangular elements.

As shown in the stress graph of a sample unit truss in Figure 2.15, the strain and stress around the nodes are usually most complicated and relatively larger in truss structures because there are considerable inter-element interactions and larger bending moment around joints (central nodes). $\underset{\sim}{u}^{(i)}$ is the nodal displacement of the i^{th} element in R^3. Compared with the other areas in struts (beams), the deformation of the cross-section plane at the middle is most least complex and mostly remain planar, and the stress and strain states are relatively simpler compared to those areas around the joints. To reduce the modeling errors caused by the strut interactions in a largest extent, it is more appropriate to divide the truss at the elements' middle planes instead of the joints.

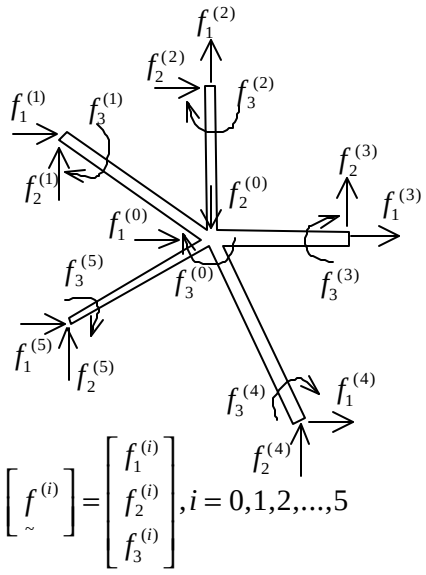

Figure 2.14 A Typical Unit Truss Model

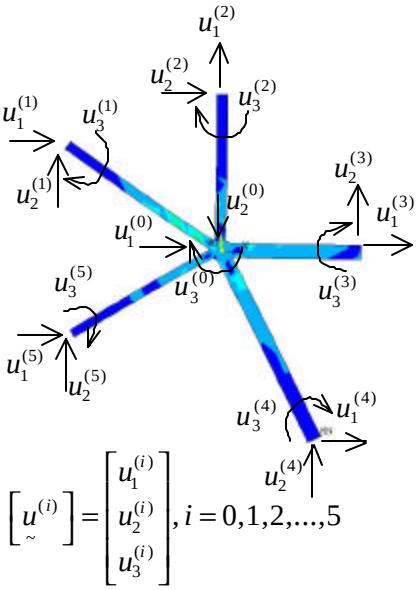

Figure 2.15 Stress Graph of a Unit Truss

2.4.2.2 Analytically Modeling Unit Truss

Continuum mechanics theory is applied to derive mechanics model of unit trusses for both linear and non-linear elastic deformations. With finite element methods, unit trusses are used as the finite elements and assembled to analyze entire structures.

Beam theory is used to derive the mechanics model of unit truss. Struts of cellular structures are assumed to be simple beams. A generalized mechanics model of unit truss is shown as Equation 2.8. $\underset{\sim}{\Psi}^{(m)}$ is the local stiffness tensor of the m^{th} unit truss in the global coordinate system. $\underset{\sim}{U}^{(m)}$ denote the displacements and $\underset{\sim}{F}^{(m)}$ denote forces on the m^{th} unit truss. $\underset{\sim}{u}^{(i)}$ and $\underset{\sim}{f}^{(i)}$ are displacements and forces referred in Figure 2.14 and Figure 2.15.

$$\underset{\sim}{\Psi}^{(m)} \cdot \underset{\sim}{U}^{(m)} = \underset{\sim}{F}^{(m)} \tag{2.8}$$

$$\left[\underset{\sim}{U}^{(m)}\right] = \begin{bmatrix} \left[\underset{\sim}{u}^{0}\right] \\ \left[\underset{\sim}{u}^{1}\right] \\ \vdots \\ \left[\underset{\sim}{u}^{N}\right] \end{bmatrix}^{(m)}, \left[\underset{\sim}{F}^{(m)}\right] = \begin{bmatrix} \left[\underset{\sim}{f}^{0}\right] \\ \left[\underset{\sim}{f}^{1}\right] \\ \vdots \\ \left[\underset{\sim}{f}^{N}\right] \end{bmatrix}^{(m)} \tag{2.9}$$

$$W_{in}^{(m)}(\underset{\sim}{u}) = \int_{\Omega^{(m)}} \frac{1}{2} \underset{\sim}{e}(\underset{\sim}{u}) : \underset{\sim}{E}^{(m)} : \underset{\sim}{e}(\underset{\sim}{u}) d\Omega^{(m)} \tag{2.10}$$

Some geometry features, such as rounding and chamfer, can influence the accuracy of analytical models. Some correcting items can be derived and added to elasticity tensor $\underset{\sim}{E}^{(m)}$, and the resulting elasticity tensor is $\underset{\sim}{\tilde{E}}^{(m)}$ as shown in Equation 2.11. Using the results of the finite element analysis, the coefficients $\underset{\sim}{a}^{(m)}$ and $\underset{\sim}{R}^{(m)}$ can be evaluated using linear regression (Neter, Kutner et al. 1996). $\underset{\sim}{a}^{(m)}$ and $\underset{\sim}{R}^{(m)}$ are functions of the shape variables under particular loads.

$$\underset{\sim}{\tilde{E}}^{(m)} = \underset{\sim}{a}^{(m)} : \underset{\sim}{E}^{(m)} + \underset{\sim}{R}^{(m)} \qquad 2.11$$

2.4.2.3 Analysis of Whole Structures

The entire system can be analyzed by mathematically assembling unit trusses. The energy bilinear form of the whole structural system is shown as Equation 2.12. M denotes the total number of unit trusses in the entire structural system. Topology synthesis by using analytical models is much faster than using numerical models.

$$W_{in} = \sum_{m=1}^{M} W_{in}^{(m)}(\underset{\sim}{u}) = \sum_{m=1}^{M} \int_{\Omega^{(m)}} \frac{1}{2} \underset{\sim}{e}(\underset{\sim}{u}) : \underset{\sim}{\tilde{E}}^{(m)} : \underset{\sim}{e}(\underset{\sim}{u}) d\Omega^{(m)} \qquad 2.12$$

2.4.3 Research Issue 3: Manufacturing

The issue about the cellular structure manufacturing is divided into two sub-issues. One is related to manufacturing process and the other is related to design process. It is necessary to investigate the state-of-art manufacturing processes and identify the manufacturing limitations. The manufacturing rules will be formulated and the manufacturability will be considered at the design stage. The tasks are to investigate the potential manufacturing processes, to identify the manufacturing rules, and to consider the manufacturing limitations during design synthesis.

Issue 3: How can adaptive cellular structures be manufactured?

Solution 3: The manufacturing rules of adaptive cellular structures can be formulated and the manufacturing limitations can be considered at the design stage.

2.4.3.1 Manufacturing Challenges and Additive Fabrication

The geometries of designed adaptive cellular structures are relatively complex and cannot be fabricated by the conventional manufacturing processes, such as machining and welding. Additive fabrication processes are utilized to manufacture

cellular structures. Additive fabrication has the unique capabilities to produce virtually arbitrary complex geometry compared to the traditional manufacturing processes (Diez 2001; Wang 2001). Additive Fabrication processes build parts by adding material, as opposed to subtracting material from a solid object. Typical processes include Stereolithography, Selective Laser Sintering, and so on (Jacobs 1996; Prinz, Atwood et al. 1997; Dutta, Prinz et al. 2001). They need minimum human intervention to operate and no part-specific tooling or fixtures. Truss structures and compliant mechanisms are two classes of shapes that can take advantage of the unique capability of these processes to produce complex geometries. Final functional metallic parts built with additive fabrication processes have been demonstrated (Daily, Lees et al. 1997; Wang 2001).

2.4.3.2 Identifying the Manufacturing Rules and Considering the Manufacturing Limitations at the Design Stage

The first issue is to identify the manufacturing rules of additive fabrication processes and investigate their limitations to manufacture cellular structures in terms of part geometric complexity, materials, and processes. It is essential to assess the effect of manufacturing processes on the part performance and form the manufacturing rules to fabricate cellular structures. These rules can be utilized to identify the ranges of design variables and consider the manufacturing limitations at the design stage.

The manufacturing limitations have great impacts on the design of cellular structures. The manufacturing rules need to be incorporated into the design synthesis process to achieve a robust and reliable design. Design for manufacturing can be realized by considering the manufacturing limitations as the bounds of design variables or the design constraints during design synthesis.

2.4.4 Research Issue 4: Design Synthesis

The design synthesis of lightweight structures and compliant mechanisms is a large-scale problem with discreet ranges of design variables. The design of compliant mechanisms can have multiple nonlinear objectives and concave design space. A design synthesis method using engineering optimization algorithms should be developed to systematically design adaptive cellular structures. A search algorithm should be identified to systematically find solutions to nonlinear, concave, and large-scale problems. The tasks are to formulate the design synthesis of adaptive cellular structure, to identify a suitable search algorithm, and to implement the design synthesis.

Issue 4: How can adaptive cellular structures be systematically designed?

Solution 4: Engineering optimization technique can be leveraged to systematically design adaptive cellular structure by integrating representation, analysis, and manufacturing.

2.4.4.1 Challenges of Design Synthesis for Cellular Structures

Challenges of the design synthesis include a huge number of design variables, multiple design objectives, nonlinearity, and factor variations. Cellular structures are represented by topologies, which are patterns of unit trusses. The strut sizes of unit trusses are design variables and modifiable to obtain the best structure. This design problem of adaptive cellular structures has a huge number of design variables. A multiple-criterion problem should be formulated since design objectives are to minimize stiffness or maximize compliance, to minimize weight, to obtain a desired natural frequency, to minimize fatigue stress, and so on. Because of the complexity of geometry and material properties, and the nonlinearity of constitutive stress/strain relations, the design synthesis of cellular structures is a nonlinear problem. Potential variations can be

such factors as operating environment, manufacturing process, and design specifications.

2.4.4.2 Design Synthesis Method For Large-scale, Multi-objective Problems

A desired design synthesis method should integrate topology representation, structural analysis, and manufacturability consideration to design cellular structures. Design objectives can be stiffness, compliance, weight, and other structural attributes. Constraints include manufacturing limitations, boundary conditions, stress, etc. Design variables are the dimensional parameters of structures and other controllable parameters related to manufacturing. Outputs are topology and strut sizes. The resulting design specifications will be used to generate the final geometric information for manufacturing.

2.4.5 Connections between Research Issues

The research issues of this dissertation are interrelated. Research Issue 1 (representation) is fundamental and supports the other three research issues (analysis, manufacturing and synthesis). Unit truss is proposed to represent the material distribution as microstructure by leveraging the concepts of ground truss approach and homogenization method. Unit truss is used as element for finite element method of mechanics analysis. Research Issue 2 (analysis) focuses on the development of the mechanics model of unit truss and analysis of the entire structure. Research Issue 3 (manufacturing) identifies the manufacturing rules, particularly for additive fabrication processes. Research Issue 4 (synthesis) integrates representation, analysis and manufacturing to systematically design adaptive cellular structures.

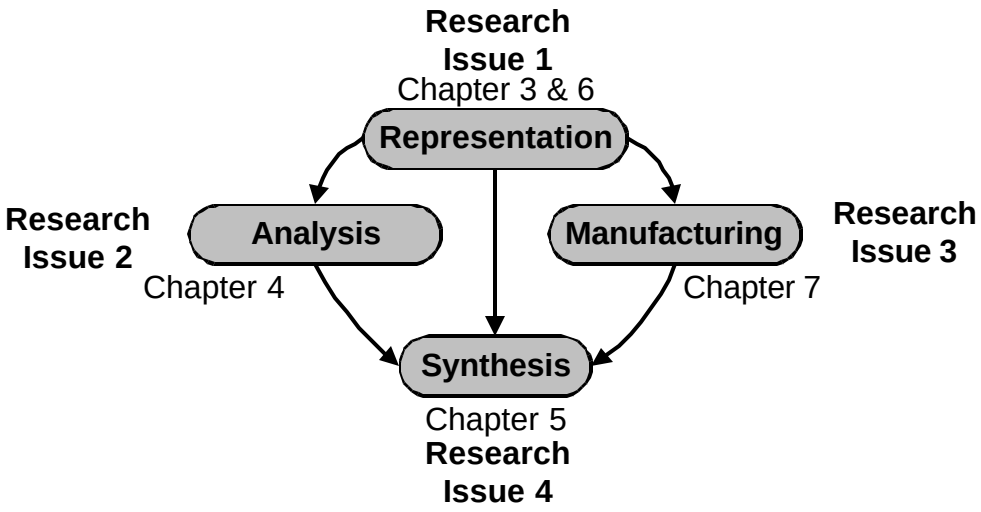

Figure 2.16 Connections Between Research Issues

2.5 Overview of Cellular Structure Design Process

There are four steps in the design process of cellular structures including lightweight structures and compliant mechanisms as shown in Figure 2.17. The inputs of the design process are the design domain and requirements. The first step (discussed in Chapter 3) is to create a conformal topology, which is adaptive to the design domain. The conformal topology is the starting topology for design synthesis (Chapter 5) to systematically design adaptive cellular structures for desired requirements, such as stress, deflection, and material volume. The design synthesis integrates mechanics analysis (Chapter 4) and iterates strut sizes' modification and mechanics analysis to find solutions. The resulting topology and size specification are the inputs for geometric modeling (Chapter 6) of cellular structures. The resulting geometric model is used for manufacturing (Chapter 7).

In Chapters 3~7, the author adapts the relevant constructs (geometric modeling, continuum mechanics and finite element method, engineering optimization, and additive fabrication) to solve the research issues ("representation", "analysis", "manufacturing",

and “synthesis”). The constructs are integrated into the new unit truss approach for designing adaptive cellular structures in Chapter 5.

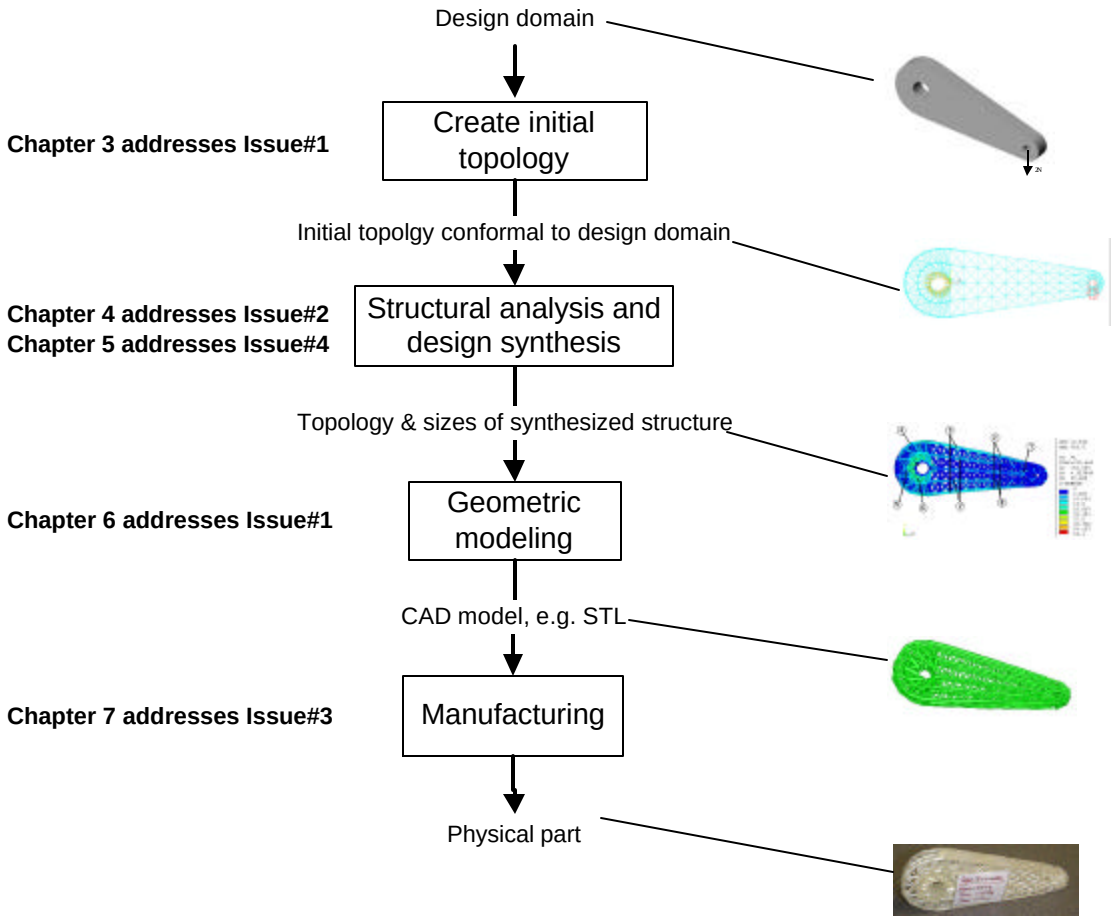

Figure 2.17 Design Process of Cellular Structures

2.6 Chapter Summary

This chapter investigates the current research status of cellular structures including lightweight structures and compliant mechanisms. It theoretically validated that conformal cellular structures are superior to uniform cellular structures. Two possible methods of designing cellular structures, ground truss approach, and homogenization method, were discussed. Unit truss approach is proposed to facilitate the design of cellular structures. Four research issues, which address representation, structural

analysis, design synthesis, and manufacturing respectively, were raised. A solution was proposed to address each research issue and the tasks are identified. The research hypothesis will be tested and validated by searching for solutions to these four research issues, in another words, developing the method constructs for the proposed unit truss approach. These method constructs are integrated together into a unit truss approach to design adaptive cellular structures.

CHAPTER 3

GEOMETRIC MODELING FOR CREATING CONFORMAL TOPOLOGY FOR ADAPTIVE CELLULAR STRUCTURE

In this chapter, the author partially addresses the "representation" issue raised in Section 2.4 with the development of two approaches to create conformal topology. The presentation of Chapter 3 follows Figure 3.1. Geometric modeling is adapted to create conformal topology for adaptive cellular structures in the specified design domain. Conformal topology is used as the starting topology for the design synthesis of lightweight truss structure and compliant mechanism. Two approaches are developed.

A parametric modeling approach is presented to create the conformal topology, which conforms to the part's shape. The approach presented in this chapter utilizes NURBS (Nonuniform Rational B-Spline) surfaces to approximate the part surfaces and trivariate NURBS volume in which the 3-D truss structure is created. Parametric truss primitives are composed using a structured mapped meshing method in order to create 3-D trusses. Truss topologies can be created for 2-D trusses and 3-D trusses. This approach requires decomposition of part surfaces into bicubic NURBS patches, construction of approximating NURBS surfaces, and solid modeling of the truss structures. A supplementary approach using meshing technique of finite element method is also presented to create the conformal truss topology. A comparison of these two approaches in terms of their advantages and disadvantages will be discussed. The focus of Chapter 3 is shown in Figure 3.2 and to create initial conformal truss topology for structural analysis and design synthesis.

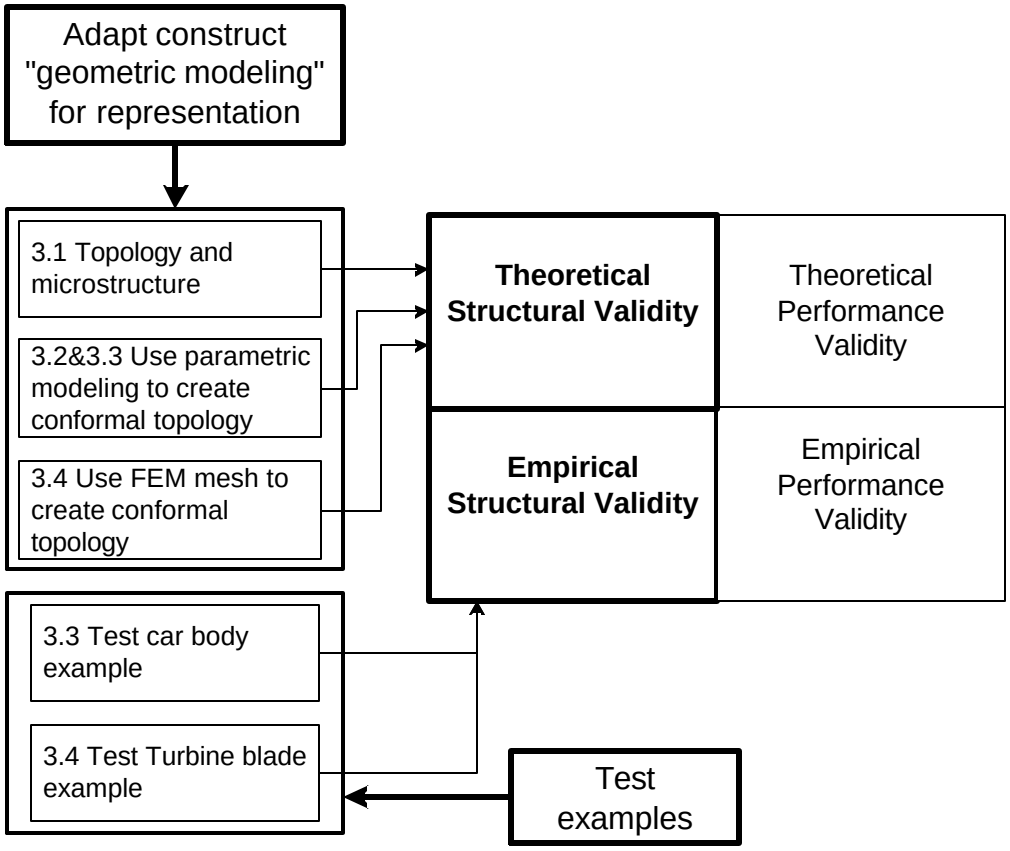

Figure 3.1 Relationship between Chapter 3 and Validation Square

3.1 Topology and Microstructures of Conformal Cellular Structures

In this section, the author discusses the initial topologies of various truss structures and their primitives (microstructures). Topology defines the connectivity between nodes in a structure. The struts of a conformal topology are adaptively oriented and sized with relatively uniform lengths and angles between struts. Trusses can be used as the internal structure of a part and should fit in the part's space (Fuller 1975; Wang and Rosen 2002). The design of compliant mechanism starts with an initial truss topology that should fit in the design domain.

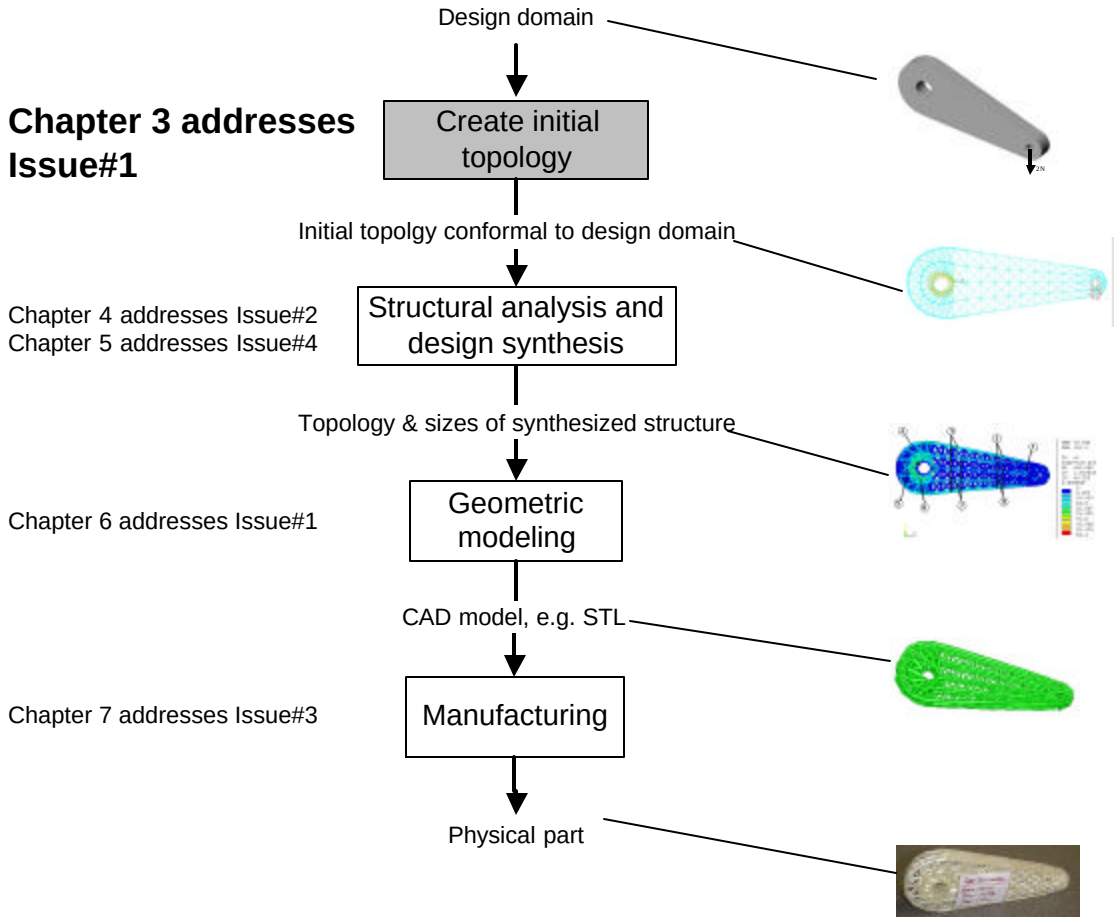

Figure 3.2 Focus of Chapter 3 in the Design Process of Cellular Structures

An example of a cylindrical surface reinforced with a two-layer conformal truss structure is shown in Figure 3.3. The truss primitives are repeated in a pattern to generate the truss structure, as shown in Figure 3.4 and Figure 3.5. Different truss primitives and patterns can generate different types of truss structures. For example, the octet truss shown in Figure 3.3 can be produced by patterning a tetrahedron shown in Figure 3.4. A Kelvin foam structure is produced using a different primitive and patterning method, as shown in Figure 3.5.

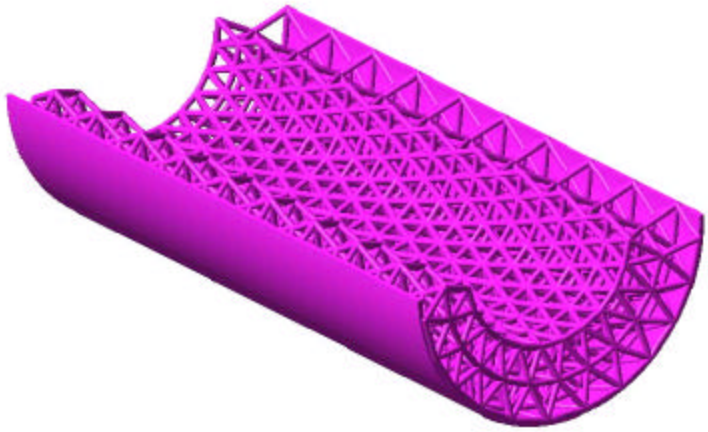

Figure 3.3 A Conformal Triangular Truss

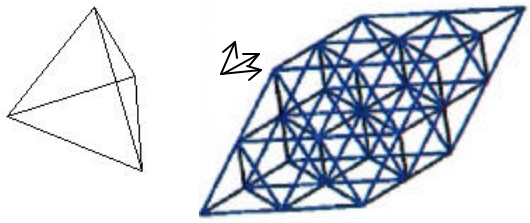

Figure 3.4 Octet Truss and Tetrahedron Microstructure

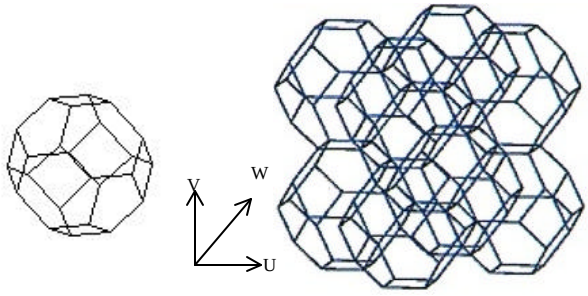

Figure 3.5 Kelvin Foam Truss and Truncated Octahedron Microstructure

Truss topology contains information about truss vertex positions and strut connectivity (**strut topology**) (Wang 2001). A truss **vertex**, or called **node**, is shown in Figure 3.6. The cylindrical shapes that connect vertices are called truss **struts** or **elements**. The truss primitives introduced in Section 3.1 are composed of truss vertices and struts.

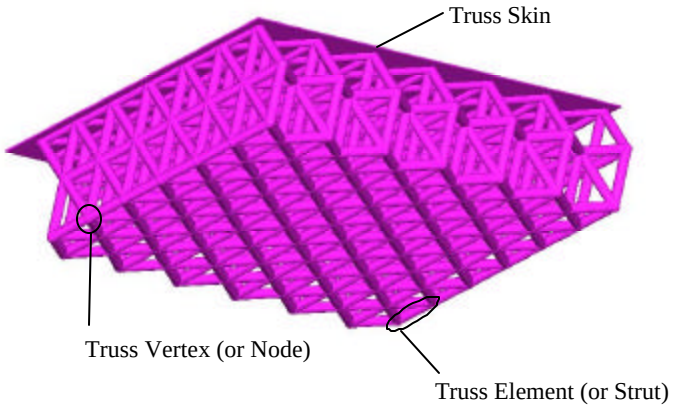

Figure 3.6 A Uniform Truss Structure

3.2 An Overview of Parametric Modeling Approach for Conformal Topology

The generation of uniform trusses is arguably simpler. Daily, *et al*. (Daily, Lees et al. 1997) created a pattern of truss struts and then repeated it in every direction to form a uniform truss structure as shown in Figure 3.6. Using their method, a void in a part could be filled easily with a latticework of repetitive truss pattern. However, this is not as structurally sound as a conformal truss, since the boundary truss nodes may not be located on the part boundaries and all truss struts are oriented into a few fixed directions. A conformal truss structure that conforms to the part's shape would fit inside the part and better distribute forces within the part (Wang 2001). The conformal truss in Figure 3.3 has boundary vertices that are located on the outer skin. Many of the truss struts are oriented in radial directions relative to the cylindrical shape, while others form triangles that stiffen the part circumferentially. Therefore, conformal trusses provide better truss configurations than uniform trusses and they tend to utilize material more efficiently.

The main concept in generating conformal trusses is illustrated in Figure 3.7. The deformed truss shape (conformal truss) can be transformed from the initial shape

(uniform truss) in a one-to-one mapping fashion by relocating the positions of the truss vertices. Vertex B_i corresponds to Vertex A_i (i=1,2,3…13). Parametric curves can be used to represent the boundary curves shown in the dashed lines. Vertices $B_{1\text{-}13}$ are located on a parametric surface. The strut connectivity of the truss vertices on the deformed shape is the same as that of the initial shape. The boundary truss vertices are located on the part surface and the resulting truss structure conforms to the part shape.

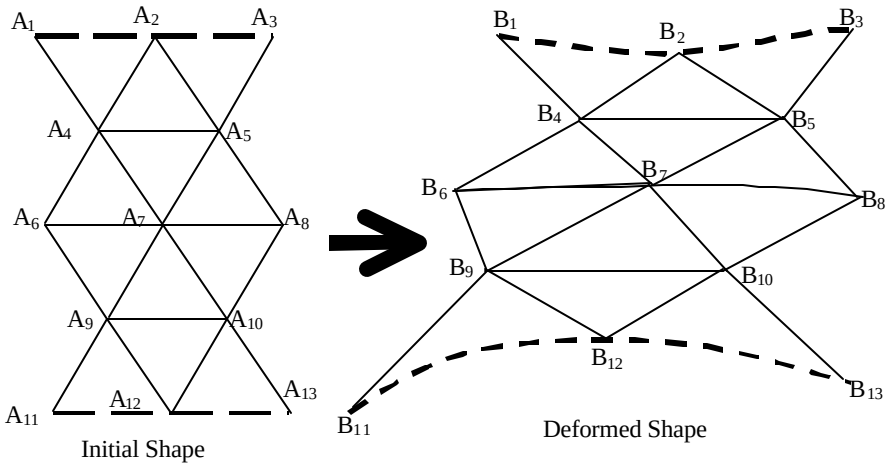

Figure 3.7 Developing Truss Topology by Mapping

There are inherent similarities between truss creation and mesh generation for finite element methods, which divides a geometric domain into small subregions (Reddy 1993). In the creation of truss structures, the subregions are replaced with truss primitives to remove material from the solid objects. To utilize the structured mesh generation (Owen 1998), the part geometry must be represented by a series of algebraic equations, and vertices/nodes are generated based on algebraic interpolation methods (Soni 2000). For both truss creation and mesh generation, geometry decomposition may be required for complicated geometric configurations, and the transitions between surface patches must be considered.

Our approach to truss topology generation utilizes the mapped meshing methods for conformal trusses. Various computer-aided design methods can be used to design and represent the truss structure. Our approach is based on parametric modeling techniques. Therefore, our truss generation process is independent of any coordinate system. It is capable to create truss structures for the parts with nonplanar surface, which is not easily represented by an ordinary nonparametric function. The method presented in this chapter is:

I. Approximate part surfaces with parametric NURBS surface patches and then construct parametric trivariate volume.

II. Generate truss topology for the parametric NURBS volume using the parametric modeling techniques:

    a. Compute vertex positions and create strut topology for each 2-D NURBS surface patch.

    b. Compute vertex positions and create strut topology for the 3-D NURBS volume.

Each pair of parametric NURBS patches encloses a 3-D NURBS volume. In many cases, the part surfaces are modeled using trimmed NURBS models. In this work, we use bicubic NURBS patches, which are extensively used in geometric modeling, such as the popular geometric kernel, ACIS. The following sections describe how to use bicubic NURBS patches to develop the trivariate parametric volume and generate the truss topology. In Section 3.3, the author will present the parametric modeling technique to create the truss topology. In Section 3.3.4, the author will discuss the formulation of NURBS surface approximating the part surface and the generation of thin skin, particularly for lightweight truss structure.

3.3 Creating Topology with Parametric Modeling

The parametric modeling technique presented in this section is used to create initial truss topology. The part surface is approximated by NURBS (Nonuniform Rational B-Spline) (Piegl and Tiller 1995) surfaces and then the truss topology is created between these NURBS surfaces. The part sections to be filled with truss structures are defined parametrically in our work as trivariate NURBS solids. The top and bottom surfaces of these NURBS solids are bicubic NURBS surface patches that approximate the actual part boundaries. Alternatively, the bottom surface may be an offset of the top surface. After the trivariate solid is developed, the truss topology is formed from filling the solid with the parametric truss primitives. Our two-step method to generate truss structures within a CAD model of a part is presented. The scope of the method is also described.

3.3.1 NURBS - Nonuniform Rational B-Spline

A brief introduction to NURBS (Nonuniform Rational B-Spline) surfaces will be provided since they were selected as the primary parametric surface used in this work. The underlying algebraic representation of the $(k-1)^{th}$ degree NURBS surface is written as Equation 3.1 (Mortenson 1997).

$$p(u,w) = \frac{\sum_{i=0}^{m}\sum_{j=0}^{n} h_{ij}\, p_{ij} N_{i,k}(u) N_{j,k}(w)}{\sum_{i=0}^{m}\sum_{j=0}^{n} h_{ij} N_{i,k}(u) N_{j,k}(w)} \qquad 3.1$$

where,

p_{ij} – $(m+1)\times(n+1)$ control points

h_{ij} – Weights to pull the NURBS toward the corresponding control points

$N_{i,k}(u), N_{j,k}(w)$ – Basis functions for B-Spline

u, w – Parameters

$$N_{i,1}(u) = \begin{cases} =1 & \text{if } t_i \le u < t_{i+1} \\ =0 & \text{otherwise} \end{cases}$$

and

$$N_{i,k}(u) = \frac{(u - t_i)N_{i,k-1}(u)}{t_{i+k-1} - t_i} + \frac{(t_{i+k} - u)N_{i+1,k-1}(u)}{t_{i+k} - t_{i+1}} \qquad 3.2$$

where,

t_i – kont values

When $k = 4$ and $h_i = 1$, the NURBS surface becomes a 3rd degree or bicubic rational NURBS surface and used as a common parametric surface in geometric modeling. A bicubic NURBS surface patch is defined by $(m+1)\times(n+1)$ control points. Its matrix form is given by Equation 3.3, where U and W are the monomial bases containing the parameters u and w $u, w \in [0,1]$, B is the matrix containing the sixteen control vertices B_{ij} $(i = s-1, s, s+1, s+2; j = t-1, t, t+1, t+2)$, and M_B denotes the bicubic NURBS basis transformation matrix (Piegl and Tiller 1987; Piegl and Tiller 1995; Mortenson 1997). In this research, the knot vector is set as $\{t_i\} = \{0,0,\cdots,0,1,1,\cdots,1\}$.

$$p_{st}(u,w) = UM_S BM_S^T W^T$$

where,

$s \in [1 : m-2]$

$t \in [1 : n-2]$ 3.3

A **surface point** is defined as a point located on a part surface. The 16 control vertices B_{ij} $(i = s-1, s, s+1, s+2; j = t-1, t, t+1, t+2)$ of a bicubic NURBS patch can be determined from 16 surface points in a closed-form manner (Mortenson 1997) as shown in Equation 3.4 by assuming that the surface points are evenly distributed in the parametric space, that is, $u \in \{0,1/3,2/3,1\}$ and $w \in \{0,1/3,2/3,1\}$. Matrix P contains the surface points measured from the part surface.

$$B = L_s L_b P L_b^T L_s^T \tag{3.4}$$

$$L_b = \begin{bmatrix} 1 & 0 & 0 & 0 \\ \frac{8}{27} & \frac{4}{9} & \frac{2}{9} & \frac{1}{27} \\ \frac{1}{27} & \frac{2}{9} & \frac{4}{9} & \frac{8}{27} \\ 0 & 0 & 0 & 1 \end{bmatrix}, L_s = \begin{bmatrix} -1 & 2 & -\frac{7}{3} & -\frac{2}{3} \\ 2 & -1 & \frac{2}{3} & \frac{1}{3} \\ -1 & 2 & -\frac{1}{3} & -\frac{2}{3} \\ 12 & -11 & \frac{22}{3} & \frac{17}{3} \end{bmatrix} \tag{3.5}$$

$$P = \begin{bmatrix} P_{11} & P_{12} & P_{13} & P_{14} \\ P_{21} & P_{22} & P_{23} & P_{24} \\ P_{31} & P_{32} & P_{33} & P_{34} \\ P_{41} & P_{42} & P_{43} & P_{44} \end{bmatrix} \tag{3.6}$$

The resulting NURBS surface is an approximation of the original part surface. The approximation accuracy is governed by the number and the measuring of $(m+1)\times(n+1)$ surface points. These surface points interpolate the NURBS surface and can be used to calculate the control points. The control points can be used to evaluate any point on the NURBS surface by giving u and w parameters with Equation 3.1.

The parametric modeling technique will be used to create initial truss topology. The part surface is approximated by NURBS (Nonuniform Rational B-Spline) (Piegl and Tiller 1995) surfaces and then the truss topology is created between these NURBS surfaces. The part sections to be filled with truss structures are defined parametrically in our work as trivariate NURBS solids. The top and bottom surfaces of these NURBS solids are bicubic NURBS surface patches that approximate the actual part boundaries. Alternatively, the bottom surface may be an offset of the top surface. After the trivariate solids are developed, the truss structures are formed by filling these solids with the parametric truss primitives.

3.3.2 Creating a 2-D Truss Topology

This subsection describes the application of the parametric modeling techniques to create a 2-D truss topology. A triangular truss for a 2-D area is shown in Figure 3.8. This area is bounded by four cubic NURBS curves, and the whole area is represented by a bicubic NURBS surface. Triangles are the primitives of this 2-D triangular truss structure. These primitive triangles in various orientations and shapes are arranged in the u and w directions and connected at the truss vertices one by one. The coordinates of all vertices in the triangular truss can be calculated using Equation 3.3 by giving values to u and w. The values for u and w are determined by the primitive spacings (Δu and Δw) in parametric space, which are given as Equation 3.7. U and W are the numbers of primitives in the u and w directions.

$$\Delta u = 1/U$$
$$\Delta w = 1/W \qquad 3.7$$

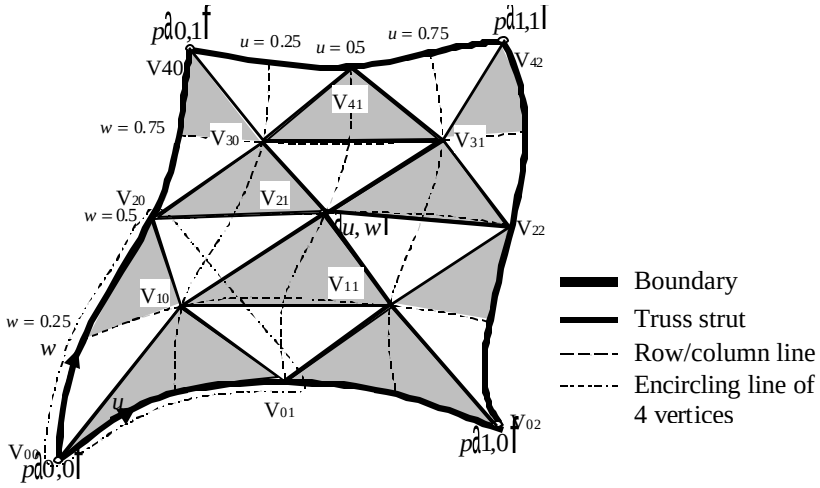

Figure 3.8 Triangular Truss Topology for a 2-D Area

In Figure 3.8, the truss primitive spacings are $\Delta u = 1/2$ and $\Delta w = 1/4$ since there are two columns of triangles in the u direction and four rows of triangles in the w

direction according to the layout of the primitive triangles. Each row of the triangles is shifted from the neighboring row by $\Delta u / 2$ in the *u* direction.

V_{ij} represents a truss vertex in the *i*th row and the *j*th column of vertices, where both *i* and *j* start at 0. For this triangular truss topology, V_{01} is shifted from V_{00} by Δu only in the *u* direction; V_{10} is shifted from V_{00} by $\frac{1}{2}\Delta u$ in the *u* direction and by Δw in the *w* direction; V_{20} is shifted from V_{00} by $2\Delta w$ only in the *w* direction. These four vertices are encircled with a closed dot-dash curve shown in Figure 3.8. Similarly, using V_{01}, we can compute the *u* and *w* values for V_{02}, V_{11}, and V_{21}. The *u* and *w* values of Vertex V_{00} are all equal to zero. By starting with V_{00} and propagating through the whole truss as shown in Figure 3.8, we can obtain the *u* and *w* values for all truss vertices similarly. Then by applying Equation 3.3, we can obtain all the truss vertex positions. The algorithm to calculate the truss vertex positions on a bicubic NURBS surface follows:

Algorithm 2D_VERTEX_POSITIONS
{
INPUT: $(m+1)\times(n+1)$ **control points, contained in Matrix** B **B, for a bicubic NURBS surface;**
INPUT: the primitive numbers, *U* and *W*, along *u* and *w* directions;
OUTPUT: Vertex Positions (x, y, z) contained in $p(V_{ij})$**;**

// Calculate the truss parameter spacing in *u* and *w* directions
$\Delta u = 1/U, \Delta w = 1/W$ **;**
// Set *u* and *w* parameters at 0th row and 0th column to 0
Vertex V_{00}**:** $u(V_{00}) = w(V_{00}) = 0$**;**
// Calculate all the *u* and *w* parameters for the vertices in
// The first even number's rows
for $i = 0; i \le W; i = i + 2$ {
  for $j = 0; j \le U - 1; j = j + 1$ {
    Vertex V_{ij+1}**:** $u(V_{ij+1}) = u(V_{ij}) + \Delta u, w(V_{ij+1}) = w(V_{ij})$**;**
    Vertex $V_{i+1\,j}$**:** $u(V_{i+1\,j}) = u(V_{ij}) + \Delta u/2, w(V_{i+1\,j}) = w(V_{ij}) + \Delta w$**;**
    Vertex $V_{i+2\,j}$**:** $u(V_{i+2\,j}) = u(V_{ij}), w(V_{i+2\,j}) = w(V_{ij}) + 2\Delta w$**;**
  }
  // If the number of rows is odd, define *u* and *w* parameters
  // For the vertices in the last row

if *W* is odd {

Vertex V_{W0}**:** $u(V_{W0}) = 0, w(V_{W0}) = 1.0$;

for $j = 0; j \le U - 1; j = j + 1$

Vertex V_{WU}**:** $u(V_{Wj+1}) = u(V_{Wj}) + \Delta u, w(V_{Wj+1}) = 1.0$;

}

Vertex V_{WU}**:** $u(V_{WU}) = w(V_{WU}) = 1.0$

}

***//* Calculate the coordinates for all vertices using Equation 3.1**

for $i = 0; i \le W; i = i + 1$

for $j = 0; j \le U; j = j + 1$

$p(V_{ij}) = p(u(V_{ij}), w(V_{ij}))$;

}

Besides calculating the vertex positions, we need to obtain the strut topology, which describes the connectivity between the truss vertices. Parametric modeling techniques are extensively used to compute the vertex positions, but they are not necessary to create strut topology. Instead, we only need to completely discuss the connection situations. The strut topology can be obtained by linking the primitive triangles one by one, such as Triangle $\Delta V_{00}V_{10}V_{01}$, $\Delta V_{01}V_{11}V_{02}$, and $\Delta V_{10}V_{21}V_{11}$ in Figure 3.8. Some single struts do not belong to any complete triangle, such as struts $\overline{V_{10}V_{20}}$ and $\overline{V_{31}V_{40}}$. Hence, it is not convenient to export the strut topology triangle by triangle. Instead, polylines are constructed by linking one vertex by one vertex; the result is exported as the strut topology. For example, in Figure 3.8, the sets of truss vertices $(V_{00}, V_{10}, V_{01}, V_{11}, V_{02})$, $(V_{20}, V_{10}, V_{21}, V_{11}, V_{22})$, (V_{10}, V_{11}), and (V_{20}, V_{21}, V_{22}) are linked into polylines $\overline{V_{00}V_{10}V_{01}V_{11}V_{02}}$, $\overline{V_{20}V_{10}V_{21}V_{11}V_{22}}$, $\overline{V_{10}V_{11}}$, and $\overline{V_{20}V_{21}V_{22}}$ as the strut topology. There are two categories of polylines: straight polyline and waved polyline. The vertices on the straight polylines have identical *w* values, such as $\overline{V_{10}V_{11}}$, and $\overline{V_{20}V_{21}V_{22}}$. The waved polylines oscillate alternatively between vertices of the i^{th} row and the $(i+1)^{th}$ row, such as $\overline{V_{00}V_{10}V_{01}V_{11}V_{02}}$ and $\overline{V_{20}V_{10}V_{21}V_{11}V_{22}}$. The following algorithm generates the 2-D strut topology on a bicubic NURBS surface.

Algorithm CREATE_2D_STRUT_TOPOLOGY
{
INPUT: the primitive numbers, *U* and *W*, along *u* and *w* directions; truss vertices V_{ij} ;
OUTPUT: Strut Topology $Topo$ (an array of struts, each strut consist of a start vertex and an end vertex);

// Link truss vertices into straight polylines
for $i=1; i \le W-1; i=i+1$ {
for $j=0; j \le U-1; j=j+1$ {Add new edge $V_{ij}V_{i(j+1)}$ into $Topo$;}
if i is even, then {Add new edge $V_{i(U-1)}V_{iU}$ into $Topo$;}
}
// Link truss vertices into waved polylines
for $i=0; i \le W-1; i=i+2$ {
for $j=0; j \le U-1; j=j+1$ {Add new edges $V_{ij}V_{(i+1)j}$, $V_{(i+1)j}V_{i(j+1)}$ into $Topo$;}
for $j=0; j \le U-1; j=j+1$ {Add new edges $V_{(i+2)j}V_{(i+1)j}$, $V_{(i+1)j}V_{(i+2)(j+1)}$ into $Topo$;}
}
if W is odd {
for $j=0; j \le U-1; j=j+1$ {Add new edges $V_{(W-1)j}V_{Wj}$, $V_{Wj}V_{(W-1)(j+1)}$ into $Topo$;}
}
}

3.3.3 Creating a 3-D Truss Topology

The method to develop a 3-D truss topology is to start with a 2-D truss topology on the top and bottom surfaces, then linearly interpolate between them. The truss vertex positions and the strut topology are developed separately using a similar method that is used to generate the 2-D truss topology. In Figure 3.9, the author shows a truss structure developed between two bicubic NURBS patches, which enclose the space into a 3-D volume. Their control vertices are represented by $b_{ij\_g}(g=0.0; i=0,1,\cdots,m; j=0,1,\cdots,n)$ and $b_{ij\_g}(g=1.0)$ respectively. The top and bottom patches must not be too skewed or twisted. The space between these two patches is considered as a trivariate NURBS solid of degree $(k-1)\times(k-1)\times 1$. Intermediate bicubic NURBS patches are used to provide multiple layers of truss structures and linearly interpolate the two boundary patches. As shown in Figure 3.9, the truss vertices are located on the intermediate bicubic NURBS patches. In some cases, the truss struts on the boundary NURBS patches are not

created to avoid the truss structures protruding through the concave part surfaces. The other truss struts, such as those in the neighboring layer, will not cause protrusions because they are always between these two boundary surfaces as shown in Figure 3.9.

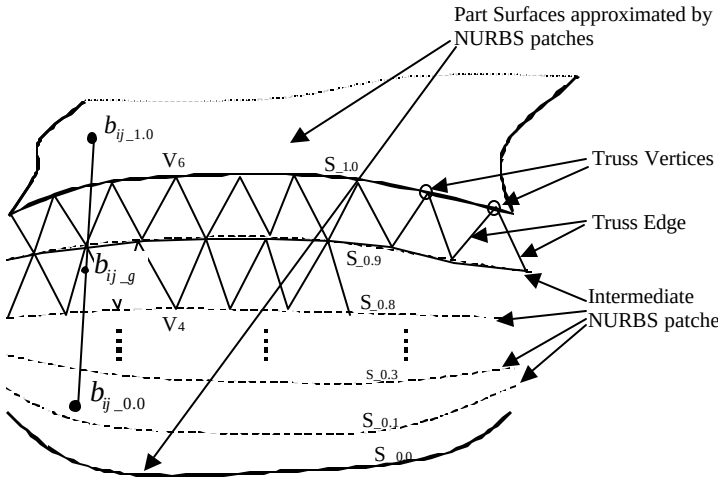

Figure 3.9 Truss Topology for a 3-D Volume

The coordinates of these control vertices are obtained using the given interpolation parameter v and the known control vertices on the part boundary surface. The intermediate bicubic NURBS surfaces are equally distributed in the parametric space between the top part surface $S_{\_1.0}$ and the bottom part surface $S_{\_0.0}$ as shown in Figure 3.9. The sixteen control vertices b_{ij_g} ($g \in [0.0,1.0]$) for each of these bicubic NURBS surfaces are located on the straight lines between the terminal control vertices known as b_{ij_0} and $b_{ij\_1.0}$, which are the control vertices for the top and bottom boundary part surfaces respectively. The parameter v ($\mathrm{v} = g$, for a particular layer) is given as $0, \Delta v, 2\Delta v, \ldots, \text{and } 1$, where Δv is the layer spacing in the v direction and is defined in Equation 3.8. Δv controls the size of the truss primitives in the V direction, such that :

$$\Delta v = 1/V \qquad 3.8$$

V is the number of primitives in the *v* direction. For the truss structure shown in Figure 3.9, $V = 10$ and $\Delta v = 0.1$.

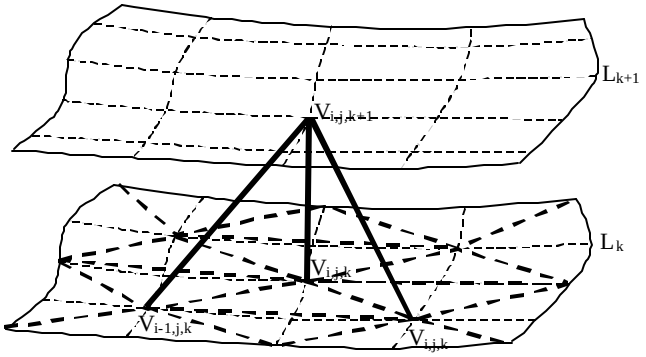

Figure 3.10 Strut Topology between Layers

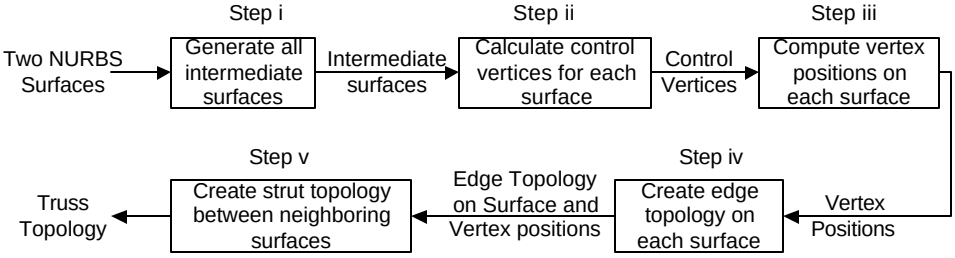

Figure 3.11 An Algorithm to Create Truss Topology

After obtaining the control vertices of each intermediate bicubic NURBS surface, we can calculate the coordinates of all the truss vertices for all bicubic NURBS surfaces including the top and bottom surfaces, as we develop the truss topology for a 2-D area. As shown in Figure 3.10, for Octet truss, each truss vertex $V_{i,j,k+1}$ on layer L_{k+1} has three vertices $V_{i-1,j,k}, V_{i,j,k}, V_{i,j+1,k}$ linked together on the lower neighboring layer L_k. The strut connections at the boundary vary from layer to layer, and all possible cases can be enumerated. The bold dashed lines represent the truss struts on the NURBS surfaces, and the bold solid lines represent the truss struts between these NURBS surfaces. In Figure 3.11, the author shows the overall algorithm to create the truss topology.

Therefore, the intermediate bicubic NURBS surfaces linearly interpolate the space between any two bounding bicubic NURBS patches, and the truss topology with a certain size of truss primitives can be created.

3.3.4 Forming The Approximating NURBS Surface and Creating Thin Skin for Lightweight Truss Structure

In Step I, the surface points are picked up from the part surface and used to interpolate the part surface. These surface points are used to define the approximating NURBS surface, which approximates the part surface. This section discusses some issues related to the formulation of NURBS and the creation of thin skin for lightweight truss structure. Thin skin is used to cover lightweight cellular structure to have a smooth surface as original solid parts.

Since the approximation of NURBS surface is based on the sampled part surface points, sometime the approximation problem happens. For the curve shown in Figure 3.12 as an example of lightweight truss structure, the space between the internal and external curves represents the thin skin of a part, and a truss structure will be created within the “part” and attached onto the internal curve. The four white stars represent the points measured from the internal curve and will be converted into the control vertices of the cubic NURBS curve. As we can see, the variation of the original internal curve is beyond the representation capability of one cubic NURBS curve. The truss vertices A, B, C and D located on the NURBS curve are far away from the original internal curve. These vertices cause vertex (node) protrusions or gaps between the vertices and the part skin. The approximation problem of NURBS surface is similar to that of NURBS curve.

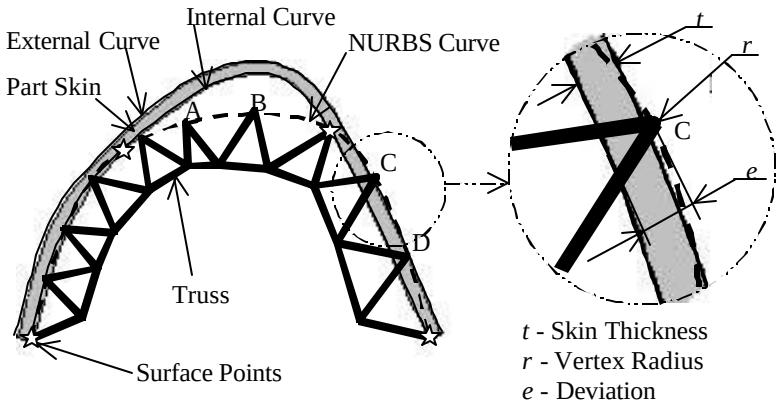

Figure 3.12 Inadequate Approximation Accuracy of NURBS Curve with 4 Interpolating Surface Points

There are two approaches to increase the approximating accuracy of NURBS surface to approximate the part surface. The first approach is to increase the number of surface points sampled from the part surface. In Figure 3.13, the author shows a new bicubic NURBS curve (dashed curve) with 7 interpolating surface points (shown as white stars) sampled from the part surface. The approximation accuracy is increased significantly and all truss vertices are located on the part skin without any vertex protrusion or gap. The approximation accuracy of the bicubic NURBS surface can be increased similarly by using more sampled surface points up to that the following tolerance is met. The approximation tolerance is $t - r$, which is determined by the part skin thickness, t, and the radius of truss vertices, r. The surface approximation error, e, is the perpendicular distance from the approximating NURBS curve/patch to the internal curve/surface of the part skin. It should satisfy $e \le t - r$ over the approximating NURBS patch, then no protrusions or gaps will occur. The baseline is to avoid vertex protrusion and gap between the part skin and the boundary truss vertices, such as Vertex C and Vertex A in Figure 3.12 respectively.

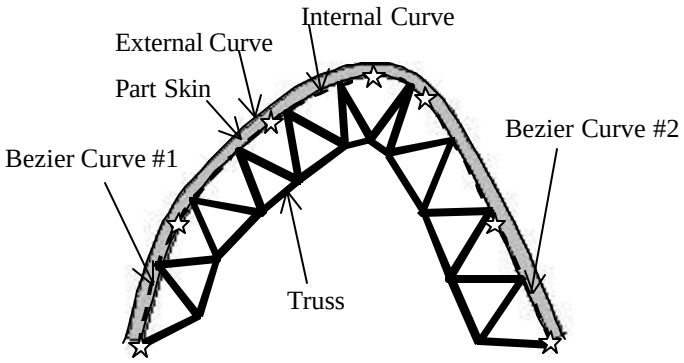

Figure 3.13 Increasing the Approximation Accuracy with 7 Interpolating Surface Points

The second approach is to replace the original internal surface of the part skin with the resulting NURBS curve as shown in Figure 3.14. This approach ensures a perfect match between part skin and truss structure. Only 4 surface points are required to sample from the part surface as compared to that 7 surface points are required in the first approach. The second approach is applied in our research and will be presented in the next section in details.

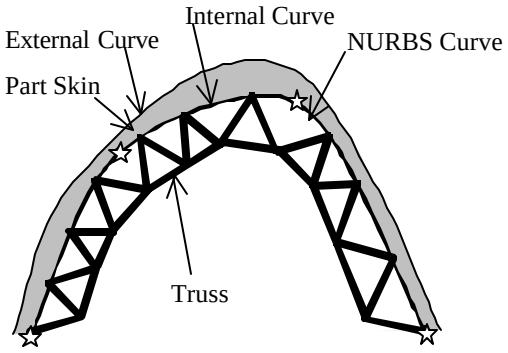

Figure 3.14 Replacing the Original Internal Curve with the NURBS Curve for Perfect Match

3.3.5 Implementation of Parametric NURBS Modeling for Creating Topology

Parametric modeling technique with NURBS is used to create the truss topology. The requirement of creating topology for compliant mechanism is not as strict as that of

lightweight truss structure. For the compliant mechanism, the design domain can be reduced without noticeable influence on the resulting design. However, the design domain cannot be varied for the lightweight truss structure design, moreover, the thin skin is not required. So this section particularly takes the lightweight truss structure as the example for the truss topology creation.

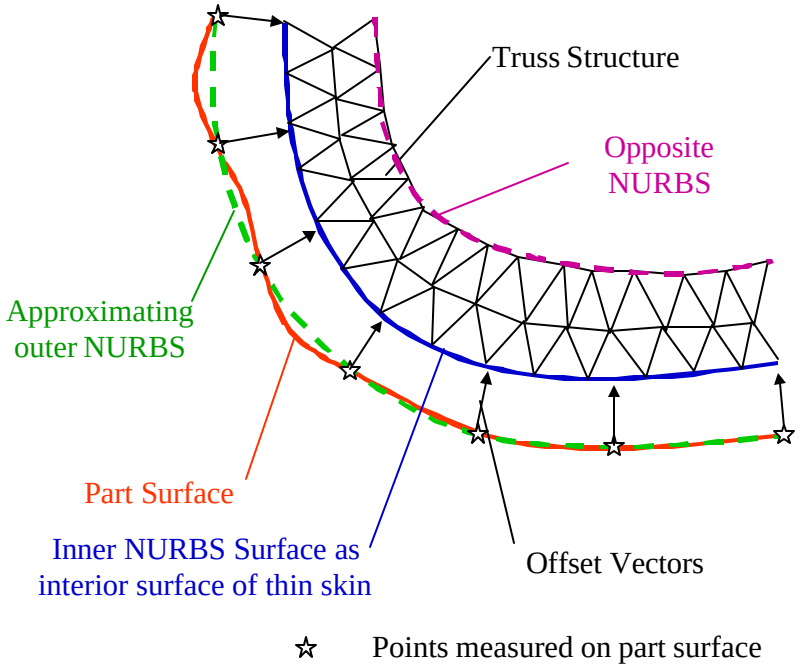

Figure 3.15 Using NURBS to Create Truss Topology

In Figure 3.15, the author shows the idea of using NURBS to create thin skin and truss topology. There are two tasks, creating thin skin and creating initial truss topology. Surface points denoted as stars are sampled from the original part surface and used to create the approximating NURBS surface represented by a dashed line. This approximating NURBS surface is offset by the distance of the desired skin thickness to obtain the inner NURBS surface. This inner NURBS surface is used as the new internal surface of the part skin, or replaces the original inner skin surface if it exists. The approximating NURBS surface is offset by another distance to obtain the opposite

NURBS denoted in dashed line. These two NURBS including the approximating NURBS surface and the opposite NURBS enclose a NURBS volume for creating truss topology.

In Figure 3.16, the author shows the implementation flowchart to create the thin skin and the initial truss topology. The software runs in the Window environment and is implemented with Visual C++, ACIS and OpenGL. A screen dump of the user interface is shown as Figure 3.17. The user interface is in the same style as the popular CAD software. STL model is the input. This approach works for any CAD format since all CAD models can be converted into STL model without any problem (Jacobs 1992).

The surface points are sampled from the part surface through the user interface and denoted by solid spheres in Figure 3.17. The sampled surface points must be an array of $(m+1)\times(n+1)$ points (for this case, $m=n=8$). The sampling process is manually performed. The larger the curvature of the surface, the more surface points sampled from the part surface. These surface points interpolate the approximating surface (or outer NURBS surface), which is offset to obtain the interior surface (or inner NURBS surface) for the thin skin. As the second approach described in Section 3.3.4 and Figure 3.14, the original part surface and resulting interior surface are used as the top and bottom surfaces of the thin skin. These top and bottom surfaces are stitched together by adding four boundary surfaces. In Figure 3.18(a), the author shows a zoomed view of the upper left corner of the gap between the part surface and the created interior skin surface. A stitching process is performed to stitch part surface and the created interior skin surface together. Before the stitching process, the boundaries of both surfaces should be identified. The boundary edges of the STL facets have only one neighboring facet. The boundary vertices of the part surface are represented as spheres as shown in Figure 3.19. In Figure 3.18(b), the author shows a zoomed view of the corner after the stitching process.

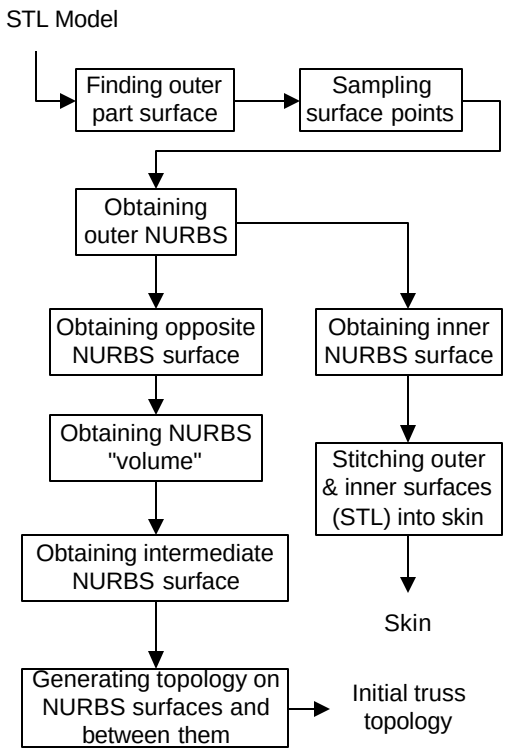

Figure 3.16 Implementation Flowchart of Using NURBS to Create Truss Topology

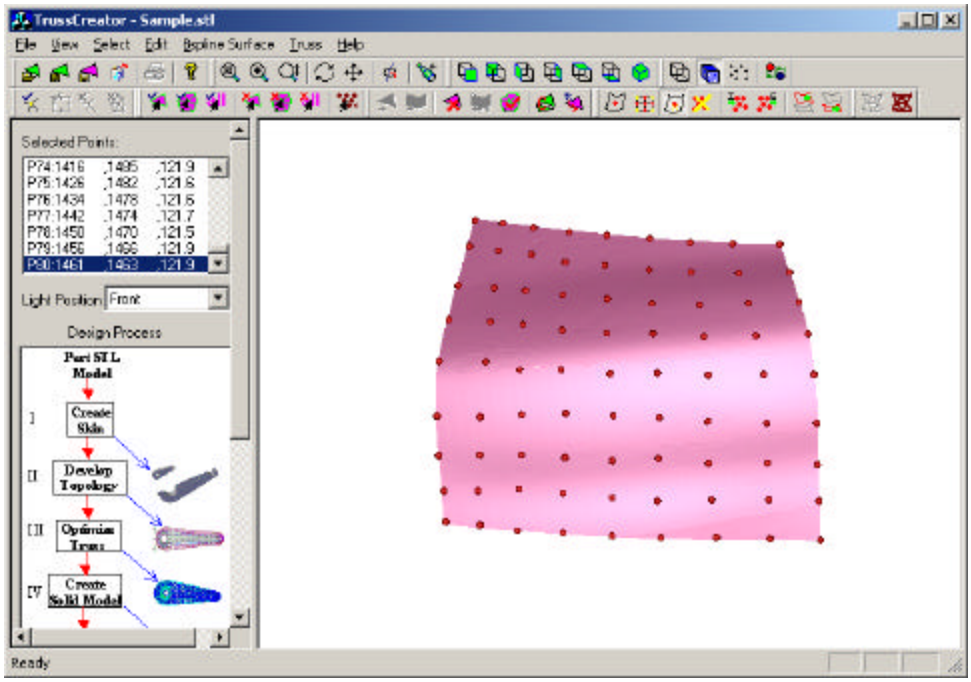

Figure 3.17 TrussCreator Software Developed to Create Truss Topology

(a) Zoomed View of the Gap at a Corner

(b) Zoomed View of the Gap after Stitching

Figure 3.18 Gap between Part surface and Created Interior Skin Surface (NURBS)

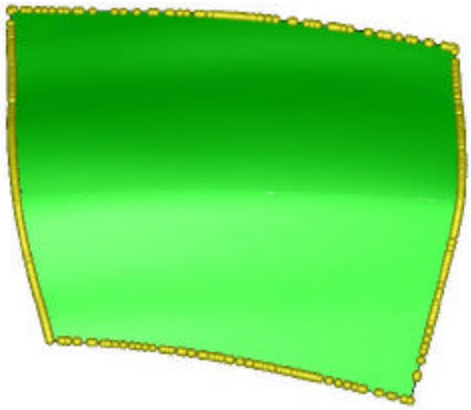

Figure 3.19 Stitching Part surface and Created Interior Skin Surface for Car Body

The inner skin surface (NURBS) is offset by a distance of the truss height to obtain the opposite surface (NURBS). The inner skin surface and the opposite surface enclose a NURBS volume, which is used to create the truss topology. The topology is created using parametric modeling method as described in Section 3.3. The resulting truss topology and thin skin are shown in Figure 3.20.

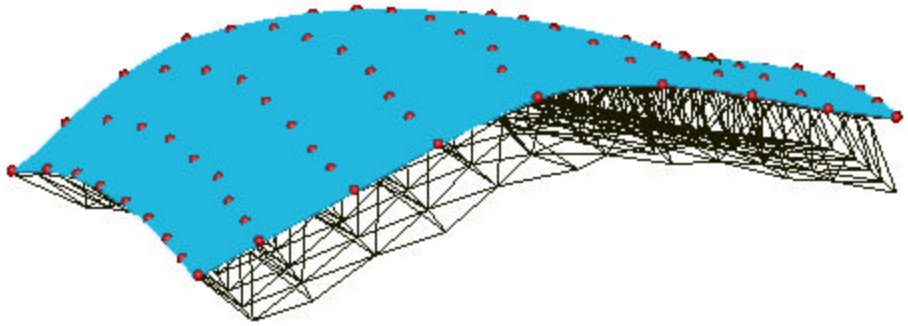

Figure 3.20 Truss Topology Created between Inner Skin Surface (NURBS) and Opposite Surface (NURBS) for Car Body

3.4 Creating Topology from FEM Mesh as Supplemental Method

The parametric modeling approach is similar to structured mesh generation, which creates mesh by mapping nodes and elements. In Step I of the parametric modeling approach, it is time consuming to decompose the part surface and difficult to automate. Multiple volumes of trusses should be generated to fill the part with complex geometry. User experience and knowledge govern the quality and time of truss generation. Hence, an interesting area using unstructured mesh generation algorithms can be explored in the future, such as Delaunay and advancing front techniques (Owen 1998). This section introduces the meshing generation approach to create conformal truss topology.

3.4.1 Overview of Meshing Approach for Creating Initial Truss Topology

There are two types of meshes for finite element method, structured mesh and unstructured mesh (Owen 1998; Soni 2000). Strictly, in a structured mesh, all interior nodes of the mesh have an equal number of adjacent elements, which are typically all 2-D quad or 3-D hexagonal (Owen 1998; Blacker 2001). The parametric modeling

approach presented in the previous sections is similar to structured meshing approach, but the elements are triangular or tetrahedral. In unstructured mesh, the node valence requirement is relaxed and the number of elements meeting at a single node is variable. 2D triangle and 3-D tetrahedron are most commonly used elements in unstructured meshes. In this chapter, the application of unstructured mesh approach in truss topology creation will be discussed.

Most meshing techniques can be categorized as three approaches: Octree, Delaunay, and Advancing Front. The Octree technique subdivides the cubes representing the geometric model until the desired resolution is reached (Shephard and Georges 1991). The interior area from the Octree technique has larger mesh size than the boundary area. However, equilateral mesh is preferred for truss topology creation to ensure the strut lengths similar. Therefore, the Octree technique is not leveraged for the truss topology creation.

Delaunay and Advancing Front algorithms are the most popular triangular and tetrahedral meshing techniques. Quite a few commercial meshing packages are available using these two techniques. In this research, they are leveraged to create the mesh for the truss topology creation. In the Delaunay technique, the Delaunay criterion is used to ensure any node not contained within the circumsphere of any tetrahedron within the mesh (George and Borouchaki 1998). The Delaunay criterion provides a criterion about how to connect existing mesh nodes in space. Nodes are inserted incrementally into the existing mesh if necessary. The Delaunay criterion is usually used with other meshing techniques, such as Advancing Front algorithm. In Advancing Front algorithm, the tetrahedra are built progressively inward from the triangulated boundary surface or curve (Lo 1991).

Quite a few commercial meshing products are available and can be leveraged to create the starting truss topology. Popular meshing packages include ANSYS (1999) and GAMBIT from Fluent. Some geometric modeling packages, such as Pro-E and Unigraphics, also provide meshing capability. ANSYS meshing product is used in this research. Its input CAD formats can be IGES, SAT, Parasolid, Unigraphics and so on. Its main meshing algorithm is Delaunay technique and the Advancing Front technique is used as an alternative algorithm.

3.4.2 Approach to Create Topology Using FEM Mesh

For lightweight truss structure, the original part geometry should be still kept and a naked truss structure is not useful. A thin skin is required to cover the truss structure, which replaces the removed material and fills the empty space. For compliant mechanism, the thin skin is not required since the original part geometry is not necessary to keep.

In Figure 3.21, the author shows an overview of the truss topology creation process using FEM mesh. This process is particularly for lightweight truss structure and there are four individual steps (Step (1), (2), (3) and (4)) for two main tasks (creating thin skin and generating initial truss topology). Steps (1), (2) and (3) are manually performed in a CAD or FEM meshing software through its user interface. Step (4) is performed in TrussCreator, which is the software developed for the lightweight truss creation.

For the topology creation of compliant mechanism, only Step (3) and Step (4) are required. In Step (3), the FEM mesh is created for the entire part geometry, not for the offset geometry.

An example shown in Figure 3.22 is used to explain the topology creation process of using FEM meshes. The geometry is relatively complex with four islands and

one cavity at the bottom. The original CAD model is made in Unigraphics. The overall size of this part is about 600mmX200mmX150mm. The creation of truss topology using FEM mesh follows the process shown in Figure 3.21.

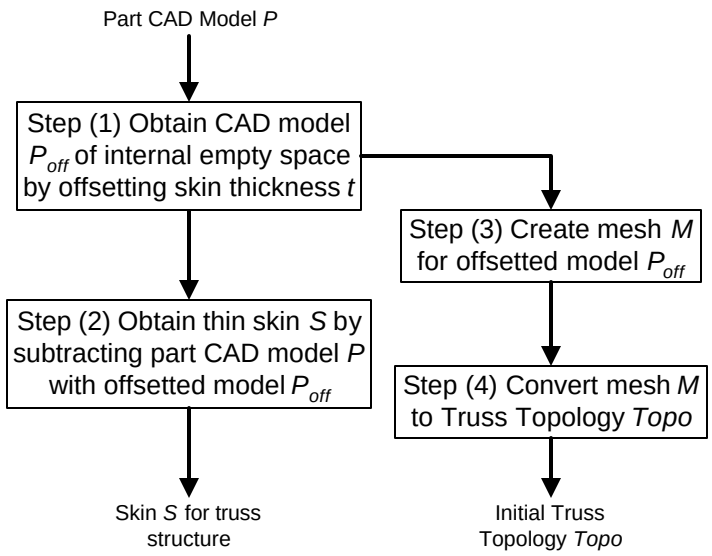

Figure 3.21 Using FEM Meshing Approach to Create Truss Topology

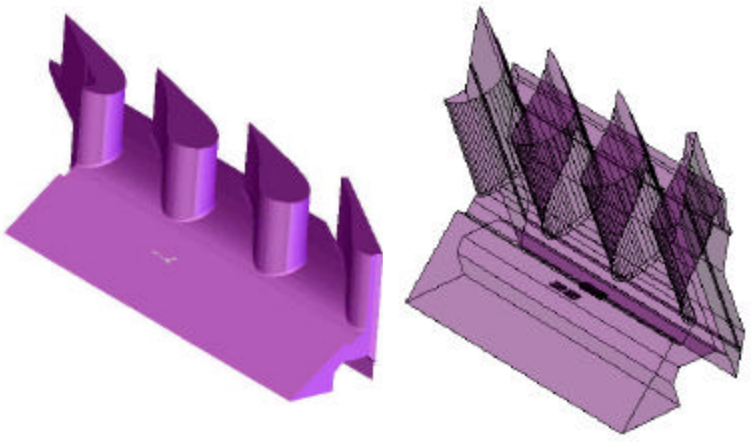

(a) Shaded View (b) Transparent View

Figure 3.22 An Turbine Blade Example of Truss Topology Creation Using FEM Meshing Approach

In Step (1), the surface of part CAD model is offset to create the CAD model for the empty space, which is the shaded view shown in Figure 3.23(a). The offsetting

distance is equal to the skin thickness. The offset model represents the empty space, which will be filled with truss structure. It is not necessary to set the offsetting distance uniform everywhere, but it can be variable. Sometime, it is even necessary to set variable distances to avoid failure during offsetting or neglect small features. It is desired to have smooth surfaces of the offset model to ensure the mesh sizes are more controllable. For convenience, the surface offsetting process was manually performed in IronCAD (1997) by importing the ParaSolid model converted from the Unigraphics model.

In Step (2), the thin skin is obtained with a subtractive Boolean operation between original part CAD model and the offset CAD model representing the empty space. Actually, the shelling operation in most CAD packages is realized through a similar subtractive Boolean operation as well. A drain hole should be made on the thin skin for the consideration of manufacturability since the internal material needs to be drained away or taken out for additive fabrication. The subtraction process in IronCAD shown in Figure 3.24(a). The drain hole made at the bottom of the thin skin is shown in Figure 3.24(b). It is relatively easy to position the parts and make drain hole on the imported CAD model in IronCAD by using its TriBall (1997). A sectioned view of the resulting thin skin is shown in Figure 3.25.

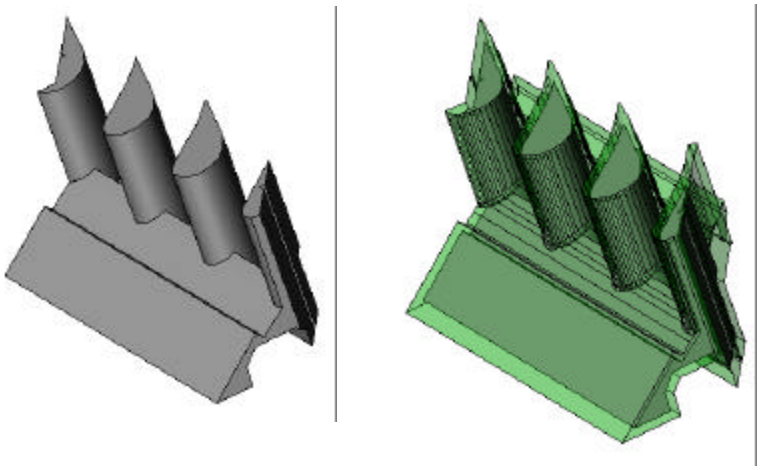

(a) Shaded View of Offset Model

(b) Transparent View of Offset Model with Part Model

Figure 3.23 Step (1) – Offsetting Original Part CAD Model by Skin Thickness for Turbine Blade Example

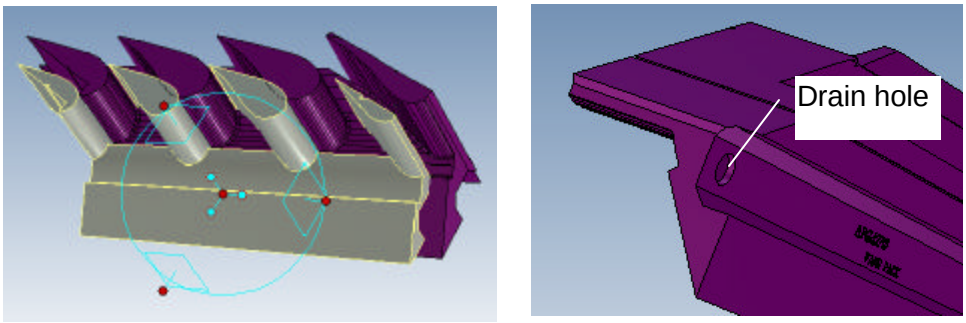

(a) Positioning and Subtracting Models

(b) Making Drain Hole

Figure 3.24 Step (2) –Subtracting Original Part CAD Model with Offset Model to Obtain Thin Skin for Turbine Blade Example

In Step (3), FEM mesh is created for the offset CAD model, which represents the empty space and will be filled with truss structures. The tetrahedron mesher of ANSYS is used to create the mesh as shown in Figure 3.27. The mesh elements are tetrahedra with average lateral length of about 20 mm. The mesh density or the element sizes are noticeably affected by the surface smoothness of the CAD model.

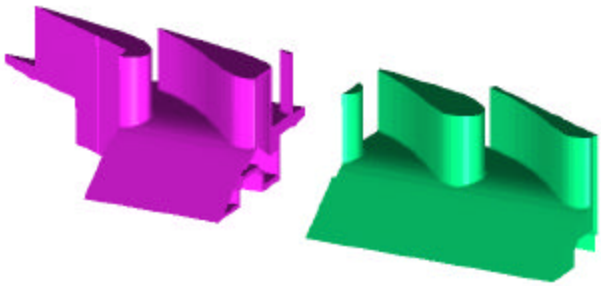

Figure 3.25 Sectioned View of the Resulting Thin Skin for Turbine Blade Example

In Step (4), the FEM mesh is converted into the truss topology using the mesh conversion functionality. Basically this step is just data conversion process. All the other three steps are performed using the existing commercial software packages. Only Step (4) is implemented through programming and integrated in our own copyrighted software, TrussCreator. The truss topology resulting from Step (4) is shown in Figure 3.27. The created truss structure and the truss covered with thin skin is shown in Figure 3.28.

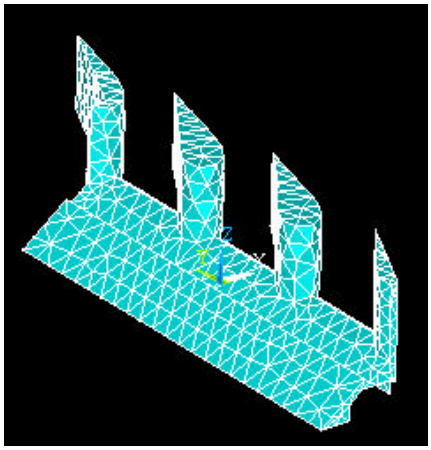

Figure 3.26 Step (3) - Creating FEM Mesh for Turbine Blade Example

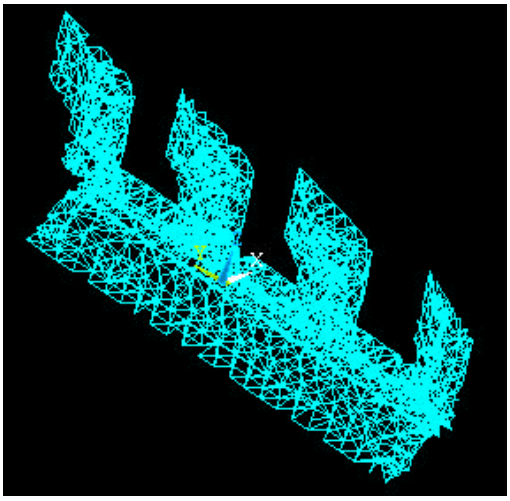

Figure 3.27 Step (4) - Converting FEM Mesh into Truss Topology for Turbine Blade Example

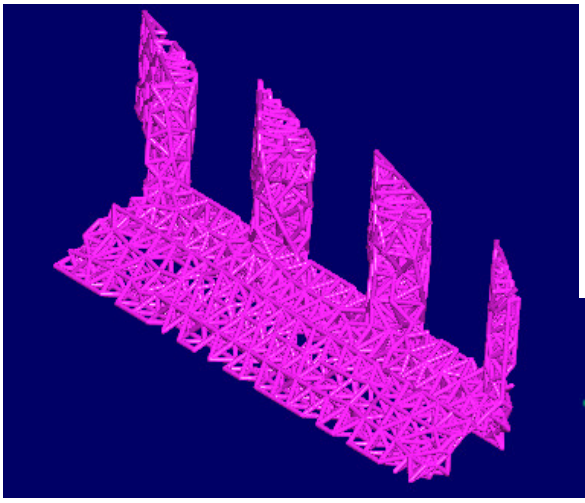

(a) Truss Structure

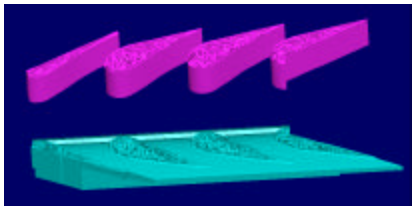

(b) Sectioned View of Truss Integrated with Thin Skin

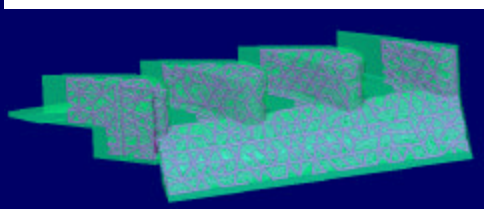

(c) Transparent View Of Truss Integrated with Thin Skin

Figure 3.28 Created Truss Structure for Turbine Blade Example

3.5 A Comparison Between Parametric Modeling And Meshing Approaches

There are inherent similarities between truss topology creation and mesh generation for finite element methods, which divides a geometric domain into small subregions (Reddy 1993). In the creation of truss topology, the subregions are replaced with truss primitives to remove material from the solid objects. To utilize the structured

mesh generation (Owen 1998), the part geometry must be represented by a series of algebraic equations, and vertices/nodes are generated based on algebraic interpolation methods (Soni 2000).

The differences between truss creation and mesh generation are also apparent. During truss creation, the boundary vertices have to be accurately positioned on the part skin. The smoothness and strut orientation of the truss are very important to best enhance a part's mechanical and/or dynamic properties. Moreover, the creation of part skin and truss solid models differentiates them in terms of computational methods and design process. The parametric modeling approach and the FEM meshing approach have their own advantages and disadvantages for creating the truss topology. A comparison between these two approaches is shown in Table 3-1.

In parametric modeling approach, the orientations and sizes of individual struts in the truss topology are more controllable. The topology contains truss primitives mapped between the two enclosing surfaces. The parametric modeling approach is good for the parts with smooth variations on the part surfaces, such as car body. Step I in the parametric modeling approach is time consuming to sample the surface points. Multiple volumes of trusses should be generated to fill the part with complex geometry. User experience and knowledge govern the quality and time of truss generation.

The FEM meshing approach works for any kind of geometries, such as those with internal cavities and obtruded islands. But the commercial FEM meshing software packages are required to support this approach. It can serve as a supplemental approach to the parametric modeling approach to create the truss topology at the current stage. However, it provides the potential to automate the process of creating truss topology. At this time, the input has to be the CAD formats that are acceptable by the FEM meshing packages, and STL model cannot be imported into ANSYS.

Table 3-1 Comparing Parametric Modeling Approach and Meshing Approach

	Parametric modeling	**FEM meshing**
Topology Quality	Very good; controllable orientations, strut sizes and density distribution; uniform node valence; smooth transition from area to area.	Good; not convenient to control strut sizes, orientations.
Compatibility of CAD Formats	STL model is the input; works for any CAD format.	Must be CAD model importable by the commercial software packages (e.g. IronCAD, ANSYS)
Geometry Complexity of The Part	Relatively simple geometry with fewer features. Works perfect for widely extended surfaces, e.g. car body.	Complex geometry with all kinds of features, such as holes, fillets, and obtrusions.
Affordability	Low cost; no extra expense except acquiring TrussCreator, which is the software developed by us and licensed by RPMI.	Relatively high cost; need to acquire the geometric modeling product for creating thin skin, and the FEM meshing product for creating mesh; need TrussCreator to convert mesh into truss topology.
User Friendliness	Using interface of TrussCreator to sample surface points, create thin skin and truss topology; experience required.	Using the commercial software packages (e.g. IronCAD, ANSYS) to create thin skin and truss topology; need to know these software packages.
Potential to Be Fully Automated	Having potential for full automation, but better to combine with some commercial software for reverse engineering to facilitate sampling surface points.	Having potential for full automation; more researches are needed to identify surface offsetting and meshing capability in the commercial software.

3.6 Chapter Summary

The computational methods based on the parametric modeling techniques were presented to create conformal truss topology as the initial topology for structural synthesis. The proposed methods use NURBS surfaces to approximate the part surface and to create a truss topology conformal to the part's shape. These methods can ensure

that the structure fits in the part space. For lightweight truss structures, most truss struts are ensured to be oriented towards the loads on the part surface. Truss topologies can be created on a 2-D surface and a 3-D truss volume. For the topology of lightweight truss structure, a thin skin with certain thickness is created to cover the naked skin. The interior surface of the thin skin perfectly matches with the nodes of the internal truss. A prototype software tool has been developed in C++ using the ACIS geometric modeling kernel to generate truss topology in parts with arbitrary shapes.

Since there is inherent similarity between truss topology creation and FEM mesh generation, the ideas and methods for mesh generation are leveraged to facilitate the truss topology creation. The meshing generation approach is formulated as a supplemental method to create conformal truss topology, particularly for the parts with complex features, such as internal holes.

Adding rounds to joints can reduce stress concentration and fatigue to enhance the structures' mechanical performance. Local Boolean operations at the common edges between neighboring unit trusses could glue the unit trusses' surfaces together and efficiently create the solid models of entire structures. These two improvements can potentially enhance the design of cellular structures and efficiently create the solid models of cellular structures. FEM mesh was successfully used to create conformal truss topology. However, the pros and cons of various meshing algorithms (e.g., advanced front method and Delaunay method) have not been sufficiently investigated as well as mesh decimation to control truss strut length (Shephard and Georges 1991; George and Borouchaki 1998; Owen 1998).

In this chapter, geometric modeling has been successfully adapted to create conformal truss topology to represent material distribution in cellular structures for analysis and design synthesis. Creating conformal truss topology addressed part of the

“representation” issue (raised in Section 2.4) and proved the theoretical structural validity (shown in Figure 1.22) of the postulated hypothesis (posted in Section 1.4).

CHAPTER 4

MECHANICS ANALYSIS OF CELLULAR STRUCTURE WITH UNIT TRUSS APPROACH

In this chapter, the “analysis” issue in unit truss approach raised in Section 2.4 is addressed by adapting continuum mechanics and finite elements method to develop the mechanics model of unit truss to accurately and efficiently analyze conformal cellular structures. The presentation of Chapter 4 follows Figure 4.1. The mechanics model of conformal structures is developed using unit truss as the microstructure or elements for finite element method. The constitutive equations of 2-D and 3-D unit trusses, as special finite elements, are derived to analyze 2-D and 3-D structures for finite element method. Nonlinear elasticity problems related to lightweight truss structure and compliant mechanisms are presented and solved with the suggested tangent stiffness method. The most possible failure modes, such as buckling and yielding, are discussed and the analysis results can be used for the designs of cellular structures. Finally, some validation examples are given to test the unit truss approach for the cellular structure analysis. The focus of Chapter 4 is the structural analysis shown in Figure 4.2. The inputs of the analysis process are the truss topology and the strut size specification. The analysis results of the structure’s mechanical behavior are used for the design optimization, which is discussed in Chapter 5.

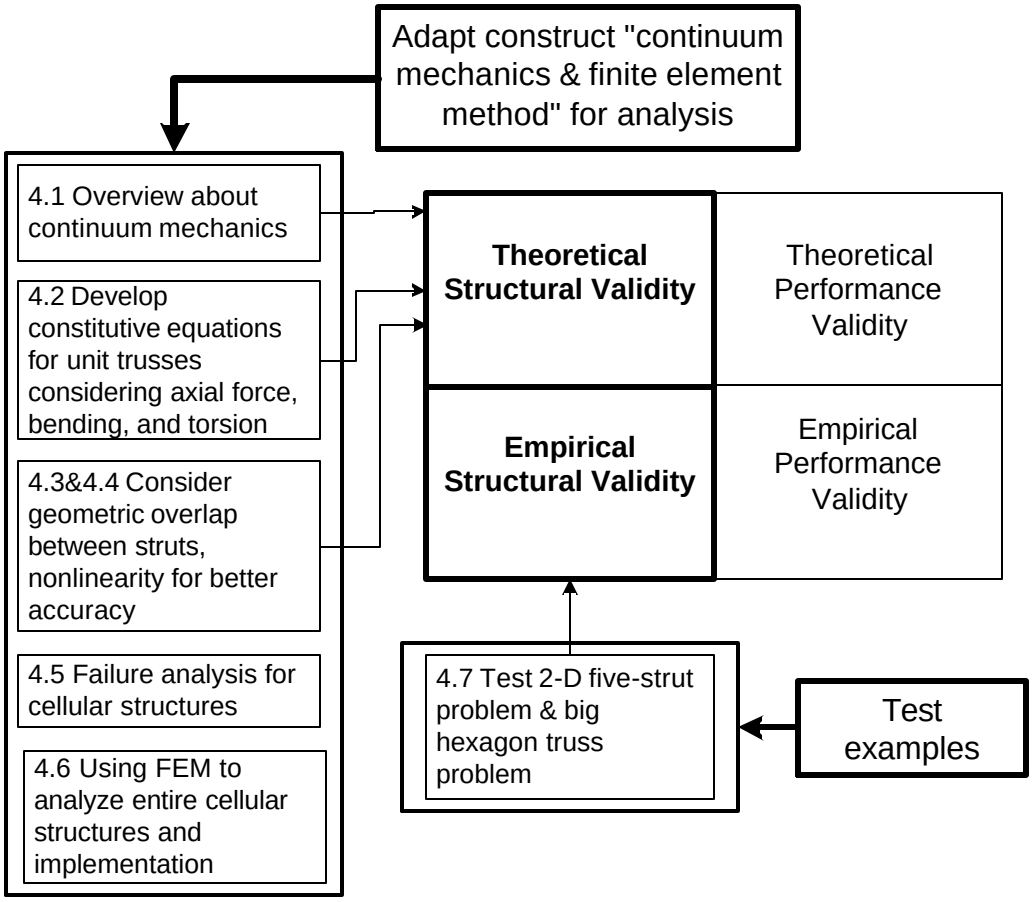

Figure 4.1 Relationship between Chapter 4 and Validation Square

4.1 Overview of Mechanics Analysis

In classical elasticity of homogeneous continuous medium, a fundamental problem is to find stress-strain relations by forces acting on the surface of elastic half-space (Malvern 1969). Stress in solids is related to strains through constitutive equations (Chung 1988), so is the stress in cellular structures. Constitutive equations are used to model mechanical behavior of material at the microscale. In a general form of isothermal elastic material with no residual stress, stress is related to strain as the constitutive equations shown in Equation 4.1 (Malvern 1969; Gould 1994), where the linear stiffness, $\underset{\sim}{C}$, is written as fourth order tensor, the infinitesimal stresses, $\underset{\sim}{s}$, and the infinitesimal

Lagrangian strains, $\underset{\sim}{e}$, as second order tensors. The nonlinear terms are neglected for linear elasticity. In Cartesian space, there are 9 components in both stress tensor $\underset{\sim}{s}$ and strain tensor $\underset{\sim}{e}$, and 81 components in linear elastic tensor $\underset{\sim}{C}$. Due to symmetry and balance of moments, the numbers of independent components in both stress tensor $\underset{\sim}{s}$ and strain tensor $\underset{\sim}{e}$ are reduced to 6, and that in linear elastic tensor $\underset{\sim}{C}$ is reduced to 36 and written in a matrix form, as shown in Equation 4.2 (Malvern 1969; Gould 1994). Each stress component can be seen as a force acting on the surface of cube in Cartesian space.

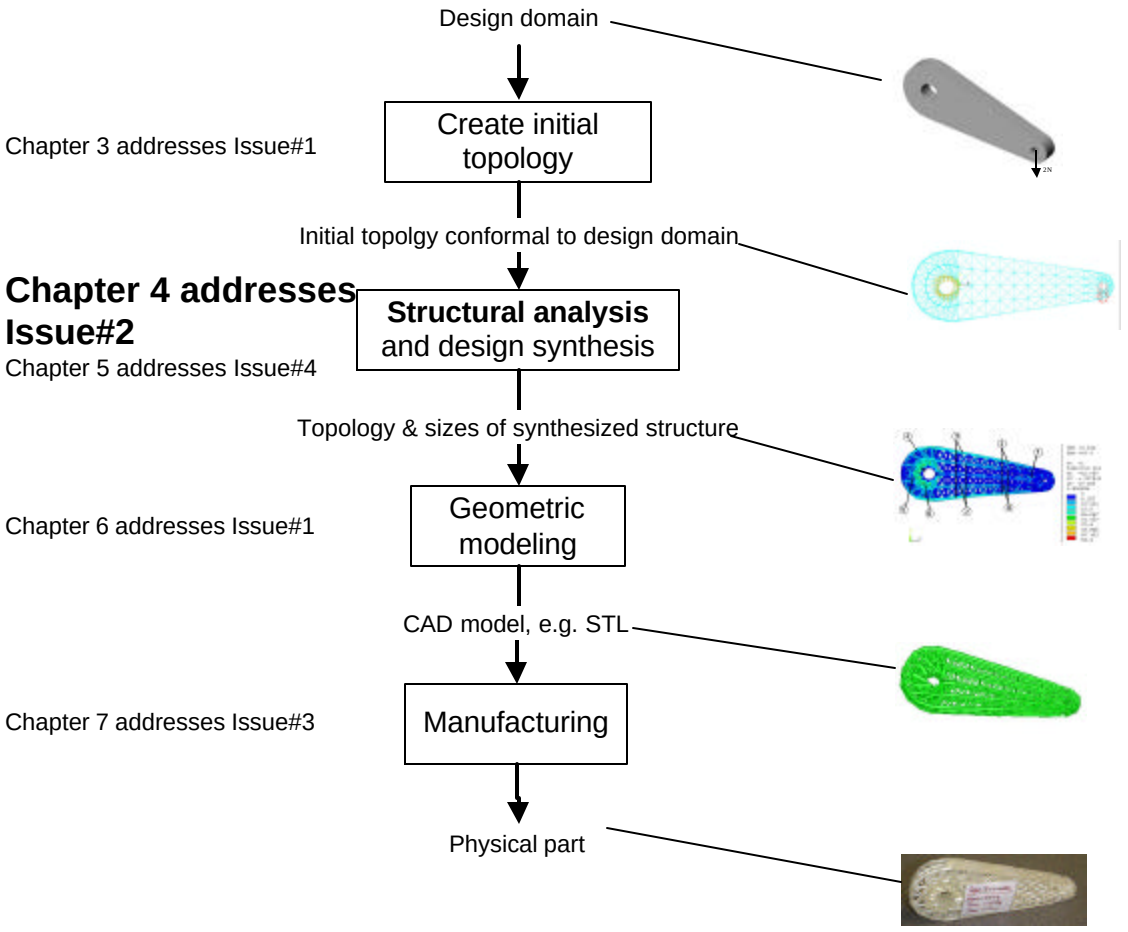

Figure 4.2 Focus of Chapter 4 in the Design Process of Cellular Structures

$$\underset{\sim}{s} = \underset{\sim}{C} : \underset{\sim}{e} + \ldots \text{ nonlinear terms in } \underset{\sim}{e} \tag{4.1}$$

$$[\underset{\sim}{s}] = \begin{bmatrix} s_1 \\ s_2 \\ s_3 \\ s_4 \\ s_5 \\ s_6 \end{bmatrix}, [\underset{\sim}{e}] = \begin{bmatrix} e_1 \\ e_2 \\ e_3 \\ e_4 \\ e_5 \\ e_6 \end{bmatrix}, [\underset{\sim}{C}] = \begin{bmatrix} c_{11} & c_{12} & c_{13} & c_{14} & c_{15} & c_{16} \\ c_{21} & c_{22} & c_{23} & c_{24} & c_{25} & c_{26} \\ c_{31} & c_{32} & c_{33} & c_{34} & c_{35} & c_{36} \\ c_{41} & c_{42} & c_{43} & c_{44} & c_{45} & c_{46} \\ c_{51} & c_{52} & c_{53} & c_{54} & c_{55} & c_{56} \\ c_{61} & c_{62} & c_{63} & c_{64} & c_{65} & c_{66} \end{bmatrix} \tag{4.2}$$

4.2 Constitutive Equations of Unit Truss

In Section 4.1, the author gives an overview of mechanics analysis of cellular structures and introduces unit truss as microstructures. This section will develop the constitutive equations of unit truss for finite element method.

The material distribution in cellular structure is neither homogeneous nor continuous since most of the part space is empty and only some space is occupied by material. Therefore, both continuity and homogeneity assumptions are not valid for lightweight cellular structure and compliant mechanism. However, at the microstructure (e.g. unit cell (Deshpande, Fleck et al. 2001) or unit truss) scale, the structure can be considered as a continuum medium. Continuum mechanics theory can still be applied to derive the constitutive equations of unit truss and its initial analytical model for both linear and non-linear elastic deformations.

The forces and the displacements of unit truss are shown in Figure 4.3 and Figure 4.4 respectively. Each unit truss has one central node and N struts connected to the central node. Unit truss is an anisotropic material structure at its size scale. The number of nodes and the degrees of freedom in unit truss are not fixed, but variable. Therefore, the constitutive equations of unit truss are different from those of such infinitesimal material volume as cube, whose constitutive equations are shown in

Equation 4.2. The following two subsections are going to derive the constitutive equations of 2-D unit truss and 3-D unit truss.

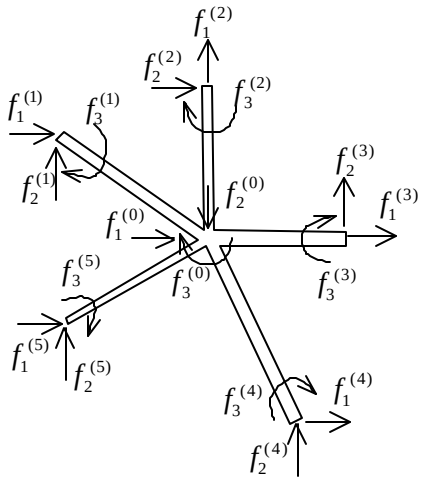

Figure 4.3 A Unit Truss Model with Five Struts

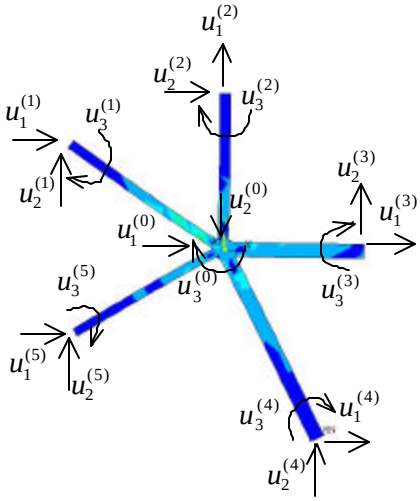

Figure 4.4 Stress Graph of A Unit Truss with Five Struts

4.2.1 Mechanics Model of 2-D Unit Truss

Development of the following analytical model is based on the assumptions concerning how the unit truss is deformed. In this research, the analytical modeling process of unit truss starts with the assumption that its struts behave as simple beams. There are three steps to derive the analytical model of unit truss with N struts: (1) finding the stiffness of each strut in the local coordinate system; (2) obtaining the

stiffness of each strut in the global coordinate system through transforming the stiffness tensor from the strut's local coordinate system to the global coordinate system; (3) assembling the stiffness tensors of all N struts into the stiffness tensor of the entire unit truss.

In Step (1), beam theory is used to find the stiffness of each strut. The constitutive equation for a single strut is shown as Equation 4.3. Every strut has one equation and a unit truss with N struts totally has N equations. $\overline{\underset{\sim}{K}}^{(i)}$ ($i = 1,...,N$) is the stiffness matrix of the i^{th} strut of a unit truss in the local coordinate system as shown in Equation 4.10. $\overline{\underset{\sim}{u}}^{(0)}$ and $\overline{\underset{\sim}{f}}^{(0)}$ represent displacements and forces respectively at the central node of the unit truss. $\overline{\underset{\sim}{u}}^{(i)}$ and $\overline{\underset{\sim}{f}}^{(i)}$ ($i = 1,2,...,N$) represent displacements and forces respectively at the i^{th} node, which is the node opposite to the central node of the i^{th} strut. Each node of the unit truss as shown in Figure 4.5 has three degrees of freedom, among which two are primary variables (translational freedom, $u_1^{(i)}$ and $u_2^{(i)}$), and one is secondary variable (rotational freedom, $u_3^{(i)}$). Totally there are six degrees of freedom in this bending beam and the stiffness tensor of i^{th} strut of a unit truss in the local coordinate system is 6×6 matrix shown as Equation 4.4 (Reddy 1993).

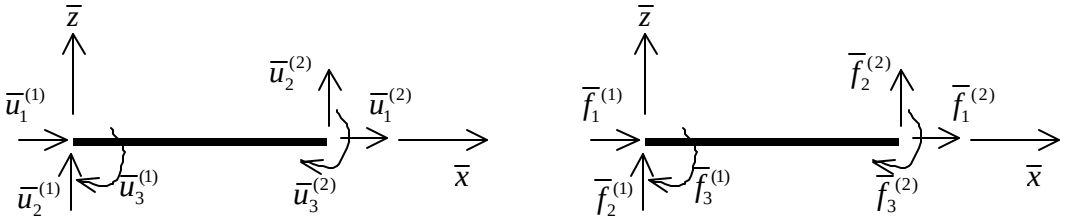

(a) Generalized Displacements (b) Generalized Forces

Figure 4.5 A 2-D Strut With Primary and Secondary Variables (or Degree of Freedom) In Local Coordinate System

$$\begin{bmatrix} \bar{f}^{(0)} \\ \tilde{\bar{f}}^{(i)} \end{bmatrix} = \left[\tilde{\bar{K}}^{(i)}\right] \bullet \begin{bmatrix} \bar{u}^{(0)} \\ \tilde{\bar{u}}^{(i)} \end{bmatrix}, \qquad i = 1,2,...,N \tag{4.3}$$

$$\left[\tilde{\bar{K}}^{(i)}\right] = \frac{2EI}{L^3} \left[\begin{array}{ccc:ccc} m & 0 & 0 & -m & 0 & 0 \\ 0 & 6 & -3L & 0 & -6 & -3L \\ 0 & -3L & 2L^2 & 0 & 3L & L^2 \\ \hdashline -m & 0 & 0 & m & 0 & 0 \\ 0 & -6 & 3L & 0 & 6 & 3L \\ 0 & -3L & L^2 & 0 & 3L & 2L^2 \end{array}\right]_{6\times 6}$$

where, (4.4)

E – Young's modulus of solid material i^{th} beam

I – Inertia of i^{th} beam along axis perpendicular to the plane

L – Length of i^{th} beam

A – Area of i^{th} beam cross-section

$$m = \frac{AL^2}{2I}$$

$$\left[\tilde{\bar{f}}^{(i)}\right] = \begin{bmatrix} \bar{f}_1^{(i)} \\ \bar{f}_2^{(i)} \\ \bar{f}_3^{(i)} \end{bmatrix}, \qquad \left[\tilde{\bar{u}}^{(i)}\right] = \begin{bmatrix} \bar{u}_1^{(i)} \\ \bar{u}_2^{(i)} \\ \bar{u}_3^{(i)} \end{bmatrix}, \qquad i = 0,1,2,...,N$$

where,

$\bar{f}_1^{(i)}, \bar{f}_2^{(i)}$ – The translational forces at the i^{th} node along x and z axes in the local coordinate system

$\bar{f}_3^{(i)}$ – The bending moment at the i^{th} node along y axis in the local coordinate system (4.5)

$\bar{u}_1^{(i)}, \bar{u}_2^{(i)}$ – The translational displacements at the i^{th}node along x and z axes in the local coordinate system

$\bar{u}_3^{(i)}$ – The rotational displacement at the i^{th} node along y axis in the local coordinate system

N – The number of struts in unit truss

In Step (2), the stiffness tensor is transformed from the local coordinate system to global coordinate system as if a strut is rotated around y axis by a as shown in

Figure 4.6. The y axis is perpendicular to Plane zox and points into the page. The constitutive equation for the i^{th} strut is shown as Equation 4.6 written in the global coordinate system. The stiffness tensor, $\underset{\sim}{K}^{(i)}$, in the global coordinate system is obtained using Equation 4.7. $\underset{\sim}{T}^{(i)}$ is the transformation tensor representing the rotation of the coordinate system around y axis by $-a$, and shown as Equation 4.8 (Reddy 1993). Equation 4.9 shows the displacements, $\underset{\sim}{u}^{(i)}$, and the forces, $\underset{\sim}{f}^{(i)}$ ($i = 0,1,...,N$), at the i^{th} node, written as in the global coordinate system. The resultant stiffness tensor $\underset{\sim}{K}^{(i)}$ is a 6×6 matrix as shown in Equation 4.10 (Reddy 1993). This global stiffness matrix is partitioned into four sub-matrices, $\Phi_{11}^{(i)}$, $\Phi_{12}^{(i)}$, $\Phi_{21}^{(i)}$ and $\Phi_{22}^{(i)}$ ($i = 0,1,...,N$), which are 3×3 matrices as shown in Equation 4.10.

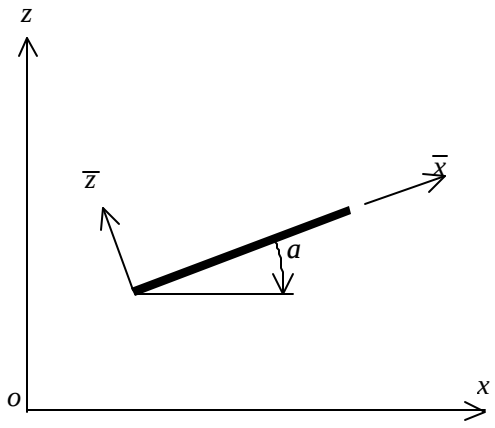

Figure 4.6 Strut Rotated from Local Coordinate System to Global Coordinate System

$$\begin{bmatrix} \underset{\sim}{f}^{(0)} \\ \underset{\sim}{\bar{f}}^{(i)} \end{bmatrix} = \left[\underset{\sim}{K}^{(i)}\right] \bullet \begin{bmatrix} \underset{\sim}{u}^{(0)} \\ \underset{\sim}{\bar{u}}^{(i)} \end{bmatrix}, \qquad i = 1,2,...,N \tag{4.6}$$

$$\underset{\sim}{K}^{(i)} = \underset{\sim}{T}^{T} \bullet \underset{\sim}{\bar{K}}^{(i)} \bullet \underset{\sim}{T} \tag{4.7}$$

where,

$\underset{\sim}{T}^{T}$ – The transpose of $\underset{\sim}{T}$

$$\left[\underset{\sim}{T}^{(i)}\right]=\left[\begin{array}{ccc:ccc} \cos a & \sin a & 0 & & & \\ -\sin a & \cos a & 0 & & 0 & \\ 0 & 0 & 1 & & & \\ \hdashline & & & \cos a & \sin a & 0 \\ & 0 & & -\sin a & \cos a & 0 \\ & & & 0 & 0 & 1 \end{array}\right]_{6\times 6} \tag{4.8}$$

where,

a – Rotating angle of i^{th} beam along axis perpendicular to the plane

$$\left[\underset{\sim}{f}^{(i)}\right]=\begin{bmatrix} f_1^{(i)} \\ f_2^{(i)} \\ f_3^{(i)} \end{bmatrix}, \qquad \left[\underset{\sim}{u}^{(i)}\right]=\begin{bmatrix} u_1^{(i)} \\ u_2^{(i)} \\ u_3^{(i)} \end{bmatrix}, \qquad i=0,1,2,...,N$$

where,

$f_1^{(i)}, f_2^{(i)}$ – The translational forces at the i^{th} node along x and z axes in the global coordinate system

$f_3^{(i)}$ – The bending moment at the i^{th} node along y axis in the global coordinate system (4.9)

$u_1^{(i)}, u_2^{(i)}$ – The translational displacements at the i^{th} node along x and z axes in the global coordinate system

$u_3^{(i)}$ – The rotational displacement at the i^{th} node along y axis in the global coordinate system

N – The number of struts in unit truss

$$\left[\underset{\sim}{K}^{(i)}\right]=\left[\begin{array}{ccc:ccc} K_{11}^{(i)} & K_{12}^{(i)} & K_{13}^{(i)} & K_{14}^{(i)} & K_{15}^{(i)} & K_{16}^{(i)} \\ K_{21}^{(i)} & K_{22}^{(i)} & K_{23}^{(i)} & K_{24}^{(i)} & K_{25}^{(i)} & K_{26}^{(i)} \\ K_{31}^{(i)} & K_{31}^{(i)} & K_{31}^{(i)} & K_{34}^{(i)} & K_{35}^{(i)} & K_{36}^{(i)} \\ \hdashline K_{41}^{(i)} & K_{42}^{(i)} & K_{43}^{(i)} & K_{44}^{(i)} & K_{45}^{(i)} & K_{46}^{(i)} \\ K_{51}^{(i)} & K_{52}^{(i)} & K_{53}^{(i)} & K_{54}^{(i)} & K_{55}^{(i)} & K_{56}^{(i)} \\ K_{61}^{(i)} & K_{61}^{(i)} & K_{61}^{(i)} & K_{64}^{(i)} & K_{65}^{(i)} & K_{66}^{(i)} \end{array}\right]_{6\times 6} = \left[\begin{array}{c:c} \Phi_{11}^{(i)} & \Phi_{12}^{(i)} \\ \hdashline \Phi_{21}^{(i)} & \Phi_{22}^{(i)} \end{array}\right]_{6\times 6} \tag{4.10}$$

In Step (3), the stiffness matrices of N struts are assembled into the stiffness tensor, $\underset{\sim}{K}^{e}$, of the entire 2-D unit truss and the entire stiffness tensor is written as Equation 4.11.

$$\left[\underset{\sim}{K}^{e}\right]=\begin{bmatrix}\sum_{i=1}^{N}\Phi_{11}^{(i)} & \Phi_{12}^{(1)} & \Phi_{12}^{(2)} & \cdots & \Phi_{12}^{(N)}\\ \Phi_{21}^{(1)} & \Phi_{22}^{(1)} & 0 & \cdots & 0\\ \Phi_{21}^{(2)} & 0 & \Phi_{22}^{(2)} & \cdots & 0\\ \vdots & \vdots & \vdots & \ddots & \vdots\\ \Phi_{21}^{(N)} & 0 & 0 & \cdots & \Phi_{22}^{(N)}\end{bmatrix}_{3(N+1)\times 3(N+1)} \qquad 4.11$$

The finite element model of this 2-D unit truss in R^2 is shown as Equation 4.12. $\underset{\sim}{K}^{e}$ is the stiffness tensor of the unit truss in the global coordinate system. $\underset{\sim}{U}^{e}$ denotes the displacements and $\underset{\sim}{F}^{e}$ denotes nodal forces on the unit truss. $\underset{\sim}{u}^{(i)}$ and $\underset{\sim}{f}^{(i)}$ are the displacements at the i^{th} node and the forces acting on the i^{th} node in Figure 4.3 and Figure 4.4. The 0^{th} node represents the central node of the 2-D unit truss.

$$\underset{\sim}{K}^{e}\cdot\underset{\sim}{U}^{e}=\underset{\sim}{F}^{e} \qquad 4.12$$

$$\left[\underset{\sim}{U}^{e}\right]=\begin{bmatrix}\left[\underset{\sim}{u}^{(0)}\right]\\ \left[\underset{\sim}{u}^{(1)}\right]\\ \vdots\\ \left[\underset{\sim}{u}^{(N)}\right]\end{bmatrix},\left[\underset{\sim}{F}^{e}\right]=\begin{bmatrix}\left[\underset{\sim}{f}^{(0)}\right]\\ \left[\underset{\sim}{f}^{(1)}\right]\\ \vdots\\ \left[\underset{\sim}{f}^{(N)}\right]\end{bmatrix} \qquad 4.13$$

4.2.2 Mechanics Model of 3-D Unit Truss

Similarly, the analytical model of 3-D unit truss in R^3 can be derived using the same approach. There are three similar steps to derive the analytical model of 3-D unit truss as of 2-D unit truss: (1) finding the stiffness of each strut in the local coordinate system; (2) obtaining the stiffness of each strut in the global coordinate system through transforming the stiffness tensor from the strut's local coordinate system to the global

coordinate system; (3) assembling the stiffness tensors of all N struts into the stiffness tensor of the entire unit truss. The main differences of deriving analytical models of 2-D unit truss and 3-D unit truss are finding the local strut stiffness in Step (1) and the transformation tensor in Step (2). This section will present the derivation of the mechanics model of 3-D unit truss with an emphasis on the differences.

In Step (1), the stiffness of each strut in the local coordinate system is obtained. A 3-D strut in the local coordinate system is shown in Figure 4.7. Each node has six degrees of freedom, among which three are primary variables (translational freedoms, $u_1^{(i)}$, $u_2^{(i)}$ and $u_3^{(i)}$), and three are secondary variables (rotational freedoms, $u_4^{(i)}$, $u_5^{(i)}$ and $u_6^{(i)}$). Totally there are twelve degrees of freedom in this 3-D bending beam and the stiffness tensor of i^{th} strut of a unit truss in the local coordinate system is 12×12 matrix shown as Equation 4.16 (McGuire, Gallagher et al. 2000). The constitutive equations of each 3-D strut are shown in Equation 4.14, which is exactly the same as that of 2-D strut shown in Equation 4.3, but the definitions of displacement vector $\underset{\sim}{\overline{u}}^{(i)}$ ($i=0,2,...,N$), force vector $\underset{\sim}{\overline{f}}^{(i)}$ ($i=0,2,...,N$) and stiffness $\underset{\sim}{\underset{\sim}{K}}^{(i)}$ ($i=1,2,...,N$) are different. The sizes of displacement vector $\underset{\sim}{\overline{u}}^{(i)}$ and force vector $\underset{\sim}{\overline{f}}^{(i)}$ are increased from 3 to 6, and the size of stiffness tensor $\underset{\sim}{\underset{\sim}{K}}^{(i)}$ is increased from 6×6 to 12×12. The components of $\underset{\sim}{\overline{u}}^{(i)}$, $\underset{\sim}{\overline{f}}^{(i)}$ and $\underset{\sim}{\underset{\sim}{K}}^{(i)}$ are given in Equation 4.15 and Equation 4.16. The components in displacement vector $\underset{\sim}{\overline{u}}^{(i)}$ and force vector $\underset{\sim}{\overline{f}}^{(i)}$ are independent. Since for small displacements the axial force effects, torsion, and bending about each axis are uncoupled, the influence coefficients relating these effects are negligible. The

constitutive relations between displacement vector $\underset{\sim}{\overline{u}}^{(i)}$ and force vector $\underset{\sim}{\overline{f}}^{(i)}$ are additive and we can derive the stiffness of the entire beam as shown in Equation 4.16. For large displacements, the effects of the force vector components are coupled and can be solved using multiple load steps to approximate the nonlinear deformation in the later section of this chapter.

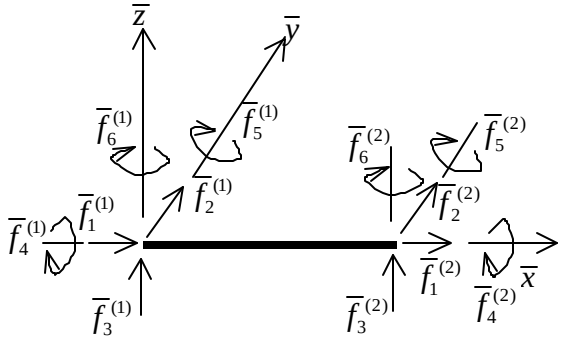

(a) Generalized Forces

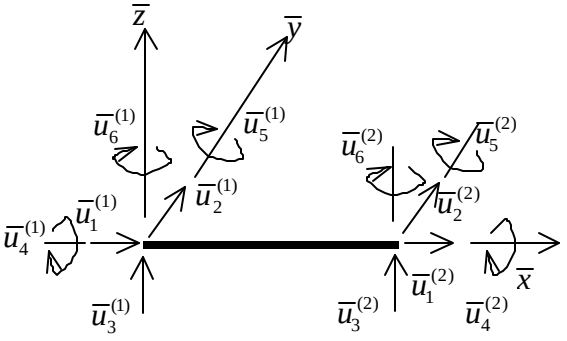

(b) Generalized Displacements

Figure 4.7 A 3-D Strut With Primary and Secondary Variables (or Degree of Freedom) In Local Coordinate System

$$\begin{bmatrix} \underset{\sim}{\overline{f}}^{(0)} \\ \hline \underset{\sim}{\overline{f}}^{(i)} \end{bmatrix} = \left[\underset{\sim}{\overline{K}}^{(i)}\right] \bullet \begin{bmatrix} \underset{\sim}{\overline{u}}^{(0)} \\ \hline \underset{\sim}{\overline{u}}^{(i)} \end{bmatrix}, \qquad i = 1,2,\ldots,N \tag{4.14}$$

$$\left[\underset{\sim}{\overline{f}}^{(i)}\right]=\begin{bmatrix}\overline{f}_1^{(i)}\\ \overline{f}_2^{(i)}\\ \overline{f}_3^{(i)}\\ \overline{f}_4^{(i)}\\ \overline{f}_5^{(i)}\\ \overline{f}_6^{(i)}\end{bmatrix},\qquad \left[\underset{\sim}{\overline{u}}^{(i)}\right]=\begin{bmatrix}\overline{u}_1^{(i)}\\ \overline{u}_2^{(i)}\\ \overline{u}_3^{(i)}\\ \overline{u}_4^{(i)}\\ \overline{u}_5^{(i)}\\ \overline{u}_6^{(i)}\end{bmatrix},\qquad i=0,1,2,...,N$$

where,

$\overline{f}_1^{(i)},\overline{f}_2^{(i)},\overline{f}_3^{(i)}$ – The translational forces at the i^{th} node along x, y and z axes in the local coordinate system

$\overline{f}_4^{(i)},\overline{f}_5^{(i)},\overline{f}_6^{(i)}$ – The bending moment or torsion at the i^{th} node around x, y and z axes in the local coordinate system

$\overline{u}_1^{(i)},\overline{u}_2^{(i)},\overline{u}_3^{(i)}$ – The translational displacements at the i^{th} node along x, y and z axes in the local coordinate system

$\overline{u}_4^{(i)},\overline{u}_5^{(i)},\overline{u}_6^{(i)}$ – The rotational displacements at the i^{th} node around x, y and z axes in the local coordinate system

N – The number of struts in unit truss

4.15

In Step (2), the stiffness tensor is transformed from the local coordinate system to global coordinate system as if a strut, whose orientation is represented as a vector $\underset{\sim}{v}$, is rotated around the three axes as shown in Figure 4.8. The transformation from the local coordinate system $\overline{xyz}$ to the global coordinate system xyz can be completed through three rotations: 1st rotation around $\overline{x}(x_1)$ by a, 2nd rotation around $z_1(z_2)$ by b, and 3rd rotation around $y_2(y)$ by g. The transformation tensor $\underset{\sim}{T}^{(i)}$ is shown as Equation 4.17, where p represents the transformation matrix given in Equation 4.18 for a single point in the 3-D space. Therefore, the stiffness tensor, $\underset{\sim}{K}^{(i)}$, in the global coordinate system is shown as Equation 4.19, which is exactly the same expression as Equation 4.7. But its size is increased to 12×12 compared with that of 2-D strut. The constitutive equation of the i^{th} 3-D strut written as in the global coordinate system is given as Equation 4.20, which is exactly the same as that of 2-D strut given in Equation

4.6. The displacements, $\underset{\sim}{u}^{(i)}$, and the forces, $\underset{\sim}{f}^{(i)}$ ($i = 0,1,...,N$), at the i^{th} node, are written in the global 3-D coordinate system and with 12 components as shown in Equation 4.21. Similarly to 2-D strut, this resulting global stiffness matrix $\left[\underset{\sim}{K}^{(i)}\right]$ of 3-D strut is partitioned into four sub-matrices, $\Phi_{11}^{(i)}$, $\Phi_{12}^{(i)}$, $\Phi_{21}^{(i)}$ and $\Phi_{22}^{(i)}$ ($i = 0,1,...,N$), which are 6×6 matrices as shown in Equation 4.22.

$$\left[\underset{\sim}{\overline{K}}^{(i)}\right] = E\bullet$$

$$\left[\begin{array}{cccccc:cccccc}
\frac{A}{L} & 0 & 0 & 0 & 0 & 0 & -\frac{A}{L} & 0 & 0 & 0 & 0 & 0 \\
0 & \frac{12I_z}{L^3} & 0 & 0 & 0 & \frac{6I_z}{L^2} & 0 & -\frac{12I_z}{L^3} & 0 & 0 & 0 & \frac{6I_z}{L^2} \\
0 & 0 & \frac{12I_y}{L^3} & 0 & -\frac{6I_y}{L^2} & 0 & 0 & 0 & -\frac{12I_y}{L^3} & 0 & -\frac{6I_y}{L^2} & 0 \\
0 & 0 & 0 & \frac{J}{2(1+u)L} & 0 & 0 & 0 & 0 & 0 & -\frac{J}{2(1+u)L} & 0 & 0 \\
0 & 0 & -\frac{6I_y}{L^2} & 0 & \frac{4I_y}{L} & 0 & 0 & 0 & \frac{6I_y}{L^2} & 0 & \frac{2I_y}{L} & 0 \\
0 & \frac{6I_z}{L^2} & 0 & 0 & 0 & \frac{4I_z}{L} & 0 & -\frac{6I_z}{L^2} & 0 & 0 & 0 & \frac{2I_z}{L} \\
\hdashline
-\frac{A}{L} & 0 & 0 & 0 & 0 & 0 & \frac{A}{L} & 0 & 0 & 0 & 0 & 0 \\
0 & -\frac{12I_z}{L^3} & 0 & 0 & 0 & -\frac{6I_z}{L^2} & 0 & \frac{12I_z}{L^3} & 0 & 0 & 0 & -\frac{6I_z}{L^2} \\
0 & 0 & -\frac{12I_y}{L^3} & 0 & \frac{6I_y}{L^2} & 0 & 0 & 0 & \frac{12I_y}{L^3} & 0 & \frac{6I_y}{L^2} & 0 \\
0 & 0 & 0 & -\frac{J}{2(1+u)L} & 0 & 0 & 0 & 0 & 0 & \frac{J}{2(1+u)L} & 0 & 0 \\
0 & 0 & -\frac{6I_y}{L^2} & 0 & \frac{2I_y}{L} & 0 & 0 & 0 & \frac{6I_y}{L^2} & 0 & \frac{4I_y}{L} & 0 \\
0 & \frac{6I_z}{L^2} & 0 & 0 & 0 & \frac{2I_z}{L} & 0 & -\frac{6I_z}{L^2} & 0 & 0 & 0 & \frac{4I_z}{L}
\end{array}\right]_{12\times12}$$

where,

E – Young's modulus of solid material i^{th} beam
I_x, I_y, I_z – Inertias of i^{th} beam along x, y, z axes
L – Length of i^{th} beam
A – Area of i^{th} beam cross-section
J – Torsion constant along x axis
u – Poisson's ratio

4.16

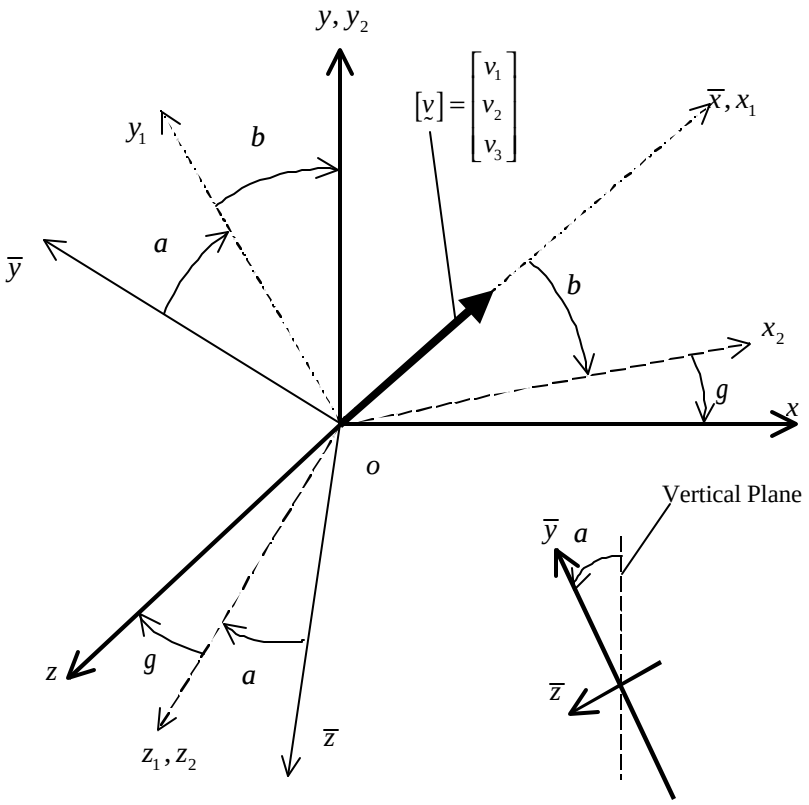

Figure 4.8 3-D Strut Rotated from Local Coordinate System to Global Coordinate System

$$\left[\underset{\sim}{T}^{(i)}\right] = \begin{bmatrix} p & 0 & 0 & 0 \\ 0 & p & 0 & 0 \\ 0 & 0 & p & 0 \\ 0 & 0 & 0 & p \end{bmatrix}_{12\times 12} \qquad 4.17$$

$$[p] = \begin{bmatrix} \cos g & 0 & \sin g \\ 0 & 1 & 0 \\ \sin g & 0 & \cos g \end{bmatrix} \bullet \begin{bmatrix} \cos b & \sin b & 0 \\ -\sin b & \cos b & 0 \\ 0 & 0 & 1 \end{bmatrix} \bullet \begin{bmatrix} 1 & 0 & 0 \\ 0 & \cos a & \sin a \\ 0 & -\sin a & \cos a \end{bmatrix}$$

Where, for a strut with an orientation represented by vector $\left[\underset{\sim}{v}\right] = \begin{bmatrix} v_1 \\ v_2 \\ v_3 \end{bmatrix}$ 4.18

a used for re-orienting crosssection and defined as shown in Figure 4.6

$b = 90^\circ - \cos^{-1}(v_2 / \|\underset{\sim}{v}\|)$

$g = \cos^{-1}(v_1 / \|\underset{\sim}{v}\|)$

$$\underset{\sim}{K}^{(i)} = \underset{\sim}{T}^{T} \bullet \overline{\underset{\sim}{K}}^{(i)} \bullet \underset{\sim}{T}$$

where, 4.19

$\underset{\sim}{T}^{T}$ – The transpose of $\underset{\sim}{T}$

$$\begin{bmatrix} \underset{\sim}{f}^{(0)} \\ \hline \underset{\sim}{f}^{(i)} \end{bmatrix} = \left[\underset{\sim}{K}^{(i)} \right] \bullet \begin{bmatrix} \underset{\sim}{u}^{(0)} \\ \hline \underset{\sim}{u}^{(i)} \end{bmatrix}, \qquad i = 1,2,...,N \tag{4.20}$$

$$\left[\underset{\sim}{u}^{(i)} \right] = \begin{bmatrix} u_1^{(i)} \\ u_2^{(i)} \\ u_3^{(i)} \\ \hline u_4^{(i)} \\ u_5^{(i)} \\ u_6^{(i)} \end{bmatrix}, \qquad \left[\underset{\sim}{u}^{(i)} \right] = \begin{bmatrix} u_1^{(i)} \\ u_2^{(i)} \\ u_3^{(i)} \\ \hline u_4^{(i)} \\ u_5^{(i)} \\ u_6^{(i)} \end{bmatrix}, \qquad i = 0,1,2,...,N$$

where,

$f_1^{(i)}, f_2^{(i)}, f_3^{(i)}$ – The translational forces at the i^{th} node along x, y and z axes in the local coordinate system

$f_4^{(i)}, f_5^{(i)}, f_6^{(i)}$ – The bending moment or torsion at the i^{th} node around x, y and z axes in the local coordinate system

$u_1^{(i)}, u_2^{(i)}, u_3^{(i)}$ – The translational displacements at the i^{th} node along x, y and z axes in the local coordinate system

$u_4^{(i)}, u_5^{(i)}, u_6^{(i)}$ – The rotational displacements at the i^{th} node around x, y and z axes in the local coordinate system

N – The number of struts in unit truss

4.21

$$\left[\underset{\sim}{K}^{(i)} \right] = \left[\begin{array}{ccc|ccc} K_{1,1}^{(i)} & \cdots & K_{1,6}^{(i)} & K_{1,7}^{(i)} & \cdots & K_{1,12}^{(i)} \\ \vdots & \ddots & \vdots & \vdots & \ddots & \vdots \\ K_{6,1}^{(i)} & \cdots & K_{6,6}^{(i)} & K_{6,7}^{(i)} & \cdots & K_{6,12}^{(i)} \\ \hline K_{7,1}^{(i)} & \cdots & K_{7,6}^{(i)} & K_{7,7}^{(i)} & \cdots & K_{7,12}^{(i)} \\ \vdots & \ddots & \vdots & \vdots & \ddots & \vdots \\ K_{12,1}^{(i)} & \cdots & K_{12,6}^{(i)} & K_{7,7}^{(i)} & \cdots & K_{12,12}^{(i)} \end{array} \right]_{12\times 12} = \left[\begin{array}{c|c} \Phi_{11}^{(i)} & \Phi_{12}^{(i)} \\ \hline \Phi_{21}^{(i)} & \Phi_{22}^{(i)} \end{array} \right]_{12\times 12} \tag{4.22}$$

Step (3) for 3-D unit truss is exactly the same as that for 2-D unit truss. The assembled stiffness tensor, $\underset{\sim}{K}^{e}$, of the entire 3-D unit truss with N struts is written as Equation 4.23. The finite element model of this 3-D unit truss in R^3 is shown as

Equation 4.24. $\underset{\sim}{K}^{e}$ is the stiffness tensor of the 3-D unit truss in the global coordinate system. $\underset{\sim}{U}^{e}$ denotes the displacements and $\underset{\sim}{F}^{e}$ denotes nodal forces on the unit truss. $\underset{\sim}{u}^{(i)}$ and $\underset{\sim}{f}^{(i)}$ are the displacements at the i^{th} node and the forces acting on the i^{th} node in the 3-D space. The 0^{th} node represents the central node of the 3-D unit truss.

$$\left[\underset{\sim}{K}^{e}\right]=\begin{bmatrix}\sum_{i=1}^{N}\Phi_{11}^{(i)} & \Phi_{12}^{(1)} & \Phi_{12}^{(2)} & \cdots & \Phi_{12}^{(N)}\\ \Phi_{21}^{(1)} & \Phi_{22}^{(1)} & 0 & \cdots & 0\\ \Phi_{21}^{(2)} & 0 & \Phi_{22}^{(2)} & \cdots & 0\\ \vdots & \vdots & \vdots & \ddots & \vdots\\ \Phi_{21}^{(N)} & 0 & 0 & \cdots & \Phi_{22}^{(N)}\end{bmatrix}_{6(N+1)\times 6(N+1)} \tag{4.23}$$

$$\underset{\sim}{K}^{e}\cdot\underset{\sim}{U}^{e}=\underset{\sim}{F}^{e} \tag{4.24}$$

$$\left[\underset{\sim}{U}^{e}\right]=\begin{bmatrix}\left[\underset{\sim}{u}^{(0)}\right]\\ \left[\underset{\sim}{u}^{(1)}\right]\\ \vdots\\ \left[\underset{\sim}{u}^{(N)}\right]\end{bmatrix},\left[\underset{\sim}{F}^{e}\right]=\begin{bmatrix}\left[\underset{\sim}{f}^{(0)}\right]\\ \left[\underset{\sim}{f}^{(1)}\right]\\ \vdots\\ \left[\underset{\sim}{f}^{(N)}\right]\end{bmatrix} \tag{4.25}$$

For the structure consisting of either 2-D or 3-D unit trusses, its energy bilinear form is defined as Equation 4.26.

$$W_{in}^{e}(\underset{\sim}{U}^{e})=\int_{\Omega^{e}}\frac{1}{2}\underset{\sim}{U}^{e}\bullet\underset{\sim}{K}^{e}\bullet\underset{\sim}{U}^{e}d\Omega^{e} \tag{4.26}$$

4.3 Adjusting Stiffness of Unit Truss with FEM

Some geometric features, such as overlapped geometries between struts, rounds and chamfers at the intersection edges, can influence the accuracy of this

analytical model. Their influences cannot be neglected when those features are large enough to affect the unit truss behavior. Most of them may be indispensable to reduce stress and increase lifetime. Ground truss approach does not count the effects of those geometry features and may incur non-negligible errors.

In Figure 4.9, the author shows a 3-D unit truss of octet truss, which is under uniform pressure on the end faces of the 12 struts. 6 struts are equally distributed in yoz plane, and 2 struts of them are oriented along the z axis. The other 6 struts are oriented by an angle of $60°$ with yoz plane and equally distributed. By assuming that the unit truss is under linear deformation and the overlap geometries at the joint can be ignored, we have the total forces on the unit truss and the resulting deformation shown in Equations 4.41 and 4.28. The equivalent elasticities in the x, y and z directions are given as 4.29. Since these three elasticities are only different within 4.9% in terms of magnitude, we may represent the equivalent elasticities with their average, E_{eff} given in Equation 4.30.

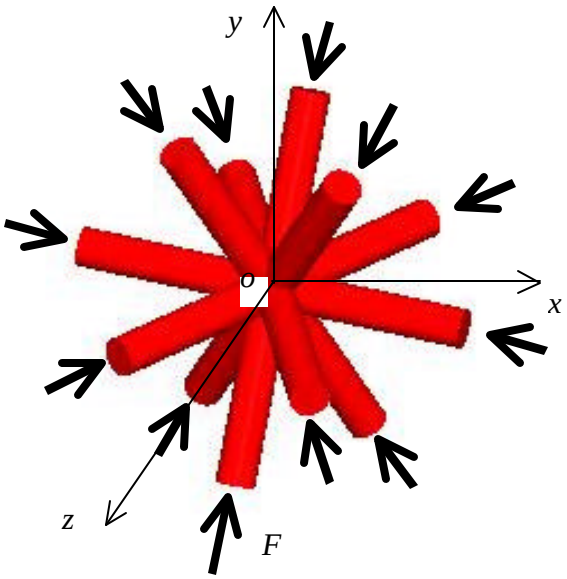

Figure 4.9 3-D Unit Truss of Octet Truss in Half Space

$$F_x = (2+\frac{\sqrt{3}}{2})F, F_y = (1+\sqrt{3})F, F_z = \frac{3\sqrt{3}}{2}F \quad (4.27)$$

where,

F – Force applied on the strut end face

$$d_x = 2\frac{FL_h}{AE_s}, d_y = \sqrt{3}\frac{FL_h}{AE_s}, d_z = \sqrt{3}\frac{FL_h}{AE_s} \quad (4.28)$$

where,

E_s – Elasticity of solid material

$A = \frac{p}{4}d^2$ – Area of strut end face

L_h – Length of half strut

d – Diameter of circular strut cross-section

$$E_x = \frac{4+\sqrt{3}}{8}\cdot\frac{E_s A}{L_h^2} \approx 0.7165\cdot\frac{E_s A}{L_h^2} \approx 0.5627\cdot E_s\left(\frac{d}{L_h}\right)^2$$

$$E_y = \frac{3+\sqrt{3}}{6}\cdot\frac{E_s A}{L_h^2} \approx 0.7887\cdot\frac{E_s A}{L_h^2} \approx 0.6194\cdot E_s\left(\frac{d}{L_h}\right)^2 \quad (4.29)$$

$$E_z = \frac{3}{4}\cdot\frac{E_s A}{L_h^2} = 0.75\cdot\frac{E_s A}{L_h^2} \approx 0.5890\cdot E_s\left(\frac{d}{L_h}\right)^2$$

$$E_{eff} = \frac{E_x + E_y + E_z}{3} \approx 0.7517\cdot\frac{E_s A}{L_h^2} \approx 0.5904\cdot E_s\left(\frac{d}{L_h}\right)^2 \quad (4.30)$$

In the above analysis, we have assumed that unit truss is under linear deformation and the geometry overlaps between struts at the joint are ignored. As a numerical approach, finite element analysis (FEA) could be used to correct the errors in the developed mechanics model. The FEA models (in ANSYS) of two unit trusses with different strut diameters while with identical half-strut length are shown in Figure 4.10. As shown in Figure 4.11, the effective elasticities from analytical and numerical analyses are fairly close when $\frac{d}{L_h} < 0.15$. When the ratio between strut diameter and half strut

length is about 0.8, the difference reaches about 40%. Therefore, it is necessary to correct the analytical modeling, in particular, the stiffness of unit truss.

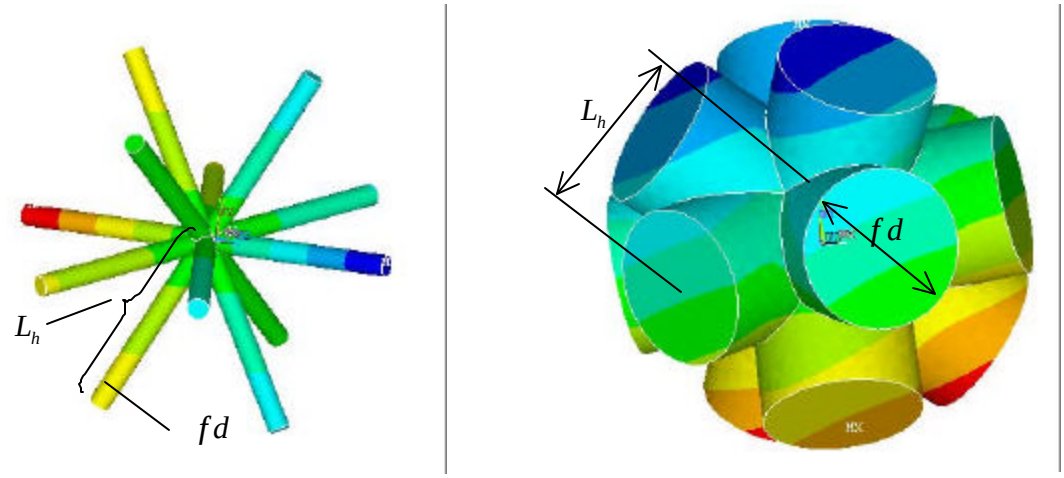

(a) $\frac{d}{L_h} = 0.1, \mathrm{Diff}(E_{eff}) = 2.57\%$, (a) $\frac{d}{L_h} = 0.8, \mathrm{Diff}(E_{eff}) = 39.9\%$,

Figure 4.10 Finite Element Analysis on Unit Truss

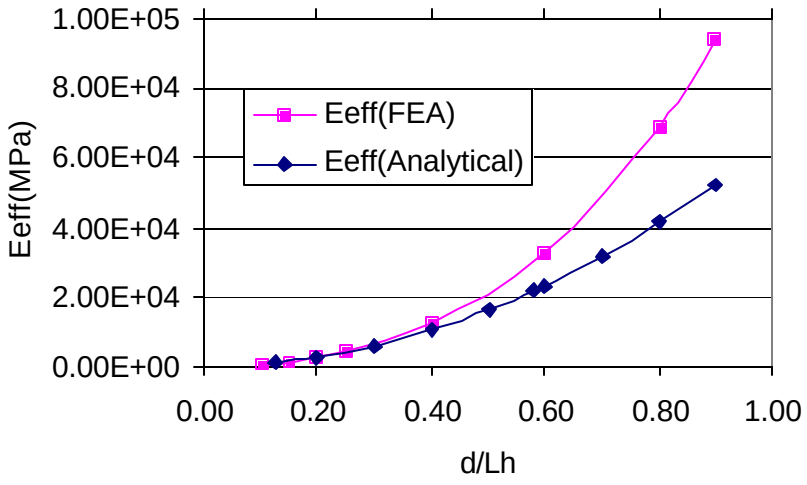

Figure 4.11 Comparing Effective Elasticities from Simplified Analytical Analysis and Finite Element Analysis

Some correcting items can be derived and added/multiplied to elasticity tensor $\underset{\sim}{K}^e$, to constitute a new elasticity tensor $\underset{\sim}{\tilde{K}}^e$. A typical correcting approach is to use a linear regression model (Neter, Kutner et al. 1996) as shown in Equation 4.31. Using the

results of the finite element analysis, the coefficients $\underset{\sim}{a}^{e}$ and $\underset{\sim}{R}^{e}$ can be evaluated through statistics. $\underset{\sim}{a}^{e}$ and $\underset{\sim}{R}^{e}$ will be functions of the shape variables under the particular loads.

$$\underset{\sim}{\tilde{K}}^{e} = \underset{\sim}{a}^{e} : \underset{\sim}{K}^{e} + \underset{\sim}{R}^{e} \qquad 4.31$$

This correcting process is time-consuming for compliant mechanisms. Fortunately, lightweight structures are stretching-dominated, and the components of stiffness matrix contributing to the bending can be neglected. The way to correct analytical model is to replace the diagonal components, $\Phi_{11}^{(i)}$ and $\Phi_{22}^{(i)}$, in the stiffness matrix with the new effective elasticity.

4.4 Consideration of Nonlinearity

In this research, the valid cellular structures undergo isothermal elastic deformation subjected to external loads and constraints. The lightweight truss structures under small load can be considered as linear elastic structure. However, both the lightweight truss under large deformation and all compliant mechanisms are concerned with nonlinear elasticity. Therefore, nonlinearity should be included when considering the strength of lightweight truss structures and the deformation of compliant mechanisms. The nonlinear elasticity is concerned with nonlinear effects associated with the deformations of elastic bodies (Fu and Ogden 2001). In nonlinear elasticity, the displacements are not linearly related to the loads, so Equation 4.12 and Equation 4.24 are no longer valid. This section presents the nonlinear elasticity problems related to cellular structures and the tangent stiffness method to solve the nonlinear problems.

4.4.1 Geometric Nonlinearity and Material Nonlinearity

There are three kinds of nonlinearity, geometric nonlinearity, material nonlinearity, and boundary nonlinearity. Boundary nonlinearity occurs when applied loads or constraints change. Boundary nonlinearity will not be discussed in our research since it is not the research focus.

Geometric nonlinearity occurs in the structures undergoing large displacements or rotations, large strain, or a combination of those. This kind of nonlinearity is due to geometry, but not due to a nonlinear stress-strain relation. For example, in a cantilever beam or a strut shown in Figure 4.12, if the maximum deflection at the right end, $d y_{\max}$, is more than 2% of the length L, or more than 20% of the short span length h, it is better to consider as nonlinear deformation under large displacement. The stress in this cantilever beam is still linearly related to strain, but the behavior or response, e.g., $d y_{\max}$, of the entire beam is not linearly dependent on the external load, P. When a beam or a strut undergoes compressional forces, the buckling is one of the failure modes and it is a geometric nonlinear problem.

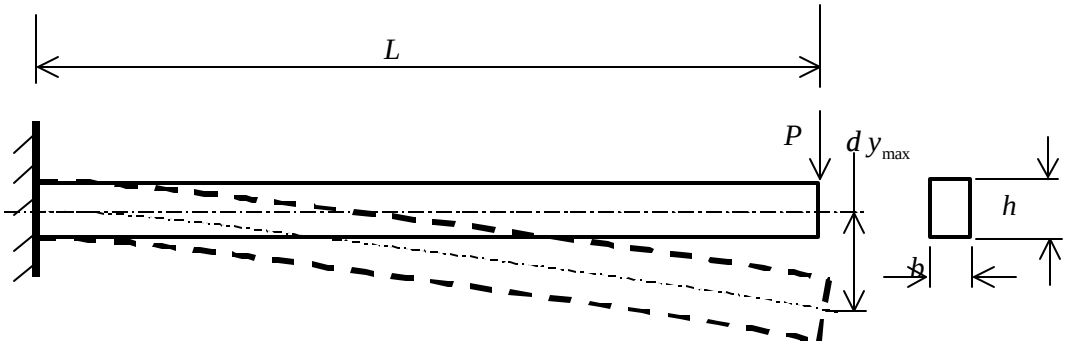

Figure 4.12 A Cantilever Beam under Geometric Nonlinear Deformation

Material nonlinearity occurs due to nonlinear stress-strain behavior. Plasticity is a typical material nonlinearity and happens when the deformation is beyond the yield point. Material nonlinearity also occurs when the stress s is between the proportional

limit s_{pl} and yield strength s_y. In Figure 4.13, the author shows the stress-strain relation of a typical plastic material in linear elasticity, nonlinear elasticity, and plasticity domains. The yield stress s_y is about equal to or slightly larger than the proportional limit s_{pl} for common engineering materials, and they are often interchangeable. In our research, only geometric nonlinearity is considered, so only the linear elasticity of stress-strain relation will be considered.

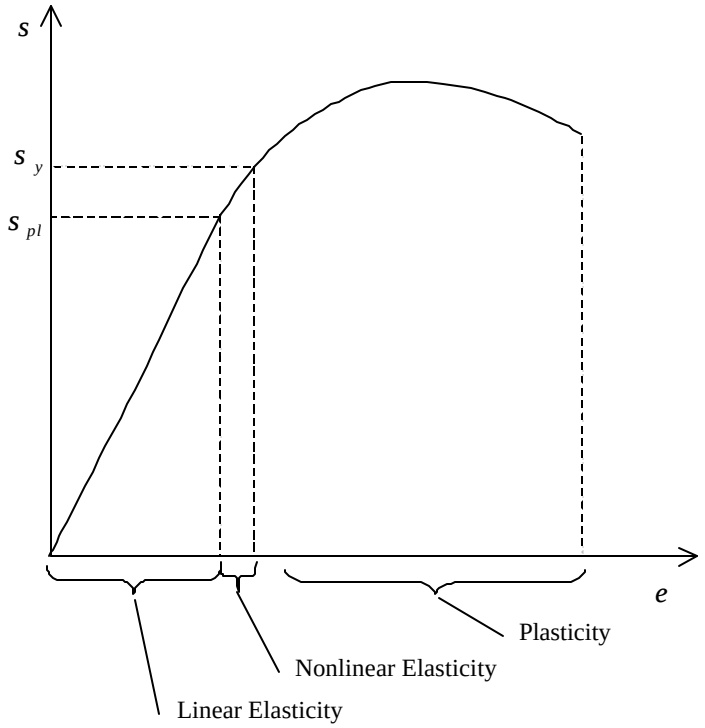

Figure 4.13 Material Nonlinearity of a Typical Plastic Material

4.4.2 Tangent Stiffness Method for Nonlinearity Analysis of Cellular Structures

A linearization approach will be applied to analyze the nonlinear elasticity problem of cellular structures. Tangent stiffness will be developed and used to represent the nonlinear behavior of individual struts, unit trusses, and entire structures. Euler method will be taken to realize the linearization of nonlinearity problem with tangent stiffness method.

4.4.2.1 Linearization of Nonlinear Problems Using Tangent Stiffness Method

In the analysis of nonlinear problems, the history of the deformation needs to be considered as if the structure undergoes progressive loading. The linearization process provides a practical way to solve nonlinear problems. Basically, nonlinear problems can be solved through a series of linear analysis steps. The linearization concept is founded on Taylor series expansion. A given set of equations as: $\underset{\sim}{f}(\underset{\sim}{x}) = \underset{\sim}{0}$, where $\underset{\sim}{f} : u \subset \underset{\sim}{x} \rightarrow \underset{\sim}{y}$ is a given map. For $\underset{\sim}{x} = \underset{\sim}{x}_0 + d\underset{\sim}{x}$, where $\underset{\sim}{x}_0$ is fixed, the linearization of the equations $\underset{\sim}{f}(\underset{\sim}{x}) = \underset{\sim}{0}$ about $\underset{\sim}{x}_0$ are the equations (Marsden and Hughes 1983):

$$\underset{\sim}{L}_{x_0}(\underset{\sim}{y}) = \underset{\sim}{0}$$

$$\text{where} \qquad \underset{\sim}{L}_{x_0}(\underset{\sim}{y}) = \underset{\sim}{f}(\underset{\sim}{x}_0) + \left.\frac{d\underset{\sim}{f}(\underset{\sim}{x})}{d\underset{\sim}{x}}\right|_{\underset{\sim}{x}=\underset{\sim}{x}_0} \bullet d\underset{\sim}{x} \tag{4.32}$$

To maintain the consistency of stiffness representation as we develop the mechanics model of unit truss in the previous section, the linearization process is presented in a matrix (2-D tensor) approach, which is taken by McGuire (McGuire, Gallagher et al. 2000). Linear elasticity theory is still used to solve the nonlinear problems. The linear elastic stiffness is designated as $\underset{\sim}{K}_e$ for any elastic deformed object (individual strut, microstructure, or entire system). The linear mechanics model is given as Equation 4.33. The subscript e denotes linear elasticity.

$$\underset{\sim}{K}_e \bullet \underset{\sim}{U} = \underset{\sim}{F} \tag{4.33}$$

According to Equation 4.32, the behavior of an elastic object can be traced back incrementally using Equation 4.34, which is still represented in a linear form (McGuire, Gallagher et al. 2000). $\underset{\sim}{K}_t$ is a tangent stiffness. $d\underset{\sim}{U}$ is incremental nodal displacements, and $d\underset{\sim}{F}$ is incremental nodal forces (including loads and reactions). $\underset{\sim}{K}_t$

consists of a linear elasticity component and one or more nonlinear components. This linearization approach to solve nonlinear problem is called Tangent Stiffness Method.

$$\underset{\sim}{K}_t \bullet d\underset{\sim}{U} = d\underset{\sim}{F} \qquad 4.34$$

The stiffness of 2nd order elasticity analysis with both geometric nonlinearity and material elastic nonlinearity accounted is shown in Equation 4.35. $\underset{\sim}{K}_g$ represents the geometric stiffness and accounts for the effects of geometric nonlinearity and nonlinear material elasticity (McGuire, Gallagher et al. 2000).

$$\underset{\sim}{K}_t = \underset{\sim}{K}_e + \underset{\sim}{K}_g \qquad 4.35$$

4.4.2.2 Tangent Stiffness of Individual Strut And Unit Truss for Geometric Nonlinearity

Since a unit truss consists of struts, the development of its geometric stiffness starts with a single strut. McGuire utilized the virtual work principle by applying virtual displacements to the reference configuration for a 2-D bending beam shown in Figure 4.5 (McGuire, Gallagher et al. 2000). The derived geometric stiffness $\underset{\sim}{K}_g^{(i)}$ of the i^{th} 2-D strut in R^2 space is shown as Equation 4.36. This geometric stiffness $\underset{\sim}{K}_g^{(i)}$ will be added onto the linear elastic stiffness $\underset{\sim}{K}_e^{(i)}$ of the i^{th} strut given in Equation 4.4 to obtain the tangent stiffness $\underset{\sim}{K}_t^{(i)}$ as shown in Equation 4.35. Then we can perform the coordinate transformation on $\underset{\sim}{K}_t^{(i)}$ from the local coordinate system to the global coordinate system and assemble the stiffness of the struts into that of the entire system as we do for the pure linear elastic stiffness using Equation 4.7 and Equation 4.11. Let $\underset{\sim}{K}_t^e$ denote the tangent stiffness of a unit truss. $d\underset{\sim}{U}^e$ and $d\underset{\sim}{F}^e$ denote the incremental displacements and forces on the nodes. Equation 4.37 shows the relation between incremental displacements and incremental forces of unit truss behavior. Therefore, the only

difference of mechanics model development between linear elasticity and nonlinear elasticity problems is the stiffness for individual struts. There is no difference in Step (2) and Step (3) of developing the constitutive equations presented in Section 4.2.1.

$$\left[\underset{\sim}{\bar{K}}_g^{(i)}\right] = \frac{F_{x_2}}{L}\left[\begin{array}{ccc|ccc} 1 & 0 & 0 & -1 & 0 & 0 \\ & \frac{6}{5} & \frac{L}{10} & 0 & -\frac{6}{5} & \frac{L}{10} \\ & & \frac{2L^2}{15} & 0 & -\frac{L}{10} & -\frac{L^2}{30} \\ \hline & & & 1 & 0 & 0 \\ & Sym. & & & \frac{6}{5} & -\frac{L}{10} \\ & & & & & \frac{2L^2}{15} \end{array}\right] \qquad 4.36$$

where,

F_{x_2} – Axial force along the beam at Node 2

L – Length of i^{th} beam

$$\underset{\sim}{K}_t^e \bullet d\underset{\sim}{U}^e = d\underset{\sim}{F}^e \qquad 4.37$$

McGuire also developed the geometric stiffness $\underset{\sim}{K}_g^{(i)}$ of the i^{th} 3-D strut in R^3 space and more information is available in Chapter 9 in his book (McGuire, Gallagher et al. 2000).

For either 2-D or 3-D unit truss, its incremental energy is given as Equation 4.38.

$$dW_{in}^e(\underset{\sim}{U}^e) = \int_{\Omega^e} (\underset{\sim}{F}^e \bullet d\underset{\sim}{U}^e) d\Omega^e \qquad 4.38$$

4.4.2.3 Using Tangent Stiffness with Euler Method for Geometric Nonlinearity

The approach of using multiple load steps is applied to solve the analysis equations (Equation 4.34) by updating the tangent stiffness $\underset{\sim}{K}_t$ ($\underset{\sim}{K}_t = \underset{\sim}{K}_e + \underset{\sim}{K}_g$) in every step. $\underset{\sim}{K}_e$ is static and without any change. $\underset{\sim}{K}_g$ is updated successively and calculated

upon certain current or reference internal forces $\underset{\sim}{F}_{ref}$. The new stiffness $\underset{\sim}{K}_t$ and reference load $\underset{\sim}{F}_{ref}$ are used to calculate the unknowns in the incremental forces $d\underset{\sim}{F}$ and the incremental displacements $d\underset{\sim}{U}$, then obtain new loads $\underset{\sim}{F}$ ($\underset{\sim}{F} = \underset{\sim}{F}_{ref} + d\underset{\sim}{F}$) and new displacements $\underset{\sim}{U}$ ($\underset{\sim}{U} = \underset{\sim}{U}_{ref} + d\underset{\sim}{U}$).

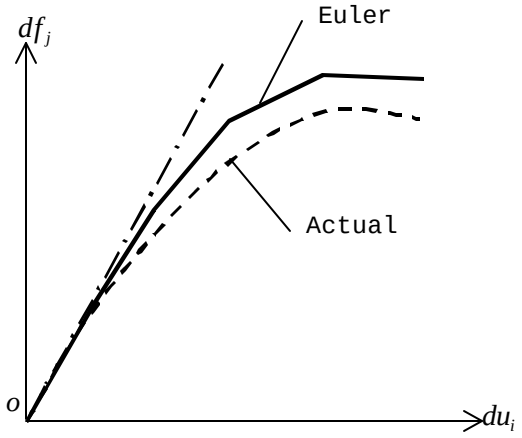

Figure 4.14 Euler Method for Multiple Load Step Approach

A variety of numerical methods is available for calculating the incremental forces $d\underset{\sim}{F}$ and the incremental displacements $d\underset{\sim}{U}$ (Faires and Burden 1998). The simplest step is to use Equation 4.34 directly to solve the unknowns in $d\underset{\sim}{F}$ and $d\underset{\sim}{U}$. This method is called Euler Method or Forward Difference Method (Faires and Burden 1998). In Figure 4.14, the author symbolically shows the solution differences of linear elasticity approach and Euler Method of 2nd order elasticity approach from the actual solution of nonlinear elasticity problems. For the nonlinear behavior analysis, the linear elasticity approach has worse accuracy to approximate the actual solution than Euler Method. Euler method is a piecewise linear approach and its accuracy depends on the number of load steps. When the strain du_i increases, the slope df_j / du_i becomes flat and the structure becomes soft. This is different from the material hardening behavior in nonlinear material deformation.

The incremental internal energy of a unit truss is given as Equation 4.39 for better accuracy, particularly useful for problems with large increments.

$$dW_{in}^{e}(\underset{\sim}{U}^{e}) = \int_{\Omega^e} ((\underset{\sim}{F}^{e} + \frac{d\underset{\sim}{F}^{e}}{2}) \bullet d\underset{\sim}{U}^{e}) d\Omega^{e} \qquad 4.39$$

4.5 Failure Mode in Cellular Structures

There are two possible failure modes in cellular structures, yielding and buckling. Yielding is the more common failure mode in all kinds of structures including lightweight truss structure and compliant mechanism. Buckling could be another main failure model for cellular structures. This section discusses the occurrence of buckling among cellular structures and identifies the most possible failure modes.

4.5.1 Failure Modes in Lightweight Truss Structures: Yielding and Buckling

Lightweight truss structure is a stretching dominated structure, where most stresses result from the tensional or compressional forces and the flexure stress from bending moment is relatively small. Compressional forces might cause the buckling failure among the long struts. The discussion of buckling issue starts with a single strut in the lightweight truss structure. If the strut is taken as a pin-jointed column, the buckling shape of the strut is shown as Figure 4.15(a). However, a buckled strut is under large deformation and the bending moments at its two joints cannot be neglected. When a strut is considered as a column with two ends clamped, the buckled shape is shown in Figure 4.15(b). The end condition of the struts in the lightweight truss structures is more like clamped ends.

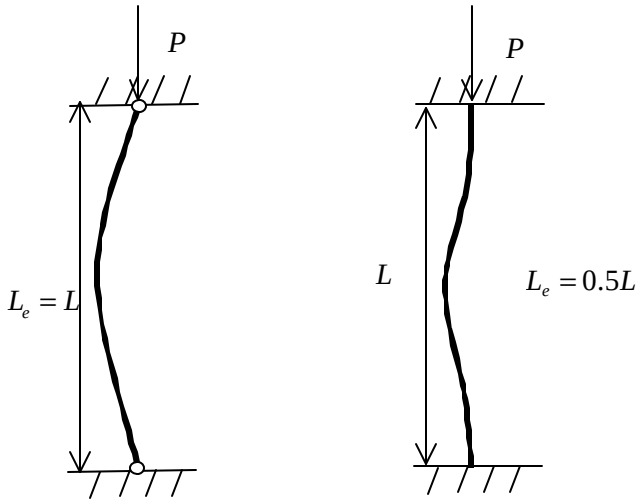

(a) Pin-jointed Strut Of The 1st Buckling Mode

(b) Clamped Strut Of The 1st Buckling Mode

Figure 4.15 Buckling of a Single Strut in Lightweight Truss Structure

For a strut with radius r, the critical compressional force P_{cr} to incur buckling is given as Equation 4.40 and the yield force P_y to incur strut yield is given as Equation 4.41. In the following discussion about failure analysis, the material is assumed to be imperfect or disturbance exists on the boundary. If the compressional force P reaches the critical force P_{cr} at first, buckling happens first. Otherwise P reaches the yield force P_y, then the yield failure happens first. The failure mode depends on the magnitude of the critical force P_{cr} and the yield force P_y. As shown in Equation 4.42, the influencing factors include Young's Modulus E, Yield Strength s_y, end condition, and Slenderness Ratio SR. For the struts in lightweight truss structure, the strut ends are considered as clamped, $K = 0.5$.

$$P_{cr} = \frac{EIp^2}{L_e^2} = \frac{Er^4 p^3}{4L_e^2}$$

where,

E – Young's Modulus

I – Area moment of cross-section inertia

L_e – Effective length of strut

r – Radius of strut cross-section

4.40

$$P_y = s_y A = s_y p r^2$$

where,

s_y – Yield strength

r – Radius of strut cross-section

4.41

$$\frac{P_y}{P_{cr}} = \frac{4s_y L_e^2}{p^2 E r^2} = \frac{4s_y}{p^2 E} \cdot K^2 \cdot SR^2$$

where,

$SR = \frac{L}{r}$ – Slenderness ratio

$L_e = K \cdot L$ – Effective length

K – Effective length factor

$K = 1$ for pin-jointed strut at both ends

$K = 0.5$ for clamped strut at both ends

4.42

In Table 4-1, the author shows the critical aspect ratios of various materials most commonly used for lightweight truss structure, which can be fabricated with Additive Fabrication (Dutta, Prinz et al. 2001). The aspect ratio is the ratio between strut length and strut diameter. Its value is half of the slenderness ratio. For the steel and aluminum structures, the critical aspect ratio is higher than that of structures manufacturable by additive fabrication, whose aspect ratios are usually less than 30. So for steel and aluminum truss structures, only yielding failure mode will happen. For SL 7510, WaterClear 10120 and ABS, buckling may happen earlier than yielding since their critical aspect ratios are only a little bit over 10. During our design process, the critical aspect ratio might be considered as a design constraint for the compressional struts. This is a

strong design constraint or strict criterion. A weak constraint or a loose constraint could be that the compressional axial forces must be less than the critical forces for the struts with aspect ratio larger than the critical aspect ratio.

Table 4-1 Critical Slenderness Ratio and Critical Aspect Ratio

Material	Yield Strength (MPa)	Young's Modulus (MPa)	Critical Slenderness Ratio	Critical Aspect Ratio
Steel	200	200000	99.35	49.67
Aluminum alloy (LM25)	150	71000	68.35	34.17
Titanium alloy	900	110000	34.73	17.37
RenShape SL 7510	57	2386	20.33	10.16
Somos WaterClear 10120	35	1960	23.51	11.75
ABS	45.7	2000	20.78	10.39

4.5.2 Failure Mode in Compliant Mechanism: Yielding

In a compliant mechanism, the structure is under large deformation. Most of the struts are bending and the flexure stress dominates those bent struts. The flexure yielding is the main failure mode for compliant mechanism. Some struts might be compression dominated. During the design process, those compression dominated struts should be re-examined for buckling failure. But very few struts need to be re-examined since most of the struts in compliant mechanism are either slender undergoing flexure or thick with bulk material.

4.6 Analysis of System Using Unit Truss as Elements

In this section, the author uses unit truss as element in finite element method to analyze entire cellular structures. Then the unit truss approach for mechanics analysis is implemented in Matlab.

4.6.1 Analysis of System Using Unit Truss as Elements

These unit trusses are special elements with bending moments and variable numbers of nodes. The elements provided by the existing commercial FEM packages (1999; 2004) cannot be customized with rotational displacements in strain tensor and bending moments in stress tensor. This section will particularly discuss the connectivity of unit trusses in the entire structural system. Imposition of boundary conditions and solution of equations will be briefly described since they are similar to those in the standard FEM process presented in Chapter 3 of Reddy's book (Reddy 1993).

To solve the total problem of the entire structure, the unit trusses are put back into their original positions. Similar to FEM process, the continuity of primary variables (nodal displacements) and the balance of the secondary variables (nodal forces) are imposed (Reddy 1993). The assembly of unit truss is carried out by imposing these two connectivity conditions shown in Equation 4.43 and Equation 4.44. The elements Ω_e and Ω_{e+1} are neighboring elements and share the same node, which is the m^{th} in the element Ω_e and the n^{th} in the element Ω_{e+1}. By following the connectivity conditions, the individual unit trusses are assembled into the entire system, and the system equations are shown in Equation 4.45. $[\underset{\sim}{U}]$ is the nodal displacement vector and $[\underset{\sim}{F}]$ the nodal load vector. N is the total number of nodes in the structure.

Continuity of nodal displacements of neighboring elements Ω_e and Ω_{e+1}

$$\underset{\sim}{u}^{(m)}|_{\Omega_e} = \underset{\sim}{u}^{(n)}|_{\Omega_{e+1}} \qquad 4.43$$

where,

$\underset{\sim}{u}^{(m)}|_{\Omega_e}$ – Displacement vector of the m^{th} node in element Ω_e

$\underset{\sim}{u}^{(n)}|_{\Omega_{e+1}}$ – Displacement vector of the n^{th} node in element Ω_{e+1}

Balance of nodal forces of neighboring elements Ω_e and Ω_{e+1}

$$\underset{\sim}{f}^{(m)}|_{\Omega_e} + \underset{\sim}{f}^{(n)}|_{\Omega_{e+1}} = \begin{cases} 0 & \text{if no external force applied} \\ \underset{\sim}{f}_0 & \text{if an external force } \underset{\sim}{f}_0 \text{ applied} \end{cases} \quad 4.44$$

where,

$\underset{\sim}{f}^{(m)}|_{\Omega_e}$ – Load vector of the m^{th} node in element Ω_e

$\underset{\sim}{f}^{(n)}|_{\Omega_{e+1}}$ – Load vector of the n^{th} node in element Ω_{e+1}

$$[\underset{\sim}{K}]\bullet[\underset{\sim}{U}] = [\underset{\sim}{F}] \quad 4.45$$

$$[\underset{\sim}{U}] = \begin{bmatrix} \left[\underset{\sim}{u}^{(0)}\right] \\ \left[\underset{\sim}{u}^{(1)}\right] \\ \vdots \\ \left[\underset{\sim}{u}^{(N)}\right] \end{bmatrix}, [\underset{\sim}{F}] = \begin{bmatrix} \left[\underset{\sim}{f}^{(0)}\right] \\ \left[\underset{\sim}{f}^{(1)}\right] \\ \vdots \\ \left[\underset{\sim}{f}^{(N)}\right] \end{bmatrix} \quad 4.46$$

For the convenience of computation, the nodal displacement vector $[\underset{\sim}{U}]$ and the nodal load vector $[\underset{\sim}{F}]$ in Equation 4.46 are written as Equation 4.48, where $\left[\underset{\sim}{U}^1\right]$ denotes the column of known displacements, $\left[\underset{\sim}{U}^2\right]$ the column of unknown displacements, $\left[\underset{\sim}{F}^1\right]$ the column of unknown loads, $\left[\underset{\sim}{F}^2\right]$ the column of known loads. Equation 4.45 is written as Equation 4.47 in the way as the standard FEM process (Hinton and Owen 1977; Reddy 1993). The sizes of sub-stiffness matrices $\left[\underset{\sim}{K}^{ij}\right]$ should correspond to the lengths of vectors $\left[\underset{\sim}{F}^i\right]$ and $\left[\underset{\sim}{U}^j\right]$.

$$\begin{bmatrix} \underset{\sim}{K}^{11} & \underset{\sim}{K}^{12} \\ \underset{\sim}{K}^{21} & \underset{\sim}{K}^{22} \end{bmatrix} \bullet \begin{bmatrix} \underset{\sim}{U}^1 \\ \underset{\sim}{U}^2 \end{bmatrix} = \begin{bmatrix} \underset{\sim}{F}^1 \\ \underset{\sim}{F}^2 \end{bmatrix} \quad 4.47$$

$$[\underset{\sim}{U}] = \begin{bmatrix} \underset{\sim}{U}^1 \\ \underset{\sim}{U}^2 \end{bmatrix}, [\underset{\sim}{F}] = \begin{bmatrix} \underset{\sim}{F}^1 \\ \underset{\sim}{F}^2 \end{bmatrix} \quad 4.48$$

The unknown displacements $\left[\underset{\sim}{U}^2\right]$ can be solved using Equation 4.49 and the unknown loads $\left[\underset{\sim}{F}^1\right]$ can solved using Equation 4.50 (Reddy 1993).

$$\left[\underset{\sim}{K}^{22}\right]\bullet\left[\underset{\sim}{U}^2\right]=\left[\underset{\sim}{F}^2\right]-\left[\underset{\sim}{K}^{21}\right]\bullet\left[\underset{\sim}{U}^1\right] \qquad 4.49$$

$$\left[\underset{\sim}{F}^1\right]=\left[\underset{\sim}{K}^{11}\right]\bullet\left[\underset{\sim}{U}^1\right]+\left[\underset{\sim}{K}^{12}\right]\bullet\left[\underset{\sim}{U}^2\right] \qquad 4.50$$

4.6.2 Implementation of Unit Truss Approach

This section presents the implementation of unit truss approach, and test examples. Some commercial finite element analysis packages, such as ANSYS, ABAQUS and FEMLAB, have been investigated for the implementation of mechanics analysis. However, none of them can provide customized elements with variable numbers of nodes and 2nd order derivatives of variables for the 2-D and 3-D problems. The mechanics analysis is implemented in MATLAB since it has superior capability of matrix computation and is much more flexible.

The implementation flowchart is shown in Figure 4.16. It follows a traditional finite element method, which has three steps: preprocessing, FEM processing, and post-processing (Reddy 1993). The traditional FEM method uses subdomains (elements) to represent the entire domain (system) with approximate behavior and the solution convergence should be verified. In contrast, the unit truss approach applied here is not an approximate approach since the unit trusses are just geometric subdomains divided from the entire structure. There is no approximation of mechanics behavior and no loss of accuracy. Therefore, convergence check is not required for unit truss approach to verify the convergence and the computation accuracy.

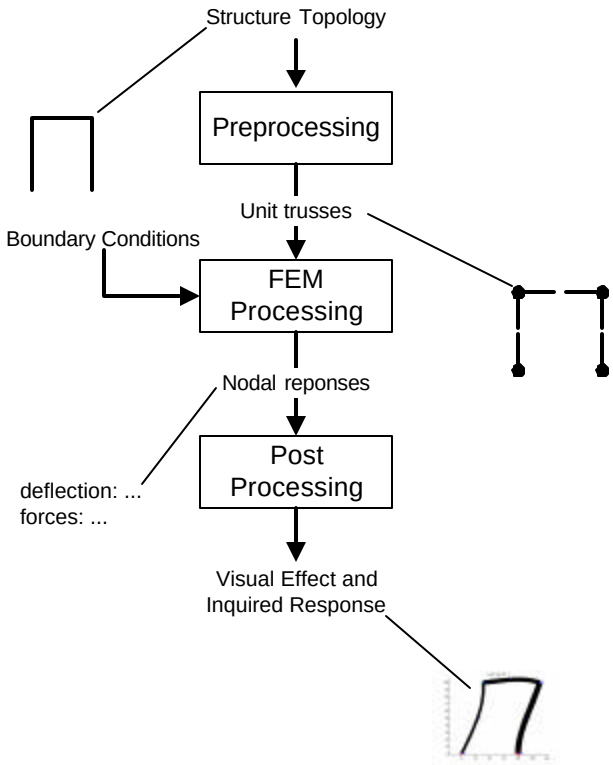

Figure 4.16 Implementation Flowchart of Mechanics Analysis

In the preprocessing step, the structure topology is formulated into unit truss. The unit truss, defined as Section 4.2, consists of one central node and the halves of the struts connected to this central node.

In the FEM processing step, the stiffness matrices of each individual unit truss and the entire structure system are calculated using Equation 4.11 and Equation 4.35, and the unknowns in the increments of the nodal displacements and forces are obtained using 4.34. For linear elasticity analysis, only one load step is required with a full load or displacement increment.

In the post-processing step, the shape of each bending strut is calculated through the interpolation of the displacements of two end nodes of the struts. The shape of an individual strut can be represented as a Hermite curve with the two known nodal

positions (obtained from translational displacements) and the two known tangent vectors (obtained from the rotational displacements) (Mortenson 1997).

4.7 Test Examples

To validate the unit truss approach for mechanics analysis, Example 10.7 from McGuire's book was taken for comparison (McGuire, Gallagher et al. 2000). The example is a frame structure with 6 nodes and 5 bending beams as shown as Figure 4.17. There are 4 vertical forces applied on the nodes on the top of the frame, 1 lateral force on the node at the upper right corner. The two nodes at the bottom of the frame are clamped. No residual stress exists before the loads are applied. The directions and the magnitudes of the loads are given as shown in Figure 4.17. The two vertical beams are identical (area A_1 and inertia I_1), and the three horizontal beams have the same cross-section areas (area A_2 and inertia I_2). The lengths and cross-section areas of the beams are indicated in Figure 4.17.

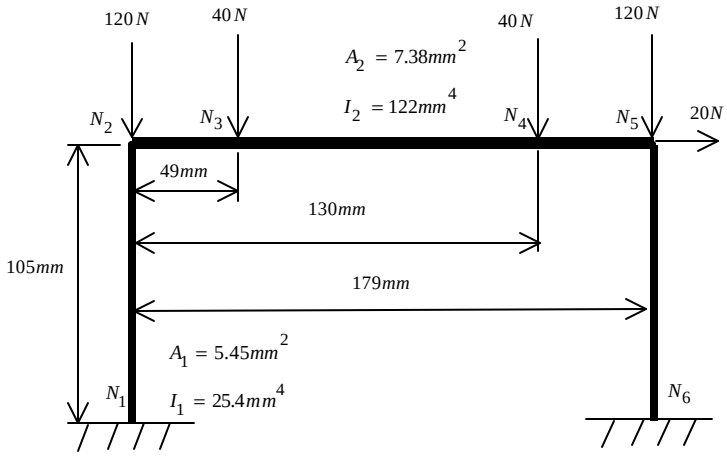

Figure 4.17 2-D Structure with Five Struts

Using the unit truss approach implemented in MATLAB, the deformed shape of the tested frame is shown as Figure 4.18 with boundary conditions, node and strut IDs

indicated. The deformed shape is identical to that resulting from MASTAN2 developed by McGuire (McGuire, Gallagher et al. 2000).

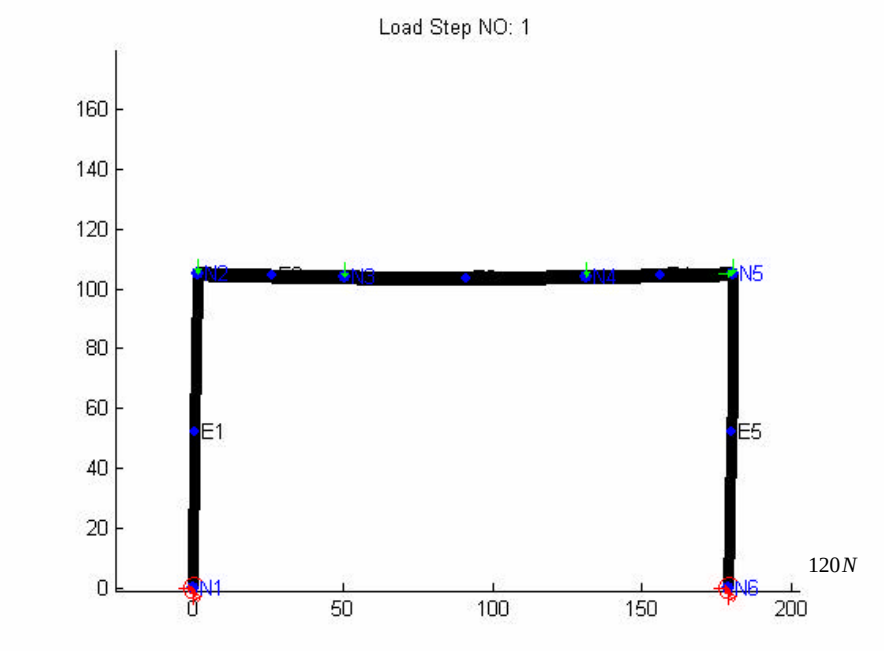

Figure 4.18 Deformed Shape of Test Example: Structure with Five Struts

In Table 4-2, the author shows the horizontal deflection of Node N_5 for linear and nonlinear elasticities as all the nodal loads incrementally change from zeroes to full loads. Load ratio denotes the ratio between the applied load and the full load. The chart of the load ratios and the specified deflections is shown in Figure 4.19. In the linear elasticity analysis, the specified deflection is proportional to the load ratio. In the nonlinear elasticity analysis, the relation between the specified deflection and the load ratio shows the nonlinearity as expected. The nonlinear behavior shown in Table 4-2 is coincident with the computational result from Example 10.7 in McGuire's book (McGuire, Gallagher et al. 2000).

Table 4-2 Horizontal Deflection of N_5 in The Test Example for Linear Analysis and Nonlinear Analysis

Load Ratio	0	0.1	0.2	0.3	0.4	0.5	0.6	0.7	0.8	0.9	1
Linear	0	0.153	0.306	0.459	0.613	0.766	0.919	1.072	1.225	1.378	1.532
Nonlinear	0	0.153	0.313	0.48	0.655	0.839	1.033	1.237	1.454	1.684	1.93

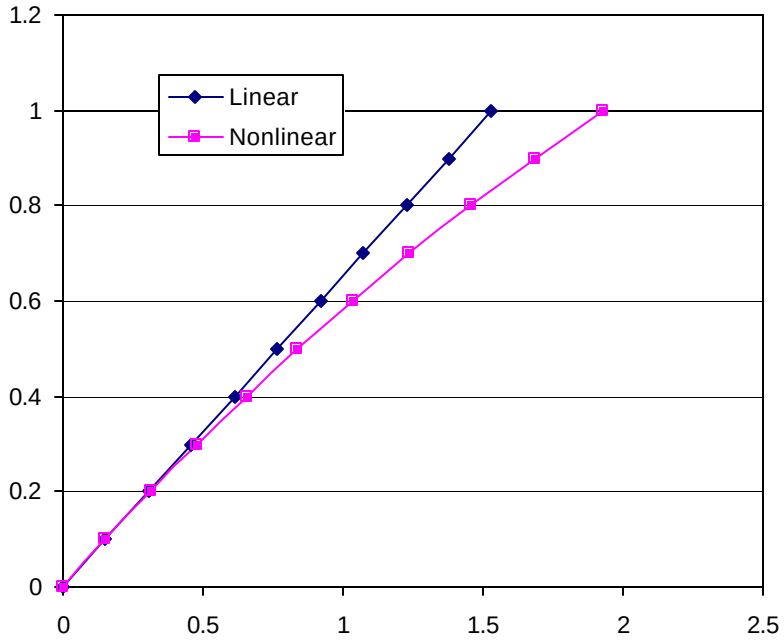

Figure 4.19 Horizontal Deflection of N_5 in the Test Example for Linear Analysis and Nonlinear Analysis

In Figure 4.20, the author shows the deformed shape of another example of hexagon truss structure analyzed by the unit truss approach. This truss structure has 88 bending struts and 66 nodes. Its overall size is about 86.6mm wide and 80 high. The maximum deflection in the structure is 9.56mm at Node N_{13}. In Figure 4.21, the author shows the deformed shaped of this structure analyzed by MASTAN2, which was provided by McGuire's book (McGuire, Gallagher et al. 2000). The analysis results from unit truss approach and MASTAN2 are exactly the same. The displacements of a few typical nodes are shown in Table 4-3. These two test examples indicated that the unit truss approach and its implementation are correct.

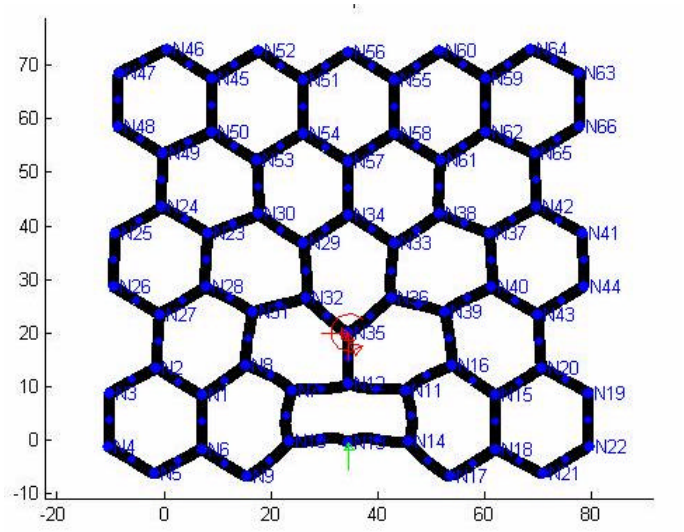

Figure 4.20 Deformed Shape of Hexagon Truss with Struts Using Unit Truss Approach

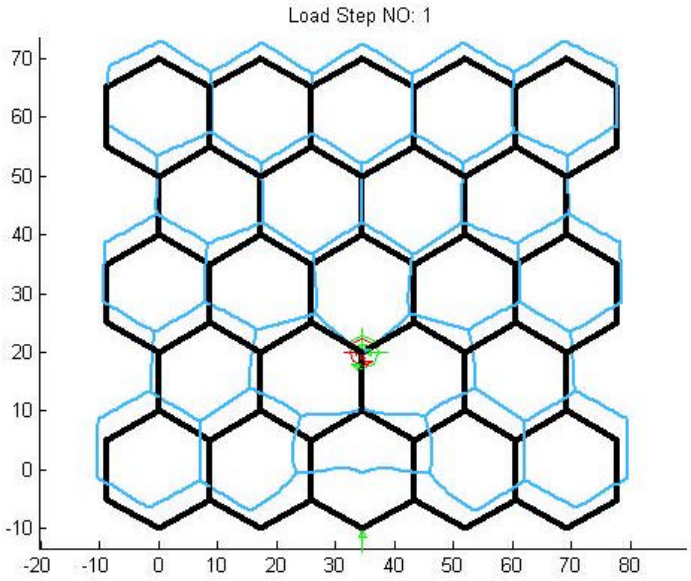

Figure 4.21 Deformed Shape of Hexagon Truss with Struts Using MASTAN2

Table 4-3 Analysis Results from Unit Truss Approach and MASTAN2

	Node N13		Node N4		Node N46		Node N64	
	x disp.	y disp.	x disp.	y disp.	x disp.	y disp.	x disp.	y disp.
Unit Truss Approach	0.0002	9.5555	-1.5864	3.7318	0.6047	2.978	-0.6051	2.9783
MASTAN2	0.0002	9.5555	-1.5864	3.7318	0.6047	2.978	-0.6051	2.9783

4.8 Chapter Summary

Unit truss is introduced and used as the common microstructure for the mechanics analysis of cellular structures, including both lightweight truss structure and compliant mechanism. The mechanics models (constitutive equations) of both 2-D unit truss structure and 3-D unit truss were developed based on beam theory. Nonlinear elasticity of the structures, particularly largely deformed truss structure and compliant mechanism, are considered using tangent stiffness method. The failure modes of cellular structure are discussed. Yielding happens first in aluminum alloy and steel structures manufacturable by additive fabrication. In SLA and ABS truss structures, buckling may happen earlier than yielding and it depends on the aspect ratio of individual struts. Yielding is the main failure mode in compliant mechanism. The unit truss approach was implemented in MATLAB. Two test examples are tested to verify the unit truss approach.

Fatigue mechanism and residual stress of cellular structures have not been discussed in this research. However, they are an important issue for the design of adaptive structures. We have performed structural analysis on adaptive cellular structures. An interesting topic about adaptive cellular structures is to design for multiple functionalities. Fatigue, residual stress and multiple functionality analysis will be important future work. “Size” effect of unit trusses remains an open issue. In this research, the size of unit trusses was given based on my own experience. It is unknown whether refining unit trusses can improve design results. We do not know what size is most appropriate for design synthesis of cellular structures. The “size” effect of unit truss could be a future work and open for further discussion.

In Chapter 4, unit truss has been successfully used to support the mechanics analysis of cellular structures. Its analytical mechanics model for finite element method was developed to analyze both 2-D and 3-D structures. Bending, torsion and nonlinearity

(geometric and material) are considered. Unit truss enabled an accurate analysis of entire cellular structures. In this chapter, the issue about “analysis” (raised in Section 2.4) was addressed. The development of mechanics model of unit truss proved the theoretical structural validity of the unit truss approach. Its empirical structural validity (shown in Figure 1.22) of the hypothesis (posed in Section 1.4) was proved through successfully solving 2-D and 3-D example problems.

CHAPTER 5

DESIGN SYNTHESIS OF CELLULAR STRUCTURES

In this chapter, the "synthesis" issue in the unit truss approach raised in Section 2.4 is addressed by the development of a systematic design synthesis for adaptive cellular structures. The organization of Chapter 5 is presented in the context of the Validation Square shown in Figure 5.1. Engineering optimization technique is adapted and integrated with representation, analysis and manufacturing to perform design synthesis. It starts with a discussion about the problem's characteristics in terms of design variables, design objectives, and constraints. The design synthesis problems of lightweight truss structure and compliant mechanism are formulated. Different search algorithms are compared and Particle Swarm Optimization is identified as the search algorithm to search for the superior solution of the design synthesis. A detailed description of Particle Swarm Optimization is given. Penalty function is introduced to consider the bounds of design variables and other inequality constraints. The Particle Swarm Optimization with unit truss approach will be implemented in MATLAB, and a validation example of lightweight truss structure will be presented. The focus of Chapter 5 is shown in Figure 5.2.

5.1 Analysis of Problem Characteristics

This section discusses the characteristics of the structural design synthesis problem of cellular structures including lightweight truss structures and compliant mechanisms.

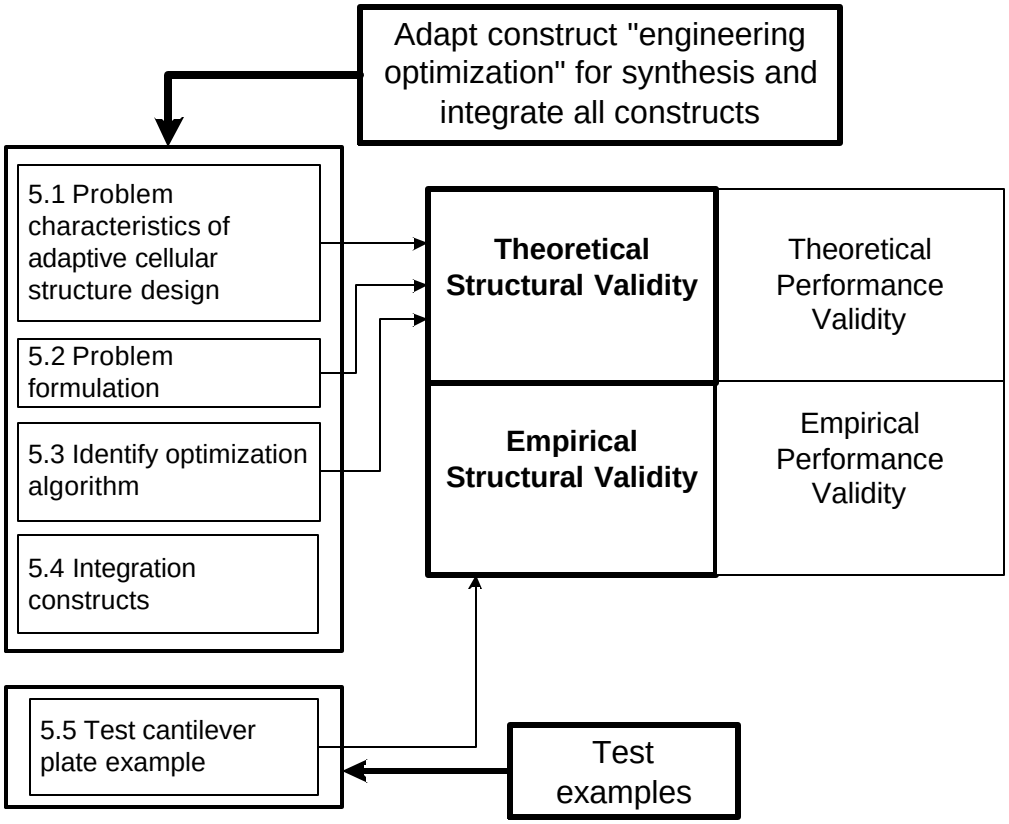

Figure 5.1 Relationship between Chapter 5 and Validation Square

5.1.1 A General Problem Formulation of Structural Design Synthesis Involving FEM

The behavior of the structures is simulated on computer using the mechanics analysis approach presented in Chapter 4. This analysis approach is a finite element method using unit trusses as microstructures or elements. Structural design synthesis problem involving finite elements can be generally expressed as Equation 5.1 (Belegundu and Chandrupatla 1999). $\{x\} = \{x_1, x_2, \ldots, x_n\}$ denotes design variables and U denotes nodal displacement vector. $f_i(x)$ is the design objective, and it can be displacement and stress. $g_i(x) \le 0$ represents inequality constraints and $h_i(x) = 0$ represents equality constraints. Displacement vector $U = U(x)$ is implicitly a function of

design variables $\underset{\sim}{x}$ as shown in the equality $h_1(x)=0$ of Equation 5.1. $K(x)$ is the stiffness of the structure and $F(x)$ is the nodal load vector. Both $K(x)$ and $F(x)$ are explicit functions of design variables x. For cellular structures, $K(x)$ is obtained using the unit truss approach, and the equality $h_1(x)=0$ of Equation 5.1 is solved as the approach described in Chapter 4.

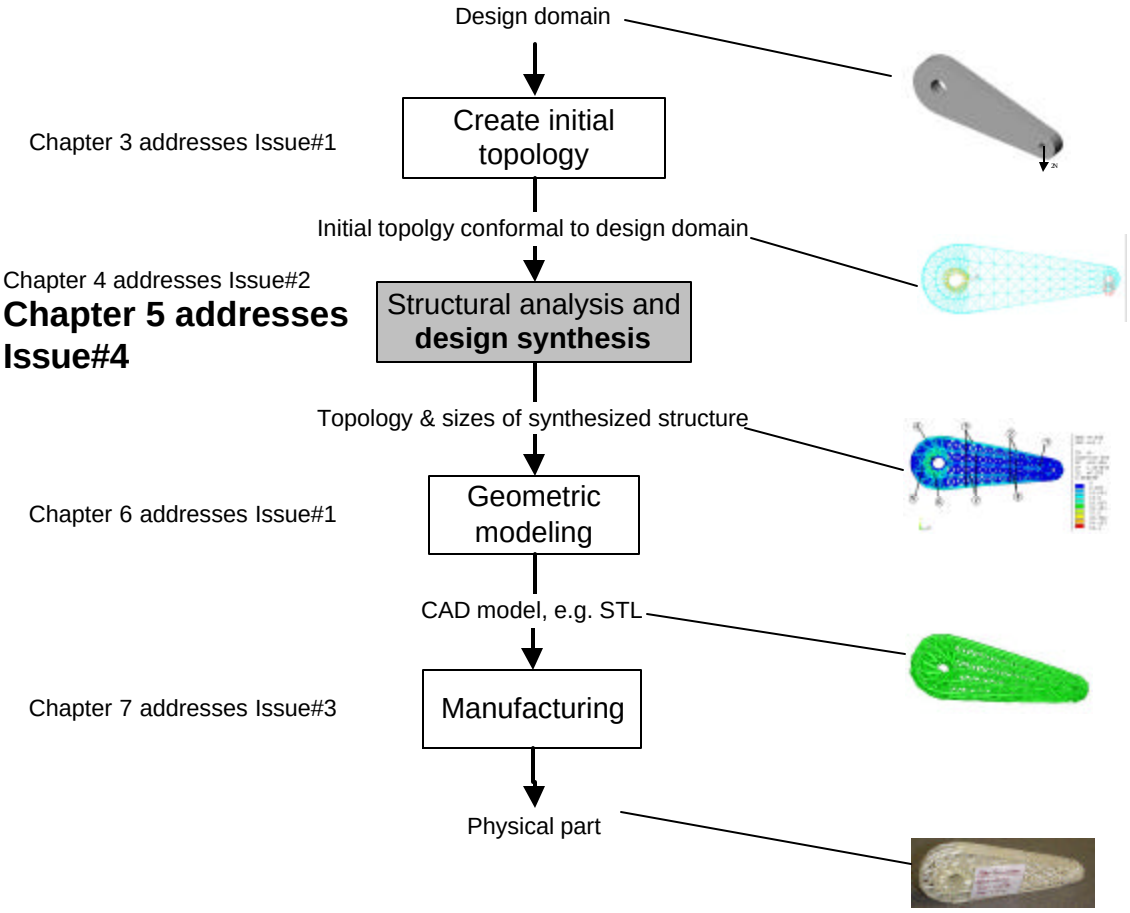

Figure 5.2 Research Focus of Chapter 5 in the Design Process of Cellular Structures

$$\begin{aligned} \text{minimize} \quad & f_i(x), i=1,2,\ldots,k \\ \text{subject to} \quad & h_1(x)=K(x)\bullet U(x)-F(x)=0 \\ & h_i(x)=0, i=2,\ldots,l \\ & g_i(x)\le 0, i=1,2,\ldots,m \end{aligned} \qquad 5.1$$

5.1.2 Design Variables

Design variables are denoted by x and can take on various forms. In homogenization method, material density, an artificial variable, is set as design variable (Bendsoe and Kikuchi 1988; Sigmund 2001). Domains with $x = 0$ or close to zero are void and with no material. Domains with $x = 1$ are solid and occupied with material. Domains with $0 < x < 1$ are partially occupied by material, but those domains do not physically exist. However, artificial material density is effective to represent material distribution for structure optimization. In cellular structures, either strut diameters or cross-section areas can be design variables if the struts of structure are cylindrical. Both widths and heights of the struts cross-sections can be design variables if the struts of structure are rectangular. The parameters of other geometry features can be design variables as well. Even the positions of the nodes can be considered. Therefore, all the variables controlling the structure's shape or topology of the body can be design variables. For cellular structures, diameters of cylindrical struts or widths and heights of rectangular struts are considered as design variables. For example, in a structure consisting of n cylindrical struts, there are n design variables, each of which corresponds to one strut diameter. Therefore, the number of design variables depends on the number of struts, and it is usually more than 50, sometime even thousands. The design synthesis problem of cellular structures is a large-scale problem with a large number of design variables. For lightweight truss structure design in our research, the strut' diameters are set as design variables. For compliant mechanism design in our research, the struts' widths and thickness are set as design variables.

5.1.3 Objective functions

Objective functions $f_i(x)$ can be to minimize deflection, strain energy, maximum stress, or even the deviations between the actual displacements and the desired

displacements. For cellular structures, the design objective could be one or multiple. For instance, the deflection minimization can be the sole objective of some lightweight truss structures with volume and stress considered as constraints. For compliant mechanisms, the design objective can be to achieve desired displacements at certain nodes. For most cases, there are multiple design variables. The objective functions $f_i(x)$ are implicit of the design variables x as described in Section 4.5. Some objectives are nonlinearly related to the design variables x even for linear deformation cases. For instance, the stress of cylindrical strut under axial force is nonlinearly related to the strut diameter and the cross-section area.

In the structural optimization of lightweight structure for minimum compliance, Sigmund considered minimization of bilinear strain energy of the entire structures as the design objective shown in Equation 5.2 (Sigmund 2001). Bendsoe used the external work as objective shown in Equation 5.3 (Bendsoe 1995). Liu and Lu set maximum displacement and maximum Von Mises stress in the structures, fundamental frequency, and total mass as design objectives (Liu and Lu 2004). In our research to design lightweight truss structure, maximum nodal displacement is set as objective.

Strain Energy $$SE = \int_{\Omega} \frac{1}{2} e^T \bullet E \bullet e \, d\Omega$$

where, 5.2

e – strain under the applied input load

E – stiffness

External work $$W_{external}(u) = \int_{\Omega} p^T \bullet u \, d\Omega + \int_{\Gamma_T} t^T \bullet u \, ds$$

where,

p – body force in domain Ω 5.3

t – traction on boundary Γ_T

u – strain

In designing compliant mechanisms shown in Figure 5.3, Kota and his colleagues set the ratio between mutual potential energy and strain energy, $\frac{SE}{MSE}$, as the objective (Canfield and Frecker 2000; Xu and Ananthasuresh 2003; Joo, Kota et al. 2004). SE and MSE are shown in Equation 5.4. Saggere, et. al. used material volume as the objective for design synthesis of planar, compliant four-bar mechanisms for motion generation (Saggere and S. 2001). Geometric Advantage, the ratio between displacement at output point and displacement at input point, was also applied to represent design objective for compliant mechanism design problem with single pair of input and output (Canfield and Frecker 1999; Kota, Joo et al. 2001). In recent publications by Lu and Kota about shape morphing, the "Least Square Error" between the deformed shape and the target shape is used as design objective (Lu and Kota 2002; Lu and Kota 2003; Lu and Kota In Press). One approach is to use "Mean Squared Deviation" of position differences (or distance) between the actual positions and the desired positions of the sampled points. The "Mean Squared Deviation" or "Mean Squared Difference" is shown in Equation 5.5 (Neter, Kutner et al. 1996; Kobayashi and Salam 2000). The function value of Mean Squared Deviation changes more smoothly than that of Standard Deviation since the square operation in Mean Squared Deviation makes the function's first derivative exist in a continuous design space. The selection of design objectives depends on the characteristics of the design problems and different objective functions have different influences on design process and results. Weighted Mean Squared Deviation (Shin and Ali H. Sayed 2004) shown Equation 5.6 can be used to assign weights of sampled points to achieve smaller deviations at certain points. In our research, Mean Squared Deviation will be used as design objective to design compliant mechanism in the case study, "Digital Clay", in which the compliant mechanism will be deformed into the desired shape.

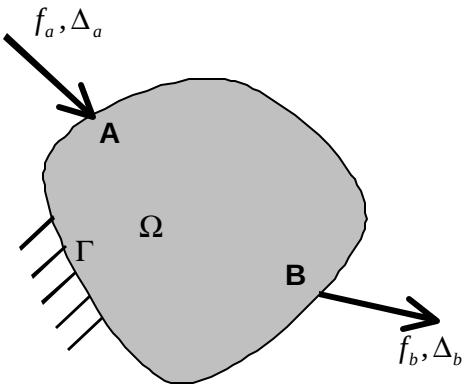

Ω – structure's domain

Γ – boundary

f_a – applied load at input point A

f_b – dummy load at output point B

Δ_a – deflection at input point A

Δ_b – deflection at input point B

Figure 5.3 An Abstract Compliant Mechanism

Mutual potential energy $MPE = V_b^T \bullet K \bullet U_a$

Strain energy $SE = \frac{1}{2} U_a^T \bullet K \bullet U_a$

where, 5.4

K – stiffness

U_a – deflection due to the applied load f_a

V_a – deflection due to the dummy load f_b

Mean Squared Deviation $MSD = \frac{1}{m} \sum_{i=1}^{m} \left\| P_{\text{actual},i} - P_{\text{desired},i} \right\|^2$

where,

m :number of sampled points from the structure

$P_{\text{actual},i} = (x_{\text{actual},i}, y_{\text{actual},i})$:actual position of the i^{th} sampled point of the deformed structure 5.5

$P_{\text{desired},i} = (x_{\text{desired},i}, y_{\text{desired},i})$:desired position of the i^{th} sampled point of the deformed the structure

$$\left\| P_{\text{actual},i} - P_{\text{desired},i} \right\| = \sqrt{(x_{\text{actual},i} - x_{\text{desired},i})^2 + (y_{\text{actual},i} - y_{\text{desired},i})^2}$$

Mean Weighted Squared Deviation $MSD_w = \frac{\sum_{i=1}^{m} w_i \left\| P_{\text{actual},i} - P_{\text{desired},i} \right\|^2}{\sum_{i=1}^{m} w_i}$ 5.6

where,

w_i – weight of the i^{th} sampled points on the mean squared deviation

Most objective functions of structural synthesis are nonlinear, such as stress and deflection, when objective functions are written in terms of size design variables. The objective functions are non-differentiable if the problem involves piecewise constraints (Reklaitis, Ravindran et al. 1983). Due to the manufacturability, the bounds of design variables of cellular structures are piecewise and the objective functions are non-differentiable. It could be differentiable after the piecewise boundedness is ignored or transformed into continuous constraints. For some objective functions, it takes huge efforts or computation resources to obtain gradients and Hessian matrices, particularly for those with no analytical models (Reklaitis, Ravindran et al. 1983; Belegundu and Chandrupatla 1999). For example, when the structural performances are simulated by finite element methods, neither gradients nor Hessian matrices can be obtained in analytical forms. Usually design objectives of structures under small deformation are convex functions, and gradient-based approaches are popularly applied. However, the design objectives of compliant mechanism are concave and one example is compliant bi-stable micro-mechanism (Howell 2001; Jensen, Parkinson et al. 2001). There could be multiple local minima in the design space. In compliant mechanisms that are under large deformation, the relation between loads and displacement is nonlinear or written as nonlinear equalities as discussed in Chapter 4. If at least one nonlinear equality is involved, the problem is non-convex (Reklaitis, Ravindran et al. 1983). The design of compliant mechanisms in our research has multiple nonlinear objective functions and some could be concave.

5.1.4 Design Constraints

Design constraints are categorized into two types: equalities $h_i(x) = 0$, and inequalities $g_i(x) \le 0$. Some constraints are bounds of design variables; others are on state variables, such as stress, volume, and even displacements.

5.1.4.1 Bounds on Design Variables

The problem boundedness always presents since design variables are limited by their physical meaning and the manufacturability of cellular structures.

In homogenization method, the design variables, artificial material density x_i, are bounded as $x_i \in [x_{\min}, 1.0]$. $x_{\min}$ is set as a non-zero positive (e.g., $x_{\min} = 0.1$) to avoid singularity in stiffness matrix. Penalization power p (e.g., $p = 3$) is used to penalize the presences of domains with densities falling between $x_{\min}$ and 1.0. The domain stiffness is artificially interpolated as Equation 5.7.

$$k_e = (x_e)^p k_s$$

where,

x_e – material density of artificial element e

k_e – stiffness of artificial element e with material density x_e

k_s – stiffness of solid element filled with regular material

p – penalization power

5.7

In our research for design synthesis of cellular structures, the diameters of cylindrical struts of lightweight truss structures are set as design variables, or the widths and thicknesses of rectangular struts of compliant mechanisms are set as design variables. The design variables are bounded by physical meaning and manufacturability as $x_i \in \{0, [x_{\min}, x_{\max}]\}$. When $x_i = 0$, there is no strut existing. $x_{\min}$ is the minimum size manufacturable by the manufacturing process. In our research, Additive Fabrication (AF) is utilized to fabricate the cellular structures. For 3D structure, a typical minimum manufacturable size $x_{\min}$ with SLA 3500 is $0.7mm$.

The strut's aspect ratio is one of the constraints that can be converted into bounds of design variables. As shown in Equation 5.8, the aspect ratio is the ratio between the length and the diameter for cylindrical struts, or the ratio between the length

and the width (or thickness, whatever smaller) for rectangular struts. For cylindrical struts, the maximum aspect ratio $AR_{\max}$ manufacturable by SLA 3500 is about 35. The diameter of cylindrical struts should be constrained as $x_i \geq L_i / AR_{\max}$ by the maximum aspect ratio. Combined with the constraint on minimum manufacturable size, the bounds of design variables of cylindrical struts are given as the inequality shown in Equation 5.9.

$$AR_i = \frac{L_i}{x_i} \leq AR_{\max}$$

where,

AR_i – aspect ratio of the i^{th} strut

$AR_{\max}$ – maximum manufacturable aspect ratio

x_i – diameter of cylindrical strut or width of rectangular strut

L_i – strut length

5.8

$$x_i \in \left\{0, \left[\max(x_{\min}, L_i / AR_{\max}), x_{\max}\right]\right\} \qquad 5.9$$

5.1.4.2 Constraints on State Variables

Most structural optimization problems are subject to constraints not only on design variables, but also on state variables, such as stress, material volume, cost. The presence of these constraints essentially reduces the region in which we search for the optimal or the superior results. In the design synthesis of cellular structures, the technical constraints, including stress and material volume, are considered.

For the lightweight truss structure design, the material volume constraint and the deflection objective are interchangeable. When the material volume is set as constraint (e.g., the maximum material volume is 30%), the design objective is to efficiently distribute the material for maximum stiffness or minimum deflection under certain load condition. On the other side, when the maximum deflection is set as a constraint, the design objective can be set to find minimum material usage. The constraints should be selected upon the design requirements, and some of them are interchangeable with the

design objectives. For the lightweight truss structure design in our research, the maximum material volume is set as constraint shown in Equation 5.10. The cross-section area of the strut is a function of the design variable and depends on its cross-section shape. For compliant mechanism design, the material volume can be set as secondary design objective to clean up trivial struts or elements, which have no stress inside and have no contribution to the structure performance. This issue will be discussed later in this chapter.

$$\text{Total material volume} \qquad V = \sum_{i=0}^{n} (L_i A(x_i)) \le V_{\max} \tag{5.10}$$

where,

$V_{\max}$ – maximum material volume allowed

$A(x_i)$ – cross-section area of the i^{th} strut

L_i – strut length

Stress everywhere in the structure should be no more than the maximum stress allowed, which is yield strength s_y. Stress constraint is shown as Equation 5.11. Axial stress shown in Equation 5.11 is caused by axial force, such as compression or tension. Axial stress is uniform everywhere in the struts. If a strut bears bending load, the maximum stress happens at one of the two farthest points on the beam cross-section from the neutral surface. One farthest point is under compression, and the other is under tension. The cross-sections of the struts in our research are symmetric and bisected by the neutral surface. So we only need to consider the magnitude of the maximum flexure stress $s_{flexture}$ due to the bending. The maximum stress in the strut is the sum of axial stress s_{axial} and flexure stress $s_{flexure}$ shown in Equation 5.13. In lightweight truss structure and compliant mechanism under small deformation, flexure stress is negligible compared with axial stress. In compliant mechanism under large deformation, flexure

stress can be the majority of the stress and should be considered. Axial force F_{axial} and axial stress s_{axial} can be obtained as discussed in Chapter 4.

Stress $s \le s_y$

where, 5.11

$s_y -$ yield strength

Axial Stress of the i^{th} strut $s_{axial} = \frac{F_{axial}}{A}$

where, 5.12

$A -$ cross-section area of the strut

$F_{axial} -$ axial force along the strut

Stress in bending strut $s = s_{axial} + s_{flexure} \le s_y$ 5.13

5.2 Problem Formulation of Design for Rigidity and Flexibility

This section will formulate the design synthesis problem of lightweight truss structure and compliant mechanism.

Lightweight truss structure design is a problem of design for rigidity. Inefficient material will be removed for minimum material usage, but without compromising stiffness and strength. In Figure 5.4, the author shows a formulation of the lightweight truss structure with given material volume for minimum deflection. The diameters of truss struts are the design variables represented by x_i $(i = 1,2,\cdots,n)$. n is the number of struts in the initial topology of structure. The total material volume is set as a constraint and the design objective is to minimize the maximum nodal deflection $\max(U)$ in the structure. The total strain energy can be used to replace the maximum nodal deflection as the design objective. The equilibrium equation is the equality constraint. The inequality constraints include stress and the total material volume. Only axial stress

$s_{axial,i}$ is accounted since the bending stress $s_{flexure,i}$ is comparatively small and negligible. For better computational efficiency, the flexure stress $s_{flexure,i}$ is ignored.

Find:	$x = \{x_1, x_2, \cdots, x_n\}$	Diameters of lattice struts
Satisfy:	Bounds: $x_i \in \{0, [x_{\min}, x_{\max}]\}$	
	Constraints:	
	$h_1 : K \bullet U = F$	static equilibrium
	$g_1 : s_{axial,i}(\mathrm{x}) \le s_{\mathrm{y}}$	axial stress
	$g_2 : V_{total} \le V_{total,\max}$	total material volume
Minimize:	$\max(U)$	maximum nodal deflection

Figure 5.4 Problem Formulation of Lightweight Truss Structure Design

Compliant mechanism design is a problem of design for flexibility. Material will be removed for desired deflections. For a 2-D compliant mechanism to match a desired shape under deformation, the widths of rectangular elements are the design variables represented by x_i ($i = 1, 2, \cdots, n$). n is the number of elements (or struts) in the starting topology of structure. In Figure 5.5, the author show a formulation of the 2-D compliant mechanism for the desired deflections at certain nodes. The first design objective is to minimize the Mean Squared Deviation between the desired shape and the actual shape under deformation. The second design objective is to minimize the total material volume and remove trivial elements as shown in Figure 5.6. Both ends of regular element should be connected to the structure. Otherwise, the dangling elements or free elements should be removed from the structures. The objective functions have different units and magnitudes. So, the values of objective functions are normalized as the ratio between the value of objective function and the reference value as shown in Equation 5.14 and Equation 5.15. For example, the reference value can be set as the value of the first run resulting from the starting design variables or upper bound. This design synthesis

problem is a multiple-objective problem. Weights w_1 and w_2 are introduced to balance the importance between the normalized mean squared deviation and the normalized material volume in the minimizing objective as shown in Figure 5.6. Obviously, minimizing the mean squared deviation is much more important than minimizing the material volume. The objective of minimizing the material volume can be even added onto the total objective $f(x)$ at the later stage of the search process. Minimizing the material volume can be performed using a local search process. For example, it is allowed to set $w_1 = 1.0$ and $w_2 = 0$ during the first 75% search process, and increase w_2 to 0.1 during the rest of search process. Mean squared deviation has already assumed that all sampled nodes have equal weights of influence on the objective function. In some applications, the designer might have different requirements on the deviations at different nodes, and mean weighted squared deviation can be set as the objective.

Normalized Mean Squared Deviation: $MSD_{norm} = \frac{MSD}{MSD_{ref}}$ 5.14

Normalized Total Volume: $V_{norm} = \frac{V}{V_{ref}}$ 5.15

Find: $x = \{x_1, x_2, \cdots, x_n\}$ Widths of elements

Satisfy: Bounds: $x_i \in \{0, [x_{\min}, x_{\max}]\}$

Constraints:

$h_1 : K_t \bullet dU = dF, U|_{x_i=0} = 0, F|_{x_i=0} = 0$ static equilibrium

$g_1 : s(x) \le s_{\max}$ stress

Minimize: $f(x,U) = w_1 \times MSD_{norm} + w_2 \times V_{norm}$

mean squared deviation and material volume

Figure 5.5 Problem Formulation of Compliant Mechanism Design

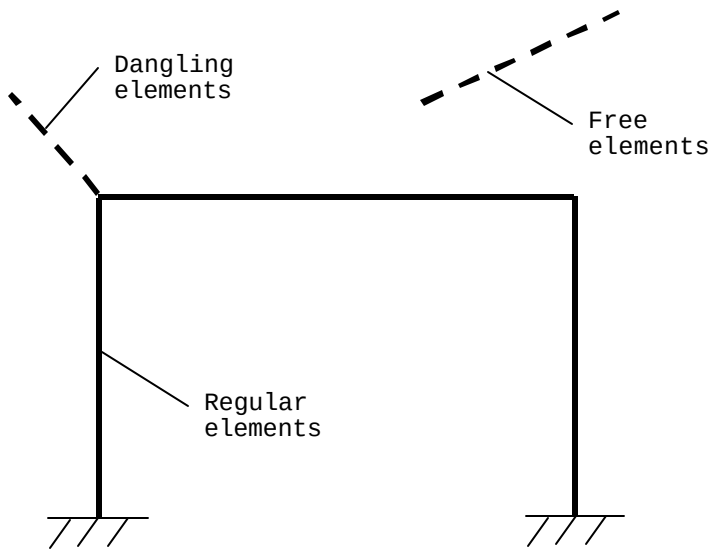

Figure 5.6 Trivial Elements: Dangling and Free Elements

5.3 Identifying Search Algorithm for Design Synthesis

In our research, a common design approach will be developed for both types of cellular structures, lightweight truss structure and compliant mechanism. In some problems, e.g. compliant plane wing (Weiss 2003), both rigidity and flexibility are desired simultaneously. The design synthesis of cellular structures is a large-scale design problem with discrete ranges of design variables, multiple nonlinear objective functions, and concave design space. This section will identify an appropriate search algorithm to search for the superior solution of the design synthesis. A desired search algorithm should be able to solve large-scale nonlinear problem. It is capable to synthesize multiple design objectives and find the global optimum in concave design space.

5.3.1 Selecting Search Algorithm

The search algorithms for small-scale problems are not appropriate for the design synthesis of cellular structures. Since it is difficult to clearly categorize optimization search algorithms, “search algorithms for small-scale problems” is just a

general term. Typical search algorithms for small-scale problems include conventional Newton's method and Cauchy's Method (Reklaitis, Ravindran et al. 1983). These search algorithms should be modified and then can be used for large-scale problems (Nocedal 1997). However, even after modifications, these search algorithms still require first order gradient or second order gradient. They utilize gradient functions and have the same issues as Optimality Criteria (OC) and Sequential Linear Programming (SLP).

The Optimality Criteria method is based on the Taylor expansion of a function of several variables (Reklaitis, Ravindran et al. 1983). Optimality Criteria shown in Equation 5.16 is effective for problems with convex design space, first and second order differentiable objective function. The differentiability of the objective function can be proved through a set of differentiation operations. However, in some cases, it is impossible to prove convexity of objective function to meet Equation 5.17 for all x. Optimality Criteria could be used for truss structure design since its design space is usually convex for the problems of continuous design variables. Sigmund used Optimality Criteria for topology optimization with homogenization method (Sigmund 2001). Sigmund assumes design variable (material densities of microstructures) continuous and sets a small density as lower bound. Constraints in Optimality Criteria should be converted to an equivalent unconstrained problem with the help of Lagrange Multipliers. Then the new gradients or Hessian matrices need to be derived from the new objective function in the equivalent unconstrained problem. It requires lots of efforts to derive gradients or Hessian matrices, and not convenient for industry applications.

x^* to be local minimum of $f(x)$ using Optimality Criteria

Necessary conditions: $\nabla f(x^*) = 0$ and $\nabla^2 f(x^*)$ is positive semidefinite — 5.16

Sufficient conditions: $\nabla f(x^*) = 0$ and $\nabla^2 f(x^*)$ is positive definite

Convexity of function $f(x)$: $x^T \bullet \nabla^2 f(x) \bullet x \geq 0$ — 5.17

Sequential Linear Programming (SLP) replaces the general nonlinear problem with a complete linearization of all problem functions at some selected estimate of the solution (Reklaitis, Ravindran et al. 1983). Sequential Linear Programming is also called Successive Linear Programming. The key limitation of SLP is the need to resort to the solution of a sequence of linear programs. It is effective and fast for the problems with modest nonlinear contributions. Therefore, SLP is appropriate for truss structure design. However, it requires substantial reductions in the step size for highly nonlinear problems, such as compliant mechanism design. The design space must be continuous and convex; otherwise, SLP would only find local minima. Kota and his colleagues used SLP for the size optimization of struts in compliant mechanism design after the topology optimization (Frecker, Ananthasuresh et al. 1997; Saggere and Kota 1997). However, the topology and size optimization are coupled and this coupling relation introduces nonlinearity and concavity.

Genetic Algorithm (GA) is an optimization technique that simulates the evolution process. GA revolves around the genetic reproduction process and "survival of the fittest" strategies (Holland 1975; Belegundu and Chandrupatla 1999). The values of design variables are encoded as binary data. Three rules dominate genetic reproduction process: selection, crossover, and mutation. During each iteration, "chromosomes" of the best solutions are selected from the population to be parents for crossover. Crossover and mutation are two basic operators of GA to create children for next iteration. GA is suitable for nonlinear, concave, and large-scale problems. It could be used for the design synthesis of cellular structure, particularly compliant mechanism.

Particle Swarm Optimization (PSO) is an optimization algorithm simulating the movement of organisms in a bird flock or fish school (Kennedy and Eberhart 1995). The social sharing of information among these organisms offers an evolutionary advantage.

It combines local search methods with global search methods by balancing explorations. It lies somewhere between genetic algorithm and evolutionary programming. Both PSO and GA do not guarantee success. PSO is an extremely simple algorithm and seems effective for large-scale, nonlinear, and concave problems with discrete design space. Compare to GA, PSO converges to the optimum more quickly, and it is simpler to formulate and implement (Fourie and Groenwold 2002). The next subsection will describe PSO in details.

In Table 5-1, the author evaluates a few typical search algorithms that are possibly used as the search algorithm of design synthesis for cellular structures. At the bottom of this table, the Applicability for each algorithm is given. SLP and OC are applicable only after certain transformations and simplifications are performed. Otherwise, SLP and OC are not able to apply in cellular structure design directly.

Table 5-1 Selecting Search Algorithms for Design Synthesis of Cellular Structures

Search Algorithm / Criterion	Algorithms for small-scale problems	Optimality Criteria	Linear Programming (SLP)	Genetic Algorithm	Particle Swarm Optimization
Capability to solve large-scale problem	No	Yes	Yes	Yes	Yes
Capability to solve nonlinear problem	Yes	Yes	Yes	Yes	Yes
Capability to solve problem with concave design space	No	No	No	Yes	Yes
Capability to solve problem with discrete design space	No	No	No	Yes	Yes
Capability to solve problem with multiple objectives	Yes	Yes	Yes	Yes	Yes
Overall	No	No	No	Yes	Yes

Both Optimality Criteria and Sequential Linear Programming would be trapped in local optima for the problems with concave objective functions and could not find the global optimum. Genetic Algorithm and Particle Swarm Optimization can avoid being trapped in local optima. In both GA and PSO, the search process jumps from one region to another in the design space, whatever is discrete or concave. GA and PSO are the

appropriate search algorithms for the design synthesis of cellular structures. However, PSO provides more flexibility to balance explorations in global search and local search. Therefore, PSO is the search algorithm in our research.

5.3.2 Particle Swarm Optimization

Particle Swarm Optimization (PSO) search algorithm is motivated by social behavior of organisms such as bird flocking and fish schooling. Dr. Eberhart and Dr. Kennedy first developed PSO in 1995 (Kennedy and Eberhart 1995). It has been successfully applied in many areas, such as function optimization and artificial neural network training. It has been shown to be robust and fast in solving nonlinear, non-differentiable, multi-model problems (Shi and Eberhart 1998). Here in our research, we would like to apply it in structural optimization.

PSO is simulation of a simplified social model and it ties to artificial life (A-life) (Heppner and Grenander 1990; Kennedy and Eberhart 1995). For example, individuals (or particles) of a school of birds, shown in Figure 5.7, adjust their flying according to their own flying experience and the other individuals' experiences during the search for food, which is unpredictably located. The individuals adjust their physical movement to avoid predators and seek food through communications and sharing information. PSO shares similarities with genetic algorithms and evolutionary programming, and lies between them. It is a combination of stochastic process and heuristic process. There is a not only competition among the individuals, but also cooperation between the individuals.

During a specific iteration, let $X_i = \{x_{id} \mid d = 1,2,\cdots, D\} = \{x_{i1}, x_{i2}, \cdots, x_{iD}\}$ represent the position of the i^{th} particle (or individual) in a D dimensional space, and $V_i = \{v_{id} \mid d = 1,2,\cdots, D\}$ represents its velocity. D can also be looked as the number of

design variables for an optimization problem. For example, D is equal to 2 for bird flocking in 3-D space.

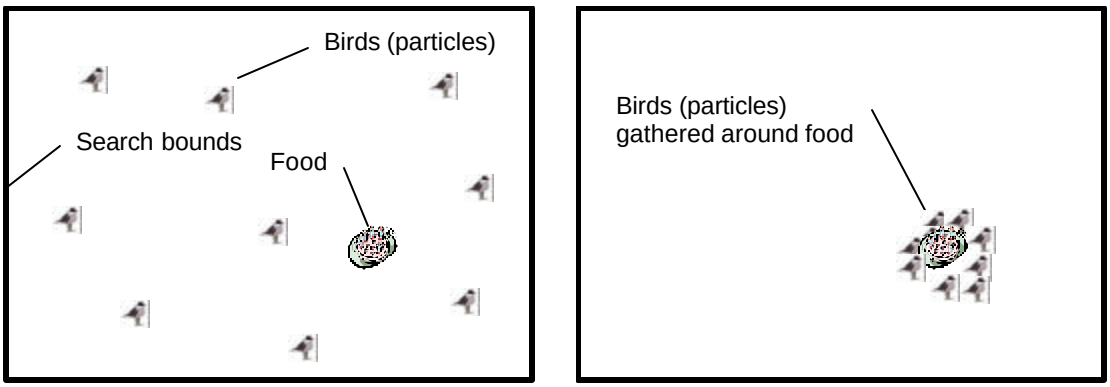

(a) Initial Status (b) Final Status

Figure 5.7 Particle Swarm Optimization Simulating A-Life

Let the best previous position of the i^{th} particle represented as $P_i = \{p_{id} \mid d = 1,2,\cdots, D\} = \{p_{i1}, p_{i2}, \cdots, p_{iD}\}$, and the best particle position among all the particles represented as $P_g = \{p_{gd} \mid d = 1,2,\cdots, D\} = \{p_{g1}, p_{g2}, \cdots, p_{gD}\}$. For each iteration, the particles' moving velocities, $V_i = \{v_{id}\}$, are updated according to Equation 5.18, and the particles' positions, $X_i = \{x_{id}\}$, are updated according to Equation 5.19 (Shi and Eberhart 1998). The selections for the learning factors j_1, j_2 and the inertia weight w can influence the search process significantly.

$$v_{id} = \underbrace{w_k \times v_{id}}_{\text{velocity inertia}} + \underbrace{j_1 \times rand() \times (p_{id} - x_{id})}_{\text{cognition behavior}} + \underbrace{j_2 \times rand() \times (p_{gd} - x_{id})}_{\text{social behavior}} \quad 5.18$$

where,

w_k – Inertia weight

j_1, j_2 – Learning factors

$rand()$ – Random function in the range $[0,1]$

$$x_{id} = x_{id} + v_{id} \quad 5.19$$

The particles' movements are updated according to the previous velocities, the particles' own best experience, and the group's best experience. The right side of the velocity equation, as shown in Equation 5.18, consists of three parts. The first part is the contribution of the particle velocity in the previous iteration. It represents the moving inertia of the moving particle. The second part is the "cognition" behavior, which represents the private thinking of the individual particle. The third part is the individual's "social" behavior, which represents the learning experiences from other particles through collaboration. The learning factors j_1 and j_2 influence the weights of the cognition behavior and the social behavior respectively. A recommended selection for j_1, j_2 is integer 2 since it on average makes the weights for "social" and "cognition" parts to be equally weighted (Kennedy and Eberhart 1995). The two random functions $rand()$ in Equation 5.18 introduce stochastic variables called craziness (Kennedy and Eberhart 1995). Some heuristic information can be added into the initial positions of the first iteration or the moving velocities in certain iterations. Therefore, PSO is a stochastic search algorithm, but it becomes heuristic with the input of heuristic information.

This manipulation strategy of the particles' positions and velocities shown in Equation 5.18 and Equation 5.19 is a modified version from the original Particle Swarm Optimization (Kennedy and Eberhart 1995) for better performance. A new parameter w, called inertial weight, is introduced to balance the global search and local search. It can be a positive constant, a positive linear or nonlinear function of time. When w is large (>1.2), the PSO is more like a global search method. It always tries to exploit new areas and converges relatively slowly, but it has more possibility to find the global optimum. When w is small (<0.8), the PSO is more like local search method. It converges quicker, but may not find the global optimum. Therefore, a decrease of inertia weight w from large value to small (e.g., from 1.4 to 0.5) can balance the explorations from a

global search method to a local search method. As shown in Figure 5.8, the values of a typical design variable x_i change randomly within the bounds in the global search stage, and then change slightly in the local search stage. A fuzzy system could be built to tune the inertia weight w during the real-time search process (Shi and Eberhart 2001). The modified PSO is a combination algorithm of global search method and local search method. In our research, a linear function of time is assigned to the inertia weight w for balancing the global search and the local search.

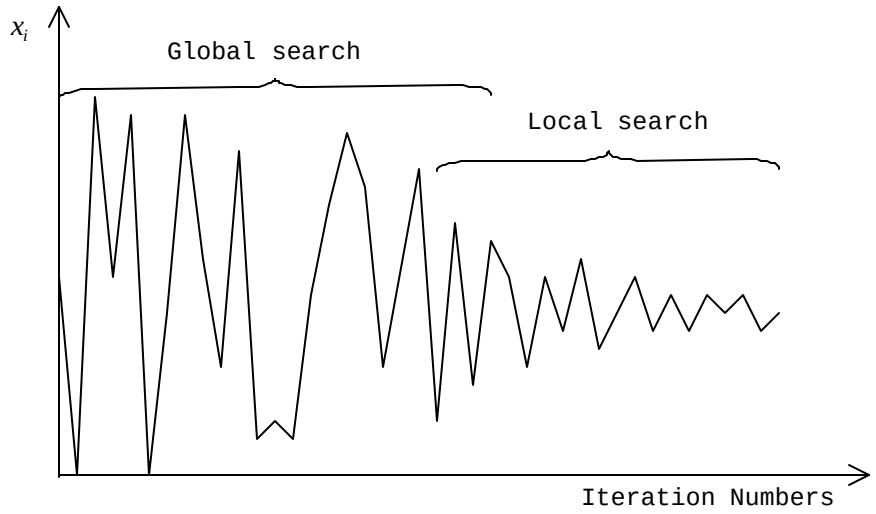

Figure 5.8 Global Search and Local Search in PSO

5.4 Constraint Consideration and System Integration Using PSO as the Search Algorithm

This section will present the penalty function approach to consider the bounds of design variables and other inequality constraints. Then this section will present the implementation of design synthesis with PSO.

5.4.1 Penalties And Composite Exponential Barrier Functions

In the design of lightweight truss structure shown in Figure 5.4, there are one equality constraint and two inequality constraints. In compliant mechanism design shown in Figure 5.5, there are one equality constraint and one inequality constraint. The equality constraint, static equilibrium equation $h_1(x) = 0$, is used to solve for the unknowns in $U(x)$ and $F(x)$ with the mechanics analysis approach described in Chapter 4. Penalty function will be applied to consider bounds and inequality constraints.

The penalty concept transforms the original constrained problem into a sequence of unconstrained problems. Equation 5.20 shows the penalty function, $P(x,R)$ (Reklaitis, Ravindran et al. 1983). The penalty term Ω forms a barrier to prevent the objective function P across the boundary of the feasible design region. The penalty term Ω is also called barrier function. Penalty terms will be used to consider design variable bounds, and design constraints for the design synthesis of cellular structures.

Penalty Function $P(x,R) = f(x) + \Omega(R, g(x), h(x))$

where,

x – design variables
R – penalty parameters
$f(x)$ – objective function
$g(x)$ – inequality constraints
$h(x)$ – equality constraints
$\Omega(R, g(x), h(x))$ – penalty terms

5.20

There are various penalty forms that have been used widely. Typical penalty functions are parabolic penalty, inverse penalty, log penalty, and bracket operator. In our research, “Composite Exponential” penalty is used as barrier function and it has capability to control the barrier shape (Qin and Nguyen 1994; Crossley and Williams 1997). Equations 5.21, 5.22, and 5.23 are barrier functions representing jump from 0 to

1, jump from 1 to 0, and jump from 0 to 1 to 0 respectively. The jump shapes of barrier values are shown in Figure 5.9, Figure 5.10, and Figure 5.11. The cutoff parameter e is slightly larger than zero, e.g., $e = 0.01$. The cutoff parameter e makes no difference for the low flat region. These barriers functions are used for minimization problems. x_0 and x_1 are the threshold values for the jumps. k is the parameter for the jump slope. The larger k value is given, the steeper the jump slope becomes.

0-1 Jump: $$b_1(x) = \begin{cases} y, & \text{if } y \geq e \\ e, & \text{if } y < e \end{cases}, y = \frac{e^{k(x-x_0)}}{e^{k(x-x_0)}+1} \qquad 5.21$$

1-0 Jump: $$b_2(x) = \begin{cases} y, & \text{if } y \geq e \\ e, & \text{if } y < e \end{cases}, y = \frac{1}{e^{k(x-x_0)}+1} \qquad 5.22$$

0-1-0 Jump:

$$b_3(x) = \begin{cases} y, & \text{if } y \geq e \\ e, & \text{if } y < e \end{cases}, y = \frac{e^{k(x-x_0)}}{e^{k(x-x_0)}+1} + \frac{1}{e^{k(x-x_1)}+1}, \quad \text{where} \quad x_0 < x_1 \qquad 5.23$$

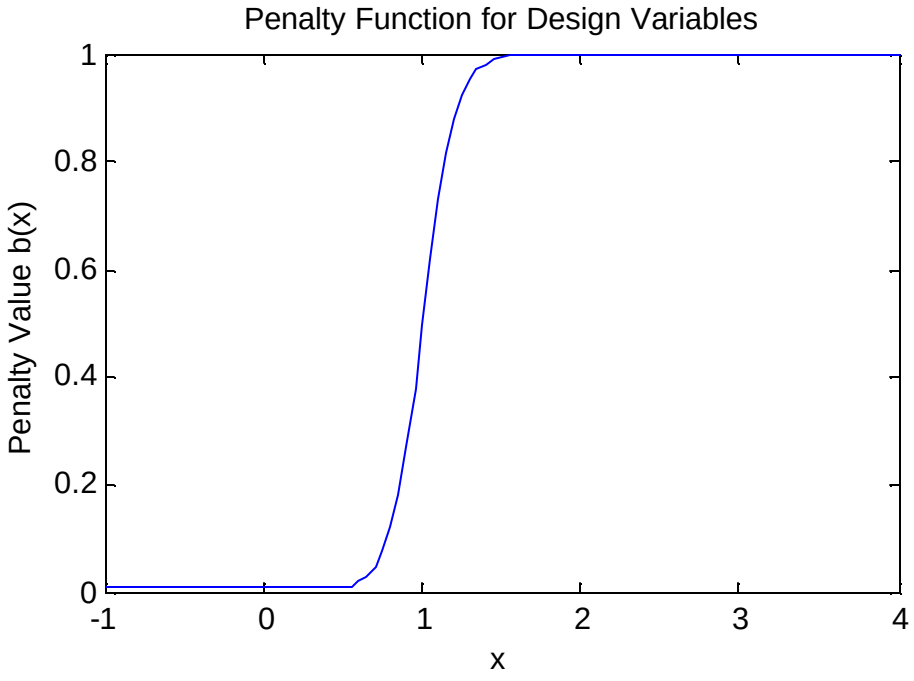

Figure 5.9 Composite Exponential Barrier Function for 0-1 Jump

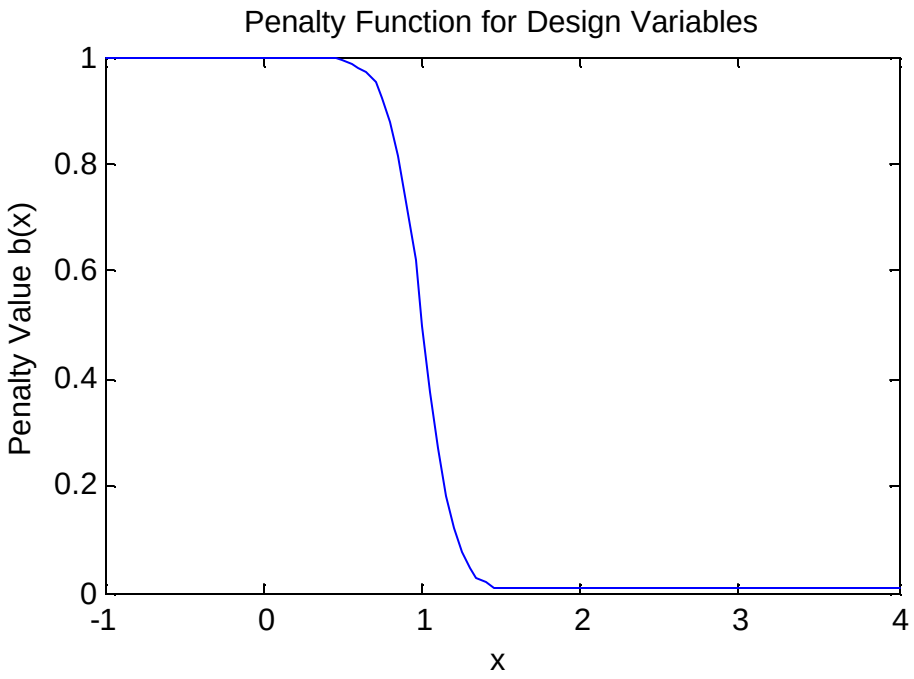

Figure 5.10 Composite Exponential Barrier Function for 1-0 Jump

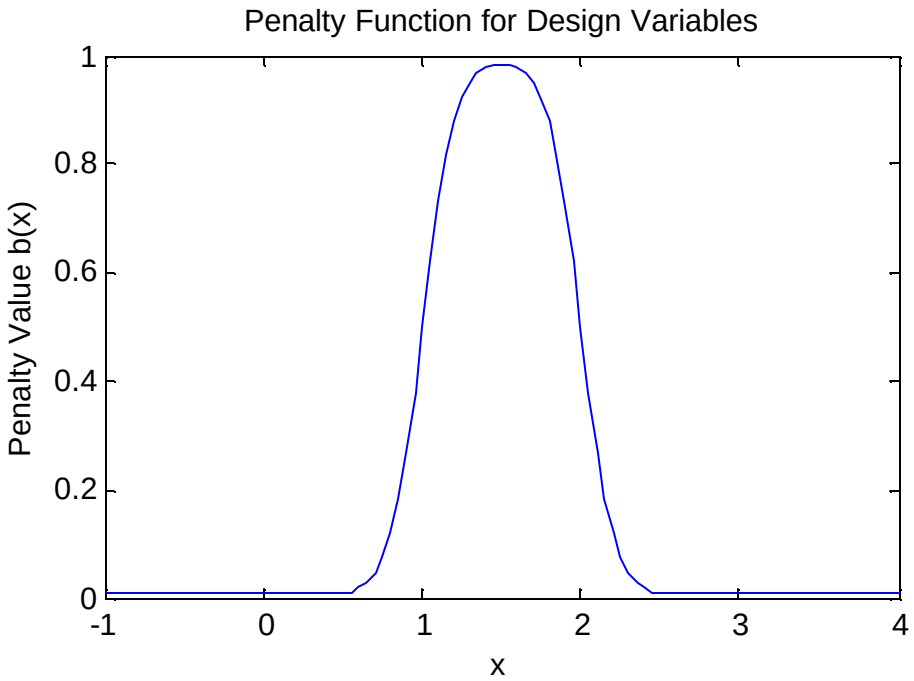

Figure 5.11 Composite Exponential Barrier Function for 0-1-0 Jump

5.4.2 Considering Constraints Using Barrier Functions

The design variables are uniformly bounded as $x_i \in \{0, [x_{\min}, x_{\max}]\}$ when the maximum manufacturable aspect ratio is not considered. Otherwise, the bound is as shown in Equation 5.9 since the minimum manufacturable size is affected by the maximum aspect ratio. When $x_i = 0$, there is no strut existing. $x_{\min}$ is the minimum size of the struts manufacturable by the manufacturing process. Practically, a small nonzero positive x_{0^+} is introduced to replace 0 and $x_{\min}$ as the lower bound. x_{0^+} is a value a little bit larger than zero, e.g. $0.01 \times x_{\min}$. The first purpose is to avoid singularity in stiffness. Now the closed continuous region $\left[x_{0^+}, x_{\max}\right]$ is used for the search process. The bounds of design variables could be considered using the updating scheme shown in Equation 5.24 by limiting the new value of design variable within the continuous region $\left[x_{0^+}, x_{\max}\right]$. New value x_i^{new} of the i^{th} design variable is set back to boundary if x_i^{new} is out of the continuous bounds $\left[x_{0^+}, x_{\max}\right]$. This updating scheme may affect the search velocity, but it is effective to consider the continuous bound constraints of design variables. The open region of $\left(x_{0^+}, x_{\min}\right)$ should be avoided since struts with sizes in this region are not manufacturable. Barrier function of design variable $\Omega_b(x_i)$ is added into objective function in the later search stage, which becomes local search method. The purpose of adding barrier function is to penalize the design variables falling in the region $\left(x_{0^+}, x_{\min}\right)$ and make them to be either close to x_{0^+} or around $x_{\min}$. A barrier function for 0-1-0 jump shown in Equation 5.23 and Figure 5.11 is used to avoid the non-manufacturable regions of design variables.

$$x_i^{new} = \begin{cases} x_{0^+}, & \text{if } x_i^{new} < x_{0^+} \\ x_{\max}, & \text{if } x_i^{new} > x_{\max} \\ x_i^{new}, & \text{otherwise} \end{cases} \quad 5.24$$

Stress $s \le s_y$ and material volume $V_{Total} \le V_{Allowed}$ are inequality constraints. Barrier function with single jump, shown in Equation 5.21 and Figure 5.9, can be used to consider these inequality constraints. The material volume value and stress value should be normalized as Equation 5.25 and Equation 5.26 before being plugged into Equation 5.21. s_i represents the maximum stress in the i^{th} element or strut.

$$V_{norm} = \frac{V_{Total}}{V_{Allowed}} \quad 5.25$$

$$s_{norm} = \frac{s}{s_y} \quad 5.26$$

Therefore, for lightweight truss structure design, the constrained problem can be transformed into an unconstrained problem shown in Figure 5.12. The bound $\left[x_{0^+}, x_{\max}\right]$ is continuous as opposed to discrete regions of design domain in the original formulation shown in Figure 5.4. The normalized maximum deflection U_{norm} represents $\frac{\max(U)}{U_{ref}}$, where $\max(U)$ is the maximum deflection in the structure and U_{ref} is the reference deflection. U_{ref} can be set as the maximum deflection of the structure before design synthesis. The equality constraint $h_1 : K(x) \bullet U(x) = F(x)$ has been used to solve the unknowns in displacements U and loads F and it is not consider as a constraint anymore. The first part in the new objective function $f(x)$ is to minimize the maximum deflection in the structure, and it is the same as the original constraint problem. The

second part in $f(x)$ is the barrier function of volume constraint. The third part is the barrier function of stress constraint. The 4th part is the bound constraint and used to avoid non-manufacturable regions of design variables. w_u, w_v, w_s, and w_x are weights for these four parts in the new objective functions.

Find: $x = \{x_1, x_2, \cdots, x_n\}$ Diameters of lattice struts

Satisfy: Bounds: $x_i \in \left[x_{0^+}, x_{\max} \right]$

Minimize:
$$f(x) = \underbrace{w_u U_{norm}}_{\text{deflection objective}} + \underbrace{w_v b_1(V_{norm})}_{\text{volume constraint}} + \underbrace{w_s \sum_{i=1}^{n} b_1(s_{norm,i})}_{\text{stress constraint}} + \underbrace{w_x \sum_{i=1}^{n} b_3(x_i)}_{\text{bounds}}$$

Figure 5.12 Constrained Design Problem of Lightweight Truss Structure after Using Penalties

For compliant mechanism design, the constrained problem can be transformed into an unconstrained problem shown in Figure 5.13. The first part in the objective function $f(x)$ is to minimize the mean squared deviation as the original constraint problem. The second part is to minimize the material and used to clean trivial elements. The third part and fourth part are stress constraint and bound constraint respectively. w_d, w_v, w_s, and w_x are weights for these four parts in the new objective functions.

Find: $x = \{x_1, x_2, \cdots, x_n\}$ Widths of elements

Satisfy: Bounds: $x_i \in \left[x_{0^+}, x_{\max} \right]$

Minimize:
$$f(x) = \underbrace{w_d \times MSD_{norm}}_{\text{mean squared deviation}} + \underbrace{w_v \times V_{norm}}_{\text{volume reduction}} + \underbrace{w_s \sum_{i=1}^{n} b_1(s_{norm,i})}_{\text{stress constraint}} + \underbrace{w_x \sum_{i=1}^{n} b_3(x_i)}_{\text{bounds}}$$

Figure 5.13 Constrained Design Problem of Compliant Mechanism After Using Penalties

In the designs of both lightweight truss structure and compliant mechanism, the fourth part is used to avoid non-manufacturable regions of design variables. The fourth part can be considered in the local search stage in the PSO process. Its weight w_v can be set to zero in the global search stage, and then it is set to nonzero in the local search stage.

The differences between the objective function $f(x)$ of lightweight truss structure design and that of compliant mechanism design are the first two parts. In lightweight truss structure design, the material distribution is optimized with the given volume of material. The material volume is a constraint. In compliant mechanism design, the objective of material volume reduction is just for cleaning up trivial elements. Therefore, the material volume objective may become effective in the local search stage, which happens later in the PSO process. Its weight w_v can be set to zero in the global search stage. In the local search stage, w_v should be set relatively smaller than other weights.

5.4.3 Implementation in MATLAB

The PSO was implemented in MATLAB. "DV" means design variables. $best(x)$ represents the best position p among the swarm with positions x and has $f(p) = \min(f_k)$. f_k represent the objective function values in the k^{th} iteration. An implementation outline of the PSO algorithm is presented as:

Algorithm PSO
{
1. Initialization:
(a) Set variables
{
f_{goal} - Target value to achieve
N_{iter} - Number of iterations
w_{start} - Start velocity inertia
w_{end} - End velocity inertia

j_1 - Cognition learning factor j_2 - Social learning factor

e_{obj} - Tolerance of objective function e_{var} - Tolerance of DV

$x_{\min}$ - Lower bound of DV $x_{\max}$ - Upper bound of DV

N_D - Number of DV N_P - Number of particles

$v_{\max}$ - Maximum moving velocity N_{iter} - Number of iterations

}

(b) Calculate the velocity inertia vector:

$$\{w_k\} = \{w_{start}, w_{start} + \Delta w, \cdots, w_{end}\},\ \Delta w = (w_{end} - w_{start}) / N_{iter}$$

(c) Generate initial particles' positions and velocities:

x_{id} and v_{id}, for $i = 1,2,\cdots,N_P$, $d = 1,2,\cdots,N_D$

(d) Evaluate the objective function $f_k = f(x)$ in Figure 5.12 or Figure 5.13 for each particle

(e) Set the current positions as the best: $p = x$, and $f_p = f_k$

(f) Set the best position of current positions as the global best: $p_g = best(x)$, and $f_g = \min(f_k)$

(g) Set iteration ID: $k := 0$

2. Optimization:

(a) Set iteration ID: $k := k + 1$

(b) Change inertia weight: $w = w_k$

(c) Calculate velocity $v = \{v_{id}\}$ using Equation 5.18.

(d) Set: $v_{id} = v_{\max}$ if $v_{id} > v_{\max}$; $v_{id} = -v_{\max}$ if $v_{id} < -v_{\max}$.

(e) Update positions $x = x_{id}$ using Equation 5.19.

(f) Set: $x_{id} = x_{\max}$ if $x_{id} > x_{\max}$; $x_{id} = x_{\min}$ if $v_{id} < x_{\min}$.

(g) Evaluate the objective function $f_k = f(x)$ in Figure 5.12 or Figure 5.13 for each particle

(h) Update $p = x$, and $f_p = f_k$ if $f_k < f_p$

(i) Update $p_g = best(x)$, and $f_g = \min(f_k)$ if $\min(f_k) < f_g$

(j) If $\left| f_g - f_{goal} \right| \le e_{obj}$ or $mean(\|v\|) \le e_{\text{var}}$ or $k \ge N_{iter}$, go to 3

(k) Go to 2(a)

3. Termination: Stop

}

The target value f_{goal} is the desired value of the objective function, which can be a sum of weighted objective values as given in Figure 5.12 and Figure 5.13. Usually, f_{goal} is set as zero. The maximum number of iterations for each run is given as N_{iter} to avoid dead loop. Automatic termination of the search process is applied when the target is reached as given in Equation 5.27 or the convergence deviation (such as standard

deviation of the search solutions) is less than the tolerance of design variables e_{var} as given in Equation 5.28. e_{obj} is the tolerance of objective function, and e_{var} is the tolerance of design variables.

$$\left| f_g - f_{goal} \right| \le e_{obj} \qquad 5.27$$

$$mean(\|v\|) \le e_{\text{var}} \qquad 5.28$$

The velocity inertia w_k linearly varies from w_{start} to w_{end}. The start velocity inertia w_{start} and the end velocity inertia w_{end} are given based on experience. The recommended values are given as $w_{start} = 0.9$ to $w_{end} = 0.4$. Increasing w_{start} and w_{end} will make the particles jump with bigger steps and have less probability to converge. The cognition learning factor j_1 and the social learning factor j_2 balance the processes for global search and local search. As mentioned in Section 5.3.2, the recommended choices of j_1 and j_2 are integer 2.

The minimum manufacturable strut size $x_{\min}$ is the lower bound of design variables. The maximum strut size $x_{\max}$ is the upper bound of design variables. For SLA 3500 machine, $x_{\min}$ is set as $0.7mm$ based on experiments and $x_{\max}$ is given as $8.0mm$ in order to consider the struts as beams.

N_D is the number of design variables, in another words, the number of struts. The number of particles N_P is given based on experience. Usually it is given as 20. A larger number of particles N_P can make the search result more reliable, but it requires more iterations to converge.

The maximum moving velocity $v_{\max}$ is usually set as the difference between the upper bound and lower bound of design variables. In fact, $v_{\max}$ can be looked as the largest allowable jump step for particles.

5.5 Validation Example

The validation example is shown as Figure 5.14, which is a 300x150x5 mm cantilever plate with elastic modulus of $200MPa$. It is loaded with a 1 N force at a distance 40 mm from the top edge. The analysis result from PSO and unit truss approach is compared with that from Optimality Criteria (OC) with homogenization method (Sigmund 2001). The goal is to optimize the material distribution with a material usage of 30% of the domain volume for minimum deflection.

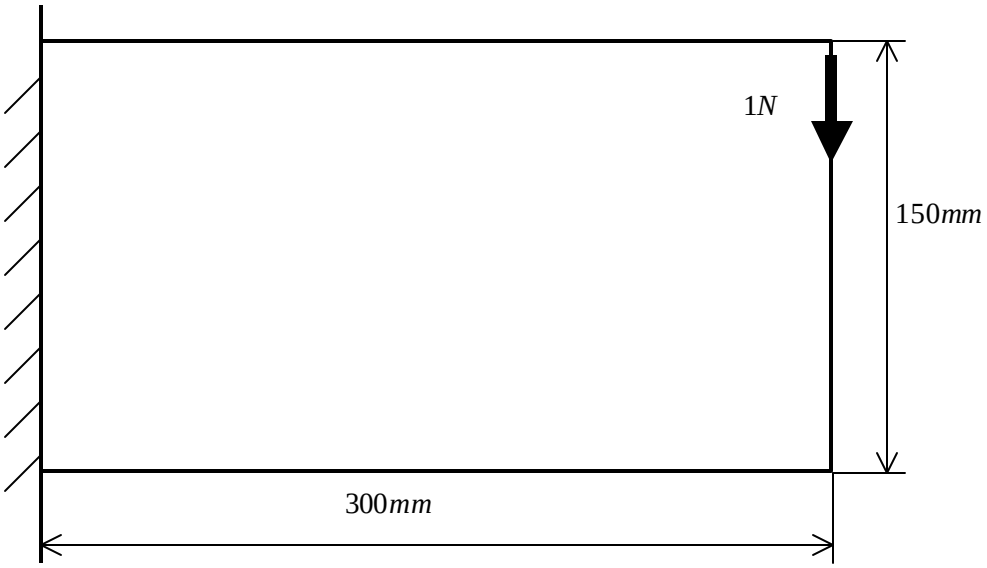

Figure 5.14 Validation Example for Design Synthesis

In Figure 5.15, the author shows the solution generated by Optimality Criteria and homogenization method for a desired average density of $r = 0.3$. In the homogenization problem, each element had one design variable, the density. Elements

were 10x10 mm in size, so the plate has 450 elements and variables. The 99-line code of OC with homogenization method by Sigmund [37] is used to solve the problem for the comparison. It required 80 iterations and about 4 minutes elapsed time on a standard PC with a 2.4GHz processor. The maximum deflection was 1.9 mm.

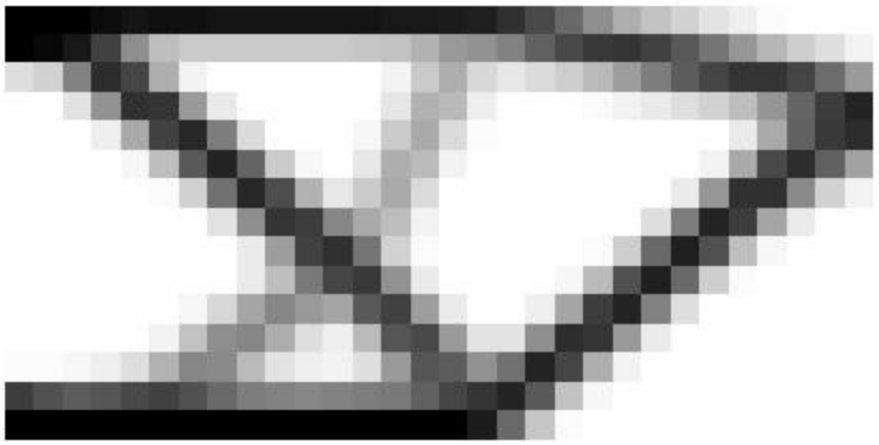

Figure 5.15 Result from Homogenization Method

In Figure 5.16, the author shows the solution using our PSO method with unit truss approach for the average density $r = 0.289$. This structure has the same thickness (5mm) as that for homogenization method. The unit truss problem had 58 struts, each of which has one variable, the strut width. The PSO with unit truss approach was run for 200 iterations with 20 particles and the resulting deflections ranged between 1.3 mm and 1.8 mm. In each iteration, the objective function is evaluated 20 times since 20 particles are used. For 200 iterations and 20 particles, the objective function is evaluated for 4000 times, and about 12 minutes elapsed time was required to solve the problem. The thin lines represent the struts with small width.

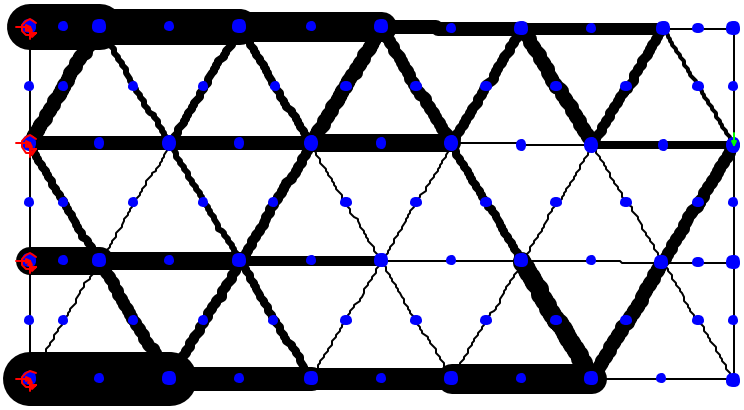

Figure 5.16 Result from Unit Truss Approach with PSO

Unit truss approach returned a solution that had the slightly smaller area and deflections than homogenization method. Though the unit truss problem had an order of magnitude fewer variables, and it took 3 times longer to reach a solution. The PSO with unit truss approach took much more runs to evaluate objective functions than OC with homogenization method. The PSO took about 4000 run (200 iterations with 20 particles), while the OC only took 80 runs. The main reason is that the OC uses gradient and Hessian matrix as the heuristic information during the search process, while the PSO does not use either of them. Regarding the geometry of the solutions, the result with the unit cell approach is manufacturable, while the gray elements in the result from homogenization are not manufacturable. This is a limitation of homogenization method.

Both homogenization method and unit truss approach have their advantages and disadvantages. However, homogenization method with optimality criteria is suitable for continuous convex design domain. It needs gradients and Hessian matrices, which can be obtained with huge efforts or computation resources. For the validation example, the design domain is continuous with design variables varying from 0.01 to 1.0. But those elements with design variables ranging between 0.01 and 1.0 are not manufacturable or do not physically exist. To precisely represent the physical meaning, the design

variables are not continuous and the design domain is discrete. Moreover, the gradients and Hessian matrices used for homogenization method are obtained by an approximation with power-law interpolation (Sigmund 2001). This power-law interpolation cannot precisely represent the true physical behavior of microstructures. When solving 3-D structural problems, the number of design variables for homogenization method is scaled much more dramatically than unit truss approach. For example, 8000 microstructures (lateral size 10mm) are needed to represent a 3D domain with lateral size 200mm. As a result, 8000 design variables are required. The research about 3-D structural homogenization method has not been explored as extensively as 2-D homogenization method because of those difficulties.

Unit truss approach with particle swarm optimization can solve problems with discrete design domains. It does not require the gradients and Hessian matrices, and make it convenient for users to use. The number of design variables is much less than the homogenization method. The number of design variables is only about 11% of that of homogenization method for the validation problem. The search time of the design synthesis process should be cut significantly with the use of unit truss approach.

5.6 Chapter Summary

In this chapter, the characteristics of the design synthesis problem of cellular structures were discussed in terms of design variables, design objectives, and constraints. Then the author formulated design synthesis problems of lightweight truss structure and compliant mechanism. Through comparing different search algorithms, Particle Swarm Optimization (PSO) was identified as the search algorithm to search for the superior solution of the design synthesis. The Particle Swarm Optimization with unit truss approach was successfully implemented in MATLAB, and

the design synthesis with PSO was validated with an example of lightweight truss structure.

Usually, the design objectives of lightweight cellular structures are not highly nonlinear. It is still feasible to obtain the derivatives of objective functions through analytical or numerical analysis. Gradient search algorithms, such as Method of Moving Asymptotes (MMA) (Svanberg 1987), are still applicable to design lightweight cellular structures and make the search process converge faster. For compliant mechanism design, it would be valuable to evaluate various algorithms (e.g. Generic Algorithm) via experiments and further explore the possibility to use gradient search algorithms.

In Chapter 5, the design synthesis problem of adaptive cellular structures was formulated through identifying design variables, constraints, and objectives. Particle Swarm Optimization (PSO) was elected as an appropriate search algorithm to systematically search for solutions. The “synthesis” issue (raised in Section 2.4) was addressed through applying engineering optimization and performing system integration. A 2-D problem was used to validate the developed design synthesis method. The theoretical structural validity (shown in Figure 1.22) of the hypothesis (posted in Section 1.4) was proved by the development of a systematic design synthesis method for adaptive cellular structures. The empirical structural validity (shown in Figure 1.22) of the hypothesis (posted in Section 1.4) was proved by the cantilever plate example.

CHAPTER 6

A HYBRID METHOD FOR GEOMETRIC MODELING OF CELLULAR STRUCTURES

In this chapter, the author completely addresses the “representation” issue raised in Section 2.4 along with the two approaches of creating conformal topology developed in Chapter 3. The organization of Chapter 6 is presented in the context of the Validation Square shown in Figure 6.1. Geometric modeling is adapted to develop a hybrid geometric modeling method and create CAD models of cellular structures effectively and efficiently, particularly for large-scale conformal lightweight truss structures. The geometry complexity of compliant mechanism is relatively less than lightweight cellular structure, so the author focuses on the geometric modeling of cellular structures. Lightweight truss structure, a typical cellular structure, can be engineered at the mesoscopic scale for high performance and multi-functional capabilities. A simple method of constructing models of uniform cellular structure is to pattern unit cells linearly within a CAD system. However, by orienting strut directions and adjusting strut sizes, such trusses can be optimized to enhance strength, stiffness, and while reducing weight. For large truss structures, computational and storage complexities cause difficulties in CAD system modeling. In this chapter, a new hybrid geometric modeling approach of directly creating tessellated models is developed to automate the geometric modeling process of conformal truss structures efficiently. This modeling approach is intended to support the design, analysis, optimization, and manufacture of conformal truss structures. Examples are presented and the computational efficiency of the hybrid method is compared with the approach of creating the complete solid model of the

cellular structures. The focus of Chapter 7 is the structural analysis shown in Figure 6.2. The input is the optimized topology of the cellular structure.

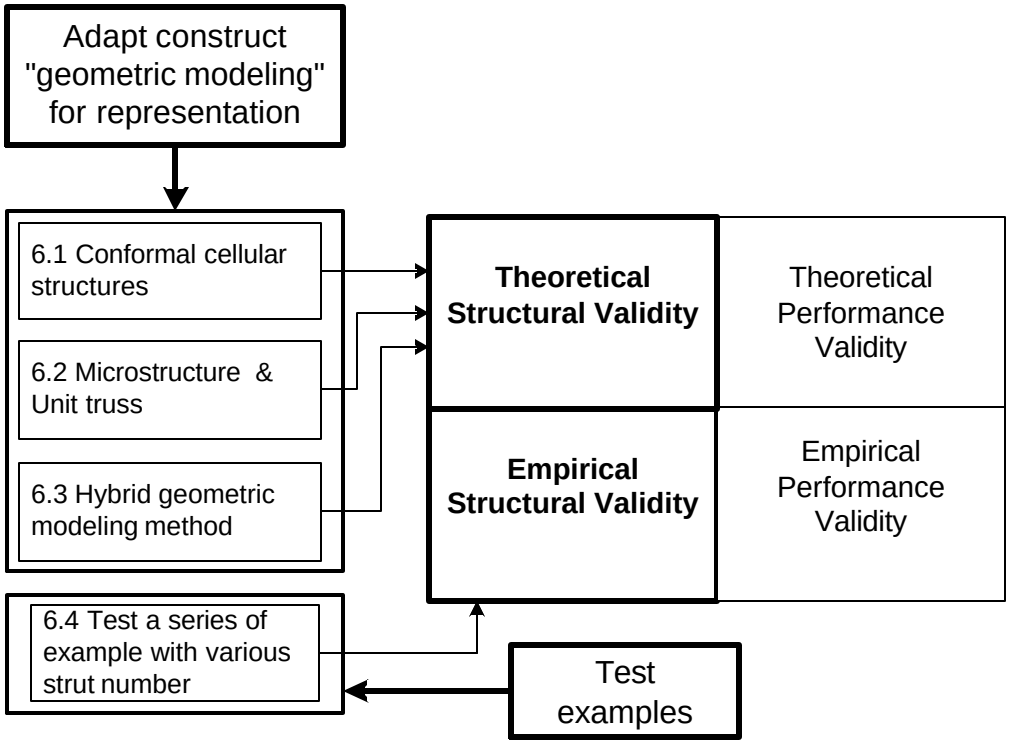

Figure 6.1 Relationship between Chapter 6 and Validation Square

6.1 Overview of Geometric Modeling for Conformal Structures

The mechanical performance of cellular structure is highly dependent on the underlying microstructures (strut topology and pattern). The anisotropy in the structure can significantly control its mechanical behavior. A conformal cellular structure resulting from the optimization of individual microstructures can better enhance the structure's performance and be adaptive to the design requirements. In the research of multifunctional cellular structure, Gibson, Ashby, Hutchinson and Evans designed and manufactured uniform octet-truss for the core of flat sandwich panels (Deshpande, Fleck et al. 2001; Wallach and Gibson 2001; Chiras, Mumm et al. 2002). The uniform truss is a

pattern of unit cells (microstructure) repeated in every direction as shown Figure 6.3. However, as discussed in Chapter 2, a conformal truss as shown in Figure 6.4 with variable adaptive strut orientations and sizes can achieve significantly better performance than a uniform truss (Wang 2001; Burns 2002; Wang and McDowell 2003). The individual strut sizes in the conformal truss can be adaptively configured through structural optimization. Moreover, a conformal truss topology with struts oriented toward external loads can better distribute loads and help the structure to be stretching-dominated, particularly for one-layer truss structure. Topology defines the strut connectivity of a structure.

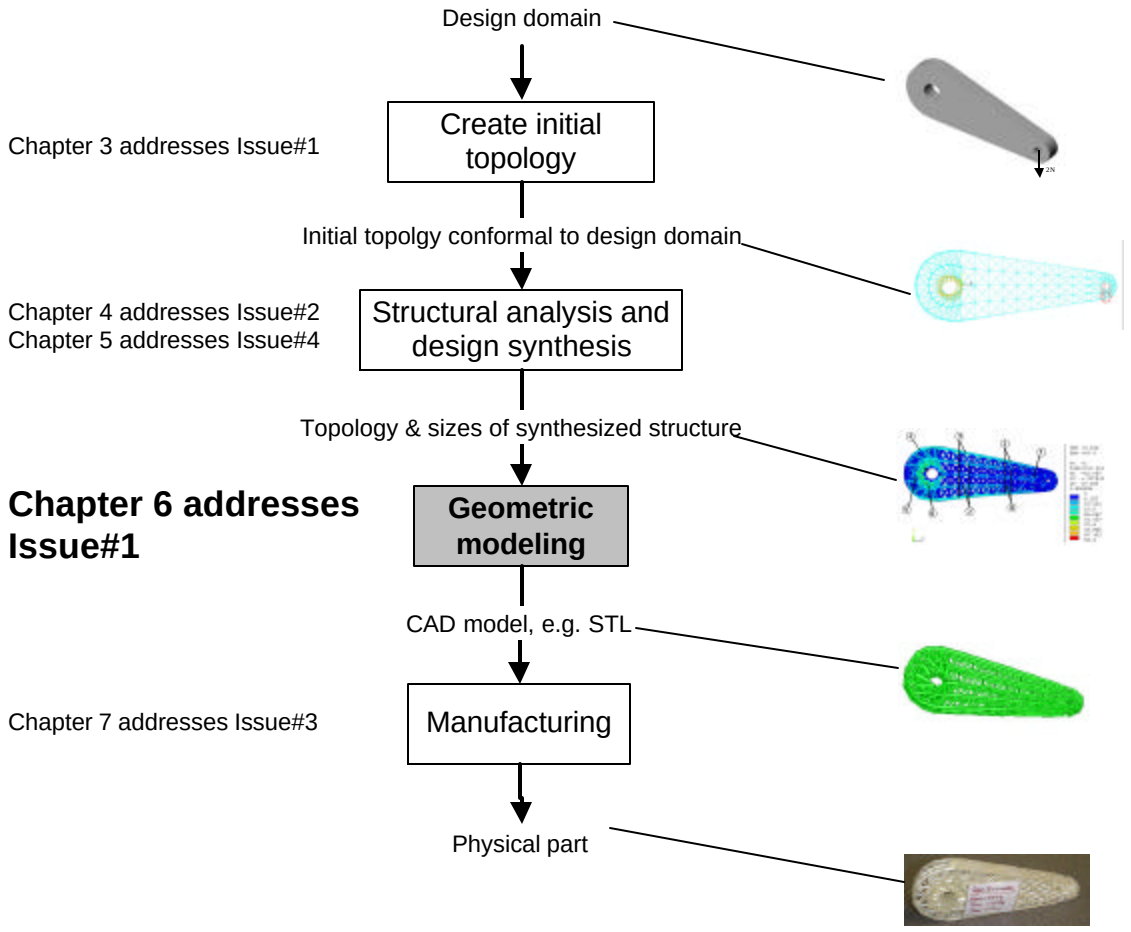

Figure 6.2 Focus of Chapter 6 in the Design Process of Cellular Structures

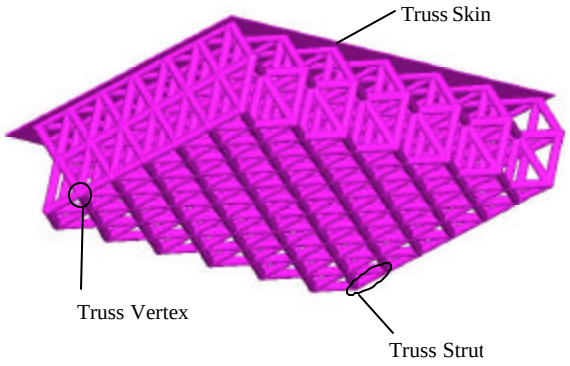

Figure 6.3 An Example of Uniform Truss

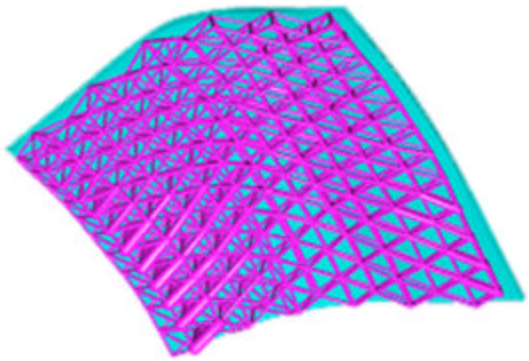

Figure 6.4 An Example of Conformal Truss

The topology and the size specifications result from a design synthesis process, e.g., a multiple objective optimization process for high strength, high stiffness, low material volume, or high heat dissipation rate (Rozvany 1997; Wang 2001; Burns 2002). Then resulting topology and size specifications are used to create a CAD model of the conformal cellular structure through geometric modeling. The obtained CAD model is used for visualization and manufacturing. This chapter mainly discusses the issues related to geometric modeling of conformal cellular structures and presents a hybrid geometric modeling method to resolve these issues.

A simple patterning operation with unit cells to create a uniform truss in a commercial geometric modeling package (e.g. Unigraphics, SolidWorks) has significant

limitations. First, uniform trusses are not as strong and stiff, per unit weight, than conformal trusses. Trusses that conform to external shapes and that enable synthesis are needed. Strut connectivity, strut size, and node positions should be design variables. Second, the construction of solid models of truss structures is limited by the computational demands of many Boolean operations and by memory limitations of computers. We are interested in designing structures with hundreds of thousands of struts, which is not possible using conventional solid modeling technology. It should also be noted that manual construction of truss structures is not feasible due to the overwhelming number of struts in an interesting truss structure. Therefore, an automatic design approach should be developed to facilitate geometric modeling of the conformal truss structures. The geometric modeling method in this design approach is intended to support the design, analysis, optimization, and manufacture of conformal truss structures.

6.2 Microstructures and Unit Truss

This section discusses the microstructures for various lightweight truss structures, such as Octet truss and Kelvin foam truss. Unit truss will be introduced as a common microstructure for both structures. The overall method of hybrid geometric modeling using unit truss will be presented.

6.2.1 Topology and Microstructures

Due to the complex geometry of truss structures, topology is used to define the strut connectivity (Wang 2001; Wang and Rosen 2002). Sample topologies of octet truss and Kelvin foam truss are given in Figure 6.5 and Figure 6.6. The complex geometries of truss structures (e.g. octet truss shown in Figure 6.4) are far beyond thoese of typical CAD models, but truss structures are composed of many simple truss primitives. Truss

primitives are repeated in certain directions as shown in Figure 6.5 and Figure 6.6. Tetrahedron (tetra) is the microstructure (unit cell) of an octet truss shown in Figure 6.5 (Fuller 1975). Truncated octahedron is the microstructure of a Kelvin foam truss (Fuller 1975). The geometries of truss joints where neighboring microstructures meet are relatively complicated for conformal truss due to the variations of struts' sizes and orientations. In Figure 6.7, the author shows that the resulting intersection curves (geometry topology) between solid struts (represented as cylinders) are different from one joint to anther joint. It is infeasible to simply stack the microstructures together into the entire truss without Boolean operations.

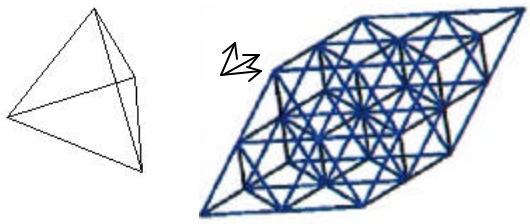

Figure 6.5 Octet Truss and Tetrahedron Microstructure

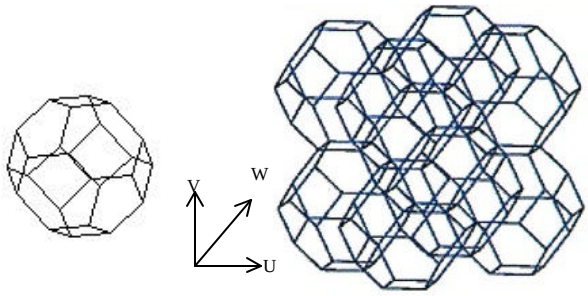

6.2.2 Using Unit Truss as the Microstructure

Superior to the microstructures discussed above, unit truss can be stacked together without Boolean operation. Moreover, unit truss can be used as a common microstructure to consist both octet truss and Kelvin foam truss. Each unit truss has one central node and semi-struts connected to the central node as shown in Figure 6.8. The

number of semi-struts in a unit truss depends on the truss type and the location of the central node. A unit truss with central node in the middle of an octet truss has 12 semi-struts. A unit with central node at the boundary of an octet truss has 9 semi-struts. The topology of unit truss is parameterizable. As shown in Figure 6.8, all unit trusses are connected at the middle of struts, and there is no overlap between unit trusses. Therefore, STL models of unit trusses can be stacked together without overlapping.

Figure 6.6 Kelvin Foam Truss and Truncated Octahedron Microstructure

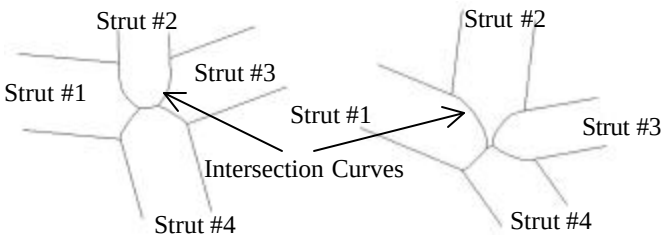

Figure 6.7 Geometry Variations at Strut Joints due to Strut Size and Orientation Changes

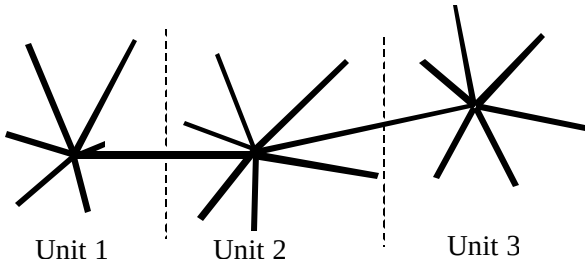

Figure 6.8 Unit Truss

The inputs are the truss topology and size specifications and the output is the STL model of the entire conformal truss. ACIS is used as the geometric modeling kernel. The overall method of hybrid geometric modeling approach for a truss structure with N nodes and M elements follows:

Repeat Step I-IV for all nodes ($i = 0,1,2,\ldots, N-1$) and start with empty STL model ($STL_{all} = null$) for the entire structure.

I. Formulate the i^{th} unit truss: find all struts connected to the i^{th} node among all M elements; let connected semi-struts represented in $E_{i,j}$ and the struts' diameters in $d_{i,j}$; totally NE_i struts are found; $j = 0,1,\ldots,NE_i - 1$

II. Create solid model of the i^{th} unit truss in the form of boundary representation (B-rep) $ACIS_i$.

III. Remove all the NE_i struts' end faces $FACE_{i,j}$ ($j = 0,1,\ldots,NE_i - 1$) from the B-rep model $ACIS_i$ of the i^{th} unit truss and obtain STL (faceted) model STL_i using surface faceting.

IV. Stack STL model STL_i of the i^{th} unit truss into the existing STL model $STL_{all} = STL_{all} \bigcup STL_i$.

Step I and Step IV are straightforward and easy to understand. Step II and Step III will be discussed in details in Section 3.

6.3 Directly Creating STL Model Using Hybrid Geometric Modeling

The presentation of hybrid geometric modeling method starts with solid modeling of unit trusses, and then discusses geometric modeling of the entire truss structure.

6.3.1 Create Solid Model of Unit Truss

During the solid modeling of unit truss in Step II, a sphere is added to its central node to smoothen the joint geometry and avoid non-manifold geometry. It is fairly obvious that the added sphere can smoothen the geometry of the joint where the connected struts meet together. In Figure 6.9, the author shows the sharp corners at the joint are removed. The smoothening process not only smoothens the joint cosmetically,

but also improves the joint's mechanical property for reducing stress convergence and crack propagation.

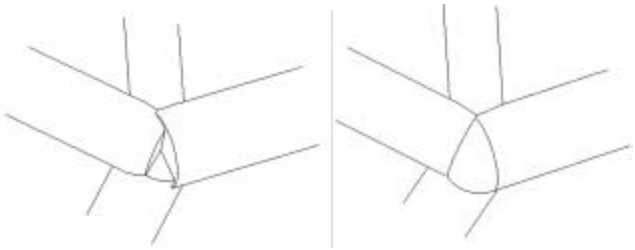

a) Joint Before Smoothening b) Joint After Smoothening

Figure 6.9 Smoothening Joint by Adding Sphere to Central Node

The second main purpose of adding sphere is to avoid the non-manifold entities. Some non-manifold entities may result from solid modeling of unit truss due to coincident lines or faces. For example shown in Figure 6.10, three cylindrical struts with equal diameters meet together at a common joint, Vertex A. The intersection edge, Curve E, between Strut 1 and Strut 2 is indicated as a bold line. The curve E is on the ending faces of both Strut 1 and Strut 2. If a new cylinder, Strut 3, is united to the existing union model of Strut 1 and Strut 2, the curve E would be on the ending face of Strut 3. So three faces would share the edge, Curve E, and the resulted union geometry is non-manifold (Mortenson 1997). Non-manifold geometry also happens when two co-linear struts with same diameters are united by Boolean operation. This 2-manifold joint model and the boundary are not topologically equivalent. According to the topology of edges and faces, one edge can only belong to two faces at the same time in the physically realizable entities. Edges belonging to more than two faces cannot be realized in ACIS (Corney and Lim 2001).

Adding spheres to the joints avoids the non-manifold entities and the result is shown in Figure 6.11. The sphere should not be equal to the diameter of any cylindrical strut. Otherwise, the sphere could not be united with that cylindrical strut since the

resulted geometry from tangent sphere and cylinder would be non-manifold as well. To avoid these non-manifold entities, it is necessary to increase the sphere diameter a little bit. In our research, the sphere diameter is 0.001% larger than the largest strut diameter among the cylindrical struts connected to the joint. The largest strut diameter can be achieved by inquiring all the diameters of the struts at this joint. Adding sphere to the joint is very effective to avoid non-manifold geometry during creating solid model of unit truss.

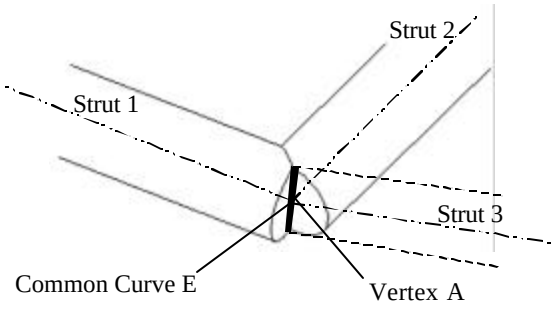

Figure 6.10 Non-manifold Entities in Truss Structures

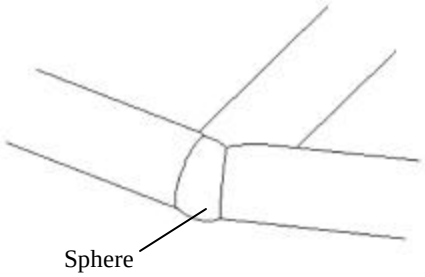

Figure 6.11 Add Sphere to Avoid Non-manifold geometry

6.3.2 Remove End Faces and Obtain STL Model of Unit Truss

After the solid model (ACIS) of unit truss is created, the struts' ending faces are removed in Step III. All the struts' ending faces are planar and different from the rest of curved faces. So these planar ending faces are easy to find and are removed from the B-rep topology of the entire solid model. An example of removing ending faces of unit

truss is shown in Figure 6.12. All the remained faces are exported as STL model using the faceting tool, which is provided by ACIS.

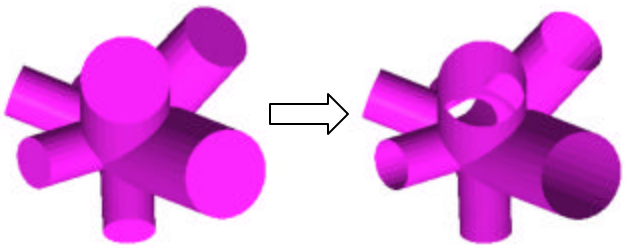

Figure 6.12 Removing Ending Faces from Unit Truss

6.3.3 Stacking Unit Trusses into the Entire Truss

After generating the STL model for all unit trusses, these STL models are stacked into the STL model of the entire truss without expensive computations as shown in Figure 6.13 in Step IV. However, it must be ensured that the triangle vertices of STL model meet up exactly with each other, without gaps or overlaps. The connection between two neighboring unit trusses is shown in Figure 6.14. The corresponding STL vertices should be coincident and there is no gap and overlap between these two units. Otherwise, a defective STL model would be resulted. The ACIS faceting tool must be configured to ensure the STL vertices along the coincident circular edge are coincident. No Boolean operation is required since the STL models of all the unit trusses are stacked together directly. The solid modeling process was implemented with C++ and ACIS. The input is the truss topology and the output is STL model of the truss structure.

6.4 Implementation of Hybrid Geometric Modeling and its Efficiency Analysis

A few examples are tested to evaluate the effectiveness and the efficiency of hybrid geometric modeling method of conformal truss structures. The test platform is a Dell Dimension XPS machine with Intel 700 MHz CPU, 512 MB RAM, and the Operating

System is Window 2000. In Figure 6.15, the author shows a half cylinder truss covered by a thin skin. The entire geometric modeling process is automated with no human interaction. No non-manifold entity is created and the resulted STL model is free of error. The half cylinder truss was built with SLA3500.

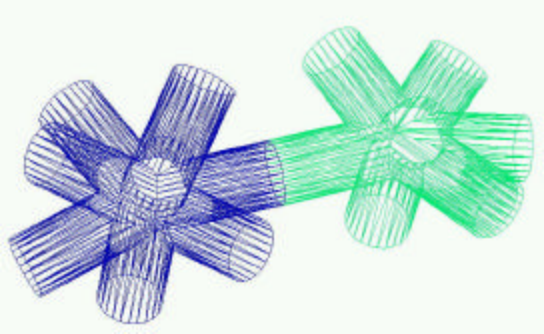

Figure 6.13 Stacking Unit Trusses into Entire Truss

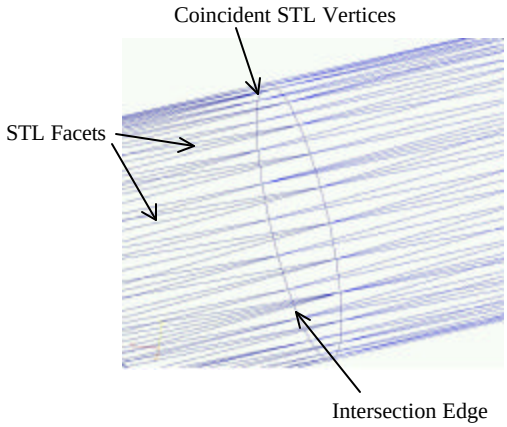

Figure 6.14 Connection between Two Neighboring Unit Trusses

a) STL Model b) SLA Part

Figure 6.15 Test Samples

Compared with the approach of creating the complete solid model, the hybrid geometric modeling method significantly saves the required computational resources for the geometric modeling of large-scale truss structures. Table 1 shows the time and memory (RAM) usage of creating complete solid model approach (labeled as ACIS) and hybrid geometric modeling method (labeled as STL). The surface smoothness is 30 during experiments.

Table 1 Time and Memory Consumption of Geometric Modeling for Truss Structures

	Number of Struts	225	480	1074	1999	4662
Time (second)	ACIS	37	107	370	2400	Infinity
	STL	80	222	539	991	1361
Memory (MB)	ACIS	52.6	95.68	321.5	500	500
	STL	32	37.5	49.316	68.04	100

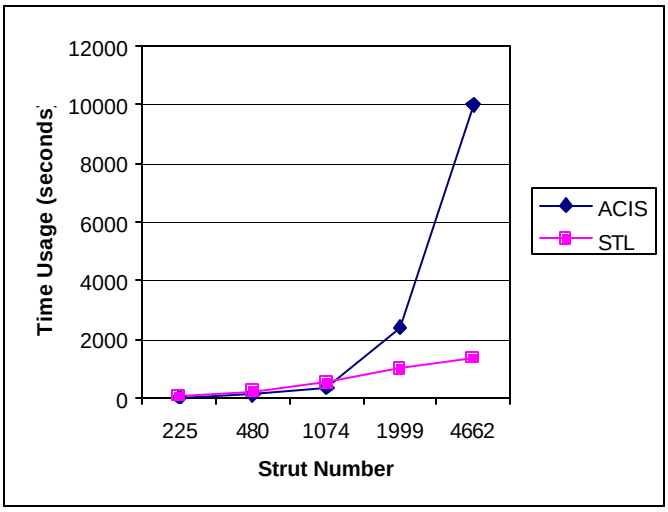

Figure 6.16 Test Result: Time vs. Strut Number

In Figure 6.16, the author shows the running time versus the number of struts in the truss structure. When the number of struts is less 1100, it takes less time to create solid (ACIS) model using completely solid modeling than to create STL model directly using hybrid geometric modeling method. It is because hybrid geometric modeling

method needs to initialize and terminate ACIS tools every time when the program creates a single unit truss. The program of creating ACIS only initializes and terminates ACIS tools once and it can save time significantly. In fact, a large portion of time is used to initialize and terminate ACIS tools for hybrid geometric modeling method. While the strut number is more than 2400, the running tme of creating complete ACIS model trends to be infinite since the memory is used up. When running a single program and the RAM is used up, the computer resorts to virtual memory on the hard drive, but this process takes a long time to exchange data between RAM with hard drive for a single program. So the running time becomes extremely large to build complete ACIS model for large-scale truss structure. The curve of creating STL model using hybrid geometric modeling method in Figure 6.16 is almost linear, which can validate that its running time is proportional to the strut number.

In Figure 6.17, the author shows the used memory versus the strut number of the truss structure. The program always keeps low memory demand for hybrid geometric modeling method. Most of used memory is to store the STL model. Even if the strut number reaches 4662, the used memory is only 150 MB, of which 120 MB memory is used to store the STL model. There are about 1200 triangular facets on one unit truss, and each facet requires 96 bytes to store it. So one unit truss requires about 115-KB memory to store its STL model. There are 1044 unit trusss in the largest truss list in Figure 6.17, so the total require memory to store STL model is about 120 MB. The ACIS components takes around 30 MB memory, and the total required memory to create the STL model is about 150 MB, which matches with the test result very well. The curve of memory usage for hybrid geometric modeling method is almost linear, which shows that the memory usage is proportional to the strut number of the truss structure.

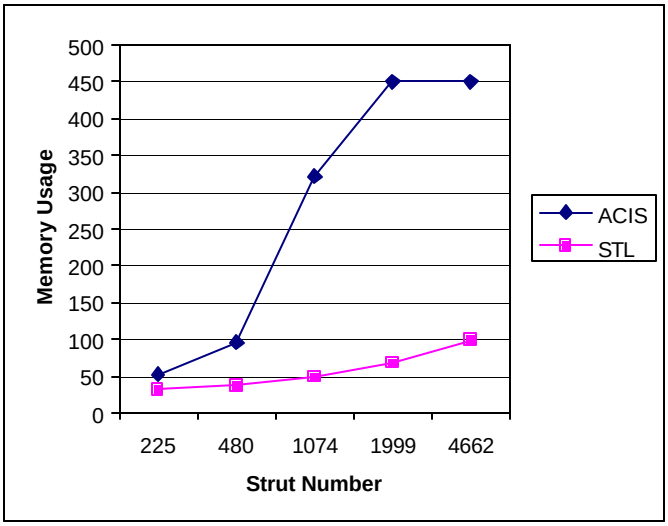

Figure 6.17 Test Result: Used Memory vs. Strut Number

The hybrid geometric modeling method can be extended as the method for other cellular structures composed of different microstructure and even some special structures with periodic topology. Choosing an appropriate microstructure is the most important step. For example, in Figure 6.18, the author shows a chainmail and its suggested microstructure for hybrid geometric modeling. No intersection or overlap between neighboring microstructures, and it is applicable to directly stack the microstructures together without Boolean operation. The hybrid geometric modeling method can significantly save the computational resources for geometric modeling.

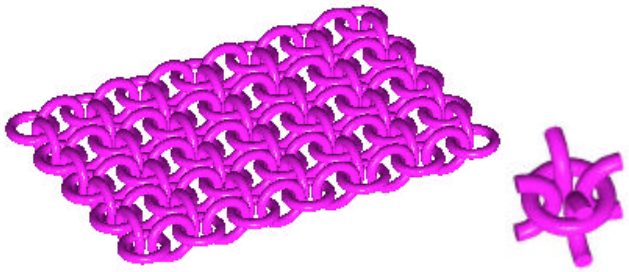

Figure 6.18 Chainmail and Its Suggested Microstructure for Geometric Modeling

6.5 Chapter Summary

The hybrid geometric modeling method of directly creating STL models can effectively and efficiently generate geometric models of large-scale conformal cellular structures. This method facilitates the design, analysis, optimization, and manufacture of cellular structures. In this chapter, conformal, mesoscale truss structures are used as the example cellular structure. An automated process is developed for constructing geometric models of truss structures by using unit truss as the microstructure. The structure's joint geometries are smoothened and non-manifold geometries are avoided. The computation efficiency of our hybrid geometric modeling method is evaluated as compared to the approach of creating complete solid model, and it is shown that the hybrid geometric modeling method is an effective and efficient approach for the geometric modeling of large-scale conformal cellular structures.

Adding rounds to the joints of cellular structures could reduce stress concentration and fatigue to enhance the structures' mechanical performance. Local Boolean operations at the common edges between neighboring unit trusses could glue the unit trusses' surfaces together and efficiently create the solid model of an entire structure. These two improvements can potentially enhance the design of cellular structures and obtain the solid models of cellular structures.

In this chapter, geometric modeling has been successfully used to create solid model of cellular structures to represent material distribution for manufacturing. A hybrid geometric modeling method using unit truss was developed to efficiently generate CAD models of large-scale conformal cellular structures. In Chapter 3, conformal topology is successfully created to represent material distribution for analysis and design synthesis. Therefore, the work presented in Chapters 3 and 6 has completely solved the issue of representation. The development of hybrid geometric modeling addressed part of the

“representation” issue (raised in Section 2.4) and proved the theoretical structural validity (shown in Figure 1.22) of the hypothesis (posted in Section 1.4). Its empirical structural validity (shown in Figure 1.22) was proved via creating a series of conformal cellular structures.

CHAPTER 7

MANUFACTURING OF CELLULAR STRUCTURES

In this chapter, the “manufacturing” issue raised in Section 2.4 is addressed through investigating the state-of-the-art manufacturing processes for cellular structures, and considering their limitations at the design stage. Additive fabrication (construct) is adapted to manufacture adaptive cellular structures and integrated into the unit truss design process.

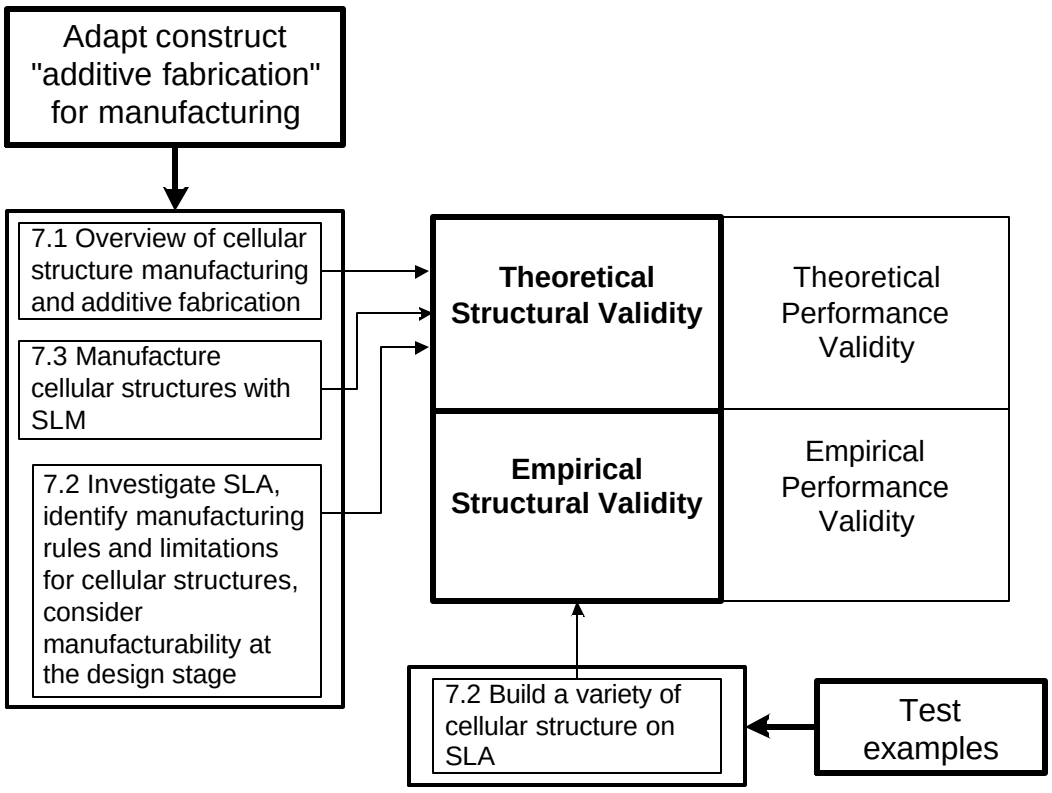

Figure 7.1 Relationship between Chapter 7 and Validation Square

The presentation of this chapter follows Figure 7.1. The author first presents the challenges to manufacture cellular structures and discusses the manufacturability of cellular structures. Additive fabrication is proposed to manufacture the cellular structures. Then, the author identifies the manufacturing rules of cellular structures with Stereolithography and considers the manufacturing limitations at the design stage. Finally, the state-of-the-art Selective Laser Melting process is investigated for the manufacturing of cellular structures. The focus of Chapter 7 is the manufacturing shown in Figure 7.2. The input is the CAD model of cellular structures.

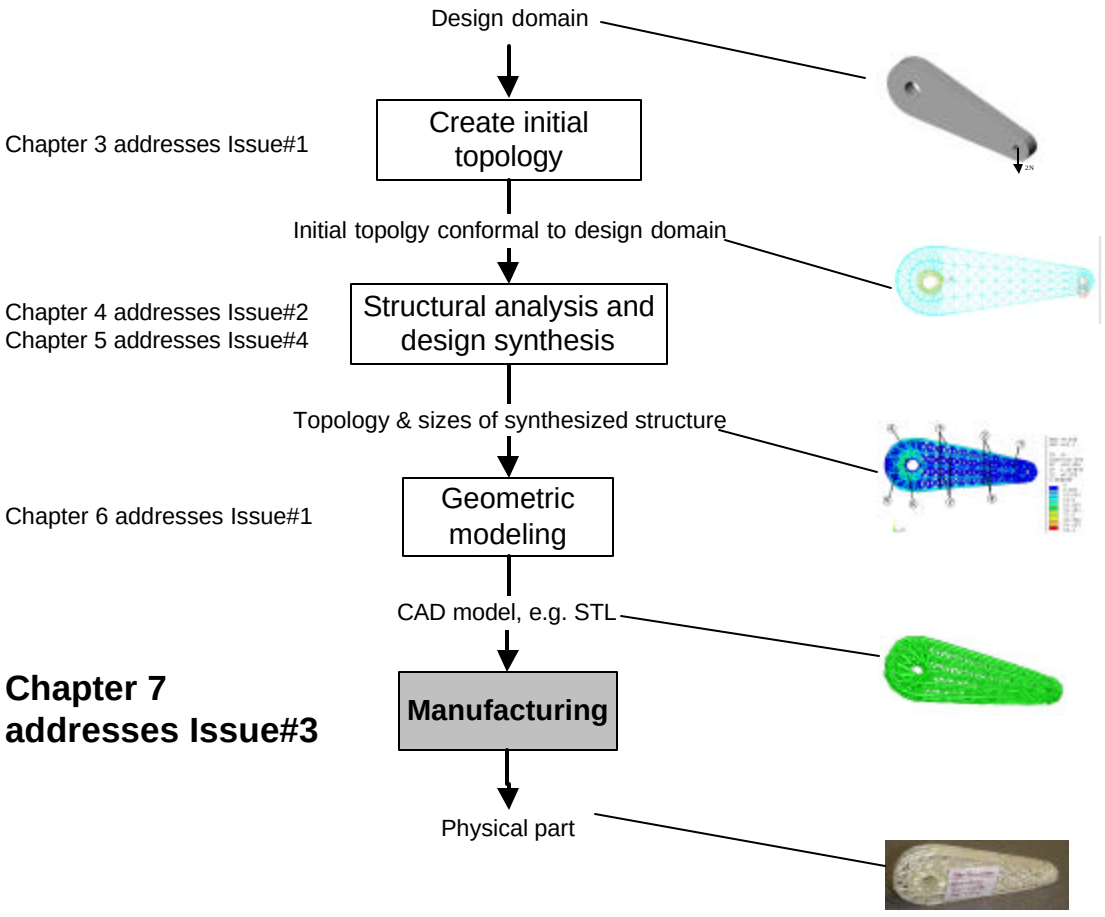

Figure 7.2 Focus of Chapter 7 in the Design Process of Cellular Structures

7.1 Overview of Cellular Structure Fabrication

This section analyzes the challenges to fabricate cellular structures and then discusses the popular manufacturing processes, particularly additive fabrication, to manufacture periodic (ordered) cellular structures.

7.1.1 Challenges of Manufacturing

Two issues are related to the manufacturability of cellular structures. One is to identify a feasible manufacturing process; the other is to identify the manufacturing rules. The cellular structures have relatively complex geometries and cannot be fabricated directly by the conventional manufacturing processes, such as machining and welding. The manufacturing process (the first issue) can be identified via leveraging the relative research works about cellular structure. The manufacturing rules (the second issue) are related to a particular manufacturing process, and have to be identified via experimentation.

The cellular structures discussed in this research have the following characteristics: **periodic structure, non-uniform mesostructure, and 3-D geometric complexity**. An example is shown in Figure 7.3.

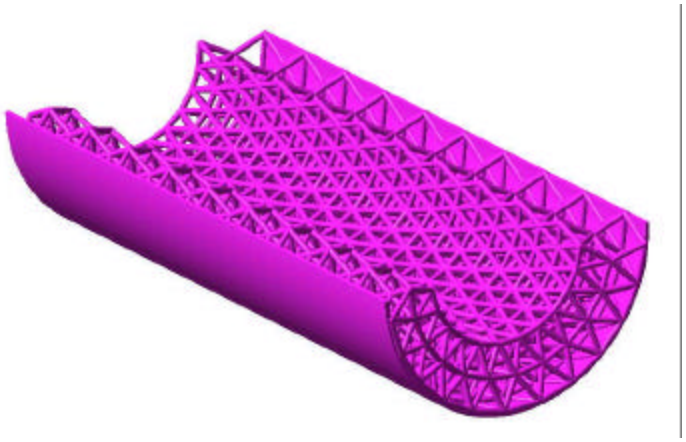

Figure 7.3 Stretching-dominated 2-D Triangular Truss Structure

7.1.2 Popular Manufacturing Processes for Periodic Cellular Structures

Researchers have developed various manufacturing processes since people started to mimic the natural occurrences 50 years ago. Corresponding to the classification of cellular structures discussed in Chapter 1, the developed manufacturing processes can be categorized as stochastic process and repeatable process. The stochastic manufacturing process, such as metal foaming, randomly distributes voids and the resulting stochastic cellular structures can show homogeneity at the part scale. In Figure 7.4, the author shows a stochastic manufacturing process using gas injection to create aluminum foams (Wadley, Fleck et al. 2003). The void and material distributions cannot be controlled during the stochastic manufacturing processes. Thus, the stochastic processes cannot be used to fabricate the adaptive cellular structures, whose void and material distributions must be well controlled.

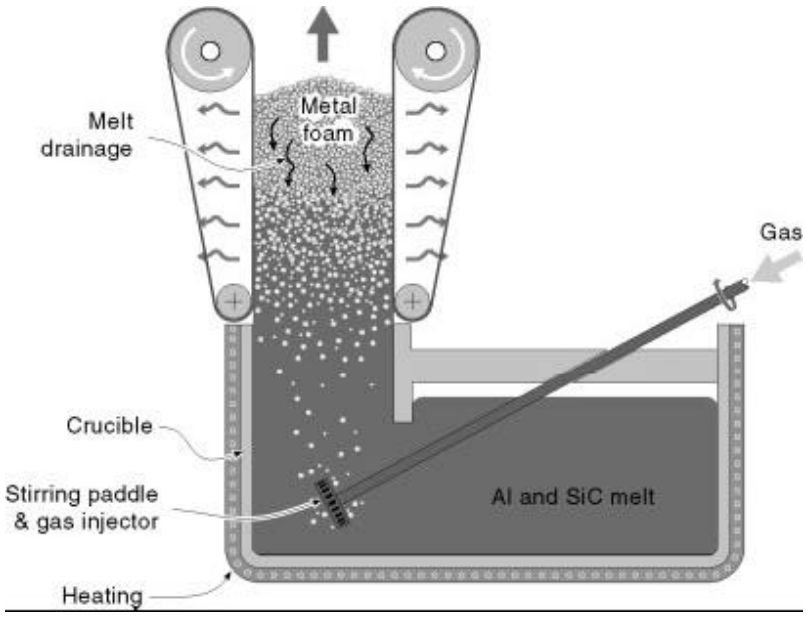

Figure 7.4 A Stochastic Cellular Material Manufacturing Process by Gas Injection

A sheet crimping and stamping process was used to fabricate periodic 2-D metallic honeycomb cores for sandwich panels (Wadley, Fleck et al. 2003). The stacked

sheets can be bonded by resistance welding or with an adhesive. The cores can be cut and adhesively bonded to face sheets to create sandwich panels. However, the geometry of the manufacturable cellular structure is limited since the wall thickness must be uniform and no geometric variation can be created in the length direction.

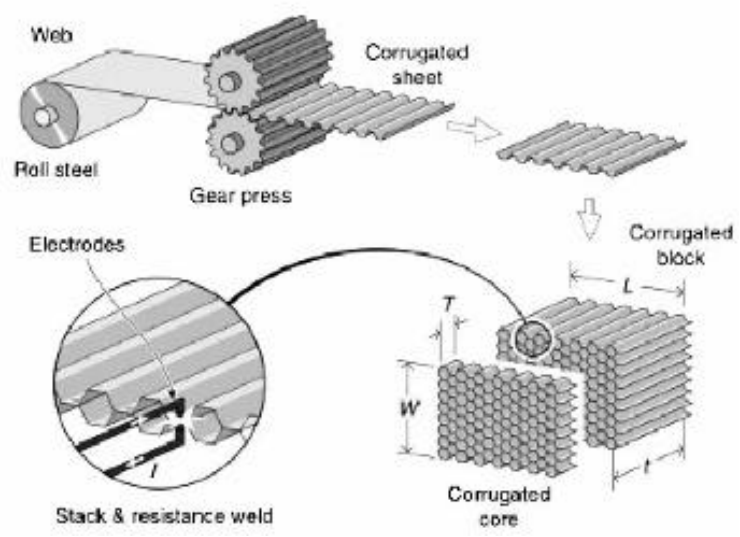

Figure 7.5 Manufacture Periodic 2-D Honeycombs by Crimping and Stamping

Cochran and his colleagues at Georgia Tech developed a process to fabricate linear cellular alloy by using conventional powder processing techniques. Precise shapes were formed with non-metal precursors and subsequently converted to the metal state by a direct reduction process as shown in Figure 7.6 (Cochran, Lee et al. 2000). The linear cellular alloy can be formed via powder forming techniques including extrusion, slurry coating of sacrificial cores, slurry casting methods, and dry pressing (Cochran, Lee et al. 2000). This slurry extrusion process can create various geometries of 2-D mesostructures by varying the cross-section shape of the honeycomb extrusion tool. The structures with non-uniform wall thickness are manufacturable. However, the manufacturable structures can only be 2.5-D and with no variations in the length direction.

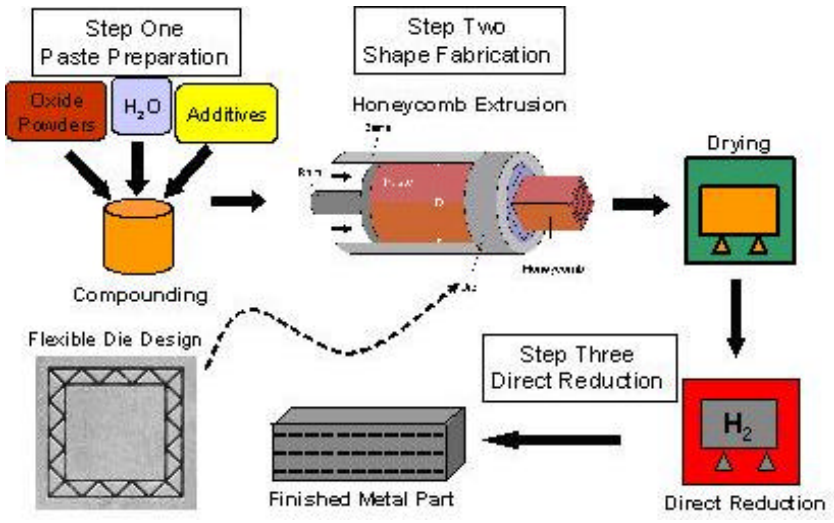

Figure 7.6 Manufacturing Linear Cellular Alloy by Extruding Slurry

Some researchers use injection modeling to fabricate truss elements (truss core, top and bottom plates) with a polymer, then assemble them into a complete lattice for investment casting if metallic structure is desired (Wallach and Gibson 2001). However, this manufacturing process is time-consuming, and cannot guarantee part accuracy. It is not capable to fabricate conformal structures or multi-layer structure.

Geodesic Inc. had pioneered the manufacturing of periodic cellular structures by using additive fabrication, namely rapid prototyping (Cheng, Stamp et al. 1999; Wang 2001; Wang and Rosen 2002). Geodesic Inc. (out of business since 2001) used Selective Laser Sintering (SLS) process to manufacture such metal geodesic structure as shown in Figure 7.7 as early as 1999. Wallach and Gibson utilized Fused Deposition Modeling (FDM) to fabricate sacrificial polymeric patterns for investment casting of metallic cellular structure as shown in Figure 7.8 (Wallach and Gibson 2001). Chiras et al. chose acrylonitrile–butadiene–styrene (ABS) to fabricate integrated truss core and face sheet sandwich panel, which were then used for investment casting from a high thermal conductivity beryllium–copper casting alloy (Cu–2%Be) (Chiras, Mumm et al. 2002; Wadley, Fleck et al. 2003).

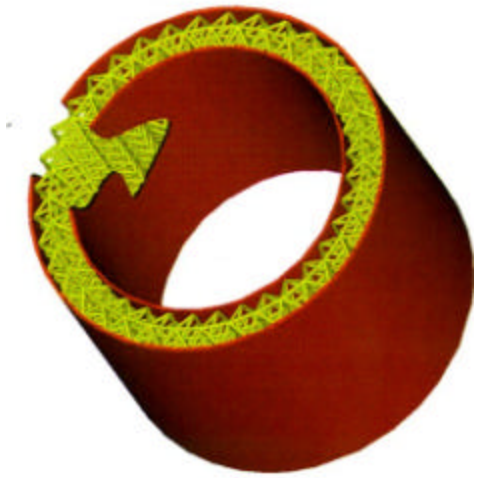

Figure 7.7 Geodesic Structure Fabricated Using SLS by Geodesic Inc.

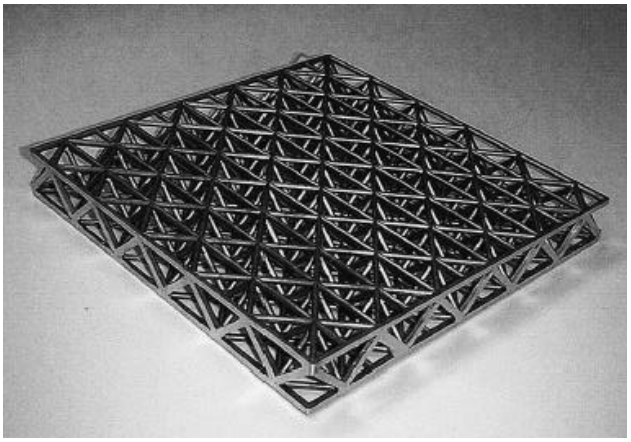

Figure 7.8 3-D Truss Panel Fabricated Using FDM and Investment Casting

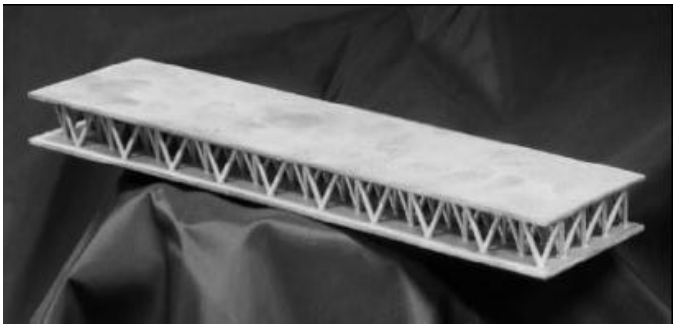

Figure 7.9 A Tetrahedral Lattice Structure Made by Rapid Prototyping Followed by Investment Casting

7.1.3 Additive Fabrication

Additive Fabrication processes build parts by adding material, as opposed to subtracting material from a solid object; additive fabrication processes include Stereolithography, Selective Laser Sintering, and so on. Additive Fabrication processes virtually can build arbitrary complex geometries. They need minimum human intervention to operate with automatic process planning. They use generic fabrication machines without the need of part-specific tooling or fixtures. (Jacobs 1992; Prinz, Atwood et al. 1997; Diez 2001; Dutta, Prinz et al. 2001; Wang 2001)

Additive fabrication has the unique capability to produce virtually arbitrary complex geometry compared to the traditional manufacturing processes. Additive fabrication processes are proposed to manufacture the cellular structure. We should investigate its limitations to manufacture the cellular structures in terms of part geometry, material, and process itself. Some researches have shown the potentials of additive fabrication to build the final functional parts (Daily, Lees et al. 1997; Wang 2001). There are two classes of additive fabrication methods that can be used to manufacture them, even the metal parts. One is direct tooling or direct manufacturing process, such as SLS RapidSteel (Radstok 1999; Stewart, Dalgarno et al. 1999; Dalgarno and Stewart 2001), 3-D Printing ProMetal (Radstok 1999) and LENS (Grylls 2003), which can fabricate the final parts without intermediate steps. The other is indirect manufacturing, such as SLA QuickCast (Hague, D'Costa et al. 2001) and FDM (Radstok 1999). For example, the SLA QuickCast patterns are first fabricated with SLA processes, and then the final parts are made by investment casting after the patterns are burned out (Hosni, Nayfeh et al. 1999).

Some resulting part geometries from topology and geometry optimization, such as 3-D truss structures and compliant mechanism, are usually very complex and difficult

to fabricate by conventional manufacturing processes. Truss structures and compliant mechanisms are two classes of shapes that can take advantage of the unique capabilities of these processes to produce complex geometries. We will explore design methods and classes of novel shapes that take advantage of additive fabrication processes' capabilities to manufacture the parts with complex shapes.

7.2 Manufacturing Cellular Structure with Stereolithography Process

In this research, we will utilize the stereolithography (SLA) process to fabricate cellular structures. We will identify the manufacturability, formulate the manufacturing rules and consider the limitations at the design stage.

7.2.1 Identify Manufacturability and Formulate Manufacturing Rules

Truss struts are the composing elements of cellular structural system. Therefore, considering truss struts' manufacturability can help identify the manufacturing limitation of the whole structural system. It is essential to assess the effect of manufacturing process on the structures' performance and form the manufacturing rules of fabricating truss struts.

Our experiments were performed on 3D Systems' Viper and SLA 3500 (2003). DSM WaterClear 10120 was used for Viper, and RenShape SL 7510 resin was used on SLA 3500. The major parameters of the manufacturing process are set as Table 7-1.

Table 7-1 Major Manufacturing Parameters of SLA 3500 to Build Cellular Structures

Machine	Resin	Layer Thickness	Z Wait	Z Dip Distance	Pre-dip Delay
Viper	DSM WaterClear 10120	4 mils	5 sec	0	10 sec
SLA3500	RenShape SL 7510	6 mils	0 sec	0	15 sec

7.2.1.1 Manufacturing Cellular Structures without Supports

Stereolithography (SLA) parts typically need support structures for the overlying surfaces during the build. Most struts of the cellular structure need support structures. However, the cellular structures have relatively complex geometries, thus the interior support structures are difficult to clean. Experiments have been done to explore the possibility of building truss structure without support structure in Stereolithography. In Figure 7.10, the author shows two truss structures with various shapes and sizes successfully built without support structure on SLA3500. The truss on left is in a kernel shape with complex surface and overhanging edges. The truss on right is a 254mm tall half-cylinder built vertically on the SLA3500 platform. The truss edges do not exhibit any curling phenomena influencing the whole structure even if almost all edges extend beyond 1.27mm from their vertices. Different from the general Stereolithography process (Jacobs 1992), the cellular structures are self-supporting and the facing-down regions can be successfully built without sag. The local inaccuracy of individual overlying struts does not cause the global inaccuracy.

Figure 7.10 Truss Structures with Various Shapes and Size without Support

7.2.1.2 Minimum Manufacturable Strut Size without Supports

Cellular structures are manufacturable without support structure within certain ranges of strut length and diameter through SLA. Due to the absence of support structure, the minimum manufacturable strut diameter is different from the machine's minimum manufacturable feature size. For example, the Viper SLA system using the High Resolution (HR) mode can provide a laser beam diameter of just 3mils with a minimum feature size of just 7mils. However, a cellular structure with the strut diameter of 7mils cannot be fabricated because the struts overlies in space without support and oriented in various directions. Therefore, the minimum manufacturable strut size should be identified. It can be identified by building cellular structures with various strut diameters.

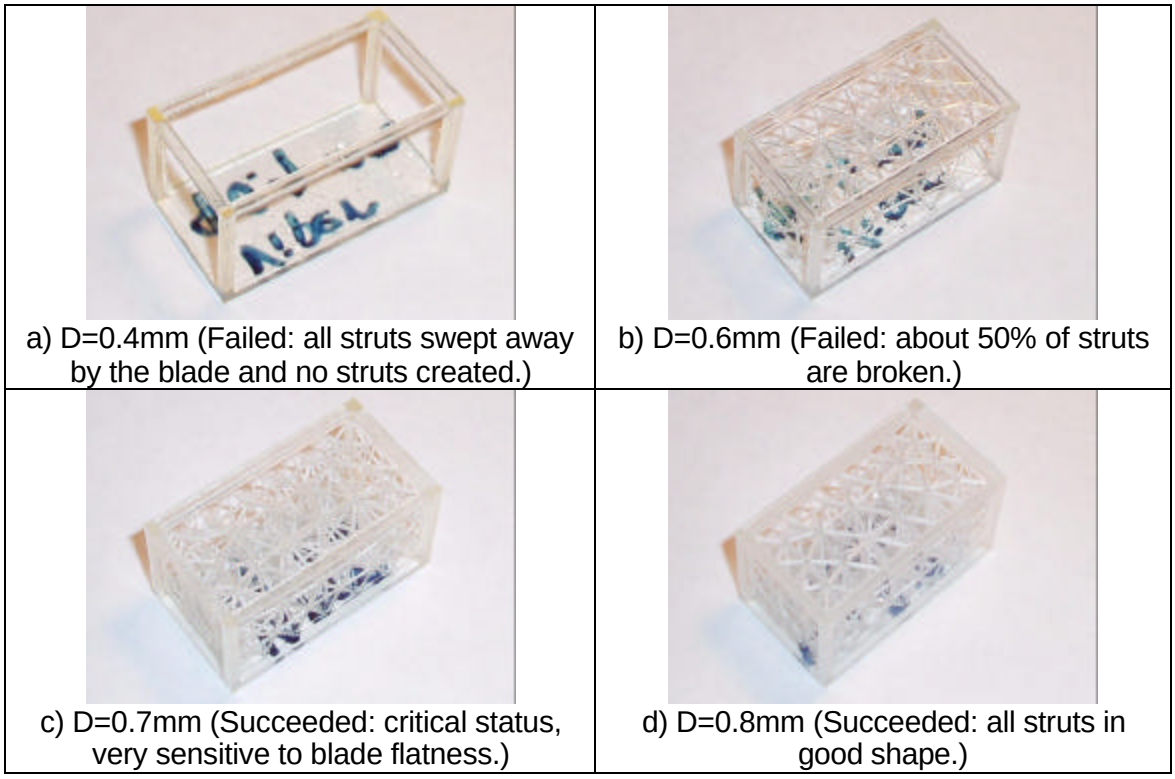

a) D=0.4mm (Failed: all struts swept away by the blade and no struts created.)

b) D=0.6mm (Failed: about 50% of struts are broken.)

c) D=0.7mm (Succeeded: critical status, very sensitive to blade flatness.)

d) D=0.8mm (Succeeded: all struts in good shape.)

Figure 7.11 Specimens to Identify Minimum Manufacturable Strut Diameter of the Viper System

In Figure 7.11, the author shows the specimens, whose strut diameter varies from 0.4mm to 0.9mm. These specimens have the same topology, and strut lengths, and

they were built on a Viper SLA system. The experiment results show that the minimum manufacturable strut diameter of cellular structures is 0.7mm for the Viper SLA system in the standard mode (with a laser beam diameter of 10mils) and with the major parameters given in Table 7-1. A similar experiment was performed on the SLA 3500 system and shows that the minimum manufacturable strut diameter is 0.8mm in the fast mode with the major parameters given in Table 7-1.

7.2.1.3 Maximum Manufacturable Strut Aspect Ratio without Supports

Due to the layer delamination, some solidified resin filaments were present inside a few cellular structures built on SLA systems. However, minor layer delamination does not have any noticeable impact on the structures' manufacturability and strength. These filaments could be avoided by using smaller layer thickness and deep dip. The strut length can range up to 85 mm with a strut diameter of 1.5 mm as the cellular structure shown in Figure 7.12. The Signature Discipline Group at Pratt & Whitney built a big triangle-like cellular structure on an SLA 7000 system. The maximum manufacturable strut aspect ratio is larger than 56.7. A comparative structure scaled down by 0.5 in each direction was unsuccessfully built on the SLA 3500 system due to the broken thin skin. However, most of the struts were built successfully. Thus, the maximum manufacturable strut aspect ratio on an SLA 3500 system should be larger than 56.7 as well.

However, as show in Table 4-1, the critical aspect ratio to avoid buckling for RenShape SL 7510 resin is 10.16, which is significantly less than the maximum manufacturable strut aspect ratio, 56.7. Thus, the maximum manufacturable strut aspect ratio may not be considered as a constraint during designing cellular structure, but the critical aspect ratio (to avoid buckling) needs to be considered as a design constraint.

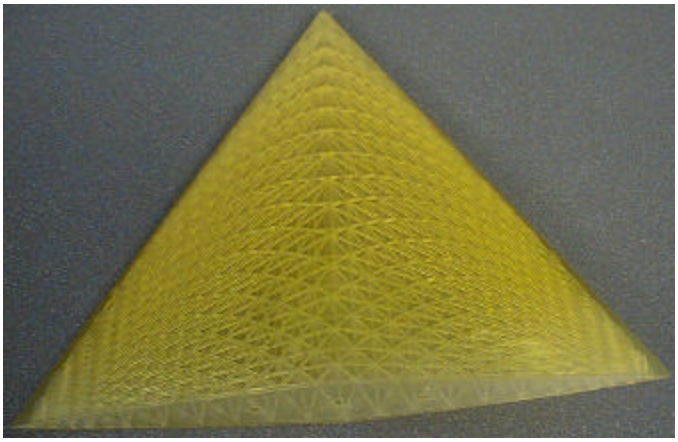

Figure 7.12 Cellular Structures with a Maximum Strut Aspect Ratio 56.7

7.2.1.4 Fabricate Metal Cellular Structure with SLA and Investment Casting

We have investigated the manufacturability to fabricate metal cellular structure with SLA and investment casting. The 3D Systems' SLA QuickCast process has three major steps: fabricate SLA prototype, create ceramic shell, and cast the part as shown in Figure 7.13 (Hague, D'Costa et al. 2001). The SLA QuickCast prototype uses shelled part filled with rib patterns; Sample rib patterns are shown in Figure 7.14 (Hague, D'Costa et al. 2001). Since the strut diameter is in the same size scale as the rib spacing, it is not necessary to create ribs inside the struts like QuickCast. The shelled cylindrical struts with a wall thickness of 0.3mm are strong and stiff enough to support themselves during SLA process. A shelled cellular structure built on SLA 3500 is shown in Figure 7.15. The wall thickness of the SLA part can influence the strength and stiffness during the ceramic shell creation. Unfortunately, due to lack of investment casting capability available at Georgia Institute of Technology, this shelled cellular structure has not been used as the sacrificial pattern for investment casting and no metal cellular structure was created using this approach.

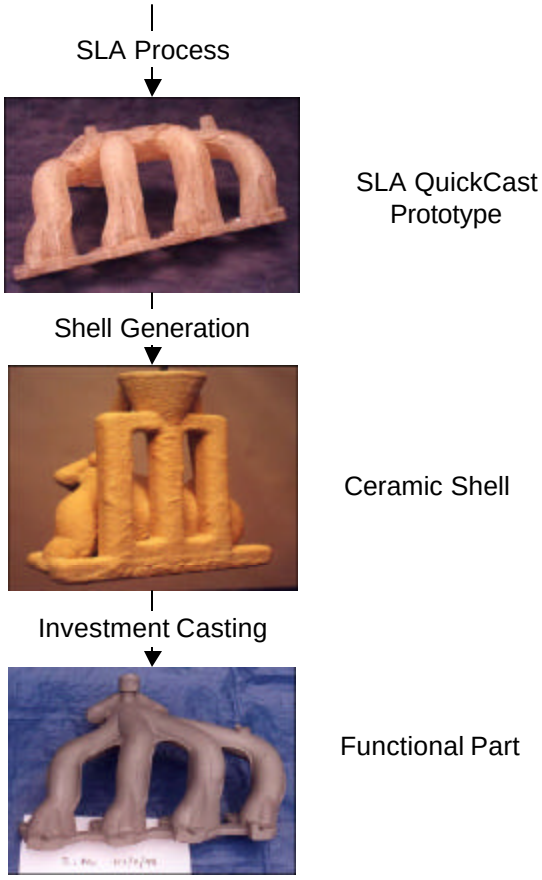

Figure 7.13 QuickCast Process to Fabricate Metal Parts and a Typical Rib Pattern

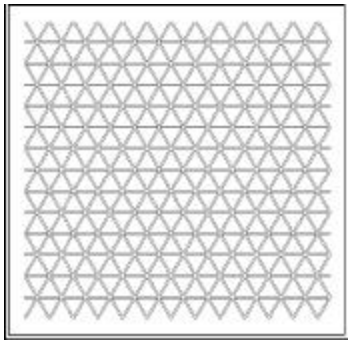

Figure 7.14 Rib Pattern for SLA QuickCast Prototype

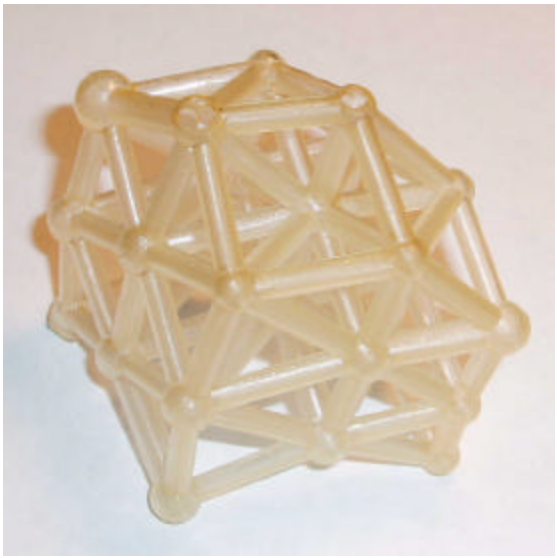

Figure 7.15 Shelled Pattern of Cellular Structure

7.2.2 Considering Manufacturing Limitations at the Design Stage

The manufacturing limitations must be considered as constraints at the design stage. The major constraint is the minimum manufacturable strut size, which limits the selection of the strut sizes during design synthesis. All strut diameters of the resulting design should be larger than the minimum manufacturable strut size. Hence, the struts should satisfy $x \geq x_{mfg_{\min}} = 0.8mm$ if using an SLA 3500 system, or $x \geq x_{mfg_{\min}} = 0.7mm$ if using a Viper SLA system. As discussed in Chapter 5, without the consideration of the minimum manufacturable strut size, the range of design variables (strut diameters) is continuous and given as $x \in \left[x_{0^+}, x_{\max} \right]$, where x_{0^+} is relatively small, e.g. $x_{0^+} = 0.01mm$. However, with the consideration of the minimum manufacturable strut size, the range of design variables becomes discreet. The diameter of the resulting design should not fall between x_{0^+} and $x_{mfg_{\min}}$. Otherwise, these struts are not manufacturable. As proposed in Chapter 4, penalty method can be used to avoid the non-manufacturable struts in the synthesized result.

The manufacturing variations of struts sizes can affect the part geometry and shift the design optimality. Unfortunately, the manufacturing variations of cellular structures with stereolithography have not been researched in our work. This problem might be a future work in our continuing research.

7.3 Manufacturing Cellular Structure with Other State-of-the-art Additive Fabrication Processes

Selective Laser Melting (SLM) is a derived process from Selective Laser Sintering (SLS) (2005; Kruth, Mercelis et al. 2005). SLM fabricates near full dense parts with mechanical properties comparable to those solid parts. The laser beam used in the SLM process can completely melt polymers and metals. The resulting parts require no post-process. Commercial SLM material includes titanium, stainless steel, cobalt and so on (2005). As claimed by MCP Group, the smallest manufacturable thickness of vertical walls can be less than $100mm$. An example of lightweight cellular structures built on SLM is shown in Figure 7.16.

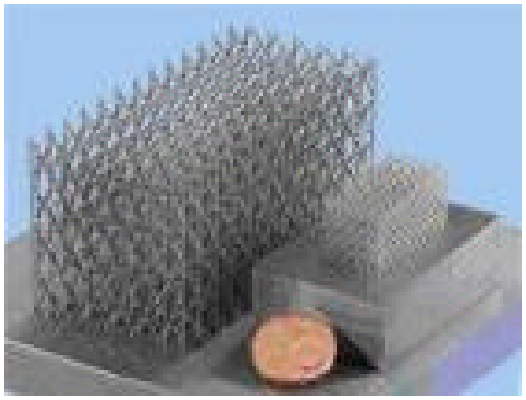

Figure 7.16 Cellular Structure Manufactured with Selective Laser Melting

The approach presented in the last section to identify the limitation on minimum strut diameter and maximum strut aspect ratio of cellular structures is applicable to other additive fabrication processes, such as Selective Laser Sintering (SLS) and Selective

Laser Melting (SLM) (Jacobs 1992; 2005). However, the applied adaptive fabrication processes need to be able to build cellular structures without supports or easily removable supports. The minimum manufacturable strut diameter and maximum manufacturable strut aspect ratio might be different from minimum manufacturable feature sizes of additive fabrication processes. These manufacturing limitations can be identified via a series of experiments as discussed in the last section.

7.4 Chapter Summary

This chapter analyzed the manufacturing challenges of cellular structures, and then discussed the manufacturability by reviewing the existing research works. As a repeatable process, additive fabrication is proposed to fabricate the periodic cellular structures with non-uniform mesostructure and complex 3-D geometries. In this research, the stereolithography (SLA) process is used to fabricate cellular structures. We successfully identified the manufacturability of SLA for cellular structures, and formulated its manufacturing rules. And we are enabled to consider the limitations at the design stage. The approach of identifying the manufacturing limitations and considering the manufacturability is applicable for other additive fabrication processes for the manufacturing of cellular structures.

Manufacturing processes can cause the variations of strut sizes and influence the structures' performance. It is desired to consider this kind of variations at the design stage through robust design (Chen, Allen et al. 1996; Seepersad 2004). More metal cellular structures are desired to manufacture and the relative manufacturing processes need to investigate. A few pieces of metallic parts can greatly reinforce our research contributions.

In Chapter 7, the potential manufacturing processes for cellular structures were investigated. As sample process, the manufacturing rules of SLA process were formulated and the limitations were identified. The manufacturing limitations (minimum manufacturable strut diameter and maximum manufacturable strut aspect ratio) are considered as constraints during design synthesis. Therefore, the issue about manufacturing (raised in Section 2.4) was successfully addressed. It proved the theoretical structural validity and empirical structural validity (shown in Figure 1.22) of the hypothesis (using unit truss) posed in Section 1.4 about manufacturing to support a systematic design of adaptive cellular structures.

CHAPTER 8

GRADED CELLULAR STRUCTURE FOR ENHANCED STABILITY ON IMPLANT-BONE INTERFACE IN UNCEMENTED PROSTHESIS – A NEW ACETABULAR IMPLANT WITH GRADIENT POROSITY FOR HIP REPLACEMENT

In this chapter, the hypothesis posed in Section 1.4 is empirically tested by using unit truss approach to design a graded cellular structure for uncemented prosthesis to enhance stability on implant-bone interface. A new acetabular implant with gradient porosity is developed for hip replacement. The state-of-the-art porous coatings become more and more popular in uncemented prostheses to make bone grow into implants for biological fixation. Gradient porous acetabular component with cellular structure could match the bone's elasticity. Material is adaptively distributed from high porosity at the bone-implant interface to solid metal at the joint's articulating surface. The new acetabular prosthesis would replace metal-on-polyethylene bearing with metal-on-metal bearing for less wear. The design problem of acetabular component is formulated and a requirement list is elaborated. Then, a detailed design of this prosthesis with graded cellular structure is performed. At last, the design concept is validated via being compared with existing products according to the design requirements.

8.1 An Overview of Implant Fixation in Hip Replacement

This section first introduces the fundamentals of hip replacement. Biological fixation with various porous coating techniques is presented as the emerging technology

for implant-bone interface in the uncemented prostheses. Finally, the major failures about the hip joint prostheses are discussed.

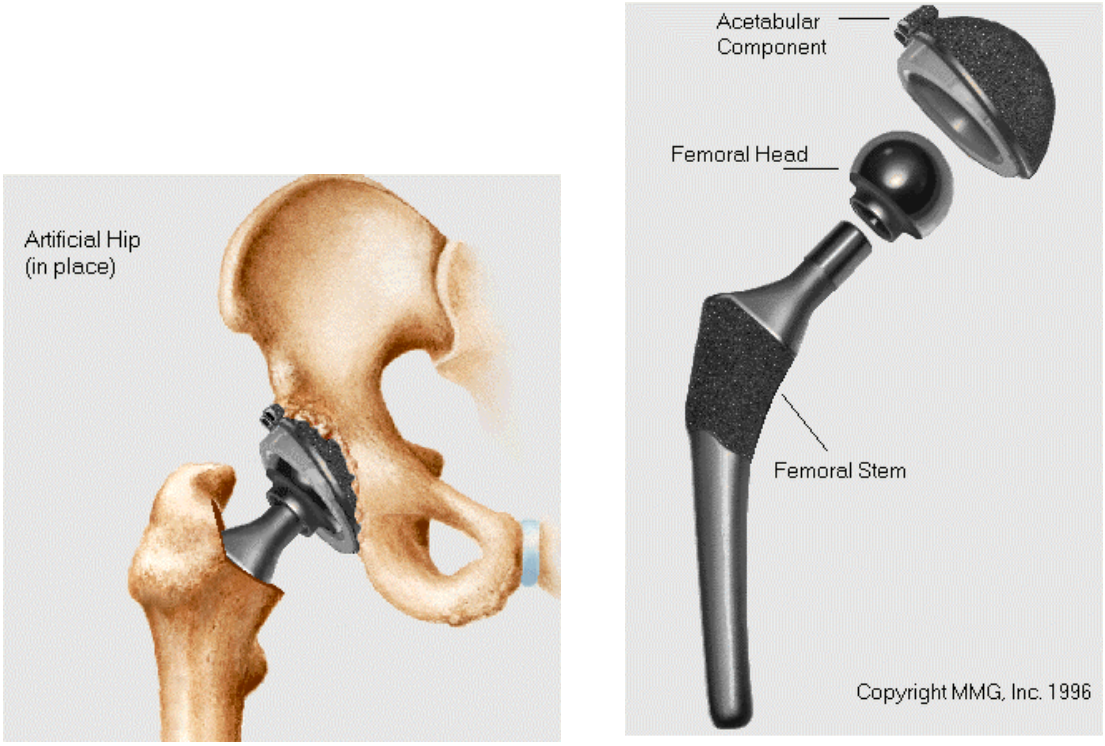

(a) Total Replaced Hip Joint (b) Hip Prosthesis Components

Figure 8.1 Total Hip Replacement and Prosthesis Components

8.1.1 Fundamentals of Hip Replacement

Hip replacement surgery becomes more common as the population of the world begins to age. The hip replacement surgery is to replace the diseased articular surface with artificial implant to prevent painful bone-bone contact. Osteoarthritis is commonly referred to as "wear and tear arthritis" and perhaps the most common cause for hip replacement surgery (2005). A total hip replacement with artificial joint components in place is shown in Figure 8.1(a) (2005). The two major hip prosthesis components, femoral component and acetabular component are shown in Figure 8.1(b) (2005). The femoral component works like femur and usually consists of a metal stem and a metal or

ceramic head. The acetabular component replaces the acetabulum of pelvis and usually consists of a polyethylene liner and a metal shell.

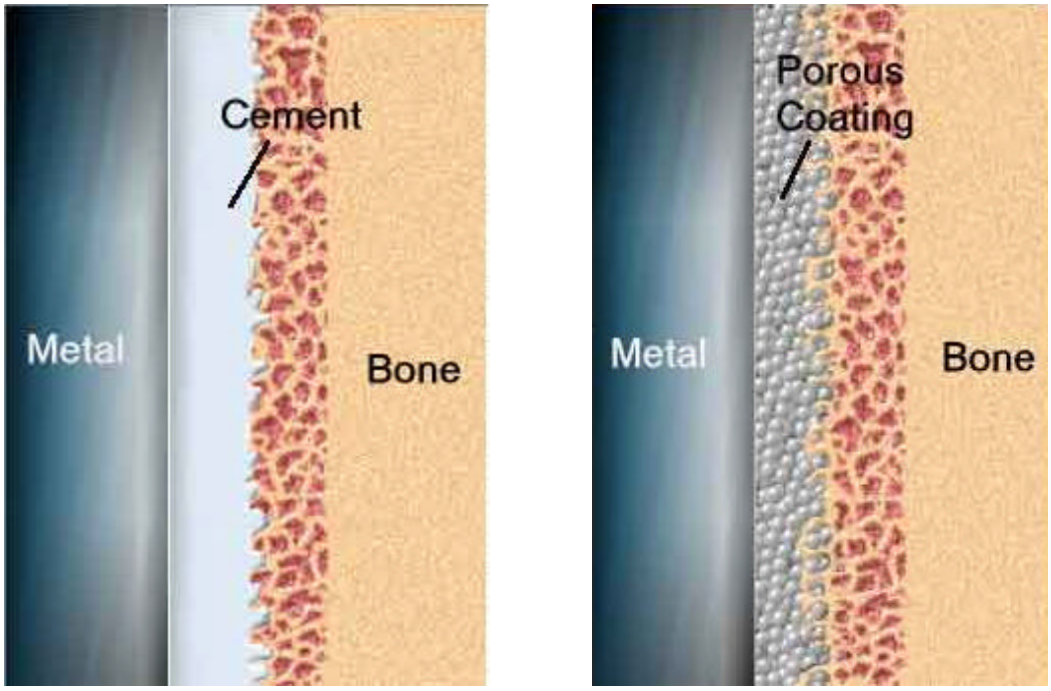

(a) Fixation with Cement (b) Fixation with Porous Metal Coating

Figure 8.2 Cemented and Uncemented Metal-Bone Interface in Prosthesis

8.1.2 Biologic Fixation with Porous Coating

One of the major design issues is about the interface (implant-bone fixation) between the prosthesis (commonly metal) and the surrounding bone. There are two widely used methods to fix the prosthesis to bone, cemented and uncemented, as shown in Figure 8.2 (2005). Cemented prosthesis uses cement, such as Polymethylmethacrylate (PMMA), to mechanically adhere the implant to the bone. Uncemented prosthesis uses a porous metal surface to create a bone ingrowth interface and biologically fix the implant to the bone without the use of cement. An uncemented prosthesis is coated with multiple layers of micro-porous metal shown in Figure 8.2(b) (Mont and Hungerford 1997; 2005). This bone ingrowth into the coating provides additional fixation to hold the implant in the desired position. The second-generation of

uncemented prostheses has shown very low aseptic loosening rates (1%-3%), and less thigh pain (under 5% in most studies) (Mont and Hungerford 1997).

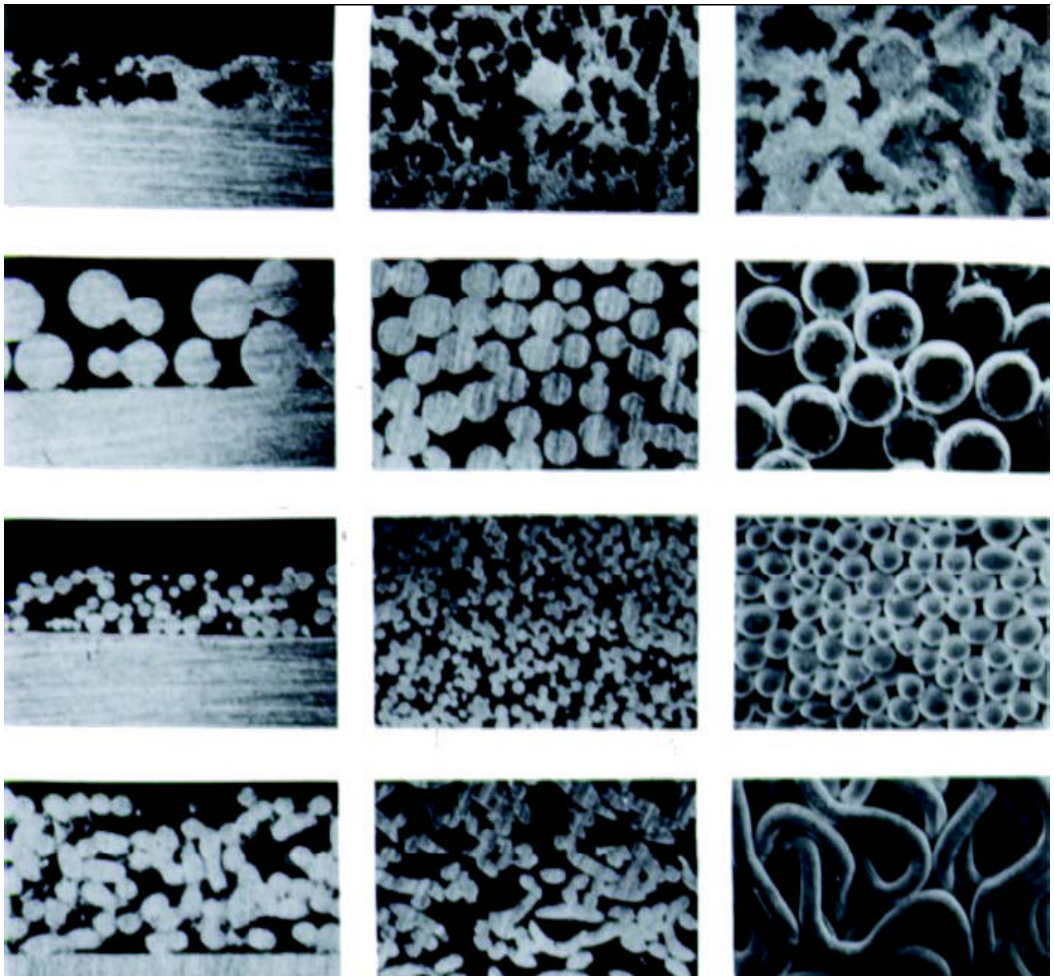

Figure 8.3 Porous Surfaces Available for Biologic Ingrowth

Different types of porous coating techniques have been developed by using biologic ingrowth. The porous surfaces for biologic ingrowth are shown in Figure 8.3. From top to bottom: plasma sprayed surfaces, sintered beaded surfaces with large spheres, sintered beaded surfaces with small spheres, and diffusion-bonded fiber-metal surfaces. The three figures from left to right in each column show representative cross-sections through the porous surfaces (Bragdon, Jasty et al. 2004). Popular metal coating materials are titanium and tantalum. Bragdon, et al., studied the significance of pore sizes on bone ingrowth, and demonstrated that their connection exists. The experimental

data shows that a mean pore size of $\geq 200mm$ and porosity of $\geq 40\%$ are experimentally optimal for bone ingrowth (Bragdon, Jasty et al. 2004). Bobyn, et al., demonstrates the intimate association between the bone and the porous tantalum acetabular prosthesis shown in Figure 8.4 (Bobyn, Poggie et al. 2004). Gross inspection shown in Figure 8.4(a) revealed large patchy areas of bone adherence to the porous tantalum. Histological analysis of undecalcified thin sections shown in Figure 8.4(b) confirmed multiple areas of bone ingrowth.

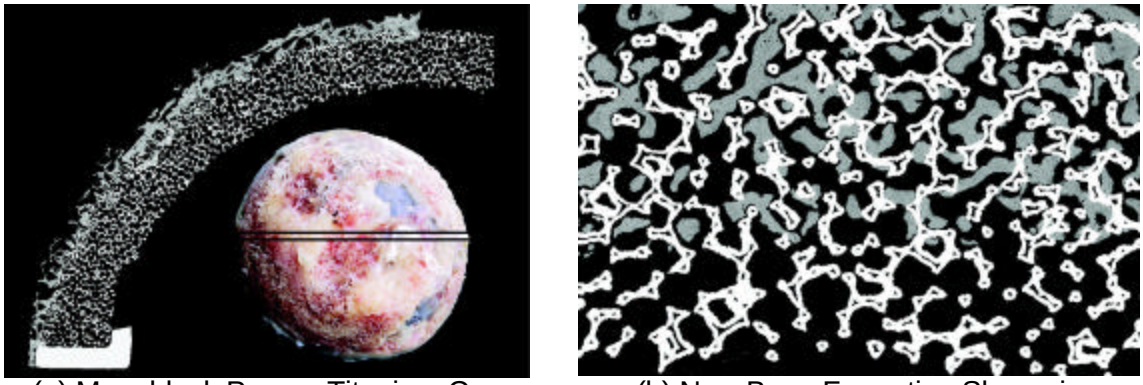

(a) Monoblock Porous Titanium Cup

(b) New Bone Formation Shown in Backscattered Scanning Electron Photomicrograph

Figure 8.4 New Bone Ingrowth into Porous Tantalum Acetabular Cup Retrieved Two Years after Surgery because of Recurrent Dislocation

8.1.3 Major Failures of Prosthesis

There are a few major complications of total hip replacement, such as vein inflammation, infection in the joint, dislocation of the joint, loosening of the joint, and osteolysis (2000; 2001; 2005). Dislocation and loosening are related to implant fixation. The dislocation may happen soon after hip replacement surgery. Loosening, mainly aseptic mechanical loosening, of the joint at the implant-bone interface is the major reason that the prostheses eventually fail. It is significantly related to the joint wear. Osteolysis, literally an "eating away" of the bone surrounding the implant, results from the wear particles of articulating surfaces. These particles insinuate their way between

the bone and the prosthesis (2000). Aseptic mechanical loosening is reported to be the most common cause of total joint failure (Fitzgerald 1992; GM, S et al. 2001). Significant factors include the fixation between the prosthesis and the bone, and wear on the articulating surfaces of the artificial joint.

8.2 Using Graded Cellular Structure in Prosthesis for Enhanced Stability

In this section, we use graded cellular structure in acetabular component for enhanced joint stability. Graded cellular structure could better strengthen the implant-bone interface, reduce the joint shock, and replace metal-on-polyethylene bearing with metal-on-metal bearing. Then, the design requirements of acetabular component for enhanced stability are identified.

8.2.1 Potential Advantages of Using Cellular Structure in Prosthesis

In the research presented in this case study, we design a new acetabular implant for hip replacement with graded cellular structure for enhanced stability of implant-bone interface. We could improve the design of joint prosthesis through changing its elasticity, porosity, interconnectivity, and wear resistance. There could be the following research opportunities: **using graded cellular structure** for better implant-bone fixation and shock reduction, **replacing metal-on-polyethylene bearing with metal-on-metal bearing** for less wear. Graded cellular structure can provide **adaptive and ordered porosity distribution.** Additive fabrication is capable to manufacture the entire acetabular component as a single part without assembly. The conventional acetabular component usually consists of polyethylene liner and metal shell as shown in Figure 8.1. Additive fabrication can build the single piece of acetabular component with varying architecture, porosity, and pore sizes of cellular structure.

The bone ingrowth adjacent to the porous implant can be greatly influenced by the chemical, mechanical and geometric characteristics of the porous coatings in uncemented prosthesis. Comparable elasticity to bone, higher porous interconnectivity, larger pore spaces, and perhaps improved surface bioactivity can significantly enhance bone growth into the gap region and into the porous coating (Jasty, Bragdon et al. 1997). The implant with comparable elasticity to the bone's elasticity has less damage on the neighboring tissue and higher fatigue resistance. Higher porous interconnectivity and larger pore spaces can improve the surface bioactivity with more breathability and enhance the prosthesis fixation through better bone ingrowth (Nancy Elftman 1998; Bragdon, Jasty et al. 2004).

Polyethylene liners are popularly used in hip replacement to reduce the shock. However, the wear debris of polyethylene is the major cause of osteolysis and aseptic mechanical loosening. The literature has demonstrated a positive correlation between the prevalence of osteolysis and the amount of polyethylene particles generated from the wearing of articulating surfaces (Chambers, Orishimo et al. 2004). Metal-on-metal bearing has wear rate that is 20 to 100 times lower than metal-on-polyethylene bearing. Metal wear particles are nanometers in linear dimension and much smaller and more numerous than the submicron polyethylene wear particles. Osteolysis seems to be relatively rare (Silva, Heisel et al. 2005). But metal-on-metal bearing may not have as good absorbability of shock and better stress distribution of ground force as metal-on-polyethylene bearing.

8.2.2 Formulating Design Requirements for Acetabular Component

In Figure 8.6, the author presents the design requirement list of an acetabular component for total hip replacement. These elaborated requirements represent the design objective, constraints, development demands and wishes. The objective is to

design an acetabular component for better stability than the existing designs, e.g., the acetabular component shown in Figure 8.1. The main goal is to reduce aseptic mechanical loosening by strengthening the implant-bone fixation and reducing the wear of the articulating surfaces. The design constraints include geometry, material, mechanical and biological properties, manufacturing and installation.

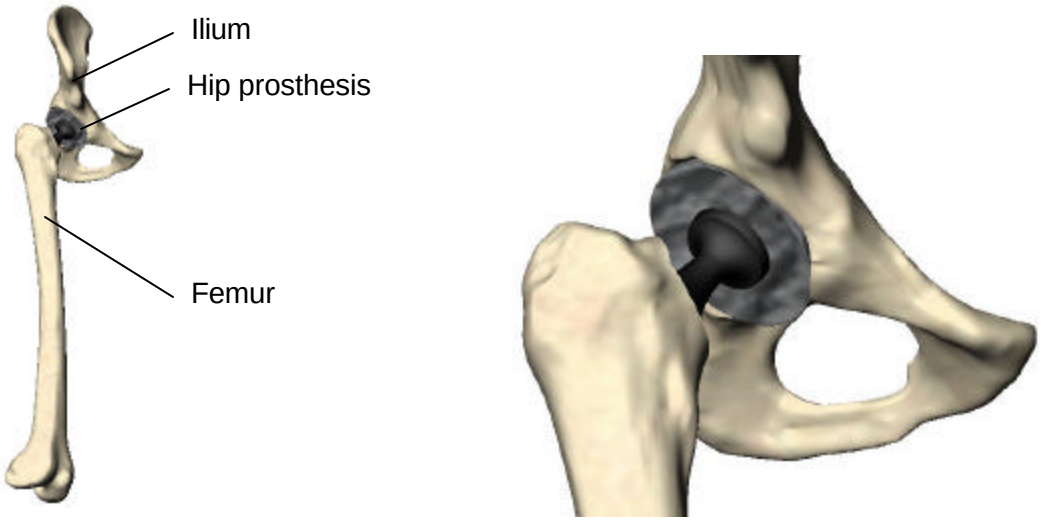

(a) Overall View (b) Close View

Figure 8.5 New Hip Prosthesis Using a Single-Piece Acetabular Component of Cellular Structure for Enhanced Stability

The CAD (IGES format) models of femur and ilium bones shown in Figure 8.5 were provided by Laboratorio di Tecnologia Medica, Istituti Ortopedici Rizzoli in Bologna, Italy, via Biomechanics European Lab (BEL) (Viceconti 2004). The NURBS surface models were derived from the CT data of a frozen cadaver with Raindrop Geomagic Studio. The CAD model of femoral component (Charnley prosthesis) was provided by Werner Schmoelz at Department of Trauma Surgery and Sports Medicine, Medical University of Innsbruck, Austria via BEL (Viceconti 2004). The femur and ilium were subtracted as the regular hip replacement surgery show in Figure 8.1. The acetabular and femoral components were inserted into the hip joint. According to the sizes of femoral component, femur and ilium measured from the given CAD models, the inner

radius and outer radius of acetabular component should be set as 13.89mm and 29.50mm. Its thickness is 15.61mm. Gaps between the implant and bone as small as 0.5mm were found to compromise bone growth into the implant. Thus, the total geometric tolerance (caused by design, manufacturing and installation) of the hemispheric implant should be no more than 0.5mm. The outer radius specification is 29.50±0.25mm. The inner surface of the liner should have very good smoothness and usually need to be polished since it is the articulating surface of the prosthesis.

Requirement List for Acetabular Component of Hip Replacement		Issued on: 10/11/2005
Problem Statement: Design a acetabular component for enhanced stability	Diseased hip joint geometry → Design → Highly stable acetabular component	
D/W	Requirements	
	1. Geometry	
D	1.1. Shape fitness (inner radius: 13.89mm; outer radius: 29.50mm; gap between implant and bone $< 0.5mm$)	
D	1.2. Cellular architecture (not discussed)	
W	1.3. Appropriate porosity ($\geq 40\%$ on implant-bone interface; solid on joint articulating interface)	
D	1.4. Pore size ($\geq 0.2mm$; avoid space collapse and best interconnectivity)	
	2. Mechanical properties	
D	2.1. Comparable elasticity to bone; graded change.	
D	2.2. Adequate strength ($\geq 500MPa$ on articulating surface)	
W	2.3. High fatigue resistance ($\geq 400MPa$ on articulating surface for 10 million cycles)	
W	2.4. Less wear and small debris	
	3. Biological properties	
D	3.1. Biocompatible with bone	
W	3.2. Less or no thrombophlebitis or infection	
	4. Manufacturability	
D	4.1. Manufacturable	
W	4.2. Less delivery time	
W	4.3. Lower cost	
	5. Installation	
W	5.1. Less or no assembly	

Figure 8.6 Requirement List of Designing Acetabular Component for Enhanced Stability

The interior region of ilium around acetabular component is spongy bone with average elasticity of 1GPa and yield strength of 5MPa. The exterior region of ilium is compact bone with average elasticity of 16GPa and yield strength of 175MPa. The elasticity of the implanted acetabular component is desired to change gradually from 1GPa at its boundary to match the elasticity of ilium (Maciel 2002; Sun, Starly et al. 2005).

8.2.3 Designing Acetabular Component with Cellular Structure

Figure 8.5 shows a computer model of the to-be-designed single-piece acetabular component and a femoral component assembled with the patient's femur and ilium. The acetabular component shown in gray is hemispherical, and would replace both polyethylene liner and metal shell shown in Figure 8.1. Its inner hemispheric surface of the liner section is the articulating surface with the spherical femoral head. The acetabular component exactly fits into the reamed acetabulum in a hemispherical shape. The new acetabular component would be mechanically fixed with screws in the same way as the regular hip prosthesis. The cellular structure in the acetabular component would biologically fix the implant to the bone via bone ingrowth to greatly enhance the fixation strength.

8.2.3.1 Material Selection and Manufacturing Process

Cellular structure, as a scaffold, can be used to increase the bone growth into the implant for better implant-bone fixation. The first design issue is the material selection. Osteoconductive materials including porous titanium guide bone ingrowth by providing cells with a microstructured scaffold that promotes sequential cell maturation. Biocompatible polymers and ceramics scaffolds, e.g., polyethylene, have been studied extensively for prosthesis components (Albrektsson and Johansson 2001). However, the mechanical properties of polymer scaffolds are insufficient to support bone growth under

loading conditions, while ceramic scaffold are too brittle. Fortunately, a few metal scaffolds, such as titanium and tantalum foam, can provide sufficient strength and fatigue resistance because they maintain sufficient mechanical strength and fatigue resistance over extended periods *in vivo* (St-Pierre, Gauthier et al. 2005). Porous titanium as well as porous metallic coating has been successful at encouraging bone ingrowth both *in vivo* and in clinical trials (LD, DE et al. 2001; Bragdon, Jasty et al. 2004). Moreover, titanium is excellently tolerated by our body tissues and popularly used for implant material. Table 8-1 shows the material properties of titanium alloy and stainless steel (Uhthoff, Bardos et al. 1981). Titanium alloy is much soft than stainless steel due to its low modulus of elasticity. Titanium has excellent fatigue and corrosion resistances. However, its known drawbacks of using titanium as a bearing include its poor resistance to wear, and notch sensitivity (Agins, Alcock et al. 1988). In our research, titanium alloy is selected as the material for cellular structure and solid liner of the acetabular component. Due to the poor wear resistance of titanium-based alloy (MK, SA et al. 1997), a layer of tantalum carbide coating (780±50nm thick and 53±4% carbon content) might be applied to the articulating surfaces to reduce the wear (Martinez, Wiklund et al. 2002). Tantalum carbide coating is a good candidate to use as protective hard coatings against wears in sliding applications (Martinez, Wiklund et al. 2002). The sliding wear resistance test on a conventional ball-on-disc test apparatus demonstrated that the friction coefficient of tantalum carbide (low carbon) coated surface can be as low as 0.15, which is comparable to the friction coefficient of untreated graphite, 0.14 (Kita, Fukushima et al. 2005).

Additive fabrication (AF) processes have the potential to manufacture the acetabular component including the porous structure and solid articulating liner section. Selective Laser Melting (SLM) is one of the possible processes to manufacture 3-D

porous metallic structures with a variety of material options, including stainless steel, titanium, and chromium-cobalt (2005; Kruth, Mercelis et al. 2005). The strut diameter of the cellular structure can be built as small as 0.1mm. Thus, the desired graded cellular titanium foam is feasible via additive fabrication. The outer surface of the liner section needs to be polished to an average roughness of 60nm for better smoothness and coated with a layer of tantalum carbide via vapor deposition (Martinez, Wiklund et al. 2002).

Table 8-1 Material Properties of Titanium Alloy and Stainless Steel

	Titanium Alloy Ti-6Al-4V	Stainless Steel 316L
Hardness	35 Rc	30 Rc
Yield Strength	900 MPa	790 MPa
Ultimate Tensile Strength	960 MPa	960 MPa
Modulus of Elasticity	110 GPA	200 GPa

8.2.3.2 Matching Elasticity with Graded Cellular Structure

The needs exist for a high porosity for helping bone ingrowth and adequate capability of withstanding physiological loads. However, the mechanical properties of the implant at the time of implantation should match that of the host tissue as closely as possible (Hutmacher 2000; Hutmacher 2001). Since the acetabular component is hosted by the spongy bone section of the acetabulum, the desired elasticity of exterior layer of cellular structure in the acetabular component is 1GPa.

We started the elasticity study with unit truss, the microstructure of the prosthesis. The elasticity of the implanted acetabular component is desired to change gradually from $E_0 = 1.0GPa$ at its boundary to $E_s = 110GPa$ of the solid titanium. We represent the equivalent elasticities with their average, E_{eff} given in Equation 8.1 according to Section 4.3. Thus, we have Equation 8.2 derived from Equation 8.1. To match the desired elasticity at the exterior surface, the effective elasticity E_{eff} needs to

be as close to $E_0 = 1.0GPa$, and the corresponding ratio between strut diameter and half-strut length would be $\frac{d}{L_h} = 0.1241$ by using Equation 8.2. The resulting slenderness ratio would be $SR = 32.2$, which is still a little bit less than the critical slenderness ratio of a single strut for buckling, $SR_{cr} = 34.73$, given by Table 4-1. The entire structure buckles after individual strut buckles. Therefore, yield would happen before buckling if the cellular structure comes to fail.

$$E_{eff} \approx 0.5904 \cdot E_s \left(\frac{d}{L_h} \right)^2 \tag{8.1}$$

$$\frac{d}{L_h} \approx \sqrt{\frac{E_{eff}}{0.5904 \cdot E_s}} \tag{8.2}$$

$$SR = \frac{L}{r} = 4\frac{L_h}{d}$$

where, (8.3)

L – Length of the entire strut

r – Radius of strut cross-section

The strut diameter linearly changes from $\frac{d}{L_h} = 0.1241$ at the exterior surface of the cellular structure to $\frac{d}{L_h} = 0.5773$ at the interior surface. The effective elasticity of the resulting cellular structure gradually changes from 1.0GPa to 21.68GPa shown as Figure 8.7.

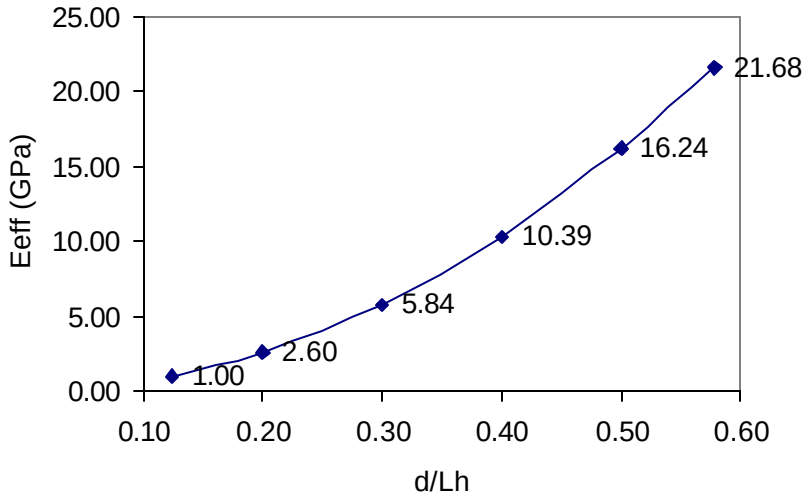

Figure 8.7 Effective Elasticity

8.2.3.3 Porosity of Graded Cellular Structure

A high degree of interconnected porosity can significantly help the bone ingrowth (St-Pierre, Gauthier et al. 2005). A porosity of 90% was recommended for optimum diffusive transport within a cell–scaffold construct under *in vitro* conditions (Hutmacher 2000). The advantage of a scaffold construct with a large surface area to volume ratio have been discussed and demonstrated (Hutmacher 2001). Figure 8.8 shows two unit trusses with different strut diameter in the representative volumes, which is a dodecahedron with 12 faces.

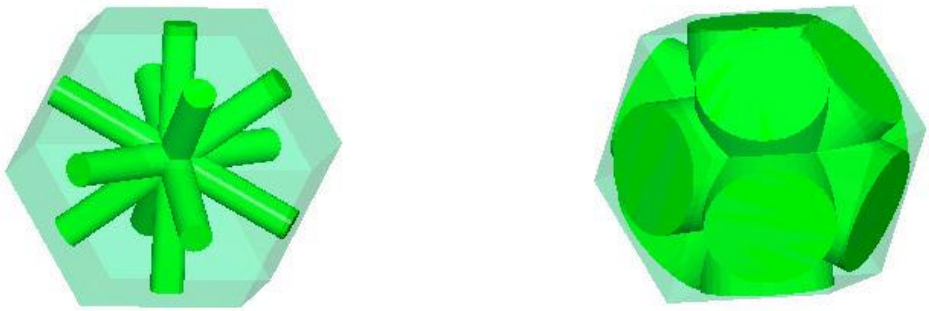

(a) $\frac{d}{L_h} = 0.1241,\ SR = 32.2$ (b) $\frac{d}{L_h} = 0.50,\ SR = 8.0$

Figure 8.8 Unit Truss in Representative Volume

The material volumes and surface area of the unit trusses with various strut diameters are measured from their solid models. The porosity and the surface/volume ratio decrease as the ratio of diameter/strut's half-length increases. When $\frac{d}{L_h} = 0.1241$, the porosity can reach as high as 91.17% and means that this section of cellular structure has excellent diffusive transporting capability. It approaches to 0% when $\frac{d}{L_h}$ is around 0.65. To avoid the material obtrusion out of the inner surface of the liner section, the strut diameter is restricted by the thickness of the liner section (skin of the cellular structure t_{inner}). For simplicity, $\frac{d}{2} \le t_{inner}$ is used and should be satisfied, whatever the pore size is. Thus, when the skin thickness is set as $t_{inner} = 3mm$, the strut diameter have $d \le 2t_{inner} = 6mm$, which is a pretty high limit. We might set $\frac{d}{L_h} = \frac{1}{\sqrt{3}} \approx 0.5773$ for the struts connected to the liner section, which is solid material. As discussed in Section 8.2.3.4, when $\frac{d}{L_h} = \frac{1}{\sqrt{3}}$, the cellular structure becomes close-cell, which is not desired for bone in-growth. Thus, the porosity of the designed graded cellular structure would gradually change from 91.17% to 10.13%. Surface/material volume ratio is proportional to the inverse of half strut length. Therefore, when evaluating the influence from strut diameter on surface/volume ratio, relative surface/volume ratio is used after multiplying surface/volume ratio with half strut length to avoid the effect of half strut length. The relative surface/volume ratio gradually decreases from 1.61 at the exterior surface to 0.35 at the inner surface as shown in Figure 8.10.

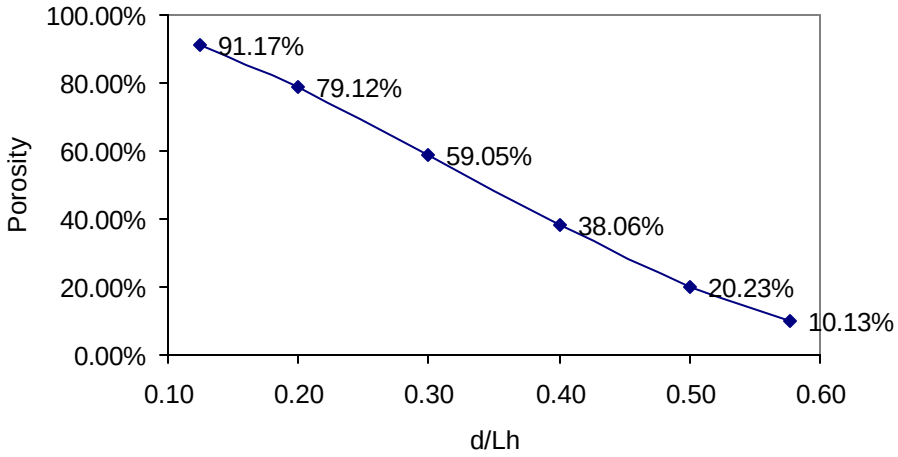

Figure 8.9 Porosity Decreases as Diameter Increases

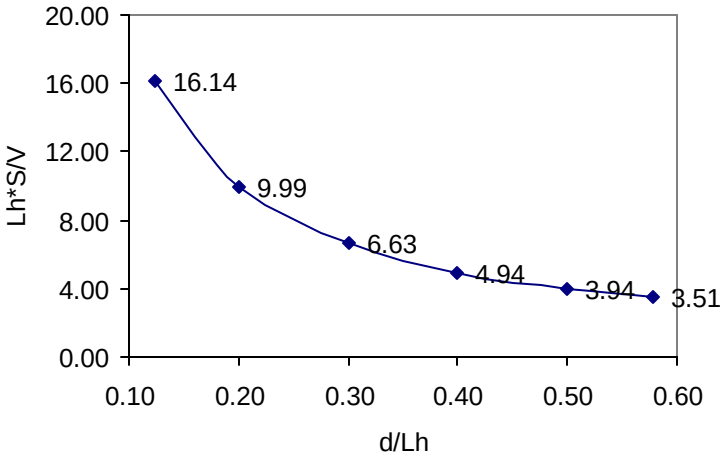

Figure 8.10 Surface/Material Volume Ratio Decreases as Diameter Increases

8.2.3.4 Pore Size of Graded Cellular Structure

Studies have been performed about the influence on tissue regeneration from the pore architectures and showed no significant difference in bone growth for 500 µm and 1,600 µm pores for PLGA scaffolds made by a 3D printing (Hollister 2005). Regarding the influence of the pore sizes of metallic foam, Brandon's studies on various metallic coatings of hip implants show that the total amount of bone ingrowth is not significantly different between the 200 and 450 µm pore sizes, but was significantly less for the 140

μm pore size (Bragdon, Jasty et al. 2004). Therefore, the optimal pore sizes for hip implant should be more than 200 μm as the lower limit. Unfortunately, little literature was found about the upper limit of pore sizes that do not create adverse effect on bone growth. The minimum feature size manufacturable by Selective Laser Melting can be as small as 100 μm (2005; Kruth, Mercelis et al. 2005). In our graded cellular structure of the designed acetabular component, the strut diameter starts from 100 μm at the outer surface of the cellular section. Therefore, to exactly match the spongy bone's elasticity $E_0 = 1.0GPa$, the half-strut length L_h should be 805.8 μm as given by Equation 8.4.

$$L_h = \frac{d}{0.1241} = \frac{100mm}{0.1241} = 805.8mm \qquad 8.4$$

The designed cellular structure must be open-cell. Otherwise, the bone cannot grow into the implant. When the strut diameter increases, the pore becomes smaller and finally the cellular structure becomes close-cell. For octet truss, whose primitive is tetrahedron, Equation 8.5 gives the largest opening size $L_{p_{\max}}$ of its triangular face as shown in Figure 8.11. The pore size is defined as the average opening size of its triangular face and given as Equation 8.6. To ensure valid open-cell cellular structure for bone ingrowth, the pore size must be larger than zero. Therefore, the strut diameter must satisfy $\frac{d}{L_h} \le \frac{2}{\sqrt{3}} \approx 1.155$. With $L_h = 805.8mm$ and $d = 100mm$ ($\frac{d}{L_h} = 0.1241$), the corresponding pore size is $L_p = 622.8mm$. With $L_h = 805.8mm$ and $d = 465.2mm$ ($\frac{d}{L_h} = 0.5773$), the corresponding pore size is $L_p = 348.9mm$.

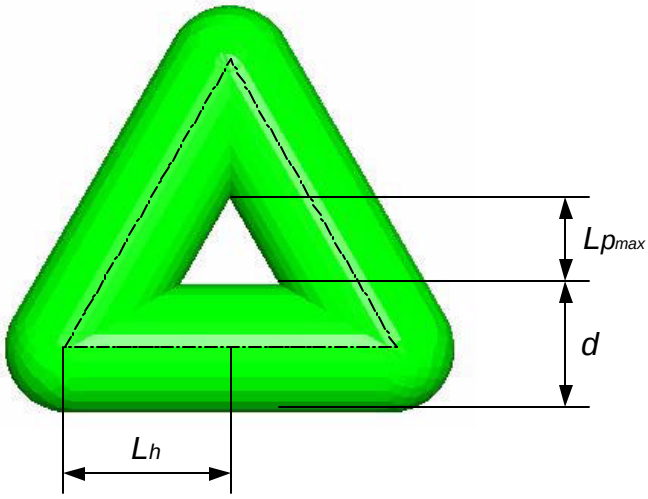

Figure 8.11 Pore Size of Octet Truss

$$L_{p_{\max}} = \begin{cases} \sqrt{3}L_h - \dfrac{3}{2}d, \text{when } L_h > \dfrac{\sqrt{3}}{2}d \\ 0, \qquad\qquad \text{when } L_h \le \dfrac{\sqrt{3}}{2}d \end{cases} \tag{8.5}$$

$$L_p = \frac{L_{p_{\max}}}{2} = \begin{cases} \dfrac{\sqrt{3}}{2}L_h - \dfrac{3d}{4}, \text{when } L_h > \dfrac{\sqrt{3}}{2}d \\ 0, \qquad\qquad \text{when } L_h \le \dfrac{\sqrt{3}}{2}d \end{cases} \tag{8.6}$$

1. Liner section in hemispherical shape
   1.1. Outer radius: $R_1 = 16.89mm$
   1.2. Inner radius: $R_2 = 13.89mm$
2. Cellular section in hemispherical shape
   2.1. Outer radius: $R_0 = 29.50mm$
   2.2. Inner radius: $R_1 = 16.89mm$
3. Cellular architecture: octet truss
   3.1. Average strut length: $L = 2L_h = 1.611mm$
   3.2. Strut diameter: gradually (linearly) increasing from $d = 100mm$ to $d = 465.2mm$

Figure 8.12 Geometric Specification of Graded Cellular Structure

8.2.3.5 Creating the Graded Cellular Structure

From the above studies, the geometric specifications of the graded cellular structures are summarized in Figure 8.12.

Conformal cellular topology was converted from finite element mesh by following the steps presented in Chapter 3. The resulting mesh and conformal topology are shown in Figure 8.13. There are 79978 struts and 15311 nodes in this cellular structure.

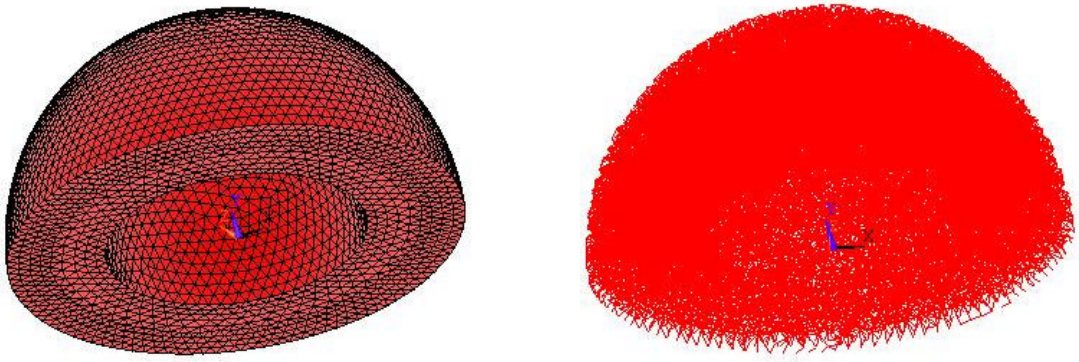

(a) FEM mesh (b) Conformal truss topology

Figure 8.13 Creating Conformal Truss Topology for Cellular Section

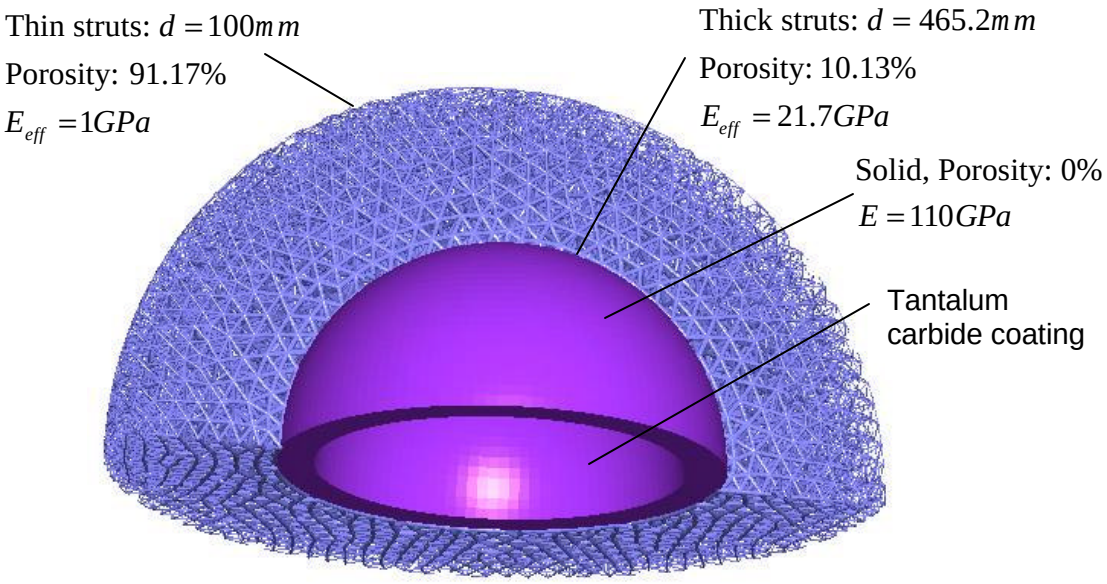

Figure 8.14 A Cross-Section View of the STL Model of the New Acetabular Component with Graded Cellular Structure

The strut diameters change linearly with the distance between the strut and hemisphere center, and increases from exterior surface to inner surface. The STL model was created by using TrussCreator and a cross-section view of the created acetabular

component with graded cellular structure and titanium liner is shown in Figure 8.14. The entire acetabular component is shown in Figure 8.15.

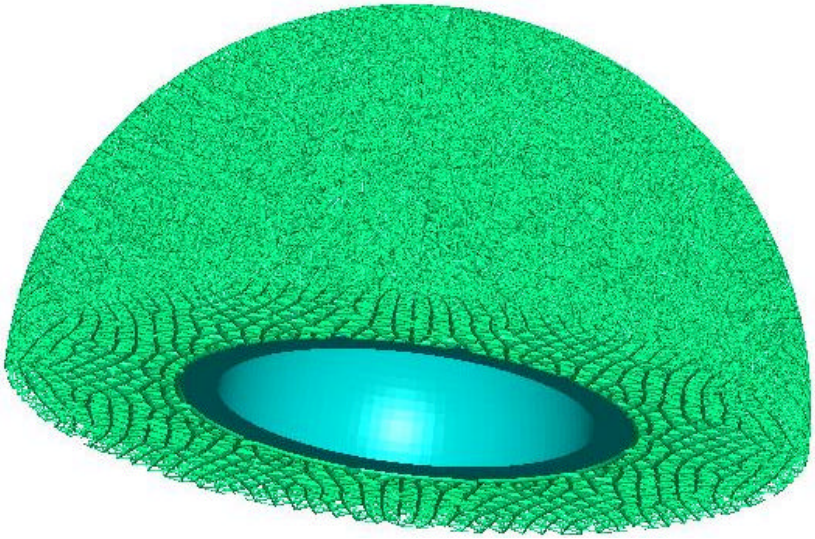

Figure 8.15 Look-through View of the Graded Cellular Section

8.2.3.6 Mechanics Analysis of the New Acetabular Component

The hip joint contact area and pressure distribution during activities of daily living vary from one movement and to another and are relatively complicated. Yoshida found that the peak pressure of moderate magnitude is located at the lateral roof of the acetabulum during fast, normal, and slow walking. The peak pressure is located at the edge of the posterior horn in standing up and sitting down, and knee bending as shown in Figure 8.16 (Yoshida, Faust et al. 2006). The peak pressure varies from 2.87MPa during slow walking to 9.36MPa during sitting down.

For simplicity, we apply a uniform pressure onto the acetabular cup (titanium liner), 1/12 of which is analyzed shown in Figure 8.17. The magnitude of the pressure on the inner surface is $8.40MPa$, which is close to the peak pressure during sitting down. The external surface is fixed in all 6 degrees of freedom. There are totally 1255 nodes attached to the inner surface (area $149.4mm^2$) and each node bears an equivalent 1.0N force along the radial direction of the hemispherical cup. The maximum deflection

among all nodes is $0.028mm$. The total strain energy stored in the cellular structure is $0.163N \cdot mm$. The effective elasticity of the cellular section in the radial direction is $3.81GPa$. The effective elasticity is $1.27GPa$ at the outer surface and $23.9GPa$ at the inner surface.

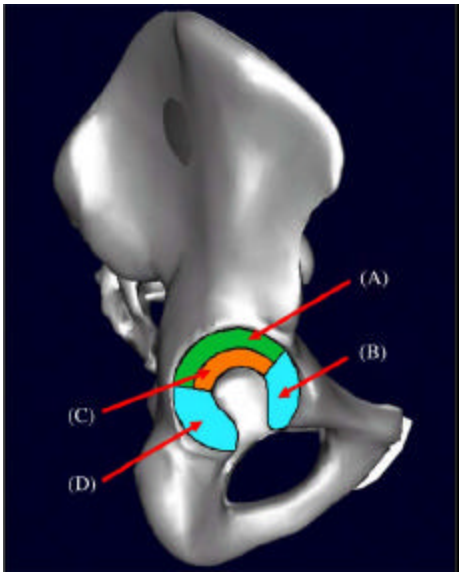

(A) Lateral roof, (B) anterior horn, (C) medial roof, (D) posterior horn.

Figure 8.16 Definition of Acetabulum Anatomic Regions

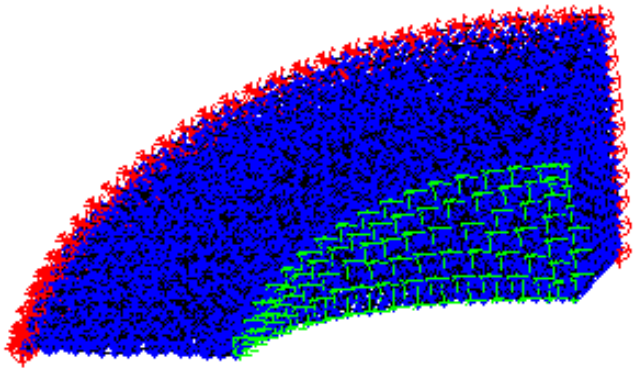

Figure 8.17 Mechanics Analysis on 1/12 of the New Acetabular Component

8.3 Critically Evaluating New Hip Prosthesis

The new design of acetabular component of hip prosthesis can be validated by evaluating the new design with the requirement list via analysis and discussion and comparing it to the existing designs. The critical evaluation is shown in Figure 8.18, where "+/-" (better/worse) means whether the new design is superior to the existing acetabular components. "0" means no improvement. All the demand requirements were well satisfied, and most of wish requirements were accommodated with improved results.

Due to the direct metal additive fabrication process, the fabricated part cannot reach very good accuracy due to such factors as shrink during material sintering/melting, and post-processing. Additive fabrication has the capability to manufacture various types of cellular architectures. In this case study, octet truss was used for cellular section of the acetabular prosthesis. However, other cellular architecture types, such as Kelvin foam, could be softer and better match elasticity with the bone. The interconnectivity of cellular structure is superior to the porous metal, which are spherical particles or diffused fibers. The elasticity of cellular structure is reconfigurable to match bone's elasticity, while the porous metal is uniform and determined by the manufacturing process and material. The new acetabular component has much better fatigue strength and significantly less wear since the metal-on-metal bearing replaces instead of metal-on-polyethylene bearing. Less assembly is required due to fewer parts. Little literature was found about the clinical trial results of the titanium alloy manufactured by SLM, and no tests was performed with the designed acetabular prosthesis. Therefore, the new design of acetabular component using graded cellular structure would superior to the existing designs.

D/W	Criteria	+/-	Comments: comparison with existing acetabular cup with porous coating
	1. Geometry		
D	1.1. Shape fitness (inner radius: 13.89mm; outer radius: 29.50mm; gap between implant and bone $< 0.5mm$)	-	Gap could be greatly influenced by the manufacturing (e.g. SLM), not as good as existing designs. But it could reach the requirement.
W	1.2. Cellular architecture	+	Type of architecture was not discussed in this research, however capable to provide various architectures. Existing designs have limitation from coating techniques.
W	1.3. Appropriate porosity ($\geq 40\%$ on implant-bone interface; solid on joint articulating interface)	+	90.17% at the implant-bone interface, solid in liner section. Superior to the existing porous coating.
D	1.4. Pore size ($\geq 0.2mm$; avoid space collapse and best interconnectivity)	+	Satisfied: average pore size 1.1mm at the implant-bone interface; good interconnectivity.
	2. Mechanical properties		
D	2.1. Comparable elasticity to bone; gradual change.	+	Satisfied: gradually from $E_0 = 1.0GPa$ to $E_s = 110GPa$
D	2.2. Adequate strength ($\geq 500MPa$ on articulating surface)	0	Satisfied: 900MPa in liner section.
W	2.3. High fatigue resistance ($\geq 400MPa$ on articulating surface for 10 million cycles)	+	700MPa in tantalum carbide coating(Niinomi 2003); 420MPa in solid titanium alloy.
W	2.4. Less wear and small debris	+	Tantalum carbide coating greatly reduces the friction and wear rate. Metal wear debris is in nano-scale.
	3. Biological properties		
D	3.1. Biocompatible with bone	0	Satisfied: perfect biocompatibility between titanium and tissue.
W	3.2. Less or no vein inflammation, infection		Not evaluated yet.
	4. Manufacturability		
D	4.1. Manufacturable	-	Satisfied: minimum manufacturable feature size can be 0.1mm by SLM
W	4.2. Less delivery time	0	A few days.
W	4.3. Lower cost	-	High cost of using rapid prototyping. But acceptable.
	5. Installation		
W	5.1. Less or no assembly	+	The regular polyethylene liner is removed. Less assembly required.

Figure 8.18 Critical evaluation on the designed acetabular component

8.4 Chapter Summary

This case study successfully use graded cellular structure in uncemented acetabular prosthesis for enhanced stability on implant-bone interface. The new acetabular component can match elasticity with the host bone and gradually changes from high porosity at the implant-bone interface to solid metal at the liner section. Other issues, such as material selection, manufacturing process, pore sizes, surface/volume ratio have been discussed.

In order to get closer to transfer this technology to clinical application, several unanswered questions related to implant design must still be addressed, such as architecture types (one of the morphology issue other than porosity and pore size), physical prototyping, part inspection method, and physical experiments for mechanical property analysis.

In this chapter, the hypothesis posed in Section 1.4 was empirically validated by testing its empirical performance validity (Shown in Figure 1.22) in this example study. A large-scale adaptive cellular structure by using unit truss via geometric modeling was successfully created for hip prosthesis to enhance stability. The mechanics analysis was performed on a section of designed adaptive cellular structure. The manufacturing limitations of using Selective Laser Melting for graded cellular structure were discussed and considered during the design stage.

CHAPTER 9

DESIGN SYNTHESIS OF COMPLIANT CELLULAR STRUCTURE FOR MORPHING WINGS

In this chapter, the hypothesis posed in Section 1.4 is empirically tested by using unit truss approach to design a compliant cellular structure for Variform morphing wing concept. This example study verifies and validates the empirical performance validity shown in Figure 1.22. The design synthesis method is used to design an airfoil with a reconfigurable shape, which can change from one type of geometry to another. The morphing wings can be used for wind tunnel tests, and even actual airfoil.

First, an overview of morphing wing technology is given, and a sample problem is provided. The design synthesis problem of the morphing wing is formulated. Then, the compliant mechanism for morphing wing is designed by using the developed design synthesis method of cellular structures. Finally, the resulting design is validated by testing its robustness and considering nonlinearity.

9.1 An Overview of Morphing Wings Technology

The aerodynamic performance of airfoil greatly depends on the airfoil geometry. The distribution of pressure over the airfoil is highly influenced by the airfoil geometry, including attack angle, chord length, camber height, and so on (Kroo 2005). The relation between the airfoil geometry and its performance is shown as Figure 9.1.

Most airplane wings are sufficiently rigid without much movement or twist during flight. For example, large aircraft wings designed for efficient high-speed flight

incorporate some form of rigid trailing edge flap and perhaps a rigid leading edge device such as a slat to achieve high aerodynamics performance. In Figure 9.2, the author shows a double-slotted flap and slat system, which is a 4-element airfoil (Kroo 2005). However, future airplanes may fly like birds with flexible wings, so-called, morphing wings. Morphing wings consist of a single piece of element with sophisticated structures that can reconfigure their geometries and adapt to changing flying conditions. These changes can affect the aerodynamics of the wing. A change in the geometry of the wing might be used to control flight, suppress flutter, reduce buffeting effects, and maximize fuel economy. Morphing wings might enable the design of multifunctional aircraft.

Figure 9.1 Relation between Airfoil Geometry and Performance

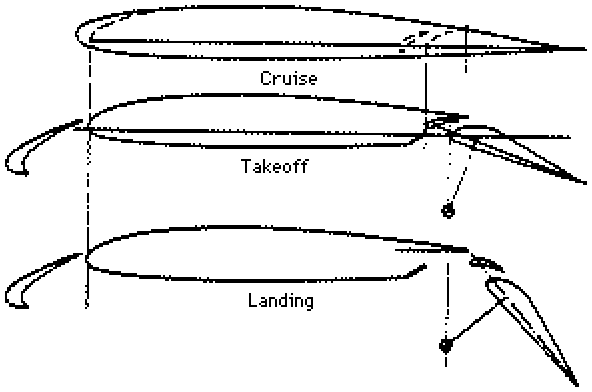

Figure 9.2 Double Slotted Flap and Slat Airfoil (Kroo 2005)

The DARPA Morphing Aircraft Structure program, when announced in 2002, stated goals to change the aircraft wing by 200% in aspect ratio, 50% in wing area, 50% in twist, and 20 degree change in wing sweep (2002; Wall 2002).

As its name implies a morphing wing changes shape from time to time. Many different mechanisms could potentially generate such a shape change. Quite a few

morphing wing designs utilize smart actuators and materials, such as lightweight piezo-composite and shape memory alloys (Martin, Redmond et al. 2000; Lim, Lee et al. 2005). However, most of those mechanisms are neither able to cause large scale effects, nor cost efficient (Lu and Kota 2003). Some researchers pioneered by using compliant mechanisms to realize shape morphing (Lu and Kota 2002; Lucato, McMeeking et al. 2005). Compliant mechanism changes shape through structural deformation, which is independent of the problem scale (Lu and Kota 2003).

9.2 Morphing Wing for AAI's Shadow UAV

In this chapter, a compliant mechanism is designed to realize the morphing wing using the design synthesis method of cellular structure. An example problem, morphing wing concept for AAI's Shadow shown in Figure 9.3 (2005), is proposed as a case study. AAI's Shadow is a small Unmanned Aerial Vehicle (UAV) for information collection (2005). The flight range and endurance of UAV are limited by the fuel storage capacity. It is greatly desired to increase the flight range and endurance without the addition of fuel.

Figure 9.3 AAI's Shadow 400 UAV System (2005)

During mission, as the fuel is burned, the total weight of the UAV decreases. Therefore, the wings' working condition changes, and a different airfoil shape would

probably better serve the aircraft. The airfoil geometry is desired to change and accommodate the changing working condition for high airfoil performance. Wings with adaptive shapes can minimize the mission drag and improve the fuel efficiency. In the AAI's Shadow example studied by Gano and Renaud, the wing cross-section morphs from NACA 23015 to FX60-126 as shown in Figure 9.4. NACA 23015 represented by large profile is bulky and has more capacity to store fuel as the starting cross-section. FX60-126 represented by the solid block is slender as the shape at the end of mission. The profile coordinates of NACA 23015 and FX60-126 airfoil cross-sections are shown in Table 9-1 and Table 9-2 respectively, which were obtained from UIUC airfoil data site (Selig 2005). The coordinated can be scaled uniformly. The chord lengths of both airfoils defined in these two tables are 300 mm.

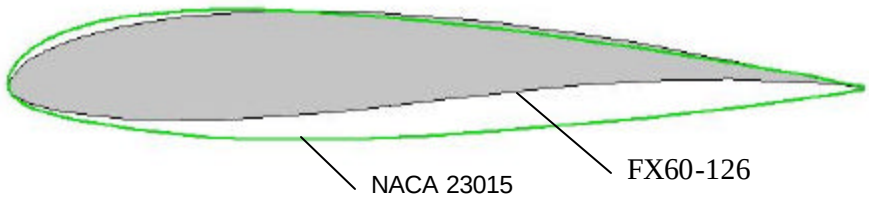

Figure 9.4 Airfoil Morphing from NACA 23015 to FX60-126

With the assumption of the linear fuel consumption over time and the constant propeller efficiency, Gano and Renaud computed the range and endurance for both variform and NACA 23015 airfoils (Gano and Renaud 2002). The variform airfoil linearly morph its shape from NACA 23015 to FX60-126, while the NACA 23015 airfoil stays static without shape change. Gano and Renaud concluded that the range of the variform wing was 22.3% further and the endurance was 22.0% longer than the initial static NACA 23015 airfoil (Gano and Renaud 2002). Thus, the morphing wing airfoil could have better performance than static airfoil. The morphing airfoils can provide better fuel efficiency to be able to fly farther.

Table 9-1 Profile Coordinates of Airfoil NACA 23015 (Unit: mm)

NO	x	y	NO	x	y	NO	x	y
1	300.000	0.000	18	70.113	27.157	35	94.285	-17.947
2	298.830	0.705	19	54.851	26.479	36	112.210	-17.925
3	295.320	1.395	20	40.388	24.934	37	130.730	-17.430
4	289.520	2.513	21	27.454	22.242	38	149.560	-16.535
5	281.530	4.016	22	16.594	18.435	39	168.400	-15.316
6	271.470	5.849	23	8.277	13.853	40	186.940	-13.852
7	259.500	7.950	24	2.749	8.982	41	204.900	-12.218
8	245.810	10.250	25	0.037	4.271	42	221.990	-10.486
9	230.620	12.679	26	0.894	-1.892	43	237.950	-8.722
10	214.160	15.164	27	4.267	-5.037	44	252.500	-6.989
11	196.690	17.629	28	9.525	-7.500	45	265.440	-5.350
12	178.490	19.993	29	16.456	-9.524	46	276.550	-3.864
13	159.840	22.170	30	24.971	-11.335	47	285.660	-2.589
14	141.040	24.069	31	35.148	-13.087	48	292.620	-1.578
15	122.370	25.599	32	46.869	-14.743	49	297.320	-0.877
16	104.140	26.671	33	61.354	-16.378	50	299.690	-0.518
17	86.630	27.210	34	77.243	-17.443	51	300.000	0.000

Table 9-2 Profile Coordinates of Airfoil FX60-126 (Unit: mm)

NO	x	y	NO	x	y	NO	x	y
1	300.000	0.000	21	48.333	23.295	41	60.545	-11.433
2	296.925	0.632	22	36.385	20.930	42	73.756	-11.244
3	289.126	2.267	23	25.430	18.017	43	87.100	-10.654
4	276.860	4.856	24	16.388	14.749	44	100.570	-9.702
5	263.237	7.719	25	9.903	11.588	45	114.195	-8.436
6	249.302	10.525	26	5.512	8.894	46	128.048	-6.934
7	235.532	13.216	27	3.268	6.647	47	142.110	-5.294
8	221.883	15.723	28	1.688	4.703	48	156.279	-3.601
9	208.284	18.006	29	0.705	3.014	49	170.379	-1.955
10	194.680	20.057	30	0.137	1.537	50	184.193	-0.453
11	181.057	21.872	31	0.000	0.000	51	197.909	0.828
12	167.394	23.454	32	0.352	-1.078	52	211.588	1.865
13	153.707	24.808	33	1.381	-2.273	53	225.205	2.641
14	140.079	25.910	34	2.997	-3.410	54	238.690	3.113
15	126.545	26.726	35	5.334	-4.618	55	252.047	3.224
16	113.110	27.211	36	8.871	-5.961	56	256.326	2.949
17	99.778	27.324	37	14.576	-7.498	57	278.271	2.289
18	86.585	27.034	38	23.504	-9.110	58	289.518	1.337
19	73.564	26.302	39	34.979	-10.414	59	296.939	0.452
20	60.780	25.072	40	47.541	-11.175	60	300.000	0.000

There could be various approaches to realize morphing wings. Gano and Renaud proposed to use fuel bladders, which interact with the structure of the wing as shown in Figure 9.5 (Gano and Renaud 2002). The shape changes of fuel bladders are used to drive the shape change of the wing airfoils. The fuel is stored in balloon-like bladders inside the wing structure. There could be a variety of fuel bladder configurations proposed. In Figure 9.5(A), symmetric bladder would be used. A non-symmetric bladder to achieve greater control of changing shape is shown in Figure 9.5(B). Multiple bladders of difference sizes and shapes are suggested as shown in Figure 9.5(C).

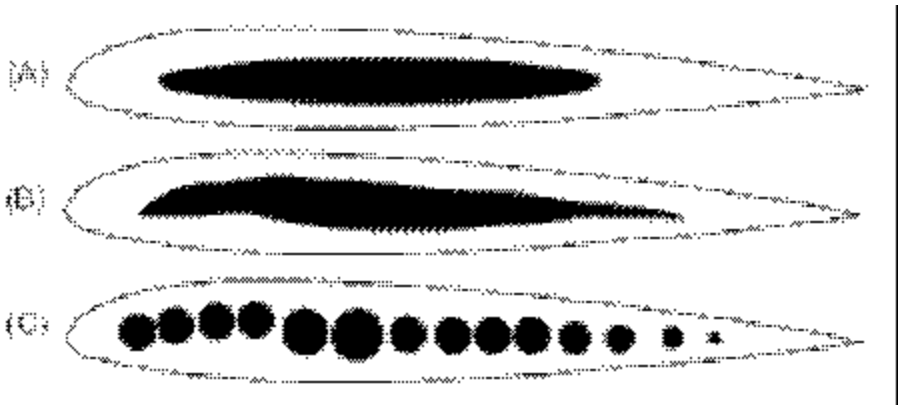

Figure 9.5 Possible Fuel Bladder Configurations (Gano and Renaud 2002)

Unfortunately, the feasible structure model and the appropriate materials of transforming the shape change of fuel bladders into the shape change of the airfoils have not been developed (Gano and Renaud 2002). This chapter focuses on the development of the structure for morphing wings. Fuel bladders or external forces might still drive and control the shape change of morphing airfoils. The allocations of these driving forces are assigned based on the structure from the design synthesis.

9.3 Preparing Design Synthesis of Compliant Mechanism for Variform Wing Concept

This section prepares the design synthesis of the compliant mechanism that enables the shape morphing from NACA 23015 to FX60-126 proposed in variform wing concept. The design constraints and the design objectives are briefly discussed. Then an initial topology is created for the design synthesis.

9.3.1 An Overview of Design Constraints and Objectives

Even though the attack angle of the airfoils changes during a mission, this change is not a shape change, but a rigid body rotation. The change of the attack angle can be realized by rotating the entire airfoil around the profile normal. Therefore, the relative positions of some specific points on the profile are assumed to be static or fixed in certain directions. For simplicity, the most left points of the profiles of both NACA 23015 and FX60-126 airfoils are coincident as shown in Figure 9.6. The most left point P_0 is fixed in both the x and y directions. The most right point P_1 is fixed in the y direction, and able to move along the x direction. Therefore, there are totally 3 constraints applied on the airfoil profile, which is fully constrained in the profile plane when considered as a rigid body. The upper and lower sections of the profile are pin-jointed with each other at points P_0 and P_1 during deformation.

The goal of the design synthesis is to design a compliant mechanism that can drive the airfoil shape to morph from the **source profile** (NACA 23015) into the **target profile** (FX60-126) under a specific loading condition. This compliant mechanism must fit in both profile shapes. The **actual deformed profile** shape is the shape of the source profile (NACA 23015) under deformation. The design objective is to approximate the actual profile shape to the target profile shape as close as possible.

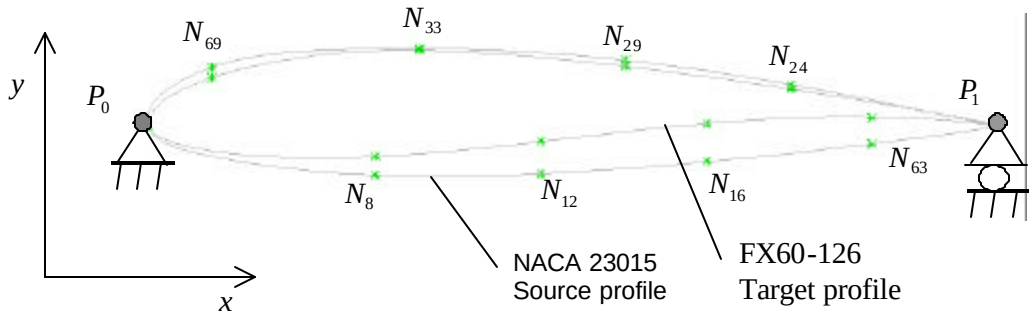

Figure 9.6 Known Boundary Condition and Sampling Points for Design Synthesis

9.3.2 Create Initial Topology for Design Synthesis

The design synthesis process starts with an initial topology, whose parameters are to be determined. A conformal topology is created using meshing approach presented in Chapter 3. Due to the curved geometry of the tested airfoil profile (NACA 23015), its curve coordinates given in Table 9-1 were imported into a CAD system, SolidWorks 2001, to create the profile's CAD model (IGS) shown in Figure 9.7. Then, the CAD model was imported into ANSYS and meshed with the use of rectangular element (PLANE42) as shown in Figure 9.8. Some nodes and elements of the resulting mesh model may be adjusted or merged manually to eliminate small mesh elements in order to reduce the element number.

Figure 9.7 CAD Model of NACA 23015 Airfoil Profile

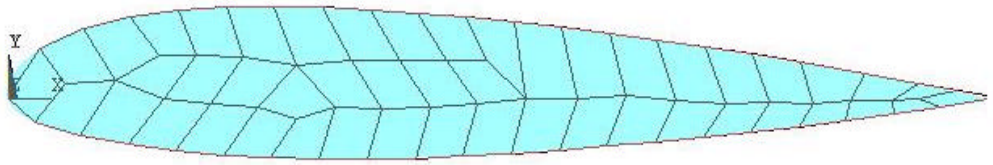

Figure 9.8 Meshing Profile Geometry in ANSYS

The resulting mesh from ANSYS was converted into the initial topology as the input for design synthesis using our developed software TrussCreator. In Figure 9.9, the author shows the resulting initial topology, which has totally 72 nodes and 117 struts. For the convenience for applying boundary constraints and loads, 2 separate nodes (N_1 and N_{72}) are created at point P_0. These 2 nodes are fixed in the x and y directions. N_1 is one node of strut 117 in the upper section, and N_{72} is one node of strut 1 in the lower section. Similarly, 2 nodes (N_2 and N_{71}) are created at point P_1. N_2 is for strut 95 in the lower section, and N_{71} is for strut 115 in the upper section.

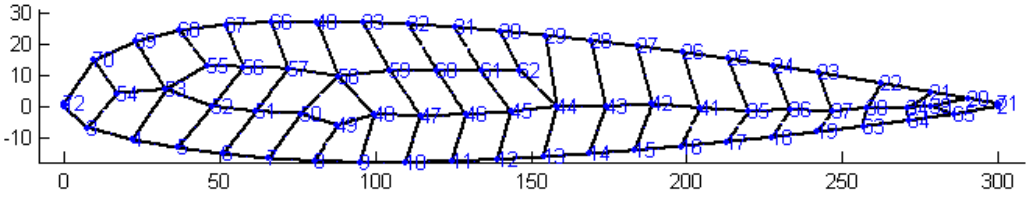

(A) Nodes of starting topology

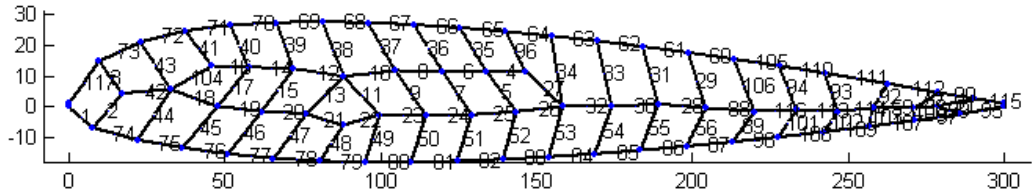

(B) Elements of starting topology

Figure 9.9 Initial Topology for Design Synthesis

9.4 Problem Formulation of Design Synthesis

This section mathematically presents the design variables, the design objective, and the problem formulation of the design synthesis.

9.4.1 Design Variables

The sizes of totally 117 struts in the initial topology are the design variables for design synthesis. This structure has uniform thickness in the normal direction of the airfoil profile. As a 2-D design problem, the strut cross-section is rectangular and the strut thickness is given as $5.0mm$. The strut widths are variables, and each of them is considered as one design variable. Additive fabrication is used to manufacture this compliant mechanism. The widths of both interior and exterior struts in the initial topology shown in Figure 9.9 must satisfy $x_i \in \left\{0, \left[x_{0^+}, x_{\max}\right]\right\}$, where $x_{0^+} = 0.7mm$ and $x_{\max} = 8.0mm$. Zero width means disappearing struts. However, zero width is replaced with a very small value, such as $x_{0^+} = 2.5e-4mm$, to avoid the singularity in the stiffness matrix. From our previous experience of design synthesis for compliant mechanisms, most of the strut widths are either very close to 0 or larger than x_{0^+}. Therefore, x_{0^+} can be set as $x_{0^+} = 2.5e-4mm$. During the post process, the struts with a width between $2.5e-4mm$ and $0.7mm$ are rounded to the closer value. Few struts' widths fall between these two values. To retain the boundary struts during design synthesis, their widths have $x_j \in \left[x_{b\min}, x_{\max}\right]$, where $x_{\max} = 8.0mm$. Therefore, the bounds of the design variables are set as Equations 9.1 and 9.2. i indicates the strut ID.

Interior struts:

$$x_i \in \left[x_{0^+}, x_{\max}\right], x_{0^+} = 2.5e-4mm, x_{\max} = 8.0mm \qquad 9.1$$
$$i = 2\sim59, 88, 89, 91\sim94, 99\sim104, 106, 113, 114, 116$$

Boundary struts:

$$x_j \in [\, x_{b\min},\, x_{\max} \,], x_{b\min} = 5.0mm, x_{\max} = 8.0mm \qquad 9.2$$
$$j = 1,60\sim87,90,95,97,98,105,107\sim112,115,117$$

9.4.2 Design Objectives

In order to mathematically represent the profile geometries for design synthesis, totally 8 discrete points, $N_k(k = 8,12,16,24,29,33,63,69)$, are sampled from the profile as shown in Figure 9.6. For simplicity, these sampled points are picked from the nodes in the initial topology. Each of upper and lower sections of the profiles is represented by 4 points besides P_0 and P_1. For better representation accuracy, more points can be sampled from the profile. The design objective is to minimize the position deviations of these sampled points on the actual deformed profile shape and the target profile shape. Due to the relative small deflection in the x direction, only the deflections in the y direction are measured. The desired deflections are measured from the corresponding points in NACA 23015 and FX60-126 airfoil profiles, and given as Equation 9.3.

Desired Deflections:

$$d_{8_{\text{target}}} = 6.58, d_{12_{\text{target}}} = 11.4, d_{16_{\text{target}}} = 13.7, d_{24_{\text{target}}} = 1.56 \qquad 9.3$$
$$d_{28_{\text{target}}} = 2.14, d_{33_{\text{target}}} = 0.0, d_{63_{\text{target}}} = 9.43, d_{69_{\text{target}}} = -3.65$$

The design objective for design synthesis consists of two parts. The first part is the normalized mean squared deviation $(\text{mean}(SD_k))_{norm}$ among all sampled nodes $N_k(k = 8,12,16,24,29,33,63,69)$. $\text{mean}(SD_k)$ is a statistical indicator to measure the closeness between the actual deformed profile and the target profile. As shown in Equation 9.4, the squared deviations are defined as the squared values of the differences between the actual deflections $d_{k_{\text{actual}}}$ and the target deflections $d_{k_{\text{target}}}$ on the measured nodes. $(\text{mean}(SD_k))_{norm}$ is the normalized value, which is the ratio between

$\text{mean}(SD_k)$ and the mean squared deviation of a "good" design before synthesis, $\text{mean}(SD_k)_{NoSyn}$, as shown in Equation 9.5. Certainly, $\text{mean}(SD_k)_{NoSyn}$ is not necessarily a precise value, but an estimated value. For this particular problem, $\text{mean}(SD_k)_{NoSyn}$ is set as 60.0. The other part in the design objective represents the goal to minimize the total volume of the structure. This goal does not contribute to minimize the deviations, but it can clean up the redundant material from the resulting structure. A normalized volume V_{norm}, the ratio between the volume of the current structure and that of the first run in the search process as shown in Equation 9.6, is used as the second part in the design objective. The contribution of the second part is much smaller than the mean squared deviation. It noticeably contributes to the design objective at a later stage of the search process for design synthesis. These two parts are compromised in the design objective. Their weights are given as $w_d = 60.0$, $w_v = 5.0$, which are decided by importance. These two weights may not be normalized since only the ratio between these two weights can influence search results. $w_d / w_v = 12.0$ tells that the mean squared deviation is much more influential than the volume on the design objective. The mean squared deviation is dominant at the early stage during the search process.

Squared Deviation: $SD_k = (d_{k_{\text{actual}}} - d_{k_{\text{target}}})^2$ 9.4

Normalized Mean Squared Deviation: $(\text{mean}(SD_k))_{norm} = \dfrac{\text{mean}(SD_k)}{\text{mean}(SD_k)_{NoSyn}}$ 9.5

Normalized volume: $V_{norm} = \dfrac{V_{total}}{V_{FirstRun}}$ 9.6

9.4.3 Problem Formulation

The problem formulation of the design synthesis for variform wing is shown in Figure 9.10. The design variables are the widths of the struts in the initial topology shown in Figure 9.9. The design objective is to minimize the compromised objective value of mean squared deviation, and the normalized volume.

Find: $x = \{x_1, x_2, \cdots, x_n\}$ Widths of lattice struts

Satisfy: Bounds:

interior struts – $x_i \in \left[x_{0^+}, x_{\max}\right]$

boundary struts – $x_j \in \left[x_{b\min}, x_{\max}\right]$

where, $x_{0^+} = 2.5e-4, x_{b\min} = 5.0, x_{\max} = 8.00$

$i = 2\sim59,88,89,91\sim94,99\sim104,106,113,114,116$

$j = 1,60\sim87,90,95,97,98,105,107\sim112,115,117$

Minimize: $f(x) = \underbrace{w_d \times (\text{mean}(SD_k))_{norm}}_{\text{mean squared deviation}} + \underbrace{w_v \times V_{norm}}_{\text{volume reduction}}$

where, $w_d = 60.0$, $w_v = 5.0$

$k = 8,12,16,24,29,33,63,69$

Figure 9.10 Problem Formulation of Compliant Mechanism for Variform Wing

9.5 Design Synthesis

Load condition is critical for this design synthesis problem. In this section, the author performs design synthesis with different load conditions. The load condition with 5 pairs of concentrated forces is proposed for the design synthesis. Then the design synthesis process is discussed and the result is presented. Due to the demand of high computational resource, only linear deformation is considered during the design synthesis. Nonlinear deformation analysis is used to verify the synthesis result from the design synthesis with linear deformation analysis.

9.5.1 Trials with Different Load Conditions

The external load condition has not been defined for this design synthesis problem. It is difficult to define due to the characteristics of the geometry. The upper section and the lower section of the airfoil profile are too close, so that the deformation cannot sufficiently propagate in such a short region. However, in the design objective, the deformation needs to propagate in both the x direction and the y direction. One load cannot give a good synthesis result. It can be seen from the following trials.

In Figure 9.11, the author shows the deformation result of the first trial that the structure is under a concentrated rotating moment, $M_{45} = 3000N \cdot mm$, at an interior node, N_{45}. The structure struts have uniform widths, $x_i = 3.0mm$ $(i = 1,2,...,117)$. The moment is perpendicular to the airfoil profile plane. Figure 9.12 shows the structure resulting from design synthesis, and its objective function value, $f(x) = 28.07$, does not represent a good result.

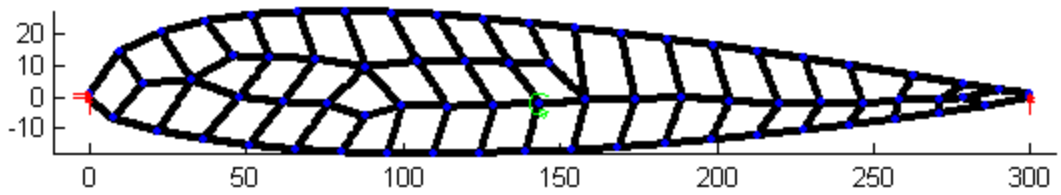

$f(x) = 66.43:\ \text{mean}(SD_k) = 65.35,\ V_{norm} = 0.2157$

Figure 9.11 Deformed Structure with 1 Concentrated Torsion before Synthesis

As a second trial shown in Figure 9.13, the same structure of uniform strut widths is deformed under 3 concentrated forces on 3 nodes. The forces are in the y direction and set as $F_{36} = 150N$, $F_{44} = 100N$, $F_{36} = -150N$. In Figure 9.14, the author shows the synthesis result, which has an objective function value, $f(x) = 19.14$ and is better than the first trial.

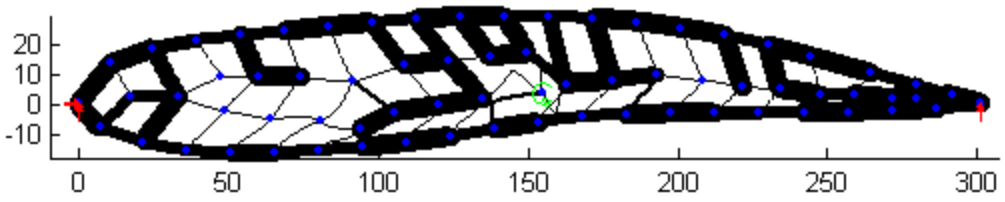

$f(x) = 28.07:\ \text{mean}(SD_k) = 26.51,\ V_{norm} = 0.3144$

Figure 9.12 Deformed Structure with 1 Concentrated Torsion after Synthesis

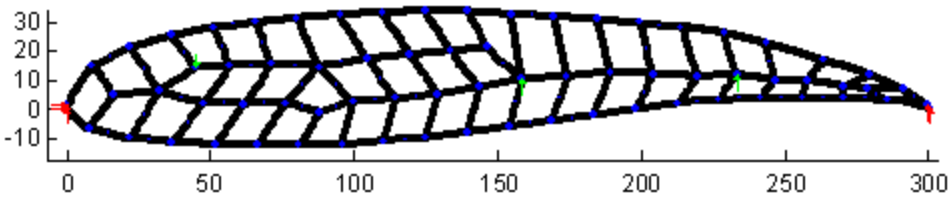

$f(x) = 35.73:\ \text{mean}(SD_k) = 34.66,\ V_{norm} = 0.2157$

Figure 9.13 Deformed Structure with 3 Concentrated Forces before Synthesis

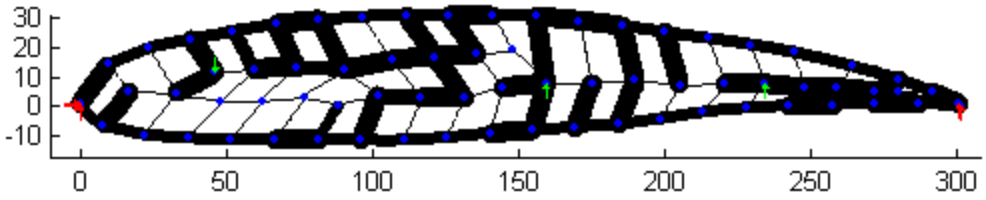

$f(x) = 19.14:\ \text{mean}(SD_k) = 17.64,\ V_{norm} = 0.3012$

Figure 9.14 Deformed Structure with 3 Concentrated Forces after Synthesis

In the third trial, to better propagate the deformation within the structure, 5 pairs of equal opposite forces are applied at the following nodes: N_4 and N_{69}, N_8 and N_{40}, N_{12} and N_{30}, N_{16} and N_{26}, N_{19} and N_{23}. The forces on these 5 pairs of nodes are all set as $F_{pair} = 21N$ in magnitude, but each pair of forces are in opposite directions. The deformation shape is shown as Figure 9.15. The synthesis result of the structure under 5 pairs of opposite forces is shown in Figure 9.16. The objective function value, $f(x) = 4.367$, is significantly less than the above two trials.

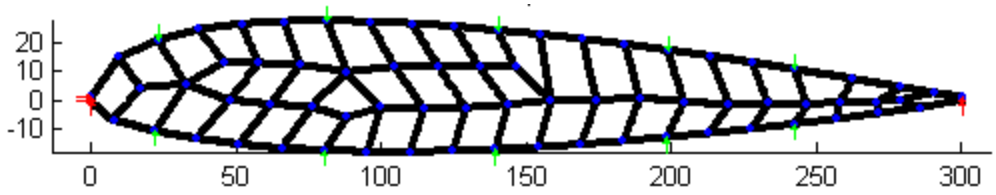

$f(x) = 59.93 :\ \text{mean}(SD_k) = 58.85\ ,\ V_{norm} = 0.2157$

Figure 9.15 Deformed Structure with 5 Pairs of Opposite Forces before Synthesis

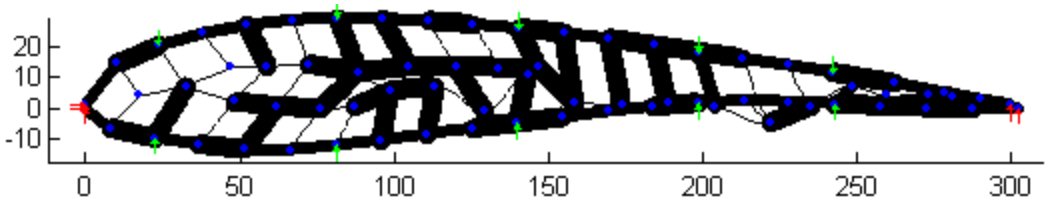

$f(x) = 4.367 :\ \text{mean}(SD_k) = 2.854\ ,\ V_{norm} = 0.3027$

Figure 9.16 Deformed Structure with 5 Pairs of Opposite Forces after Synthesis

9.5.2 Design Synthesis Process

The Particle Swarm Optimization (PSO) search algorithm is used for design synthesis to search for a superior solution (Kennedy and Eberhart 1995). The design synthesis problem for variform airfoil concept has 117 design variables and 2 weighted design objectives. It is constrained by bounds of design variables. The parameters of PSO are set as Figure 9.17. Totally 10 runs were performed with 38300 evaluations of the objective function for 4.81 hours of CPU time. Each evaluation of the objective function takes about 0.612 seconds. The experiment computer has Intel P4 2.4GHz CPU and 512MB RAM.

The final objective function value of each PSO run is listed in Table 9-3. The average value is 12.18, which is better than the other two trials with different load conditions. The best run (the 3rd run) has the objective function value, $f(x) = 4.37$, and its deformed shape is shown in Figure 9.16.

$f_{goal} = 0.0$ - Target value to achieve

$N_{iter} = 150$ - Number of iterations

$w_{start} = 0.95$ - Start velocity inertia

$w_{end} = 0.40$ - End velocity inertia

$j_1 = 2.0$ - Cognition learning factor

$j_2 = 1.25$ - Social learning factor

$e_{obj} = 0.01$ - Tolerance of objective function

$e_{\text{var}} = 0.001$ - Tolerance of Design Variable

$$x_{i_{\min}} = \begin{cases} 2.5e-4, i \in \{2\sim59,88,89,91\sim94,99\sim104,106,113,114,116\} \\ 5.0, i \in \{1,60\sim87,90,95,97,98,105,107\sim112,115,117\} \end{cases}$$

- Lower bound of Design Variable

$x_{\max} = 8.0$ - Upper bound of Design Variable

$N_D = 117$ - Number of Design Variable

$N_P = 20$ - Number of particles (swarm size)

$v_{i_{\max}} = x_{\max} - x_{i_{\min}}$ - Maximum moving velocity

$N_{iter} = 150$ - Maximum number of iterations

Figure 9.17 Parameter Setting for Design Synthesis

Table 9-3 Objective Function of PSO Results

Run NO.	1	2	3	4	5	6	7	8	9	10	Average
f(x)	10.71	13.25	4.37	11.00	21.34	10.75	10.41	9.96	9.65	20.39	12.18

A topology cleaning process is performed on the resulting synthesized topology by removing “zero-width” struts, of which the widths are close to 0.00025. During the cleaning process, the dangling elements should be removed as well. The cleaned structure has 68 struts and 60 nodes as shown in Figure 9.18 (A) and (B). After cleaning, the objective function value $f(x) = 5.012$ is a little larger than that before cleaning. It is caused by the removed struts that contribute to the structure’s stiffness even if their widths are relatively small. However, this does not extensively influence our design synthesis result.

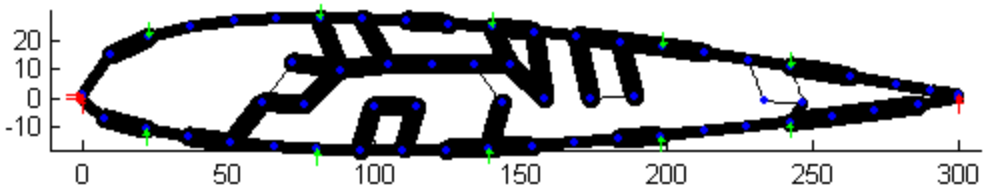

(A) Before Deformation

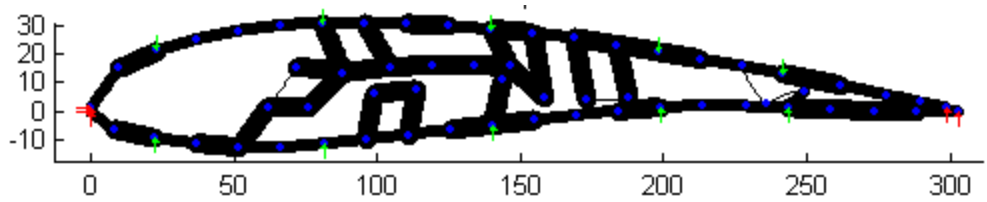

$f(x) = 5.012 : \text{mean}(SD_k) = 3.690 , V_{norm} = 0.2643$

(B) After Deformation

Figure 9.18 Cleaning Topology by Removing Zero-width Struts

In Table 9-4, the author shows the deflection deviations of the sampled nodes between the actual profile and the target profile. The deflection deviations of the sampled nodes are significantly improved if compared to those before design synthesis.

Table 9-4 Deviations between Actual and Target Deflections of Sampled Nodes

	Node ID	8	12	16	24	28	33	63	69
	Target	6.580	11.400	13.700	1.560	2.140	0.000	9.430	-3.650
Before synthesized	Actual	-6.397	-11.360	-13.759	-1.686	-2.250	-0.020	-9.427	3.645
	Deviation	-12.977	-22.760	-27.459	-3.246	-4.390	-0.020	-18.857	7.295
After synthesized	Actual	5.226	11.515	13.532	1.250	3.125	3.031	6.848	0.225
	Deviation	-1.354	0.115	-0.168	-0.311	0.985	3.031	-2.582	3.875

9.5.3 Refining Load Condition

As shown in Table 9-4, the deflection deviations of Nodes 33, 63, and 69 are relatively larger than those of the other sampled nodes. The deflection deviations can be reduced through running another sub design synthesis to find the most appropriate force magnitudes. In Figure 9.19, the author shows the problem formulation of the design synthesis to search for the magnitudes of paired forces. The design variables are the magnitudes of 5 pairs of forces shown in Figure 9.18. The sub search process has the same design objective as the design synthesis to find the appropriate strut widths, which

is to minimize the compromised objective value of mean squared deviation and the normalized volume.

Find: $F = \{F_{p1}, F_{p2}, F_{p3}, F_{p4}, F_{p5}\}$

F_{p1} - Magnitude of paired forces on N_4 , N_{69}

F_{p2} - Magnitude of paired forces on N_8 , N_{40}

F_{p3} - Magnitude of paired forces on N_{12} , N_{30}

F_{p4} - Magnitude of paired forces on N_{16} , N_{26}

F_{p5} - Magnitude of paired forces on N_{19} , N_{23}

Satisfy: Bounds: $F_{pi} \in \left[F_{p_{\min}}, F_{p_{\max}} \right], i = 1,2,3,4,5$

where, $F_{p_{\min}} = 0.0, F_{p_{\max}} = 200.0$

Minimize: $f(x) = \underbrace{w_d \times (\text{mean}(SD_k))_{norm}}_{\text{mean squared deviation}} + \underbrace{w_v \times V_{norm}}_{\text{volume reduction}}$

where, $w_d = 60.0 \quad w_v = 5.0$,

$k = 8,12,16,24,29,33,63,69$

Figure 9.19 Problem Formulation of Searching for Appropriate Magnitudes of Paired Forces

This design synthesis problem has only 5 design variables and can be solved by using a small-scale search algorithm. Sequential quadratic programming (SQP) method provided by Matlab is applied to search for the superior solution (Fletcher and Powell 1963; Reklaitis, Ravindran et al. 1983). The search process took 53 seconds of CPU time to get convergence on a computer with Intel P4 2.4GHz CPU and 512MB RAM. The resulting paired force magnitudes are shown as Equation 9.7. The resulting objective function value is $f(x) = 3.668$, which is slightly better than the uniform force magnitude on all the applied nodes.

$$F_{p1} = 108.35,\ F_{p2} = 37.00,\ F_{p3} = 9.40,\ F_{p4} = 39.16,\ F_{p5} = 4.68 \qquad 9.7$$

9.6 Critically Evaluating the New Morphing Airfoil

This section discusses the robustness of the obtained result against the variations of the load condition and the strut widths. Then, it presents the difference of the structure's performances with linear and nonlinear deformation analyses.

9.6.1 Robustness Analysis

In Figure 9.20, the author shows that the objective function reliably changes against the variations of the load condition, which could be caused by the operating environment. When the force magnitude changes around the designated value, $F_{pair} = 21N$, by 4.76%, the objective function changes by 2.63%, which means a relatively small change.

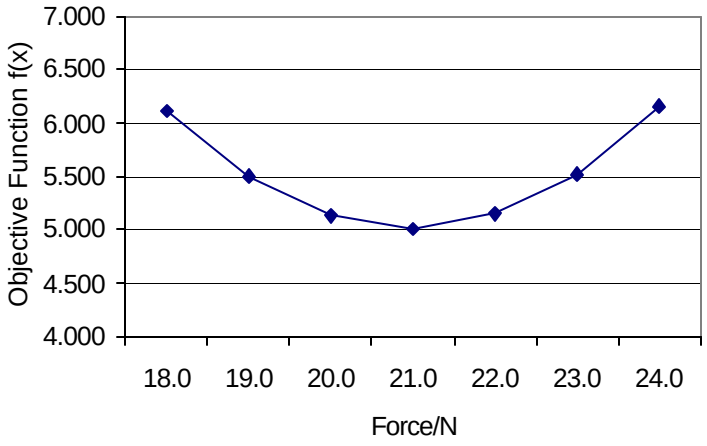

Force/N	18.0	19.0	20.0	21.0	22.0	23.0	24.0
f(x)	6.116	5.498	5.129	5.012	5.144	5.528	6.162

Figure 9.20 Objective Function Changes against Load Condition Variations

The variations of design variables could be mainly caused by the manufacturing process. The variations of the thin struts can incur large changes in the objective function as shown in Figure 9.21. The variation of the thin struts width by 0.05mm can cause 200% change in the objective function. As shown in Figure 9.22, the variations of

the thick struts do not influence the objective function much. When the width of the thick struts changes by 0.1 mm, the objective function changes about 4.37%. Thus, the variations of the thick struts are not critical to the mechanism's performance, while the variations of the thin struts are very influential. It can be an issue for future research.

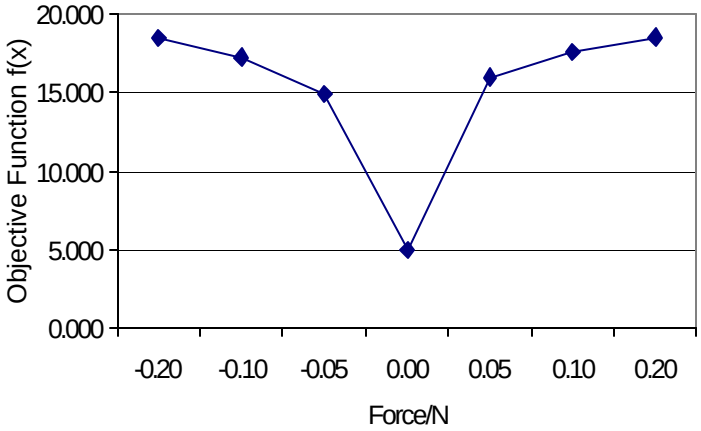

Width Deviation	-0.20	-0.10	-0.05	0.00	0.05	0.10	0.20
f(x)	18.431	17.259	14.929	5.012	15.986	17.555	18.506

Figure 9.21 Objective Function Changes against Width Variations of Thin Struts

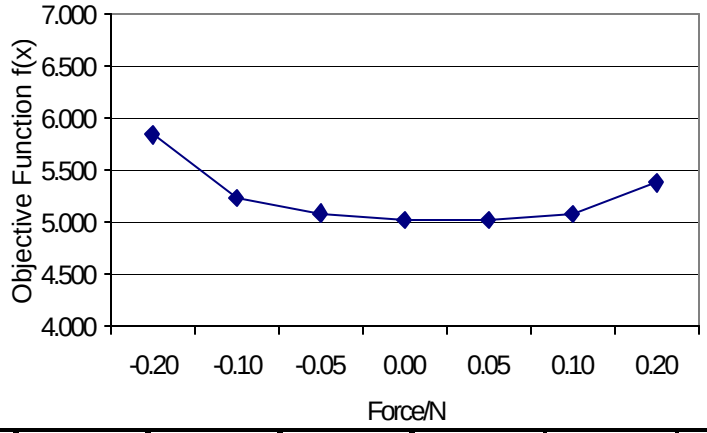

Width Deviation	-0.20	-0.10	-0.05	0.00	0.05	0.10	0.20
f(x)	5.837	5.231	5.081	5.012	5.014	5.080	5.375

Figure 9.22 Objective Function Changes against Width Variations of Thick Struts

9.6.2 Nonlinear Deformation

In Figure 9.23, the author shows that the objective function changes under nonlinear deformation caused by geometry nonlinearity. The tangent stiffness method

discussed in Chapter 4 is used for the nonlinear deformation analysis with 10 steps of linear analysis (Marsden and Hughes 1983). The nonlinear deformation analysis could be considered during design synthesis. However, the total computation time would be scaled up by the number of steps since only one step is used during linear deformation analysis. When the force is maintained as $F_{pair} = 21N$, the objective function is $f(x) = 16.059$, which is much larger than that under linear deformation. The deformation shape shows that the structure is over-deformed. According to the chart shown in Figure 9.23, the objective function reaches the minimum $f(x) = 5.548$ when $F_{pair} = 16N$. The geometric nonlinearity makes the structure softer under large deformation. The resulting design is reliable against the variations of the loads as well. $F_{pair} = 16N$ is proposed for the magnitude of the 5 pairs of nodal forces when considering geometric nonlinearity.

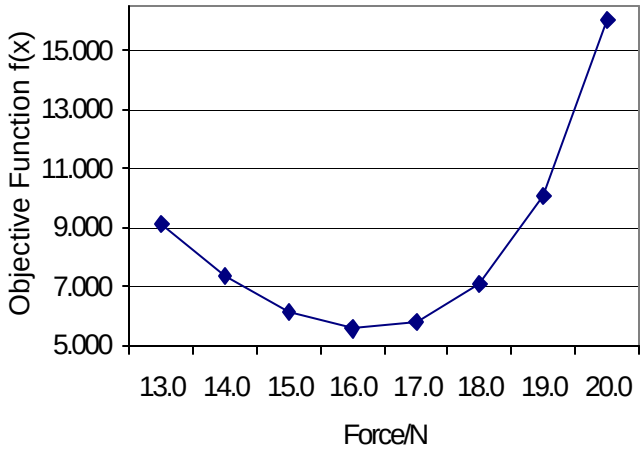

Force/N	13.0	14.0	15.0	16.0	17.0	18.0	19.0	20.0
f(x)	9.100	7.347	6.126	5.548	5.779	7.089	10.041	16.059

Figure 9.23 Variations under Nonlinear Deformation

9.7 Chapter Summary

This chapter successfully utilized the proposed design synthesis method to design a compliant structure for variform morphing wing concept of AAI's Shadow UAV.

Various load conditions were discussed and a suitable load form was suggested. The load magnitudes can be refined with a sub design synthesis to find the more suitable magnitudes. As one of the future work, the load conditions should be considered as design variables during the design synthesis, instead of a follow-up refining process.

The robustness of the resulting design was tested and the nonlinear deformation was considered. The design objective function is relatively not sensitive to the variations caused by the external load magnitudes or the widths of the thick struts. However, it is sensitive to the variations incurred by the widths of thin struts. In the future work, the sensitivity of the design variables needs to be considered during design synthesis. The robust design methodology could be applied (Chen, Allen et al. 1996; Seepersad, Allen et al. 2003; Seepersad 2004).

In this chapter, the hypothesis posed in Section 1.4 was empirically validated by testing its empirical performance validity (shown in Figure 1.22) in this example study. The starting conformal topology for design synthesis of morphing airfoil was created successfully. Shearing, bending, and torsion as well as nonlinearity of the designed morphing airfoil were considered during design synthesis. The developed design synthesis with Particle Swarm Optimization was used to systematically design compliant mechanism for morphing wings.

CHAPTER 10

CLOSURE

The principal goal in this dissertation is to develop a unit truss approach that facilitates the design, including representation, analysis, design synthesis, and manufacturing, of conformal cellular structures.

The motivation of developing the unit truss approach, the details of this approach, and the results of its applications to conformal cellular structures are summarized in Section 10.1. In Section 10.2, the research question identified in Chapter 1 is revisited and the research hypothesis is critically re-evaluated. Based on the critical evaluations, the research contributions of this dissertation are reported in Section 10.3 and the future work is identified in Section 10.4.

10.1 A Summary of this Dissertation

Cellular structures are present from the atomic level all the way up to patterns found in human skeleton. They are prevailing structures in the nature and known for their excellent mechanical, thermal and acoustic properties. Two typical types of cellular structures, lightweight structures and compliant mechanisms, are investigated. Lightweight structures are rigid and designed to reduce weight, while increasing strength and stiffness. Compliant mechanisms are designed to transform motions and forces. Most available artificial lightweight structures are patterns of primitives. However, the performance of lightweight structures can be enhanced by using adaptive cellular structures with conformal strut orientations and sizes, like the trabeculae in femoral

bone. Bending, torsion, and nonlinear behaviors of compliant mechanisms have not been sufficiently studied.

In order to design adaptive cellular structures, a new unit cell, the unit truss is proposed. The unit truss approach facilitates the design of adaptive cellular structures for enhanced mechanical properties via geometric modeling, finite element analysis, geometry optimization, and additive fabrication. Four research issues, which address representation, structural analysis, design synthesis, and manufacturing respectively, are raised and solved. Unit truss enables representation and mechanics analysis for adaptive cellular structures. A synthesis method using engineering optimization algorithms is developed to systematically design adaptive cellular structure. Two examples, graded cellular structure for prosthesis and compliant mechanism for morphing wings, are studied to test the unit truss approach.

10.2 Answering the Research Question and Validating the Research Hypothesis

Research Question: How can adaptive cellular structures be accurately analyzed, efficiently created, and systematically designed?

Research Hypothesis: Unit truss can be used as unit cell to facilitate the design of adaptive cellular structure via geometric modeling, finite element analysis, engineering optimization, and additive fabrication.

In general, a research question is answered when the corresponding hypothesis is validated. In order to answer the research question, the author validates the posed hypothesis. As discussed in Section 1.6, the validation square is used to test the hypothesis (Pedersen, Emblemsvag et al. 2000).

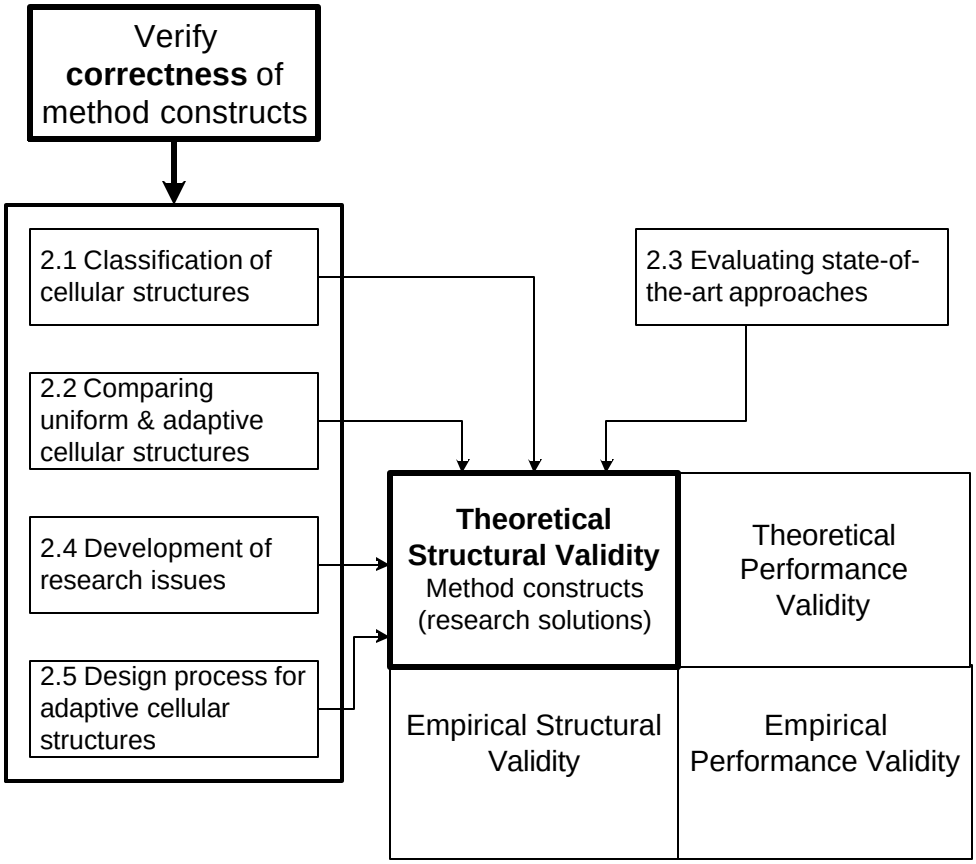

Figure 10.1 Test Theoretical Structural Validity by Literature Review and Critical Thinking

10.2.1 Theoretical Structural Validation and Empirical Structural Validation

The **theoretical structural validity** of the new unit truss approach is verified via the literature review in Chapter 2 as shown in Figure 10.1, and the adaptations of the method constructs ("geometric modeling", "continuum mechanics and finite element method", "engineering optimization", and "design for manufacturing") as well as their integration into the unit truss approach in Chapters 3~7 as shown in Figure 10.2. The four individual constructs constituting the method are accepted (**Step 1** in Validation Square) as well as the internal consistency of the way to put together into the new unit truss approach (**Step 2** in Validation Square). The correctness of constructs is proved

when they are separate and integrated. The effectiveness of the unit truss approach proposed in the hypothesis is demonstrated empirically with the examples presented in Chapters 3~7 as shown in Figure 10.2 (**Step 3** in Validation Square). So, the **empirical structural validity** of the new unit truss approach is verified.

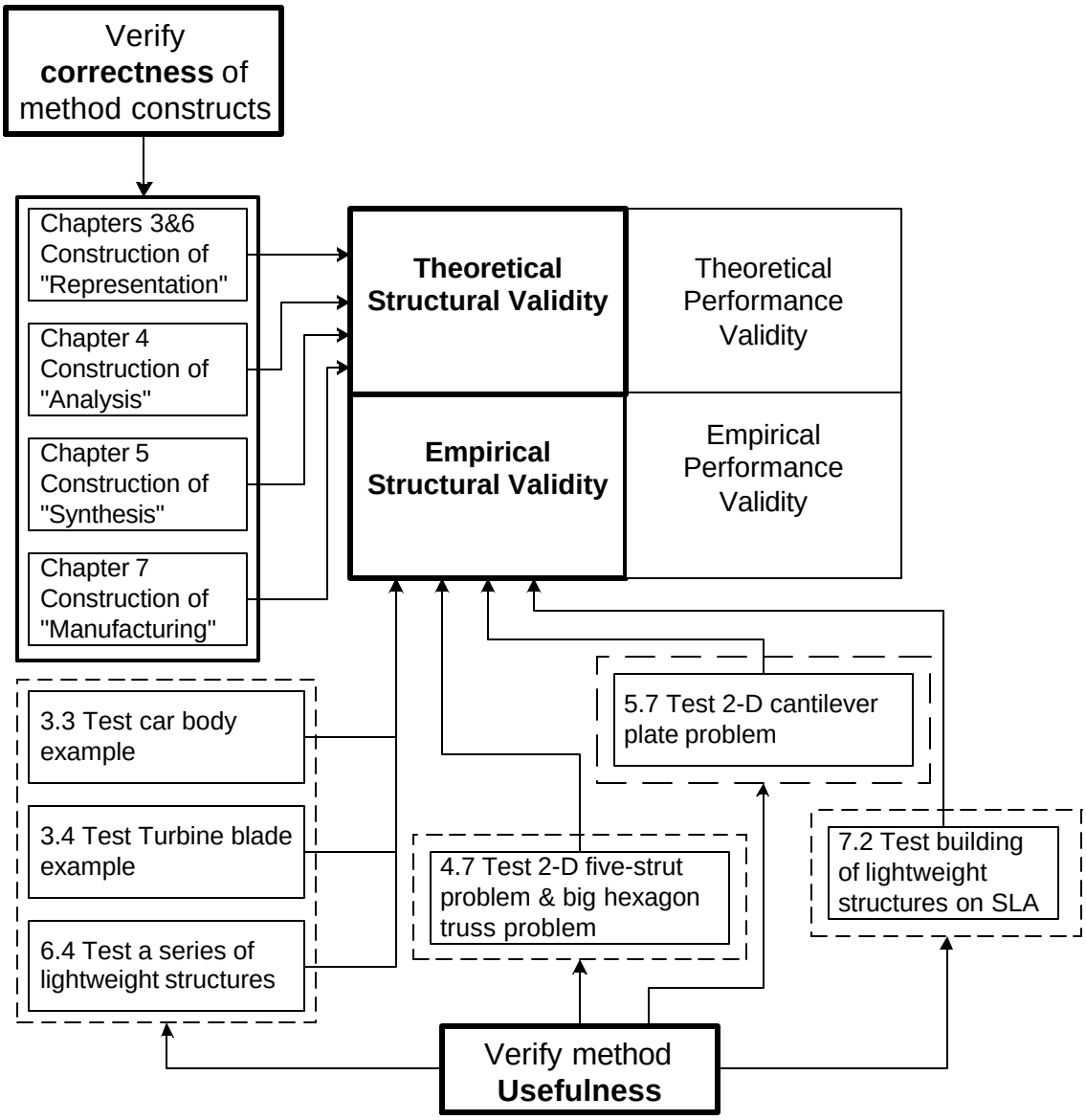

Figure 10.2 Test Theoretical Structural Validity and Empirical Structural Validity with Method Constructs and Example Problems in the Context of Validation Square

In Chapter 2, the author performs a literature review as shown in Figure 10.1. The unit truss approach posed in the hypothesis should address four research issues. Four constructs are adapted to solve these research issues ("representation", "analysis", "manufacturing", and "synthesis") respectively.

In Chapters 3~7, the author elaborately addresses how these four relevant constructs are adapted to solve the four research issues and integrated into the new unit truss approach. The correctness of the constructs during individual adaptations and integration prove the theoretical structural performance of the new unit truss approach as Figure 10.2.

In Chapter 3, two approaches (parametric modeling method and approach of using finite element mesh data) were developed to create conformal truss topology. In Chapter 6, a hybrid geometric modeling is developed to perform the geometric modeling of conformal cellular structures. Therefore, the construct of "geometric modeling" proved the **theoretical structural validity** of the hypothesis and well address the issue of "representation". In Section 6.4, a few conformal cellular structures were successfully created, including those lightweight structures with more than 2000 struts. This usefulness of unit truss approach proved **empirical structural validity** of the hypothesis about "representation".

In Chapter 4, the mechanics model of unit truss has been successfully developed and used to more accurately analyze cellular structures (2-D and 3-D). The construct of "continuum mechanics and finite element method" proved the **theoretical structural validity** of the hypothesis and well address the issue of "analysis". In Section 4.7, the unit truss approach was tested with a few sample problems and compared to MASTAN2 (McGuire, Gallagher et al. 2000). The usefulness of unit truss approach proved **empirical structural validity** of the hypothesis of the hypothesis about "analysis".

In Chapter 5, a design synthesis method was developed to systematically design adaptive lightweight structures for enhanced performance and compliant mechanisms with multiple inputs/outputs. It enabled the design of 3D compliant mechanisms. It proved the **theoretical structural validity** of the hypothesis using unit truss approach. In Section 5.5, a lightweight structure problem was used to test the unit truss approach and resolved successfully. This test proved the **empirical structural validity** of the hypothesis about "synthesis".

In Chapter 7, the author performed a literature review about the manufacturing processes of cellular structures. Then the author demonstrated the identification of manufacturing rules for cellular structures and the consideration of limitations during design using SLA process using the principles of design for manufacturing. From the investigation of AF processes, the author concluded that SLM as a state-of-the-art process can directly fabricate final functional cellular structures for industry applications. It proved **theoretical structural validity** and **empirical structural validity** of the hypothesis through a critical literature review about the cellular structure manufacturing and experiments of building various cellular structures with Additive Fabrication processes.

10.2.2 Empirical Performance Validation

The author tested the hypothesis with two examples in Chapters 8 and 9 and successfully designed graded cellular structure for prosthesis and compliant mechanism for morphing wings. In Chapter 8, a new acetabular implant with graded cellular structures was developed for hip prosthesis. With the comparison to the state-of-the-art porous coated prosthesis, the graded cellular structure designed with unit truss approach has better stability. In Chapter 9, a compliant cellular structure for Variform morphing wing concept. Axial forces, bending, and torsion were considered

simultaneously and nonlinearity was analyzed for better analysis accuracy. The morphing airfoil design problem has 117 design variables and multiple design objectives. Through two example presented in Chapters 8 and 9, the research hypothesis was tested empirically. The outcome of the new unit truss approach is useful with respect to the initial purpose for these two example problems (**Step 4** in Validation Square). The achievements of enhanced performances in the designed hip prosthesis and morphing airfoil resulted from the unit truss approach (**Step 5** in Validation Square). The successful applications of the examples problems proved the **empirical performance validity** of the hypothesis.

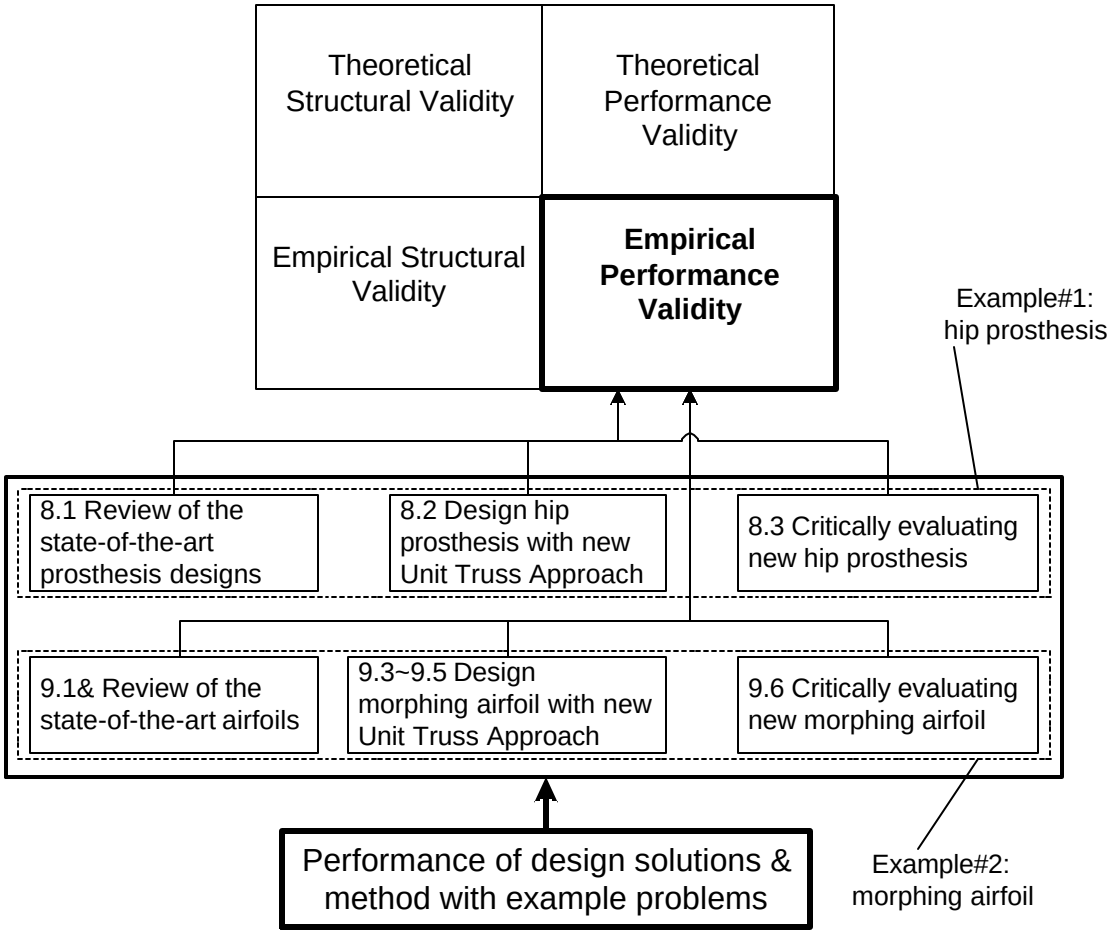

Figure 10.3 Test Empirical Performance Validity by using Example Problems in the Context of Validation Square

10.2.3 Theoretical Performance Validation

"Theoretical performance validity involves establishing that the proposed methods are useful beyond the example problems. This involves determining the characteristics of the example problems that make them representative of general classes of problems. Based on the utility of the method for these example problems, its usefulness for general classes of problems is inferred." (Seepersad 2004) For empirical structural validation, it is argued in Sections 3.3, 3.4, 4.7, 7.2, 5.5 and 6.4, that the example problems are collectively representative of a general class of problems, defined by the following characteristics:

- Parametric modeling approach is available to create conformal truss topology for parts with widely extended surfaces. FEM meshing approach is available to create topology for parts with arbitrary geometries but with no full control of strut sizes and orientations. (Chapter 3)
- CAD models can be created for arbitrary truss topologies as long as the used computer has enough memory. The storage memory of cellular structures is proportional to the number of struts with 115 KB/Unit Truss. (Chapter 6)
- The mechanics model of unit truss is suited to both lightweight structure and compliant mechanisms. Cellular structures can consists of various primitives, including triangle, rectangle, hexagon, octahedron, and truncated octahedron. Matlab limits the scale of analyzable cellular structures in this research. (Chapter 4)
- SLA is used to demonstrate formulating manufacturing rules and identifying manufacturing limitations. Supports are not required during the fabrication. Any manufacturing limitations can be included as constraints or bounds in the design synthesis. This process can be leveraged to other additive fabrication processes that

can build cellular structures without supports or easily removable supports. (Chapter 7)

– The developed design synthesis method with Particle Swarm Optimization is suited to both 2-D and 3-D adaptive cellular structure designs as long as starting topologies are provided. It is applicable to problems with multiple design objectives and discrete design domains. The scale of the starting cellular structures greatly influences the search time.

In Chapters 3~9, it has been demonstrated that the unit truss approach is effective for the example problems with these characteristics. Therefore, we take a leap of faith to believe that the unit truss approach is effective for general classes of problems with these characteristics. The usefulness of the method is beyond the example problems (**Step 6** in Validation Square). The unit truss approach may be applied to broader classes of problems, such as tissue engineering (scaffolds) and materials design (structure). At this point, **theoretical performance validity** of the hypothesis is proved.

10.3 Contributions

As a result of the research efforts, these are the following principal contributions:

1. This research enabled the users of my results to create conformal topology for adaptive cellular structures and formulate topology into unit trusses. This research enabled geometric modeling and mechanics analysis of adaptive cellular structures. This is presented in Chapters 3, 4 and 6.

2. In Chapter 4, unit truss is unitized as a new unit cell for structural analysis of adaptive cellular structure with the simultaneous considerations of bending, torsion, nonlinearity, and buckling. The mechanics model of unit truss can

provide better accuracy to estimate the effective properties by correcting the stiffness for lightweight structure. The geometric nonlinearity and material nonlinearity can be considered by using tangent stiffness method.

3. Through the research on manufacturing in Chapter 7, I advanced the understanding of AF for cellular structures manufacturing and led to extend the applications of AF into new mesoscopic material structure design.

4. In Chapter 5, a design synthesis method using particle swarm optimization is developed to systematically design adaptive cellular structures, including lightweight cellular structures with better performance, compliant mechanisms with multiple inputs/outputs for morphing shape and potentially for 3-D compliant mechanisms.

10.4 Limitations and Future Work

The limitations and future work of this dissertation are outlined in the areas of representation, analysis, manufacturing, and synthesis.

1. Adding rounds to the joints of cellular structures cab reduce stress concentration and fatigue to enhance the structures' mechanical performance. Local Boolean operations at the common edges between neighboring unit trusses could glue the unit trusses' surfaces together and efficiently create the solid model of an entire structure. These two improvements can potentially enhance the design of cellular structures and create the solid models of cellular structures efficiently. FEM mesh was applied to created conformal truss topology. However, meshing algorithms and mesh decimation have not been sufficiently studied and are future work.

2. Fatigue mechanism and residual stress of cellular structures have not been discussed in this research. However, they are important issues for the design of adaptive structures. We have performed structural analysis on adaptive cellular structures. An interesting topic about adaptive cellular structures is to design for multiple functionalities. Fatigue, residual stress and multiple functionality analysis should be one of future work.

3. Manufacturing processes can cause the variations of strut sizes and influence the structures' performance. It is desired to consider the manufacturing variations at the design stage using robust design.

4. Even though the literature survey has been used to support the selection of search algorithm, and the design synthesis with particle swarm optimization algorithm can reach convergence, the number of iterations is still numerous and inferior to gradient search algorithms. It is important to evaluate various algorithms via experiments and further explore the possibility to use gradient search algorithms.

"Size" effect of unit trusses remains an open issue. In this research, the size of unit trusses was given based on my own experience. It is unknown whether refining unit trusses can improve design results. We do not know what size is most appropriate for design synthesis of cellular structures. The cellular structures presented in this research are in mesoscopic scale. Is this unit truss approach still valid in microscopic scale or nanoscopic scale? One sample problem would be living cells, whose scaffolds simultaneously provide high mechanical strength and enhanced flexibility (Ingber 1993; Bray).

REFERENCES

"*Hip Replacement*", http://www.biomet.com/patients/hip_replacement.cfm, Biomet, Inc.

"*Pro/Mesh & Pro/FEM-Post user's guide*", 1997, Parametric Technology Corporation,

1998, "Materials for lean weight vehicles: the battle for a better body." *Steel Times (UK)* **226**(2): 73-74.

"*ANSYS advanced analysis techniques guide*", 1999, ANSYS, Inc.,

2000, Longer-Lasting Implants Used for Total Hip Replacement. Cornerstone. Mineola, NY, Winthrop-University Hospital. **10**.

"*Questions and Answers about Hip Replacement*", 2001, http://www.niams.nih.gov/hi/topics/hip/hiprepqa.pdf, National Institute of Arthritis and Musculoskeletal and Skin Diseases Information Clearinghouse

"*Morphing Aircraft Structures*", 2002, http://www.darpa.mil/dso/thrust/matdev/mas.htm, DARPA Defense Sciences Office

"*GEO structures, shaping the future of spine surgery*", 2003, http://www.interpore.com/product_geo.html, Interpore Cross International, Inc.

"*SLA 3500 System*", 2003, http://www.3dsystems.com, 3D Systems, Inc.

"*ABAQUS Analysis User's Manual Version 6.4*", 2004, Abaqus, Inc.,

"*AAI RQ-7 Shadow 200*", 2005, http://juav.janes.com/, Jane's Information Group

"*A NEW world-class generative process developed for direct product realisation with SELECTIVE LASER MELTING (SLM)*", 2005, http://www.mcp-group.com/rpt/rpttslm.html, MCP Group

"*A Patient's Guide to Total Hip Replacement Surgery*", 2005, http://www.healthpages.org/AHP/LIBRARY/HLTHTOP/THR/INDEX.HTM, Medical Multimedia Group

"*Shadow 400 UAV system*", 2005, http://www.aaicorp.com, AAI Corporation

Agins, H., N. Alcock, et al., 1988, "Metallic wear in failed titanium-alloy total hip replacements. A histological and quantitative analysis." *The Journal of Bone and Joint Surgery* **70**: 347-356.

Albrektsson, T. and C. Johansson, 2001, "Osteoinduction, osteoconduction and osseointegration." *European Spine Journal* **10**(0): 96-101.

An, C. H., C. G. Atkeson, et al., 1988, *Model-based control of a robot manipulator*, MIT Press.

Ananthasuresh, G. K. and S. Kota, 1995, Designing compliant mechanisms. ASME Mechanical Engineering. **117:** 93-96.

Ananthasuresh, G. K., S. Kota, et al., 1994, *Strategies for systematic synthesis of compliant MEMS*. ASME Winter Annual Meeting

Ananthasuresh, G. K., L. Saggere, et al., 1994, *A single-piece compliant stapler*. ASME Mechanisms Conference-Student Design Competition

Belegundu, A. D. and T. R. Chandrupatla, 1999, *Optimization concepts and applications in engineering*, Prentice Hall.

Bendsoe, M. P., 1995, *Optimization of structural topology, shape, and material*. Berlin Heidelberg, Springer-Verlag.

Bendsoe, M. P. and N. Kikuchi, 1988, "Generating optimal topologies in structural design using a homogenization method." *Computer Methods in Applied Mechanics and Engieering* **71**: 197-224.

Blacker, T., 2001, "Automated conformal hexahedral meshing constraints, challenges and opportunities." *Engineering with Computers* **17**: 201-210.

Bobyn, B. J. D., R. A. Poggie, et al., 2004, "Clinical Validation Of A Structural Porous Tantalum Biomaterial For Adult Reconstruction." *The Journal Of Bone And Joint Surgery* **86-A**(Supplement 2).

Bragdon, C. R., M. Jasty, et al., 2004, "Biologic Fixation of Total Hip Implants." *Journal of Bone & Joint Surgery* **86**(Dec2004 Supplement): 105-117.

Bray, D., "*Cell*", 2005, http://au.encarta.msn.com, Microsoft® Encarta® Online Encyclopedia

Burns, S. A., Ed. 2002, *Recent advances in optimal structural design*, American Society of Civil Engineers.

Canfield, S. and M. Frecker, 1999, *Design Of Compliant Mechanisms For Amplification Of Induced Strain Actuators*. ASME Design Engineering Technical Conferences, Las Vegas, Nevada

Canfield, S. and M. Frecker, 2000, "Topology Optimization of Compliant Mechanical Amplifiers for Piezoelectric Actuators." *Structural and Multidisciplinary Optimization* **20**(4): 269-279.

Chambers, I., K. F. Orishimo, et al., 2004, "Relationship Between Polyethylene Wear and Osteolysis in Hips with a Second-Generation Porous-Coated Cementless Cup." *Journal of Bone & Joint Surgery* **86**(5): 1097 - 1098.

Chen, W., J. K. Allen, et al., 1996, "A concept exploration method for determining robust top-level specifications." *Engineering Optimization* **26**(2): 137-158.

Cheng, Y.-L., J. Stamp, et al., 1999, *Additive/Subtractive Material Processing for Mesoscopic Parts*. Solid Freeform Fabrication Symposium, Austin, Texas

Chiras, S., D. R. Mumm, et al., 2002, "The structural performance of near-optimized truss core panels." *International Journal of Solids and Structures* **39**(15): 4093-4115.

Chung, T. J., 1988, *Continuum mechanics*, Prentice Hall.

Cochran, J. K., K. J. Lee, et al., 2000, *Low Density Monolithic Metal Honeycombs by Thermal Chemical Processing*. Fourth Conference on Aerospace Materials, Processes, and Environmental Technology, Huntsville, AL

Corney, J. and T. Lim, 2001, *3D modeling with ACIS*, Saxe-Coburg Publications.

Crossley, W. A. and E. A. Williams, 1997, *A study of adaptive penalty functions for constrained genetic algorithm-based optimization*. Aerospace Sciences Meeting and Exhibit, 35th, Reno, NV, AIAA,

Daily, C., D. Lees, et al., 1997, Truss structure design. United States Patent.

Dalgarno, K. and T. Stewart, 2001, "Production tooling for polymer moulding using the RapidSteel process." *Rapid Prototyping Journal* **7**(3): 173-9.

Deshpande, V. S., N. A. Fleck, et al., 2001, "Effective properties of the octet-truss lattice material." *Journal of the Mechanics and Physics of Solids* **49**(8): 1747 – 1769.

Deshpande, V. S., N. A. Fleck, et al., 2001, "Foam topology: bending versus stretching dominated architectures." *Acta Materialia* **49**(6): 1035-1040.

Diez, J., 2001, Design for additive fabrication: building miniature robotic mechanisms. School of Mechanical Engineering. Atlanta, GA, Georgia Institute of Technology.

Dutta, D., F. B. Prinz, et al., 2001, "Layered manufacturing: current status and future trends." *ASME Journal of Computing and Information Science in Engineering* **1**(1): 60-71.

Eringen, A. C., 1971, *Continuum physics*. New York,, Academic Press.

Eringen, A. C., 1999, *Microcontinuum field theories*. New York, Springer.

Eschenauer, H. A. and N. Olhoff, 2001, "Topology optimization of continuum structures." *Applied Mechanics Reviews* **54**(4): 331-390.

Evans, A. G., J. W. Hutchinson, et al., 2002, "The topological design of multifunctional cellular metals." *Progress in Materials Science* **46**: 309-327.

Faires, J. D. and R. L. Burden, 1998, *Numerical methods*, Brooks/Cole Pub. Co.

Fitzgerald, R. H., 1992, "Total hip arthroplasty sepsis." *Orthopedic Clinics of North America* **23**: 259-264.

Fletcher, R. and M. J. D. Powell, 1963, "A Rapidly Convergent Descent Method for Minimizatio." *Computer Journal* **6**: 163-168.

Fourie, P. C. and A. A. Groenwold, 2002, "The particle swarm optimization algorithm in size and shape optimization." *Structural and Multidisciplinary Optimization* **23**(4): 259 - 267.

Frecker, M., G. K. Ananthasuresh, et al., 1997, "Topological synthesis of compliant mechanisms using multi-criteria optimization." *ASME Journal of Mechanical Design* **119**(2): 238-245.

Fu, Y. B. and R. W. Ogden, 2001, *Nonlinear elasticity : theory and applications*, Cambridge University Press.

Fuller, R. B., 1975, *Synergetics, explorations in the geometry of thinking*, Macmillan Publishing.

Gano, S. E. and J. E. Renaud, 2002, *Optimized Unmanned Aerial Vehicle With Wing Morphing For Extended Range And Endurance*. 9th AIAA/ISSMO Symposium and Exhibit on Multidisciplinary Analysis and Optimization, Atlanta, GAAIAA-2002-5668

George, P.-L. and H. Borouchaki, 1998, *Delaunay Triangulation and Meshing: Application to Finite Elements*. Paris, France, Hermes.

Gibson, L. J., 2003, Cellular solids. MRS Bulletin, Materials Research Society. **4:** 270-271.

Gibson, L. J., 2005, "Biomechanics of cellular solids." *Journal of Biomechanics* **38**: 270-271.

Gibson, L. J. and M. F. Ashby, 1997, *Cellular solids : structure and properties*, Cambridge University Press.

GM, S., K. S, et al., 2001, "Early failure of a roughened surface, precoated femoral component in total hip arthroplasty." *Journal of Arthroplasty* **16**(2): 141-148.

Gould, P. L., 1994, *Introduction to linear elasticity*, Springer-Verlag.

Gray, H., 1918, *Anatomy of the Human Body*. Philadelphia, Lea & Febiger.

Grylls, R., 2003, "Laser Engineered NET SHAPES." *Advanced Materials & Processes* **161**(1): 45.

Hague, R., G. D'Costa, et al., 2001, "Structural design and resin drainage characteristics of QuickCast 2.0." *Rapid Prototyping Journal* **7**(2).

Hague, R., G. D'Costa, et al., 2001, "Structural design and resin drainage characteristics of QuickCast 2.0." *Rapid Prototyping Journal* **7**(2): 66-73.

Harris, T., "*Shark Anatomy*", http://science.howstuffworks.com/shark.htm, HowStuffWorks.com, Convex Group, Inc.

Hassani, B. and E. Hinton, 1999, *Homogenization and structural topology optimization: theory, practice and software*. Verlag, Springer.

Hayes, A. M., A. Wang, et al., 2004, "Mechanics of linear cellular alloys." *Mechanics of Materials* **36**(8): 691-713.

Heppner, F. and U. Grenander, 1990, *A stochastic nonlinear model for coordinated bird flocks*. The Ubiquity of Chaos. E. S. Krasner. Washington, DC, AAAS Publications.

Hetrick, J. A. and S. Kota, 1998, *Size and shape optimization of compliant mechnisms: an efficiency formulation*. ASME Design Engineering Technical Conference, Atlanta, GA

Hinton, E. and J. Owen, 1977, *Finite element programming*, Academic Press.

Holland, J. H., 1975, *Adaption in Natural and Artifical Systems*. Ann Arbor, MI, University of Mechigan Press.

Hollister, S. J., 2005, "Porous scaffold design for tissue engineering." *Nature Materials* **4**(7): 518–524.

Hosni, Y. A., J. Nayfeh, et al., 1999, "Investment Casting Using Stereolithography: The Case of Complex Objects." *Rapid Prototyping Journal* **5**(1): 1-5.

Howell, L. L., 2001, *Compliant mechanisms*. New York, NY, John Wiley & Sons.

Hutmacher, D. W., 2000, "Scaffolds in tissue engineering bone and cartilage." *Biomaterials* **21**(24): 2529-2543.

Hutmacher, D. W., 2001, "Scaffold design and fabrication technologies for engineering tissues — state of the art and future perspectives." *Journal of Biomaterials Science -- Polymer Edition* **12**(1): 107-124.

Ingber, D. E., 1993, "Cellular tensegrity: defining new rules of biological design that govern the cytoskeleton." *Cell Science* **104**(3): 613-627.

Ingber, D. E., 1998, "The architecture of life." *Scientific American*.

Jacobs, P., 1992, *Rapid prototyping & manufacturing: fundamentals of stereolithography*. Dearborn, MI, SME.

Jacobs, P., 1996, *Stereolithography and other RP&M technologies: from rapid prototyping to rapid tooling*. Dearborn, MI, Society of Manufacturing Engineers.

Jasty, M., C. Bragdon, et al., 1997, "In vivo skeletal responses to porous-surfaced implants subjected to small induced motions." *Journal of bone and joint surgery* **79**: 707-714.

Jensen, B. D., M. B. Parkinson, et al., 2001, *Design Optimization Of A Fully-Compliant Bistable Micro-Mechanism*. ASME International Mechanical Engineering Congress and Exposition, New York, NY

Joo, J., S. Kota, et al., 2000, "Topological Synthesis of Compliant Mechanisms Using Linear Beam Elements." *Mechanics of Structures and Machines* **28**(4): 245-280.

Joo, J., S. Kota, et al., 2001, *Large Deformation Behavior of Compliant Mechanisms*. ASME Design Engineering Technical Conferences, Pittsburgh, PA

Joo, J., S. Kota, et al., 2001, *Nonlinear Synthesis of Compliant Mechanisms: Topology Design*. ASME Design Engineering Technical Conferences, Pittsburgh, PA

Joo, J., S. Kota, et al., 2004, "Topological Synthesis of Compliant Mechanisms Using Nonlinear Beam Elements." *Mechanics Based Design of Structures and Machines* **32**(1): 17 - 38.

Kanit, T., S. Forest, et al., 2003, "Determination of the size of the representative volume element for random composites: statistical and numerical approach." *International Journal of Solids and Structures* **40**: 3647–3679.

Kennedy, J. and R. C. Eberhart, 1995, *Particle swarm optimization*. Proceedings of IEEE International Conference on Neural Networks, Piscataway, NJ

Kita, H., M. Fukushima, et al., 2005, "Oxidation Resistance and High-Temperature Lubricating Properties of Magnesium-Phosphate-Treated Graphite." *Journal of the American Ceramic Society* **88**(9): 2632-2634.

Kobayashi, K. and M. U. Salam, 2000, "Comparing Simulated and Measured Values Using Mean Squared Deviation and its Components." *Agronomy Journal* **92**: 345-352.

Kota, S., J. Joo, et al., 2001, "Design of compliant mechanisms: applications to MEMS." *Analog Integrated Circuits and Signal Processing* **29**(1): 7-15.

Kroo, I., "*Applied Aerodynamics: A Digital Textbook*", 2005, http://www.desktopaero.com/appliedaero/, Desktop Aeronautics, Inc.

Kruth, J.-P., P. Mercelis, et al., 2005, "Binding mechanisms in selective laser sintering and selective laser melting." *Rapid Prototyping Journal* **11**(1): 26-36.

Kumar, R. S. and D. L. McDowell, 2004, "Generalized continuum modeling of 2-D periodic cellular solids." *International Journal of Solids and Structures* **41**(26): 7399-7422.

Larsen, U. D., O. Sigmund, et al., 1997, "Design and fabrication of compliant mechanisms and material structures with negative Poisson's ratio." *Journal of Microelectromechanical Systems* **6**(2): 99-106.

LD, Z., P. DE, et al., 2001, "Structure, metallurgy, and mechanical properties of a porous tantalum foam." *Journal of Biomedical Materials Research* **58**(2): 180-187.

Lim, S. M., S. Lee, et al., 2005, "Design and demonstration of a biomimetic wing section using a lightweight piezo-composite actuator (LIPCA)." *Smart Materials and Structures* **14**(4): 496-503.

Liu, J.-S. and T. J. Lu, 2004, "Multi-objective and multi-loading optimization of ultralightweight truss materials." *International Journal of Solids and Structures* **41**: 619–635.

Lo, S. H., 1991, "Volume Discretization into Tetrahedra - II. 3D Triangulation by Advancing Front Approach." *Computers and Structures* **35**(5): 501-511.

Lu, K.-J. and S. Kota, 2002, *Compliant Mechanism Synthesis for Shape-Change Applications: Preliminary Results*. Proceedings of the 2002 SPIE Modeling, San Diego, CA

Lu, K.-J. and S. Kota, 2003, "Design of Compliant Mechanisms for Morphing Structural Shapes." *Journal of Intelligent Material Systems and Structures* **14**: 379-391.

Lu, K.-J. and S. Kota, In Press, "An Effective Method of Synthesizing Compliant Adaptive Structures Using Load Path Representation." *Journal of Intelligent Material Systems and Structures*.

Lucato, S. L. d. S. e., R. M. McMeeking, et al., 2005, "Actuator placement optimization in a Kagome based high authority shape morphing structure." *Smart Materials and Structures* **14**(4): 869-875.

Maciel, A., "*Biomechanics of Hip Joint Capsule*", 2002, Computer Graphics Lab, Institute of Computing and Multimedia Systems, School of Computer and Communication Sciences, Swiss Federal Institute of Technology,

Malvern, L. E., 1969, *Introduction to the mechanics of a continuous medium*. Englewood Cliffs, New Jersey, Prentice-Hall, Inc.

Marieb, E. N., J. Mallatt, et al., 2004, *Human Anatomy*, Benjamin-Cummings Publishing Company.

Marsden, J. E. and T. J. R. Hughes, 1983, *Mathematical foundations of elasticity*, Prentice-Hall.

Martin, J. W., J. M. Redmond, et al., 2000, "Distributed Sensing and Shape Control of Piezoelectric Bimorph Mirrors." *Journal of Intelligent Materials Systems and Structures* **11**: 744–757.

Martinez, E., U. Wiklund, et al., 2002, "Tribological performance of TiN supported molybdenum and tantalum carbide coatings in abrasion and sliding contact." *Wear* **253**: 1182–1187.

Maxwell, J. C., 1864, On the calculation of the equilibrium and stiffness of frames. Philosophical Magazine. **27:** 294.

McDowell, D. L., "*New Directions in Materials Design Science and Engineering (MDS&E), Report of a Workshop Sponsored by the U.S. National Science Foundation,*" 1998, Georgia Institute of Technology and Morehouse College, Atlanta, GA

McGuire, W., R. H. Gallagher, et al., 2000, *Matrix structural analysis*, John Wiley.

Michell, A. G. M., 1904, The limits of economy in frame structures. Philosophical Magazine Sect. 6. **8:** 589-597.

Midha, A., T. W. Norton, et al., 1994, "On the nomenclature, classification, and abstractions of compliant mechanisms." *ASME Journal of Mechanical Design* **116**(1): 270-279.

MK, H., B. SA, et al., 1997, "Wear analysis of a retrieved hip implant with titanium nitride coating." *Journal of Arthroplasty* **12**(8): 938-945.

Mont, M. A. and D. S. Hungerford, 1997, "Proximally Coated Ingrowth Prostheses: A Review." *Clinical orthopaedics and related research* **344**: 139-149.

Mortenson, M. E., 1997, *Geometric modeling*. New York, John Wiley & Sons, Inc.

Nancy Elftman, 1998, Orthotic Materials: Cellular urethanes combine durability with breathability. BioMechanics.

Neter, J., M. H. Kutner, et al., 1996, *Applied linear statistical models*. Chicago, Boston, Mass., Irwin/McGraw-Hill.

Niinomi, M., 2003, "Fatigue performance and cyto-toxicity of low rigidity titanium alloy, Ti-29Nb-13Ta-4.6Zr." *Biomaterials* **24**(16): 2673-2683.

Nocedal, J., 1997, *Large Scale Unconstrained Optimization*. The State of the Art in Numerical Analysis. A. Watson and I. Duff., Oxford University Press.

Nowacki, W. and International Centre for Mechanical Sciences., 1970, *Theory of micropolar elasticity*. Wien ; New York, Springer-Verlag.

Owen, S. J., 1998, *A Survey of Unstructured Mesh Generation Technology*. 7th International Meshing Roundtable, Dearborn, Michigan

Panchal, J. H., 2005, "*A Framework for Simulation-Based Integrated Design of Multiscale Products and Design Processes*". Department of Mechanical Engineering. Atlanta, Georgia Institute of Technology**:** 557.

Pedersen, K., J. Emblemsvag, et al., 2000, *Validating Design Methods and Research--The Validation Square*. ASME Design Theory and Methodology Conference, Baltimore, MD

Piegl, L. and W. Tiller, 1987, "Curve and surface constructions using rational B-splines." *Computer Aided Design* **19**(9): 485-498.

Piegl, L. and W. Tiller, 1995, *The BURBS Book*. Berlin, Springer Verlag.

Prinz, F. B., C. L. Atwood, et al., "*Rapid prototyping in Europe and Japan: Volume I. analytical chapters*", 1997, The World Technology (WTEC) Division of Loyola College, Baltimore, MD

Qin, J. and D. T. Nguyen, 1994, *Generalized exponential penalty function for nonlinear programming*. AIAA/ASME/ASCE/AHS/ASC Structures, Structural Dynamics, and Materials Conference, 35th, Hilton Head, SC

Radstok, E., 1999, "Rapid tooling." *Rapid Prototyping Journal* **5**(4): 164-9.

Reddy, J. N., 1993, *An introduction to the finite element method*, McGraw-Hill, Inc.

Reklaitis, G. V., A. Ravindran, et al., 1983, *Engineering optimization: methods and applications*. New York, John Wiley and Sons.

Rietz, A., 2001, "Sufficiency of a finite exponent in SIMP (power law) methods." *Structural and Multidisciplinary Optimization* **21**(2): 159 - 163.

Rosen, D. W., "*NSF Proposal: Synthesis Methods for Structural and Compliant Mesostructured Parts*", 2003, Georgia Institute of Technology, Atlanta, GA

Rozvany, G. I., Ed. 1997, *Topology Optimization in Structural Mechanics*, Springer Verlag.

Rule, W. K., 1994, "Automatic truss design by optimized growth." *Journal of Structural Engineering* **120**(10): 3063-3070.

Saggere, L. and S. Kota, 1997, *Synthesis of distributed compliant mechanisms for adaptive structures application: an elasto-kinematic approach*. ASME Design Engineering Technical Conferences, Sacramento, CA

Saggere, L. and K. S., 2001, "Synthesis of Planar, Compliant Four-Bar Mechanisms for Compliant-Segment Motion Generation." *ASME Journal of Mechanical Design* **123**: 535-541.

Seepersad, C. C., 2004, A Robust Topological Preliminary Design Exploration Method With Materials Design Applications. School of Mechanical Engineering. Atlanta, GA, Georgia Institute of Technology**:** 565.

Seepersad, C. C., J. K. Allen, et al., 2003, *Robust topological design of cellular materials*. ASME Design Automation Conference, Chicago, ILPaper Number: DAC-48772

Seepersad, C. C., K. Pedersen, et al., 2005, *The Validation Square: How Does One Verify and Validate a Design Method?* Decision-Based Design: Making Effective Decisions in Product and Systems Design. W. Chen, K. Lewis and L. Schmidt. NY, ASME Press.

Selig, M., "*UIUC Airfoil Coordinates Database - Version 2.0*", 2005, http://www.ae.uiuc.edu/m-selig/ads.html, Department of Aerospace Engineering, University of Illinois at Urbana-Champaign, Urbana, Illinois 61801

Shephard, M. S. and M. K. Georges, 1991, "Three-Dimensional Mesh Generation by Finite Octree Technique." *International Journal for Numerical Methods in Engineering* **32**: 709-749.

Shi, Y. and R. C. Eberhart, 1998, *A modified particle swarm optimizer*. Proceedings of the IEEE Congress on Evolutionary Computation, Piscataway, NJ

Shi, Y. and R. C. Eberhart, 2001, *Fuzzy adaptive particle swarm optimization*. Proceedings of the IEEE Congress on Evolutionary Computation, Seoul, Korea

Simpson, T. W., J. K. Allen, et al., 1998, *Spatial Correlation Metamodels for Global Approximation in Structural Optimization*. ASME Advances in Design Automation Conference., Atlanta, GA

Shin, H.-C. and Ali H. Sayed, 2004, "Mean-Square Performance of a Family of Affine Projection Algorithms." *IEEE TRANSACTIONS ON SIGNAL PROCESSING,* **52**(1): 90-102.

Sigmund, O., 2001, "A 99 line topology opitimization code written in Matlab." *Struct Multidisc Optim* **21**: 120-127.

Silva, M., C. Heisel, et al., 2005, "Metal-on-Metal Total Hip Replacement." *Clinical orthopaedics and related research* **430**: 53–61.

Soni, B. K., 2000, "Grid generation: past, present, and future." *Applied Numerical Mathematics* **32**: 361-369.

Stewart, T. D., K. W. Dalgarno, et al., 1999, "Strength of the DTM RapidSteel ™ 1.0 material." *Materials and Design* **20**(2-3): 133-8.

St-Pierre, J.-P., M. Gauthier, et al., 2005, "Three-dimensional growth of differentiating MC3T3-E1 pre-osteoblasts on porous titanium scaffolds." *Biomaterials* **26**(35): 7319-7328.

Sun, W., B. Starly, et al., 2005, "Bio-CAD modeling and its applications in computer-aided tissue engineering." *Computer-Aided Design* **37**: 1097–1114.

Svanberg, K., 1987, "The Method of Moving Asymptotes--A New Method for Structural Optimization." *International Journal for Numerical Methods in Engineering,* **24**: 359-373.

Uhthoff, H., D. Bardos, et al., 1981, "The advantages of titanium alloy over stainless steel plates for the internal fixation of fractures: an experimental study in dogs." *The Journal of Bone and Joint Surgery* **63**: 427-434.

Viceconti, M., "*Visible Human Male - Bone surfaces*", 2004, http://www.tecno.ior.it/VRLAB/researchers/repository/BEL_repository.html, Laboratorio di Tecnologia Medica, Istituti Ortopedici Rizzoli

Wadley, H. N. G., N A. Fleck, et al., 2003, "Fabrication and structural performance of periodic cellular metal sandwich structures." *Composites Science and Technology* **63**: 2331-2343.

Wall, R., 2002, Darpa Eyes Materials For 'Morphing' Aircraft. Aviation Week & Space Technology. **156:** 36.

Wallach, J. C. and L. J. Gibson, 2001, "Mechanical behavior of a three-dimensional truss material." *International Journal of Solids and Structures* **38**(41): 7181-7196.

Wang, A.-J. and D. L. McDowell, 2003, "Optimization of a metal honeycomb sandwich beam-bar subjected to torsion and bending." *International Journal of Solids and Structures* **40**(9): 2041-2320.

Wang, H., 2001, Computer-aided design methods for the additive fabrication of truss structure. School of Mechanical Engineering. Atlanta, GA, Georgia Institute Of Technology**:** 171.

Wang, H., 2005, A unit cell approach for lightweight structure and compliant mechanism. School of Mechanical Engineering. Atlanta, GA, Georgia Institute Of Technology**:** 330.

Wang, H., Y. Chen, et al., 2005, *A Hybrid Geometric Modeling Method For Large Scale Conformal Cellular Structures*. ASME Computers and Information in Engineering Conference, Long Beach, CaliforniaPaper Number: DETC02/CIE-34495

Wang, H. and D. W. Rosen, 2002, *Computer-aided design methods for additive fabrication of truss structures*. International Conference on Manufacturing Automation (ICMA2002), Hong Kong, China, SPIE,

Wang, H. and D. W. Rosen, 2002, *Parametric modeling method for truss structures*. ASME Computers and Information in Engineering Conference, Montreal, CanadaPaper Number: DETC02/CIE-34495

Wang, X. L. and W. J. Stronge, 1999, "Micropolar theory for two-dimensional stresses in elastic honeycomb." *Proceedings: Mathematical, Physical & Engineering Sciences* **455**(1986): 2091-2116.

Weiss, P., 2003, Shape-shifting aircraft may ply future skyways. Science News. **164:** 359.

Wicks, N. and J. W. Hutchinson, 2004, "Performance of sandwich plates with truss cores." *Mechanics of Materials* **36**: 739–751.

Xie, Y. M. and G. P. Steven, 1997, *Evolutionary structural optimization*. Berlin Heidelberg, Springer-Verlag.

Xu, D. and G. K. Ananthasuresh, 2003, "Freeform Skeletal Shape Optimization of Compliant Mechanisms." *Journal of Mechanical Design* **125**: 253-261.

Xue, Z. and J. W. Hutchinson, 2003, "Preliminary assessment of sanwich plates subject to blast loads." *International Journal of Mechanical Sciences* **45**: 687-705.

Yang, D. U., S. Lee, et al., 2003, "Geometric effects on micropolar elastic honeycomb structure with negative Poisson's ratio using the "nite element method." *Finite Elements In Analysis And Design* **39**: 187–205.

Yoshida, H., A. Faust, et al., 2006, "Three-dimensional dynamic hip contact area and pressure distribution during activities of daily living." *Journal of Biomechanics* **39**(1).

VITA

Hongqing Vincent Wang was born at Xiaoshan, Hangzhou, China on November 25, 1974. He grew up in the same city and attended Linpu High School. He earned a Bachelor of Science degree in Mechanical Engineering from Tsinghua University in 1997. He worked for Motorola (China) as a process engineer between 1997 and 1999. He earned a Master of Science degree in Mechanical Engineering from the Georgia Institute of Technology in 2001. His graduate work was funded by the RPMI industrial members and the NSF-ITR “Digital Clay” project. Vincent is an R&D engineer at IronCAD Inc. in Atlanta, Georgia since April 2005.